The Dissertation Committee for Roy Damar Raharjo Certifies that this is the approved version of the following dissertation:

Mixed Gas Sorption and Transport Study in Solubility Selective Polymers

Committee:

Benny D. Freeman, Supervisor

Donald R. Paul

Isaac C. Sanchez

R. Bruce Eldridge

Edgar S. Sanders

Mixed Gas Sorption and Transport Study in Solubility Selective Polymers

by

Roy Damar Raharjo, B.S.

Dissertation

Presented to the Faculty of the Graduate School of

The University of Texas at Austin

in Partial Fulfillment

of the Requirements

for the Degree of

Doctor of Philosophy

The University of Texas at Austin

December 2007

Dedication

To my parents for their constant love and support

Acknowledgements

First and foremost, I would like to express my deepest gratitude to my advisor, Dr. Benny D. Freeman, for his continuous support, guidance, and encouragement during my study. I am also thankful for my thesis committee members – Dr. Donald R. Paul, Dr. Isaac C. Sanchez, Dr. Bruce R. Eldridge, and Dr. Edgar S. Sanders – as they have been helpful in discussions and guidance on this project.

Several people have contributed to this project in various ways. Dr. Lora G. Toy at Research Triangle Institute (RTI) provided invaluable inputs on the design of the mixed gas sorption and permeation system. Dr. Timothy C. Merkel at Membrane Technology and Research (MTR) hosted many helpful discussions. Dr. Rajeev Prabhakar at Air Liquide provided many useful tips on the mixed gas permeation measurements. I would also like to thank Dr. Valeriy Bondar at RTI, who built the original dilation equipment, for the tips and tricks on running the dilation measurements. I also gratefully acknowledge the fund sources for this research. This research was partially supported by the U.S. Department of Energy (grant no. DE-FG03-02ER15362) and the National Science Foundation (grant no. CTS-0515425).

Past and present members of the Freeman Polymer Research Group are also in need of acknowledgement for their technical advice, support, and encouragement. In particular, interactions with the following members have been helpful: Dr. Hyuck J. Lee,

Dr. Ho Bum Park, Dr. Rajeev Prabhakar, Dr. Haiqing Lin, Scott Matteucci, Scott Kelman, Victor Kusuma, Hao Ju, Richard Li, and Keith Ashcraft. Very special thanks go to Dr. Hyuck J. Lee and Dr. Rajeev Prabhakar for their constant help in the early years of my graduate study. I am also grateful to Dr. Haiqing Lin for his tremendous support and many insightful comments on research and life, in general. I would also like to thank the "lunch-regulars" – Scott Matteucci, Keith Ashcraft, David Sanders, Hao Ju, Richard Li, Bryan McCloskey, Scott Kelman, and Dr. Ho Bum Park – for brightening the days of research with humor and laughter. A special thank goes to my officemate, Scott Matteucci, for always entertaining me with his humors and his vast knowledge on world history. I thank you all for making my experience in graduate school a pleasant one.

Finally, I would like to thank my parents, sister, and brother for their unconditional love and constant support during my study.

Mixed Gas Sorption and Transport Study in Solubility Selective Polymers

Publication No._____

Roy Damar Raharjo, Ph.D.

The University of Texas at Austin, 2007

Supervisor: Benny D. Freeman

Membrane separation technology has recently emerged as a potential alternative technique for removing higher hydrocarbons (C_{3+}) from natural gas. For economic reasons, membranes for this application should be organic vapor selective materials such as poly(dimethylsiloxane) (PDMS) or poly(1-trimethylsilyl-1-propyne) (PTMSP). These polymers, often called solubility selective polymers, sieve penetrant molecules based largely on relative penetrant solubility in the polymer.

The sorption and transport properties in such polymers have been reported previously. However, most studies present only pure gas sorption and transport properties. Mixture properties, which are important for estimating membrane separation performance, are less often reported. In addition, mixed gas sorption and diffusion data in such polymers, to the best of our knowledge, have never been investigated before.

This research work provides a fundamental database of mixture sorption, diffusion, and permeation data in solubility selective polymers. Two solubility selective polymers were studied: poly(dimethylsiloxane) (PDMS) and poly(1-trimethylsilyl-1-

propyne) (PTMSP). The vapor/gas mixture was *n*-C_4H_{10}/CH_4. CH_4 partial pressures ranged from 1.1 to 16 atm, and *n*-C_4H_{10} partial pressures ranged from 0.02 to 1.7 atm. Temperatures studied ranged from -20 to 50^oC. The pure and mixed gas *n*-C_4H_{10} and CH_4 permeability and solubility coefficients in PDMS and PTMSP were determined experimentally using devices constructed specifically for these measurements. The pure and mixed gas diffusion coefficients were calculated from permeability and solubility data.

In rubbery PDMS, the presence of *n*-C_4H_{10} increases CH_4 permeability, solubility, and diffusivity. On the other hand, the presence of CH_4 does not measurably influence *n*-C_4H_{10} sorption and transport properties. The *n*-C_4H_{10}/CH_4 mixed gas permeability selectivities are lower than those estimated from pure gas measurements. This difference is due to both lower solubility and diffusivity selectivities in mixtures relative to those in pure gas. Plasticization of PDMS by *n*-C_4H_{10} does little to *n*-C_4H_{10}/CH_4 mixed gas diffusivity selectivity. Increases in mixed gas permeability selectivity with increasing *n*-C_4H_{10} activity and decreasing temperature were mainly due to increases in solubility selectivity.

Unlike PDMS, the presence of *n*-C_4H_{10} decreases CH_4 permeability, solubility, and diffusivity in PTMSP. The competitive sorption and the blocking effects significantly reduce CH_4 solubility and diffusion coefficients in the polymer, respectively. However, similar to PDMS, the presence of CH_4 has no measurable influence on *n*-C_4H_{10} sorption and transport properties. *n*-C_4H_{10}/CH_4 mixed gas permeability selectivities in PTMSP are higher than those determined from the pure gas measurements. This deviation is a result of higher solubility and diffusivity selectivities in mixtures relative to the pure gas values. Mixed gas permeability, solubility, and diffusivity selectivities in PTMSP increased with increasing *n*-C_4H_{10} activity and decreasing temperature.

The partial molar volumes of *n*-C_4H_{10} and CH_4 in the polymers were determined from sorption and dilation data. The dilation isotherms of PDMS and PTMSP in mixtures agree with estimates based on pure gas sorption and dilation measurements. The partial molar volumes of *n*-C_4H_{10} and CH_4 in PDMS are similar to those in liquids. In contrast, the partial molar volumes of *n*-C_4H_{10} and CH_4 in glassy PTMSP are substantially lower than those in liquids.

Several models were used to fit the experimental data. For instance, the FFV model, the activated diffusion model, and the Maxwell-Stefan model were employed to describe the mixture permeability data in PDMS. Based on the Maxwell-Stefan analysis, the influence of coupling effects on permeation properties in PDMS were negligible. The dual mode sorption and permeation models were used to describe the mixed gas data in PTMSP. The dual mode permeability model must be modified to account for *n*-C_4H_{10}-induced reductions in CH_4 diffusion coefficients (*i.e.,* the blocking effect). The FFV model provides poor correlations in PTMSP. There seems to be other factors, besides FFV per se, contributing to the temperature and concentration dependence of diffusion coefficients in PTMSP.

Table of Contents

List of Tables xiv

List of Figures xv

Chapter 1: Introduction 1

1.1 Membrane Separation for Higher Hydrocarbon Removal from Natural Gas... 1

1.2 Pure vs. Mixed Gas Permeation Property Measurements 2

1.3 Goals and Organization of the Dissertation 6

1.4 References 7

Chapter 2: Background 9

2.1 Fundamentals of Permeation in Polymer Membranes 9

2.2 Sorption and Transport in Rubbery Polymers 11

2.2.1 Pure Gas 11

2.2.2 Mixed Gas 12

2.3 Sorption and Transport in Glassy Polymers 13

2.3.1 Pure Gas 13

2.3.2 Mixed Gas 14

2.4 Gas Phase Nonidealities 15

2.5 References 18

Chapter 3: Materials and Experimental Methods 21

3.1 Materials 21

3.1.1 Poly(dimethylsiloxane) (PDMS) 21

3.1.2 Poly(1-trimethylsilyl-1-propyne) (PTMSP) 22

3.1.3 Gases 24

3.2 Pure and Mixed Gas Permeability Measurements 24

3.3 Pure and Mixed Gas Sorption Measurements 27

3.4 Pure and Mixed Gas Dilation Measurements 30
3.5 References.....33

Chapter 4: Pure and Mixed CH_4 and *n*-C_4H_{10} Sorption and Dilation in Poly(dimethylsiloxane).....35
4.1 Pure Gas Solubility 35
4.2 Effect of Temperature on Pure Gas Solubility.....40
4.3 Pure Gas Dilation.....41
4.4 Mixed Gas Solubility 47
4.5 Effect of Concentration on Enthalpy of Sorption 56
4.6 Mixed Gas Dilation.....59
4.7 Solubility Selectivity.....63
4.8 Conclusions.....64
4.9 References.....65

Chapter 5: Pure and Mixed Gas CH_4 and *n*-C_4H_{10} Permeability and Diffusivity in Poly(dimethylsiloxane).....68
5.1 Pure Gas Permeability.....68
5.2 Pure Gas Diffusivity 71
5.3 Effect of Temperature on Pure Gas Permeability and Diffusivity.....73
5.4 Mixed Gas Permeability 73
5.5 Mixed Gas Diffusivity 79
5.6 Effect of Concentration on Activation Energy of Permeation and Diffusion 83
5.7 Modeling.....86
5.7.1 FFV Model.....86
5.7.2 Activated Diffusion Model 90
5.7.3 Maxwell-Stefan Model 93
5.8 Selectivity 96
5.8.1 Permeability Selectivity.....96
5.8.2 Diffusivity Selectivity.....99
5.9 Conclusions.....100
5.10 References.....101

Chapter 6: Pure and Mixed Gas CH_4 and *n*-C_4H_{10} Sorption and Dilation in Poly(1-trimethylsilyl-1-propyne) 104
6.1 Experimental 104
6.1.1 Hysteresis Effects 104
6.1.2 Checking for Isotropic Expansion 105
6.2 Pure Gas Solubility 105
6.3 Mixed Gas Solubility 111
6.4 Dual Mode Mixture Sorption Model 116
6.5 Effect of Concentration on Enthalpy of Sorption 122
6.6 Solubility Selectivity 124
6.7 Pure Gas Dilation 126
6.8 Mixed Gas Dilation 137
6.9 Conclusions 139
6.10 References 140

Chapter 7: Pure and Mixed Gas CH_4 and *n*-C_4H_{10} Permeability and Diffusivity in Poly(1-trimethylsilyl-1-propyne) 143
7.1 Physical Aging and Hysteresis During Measurements 143
7.2 Pure Gas Permeability 144
7.3 Pure Gas Diffusivity 147
7.4 Mixed Gas Permeability 147
7.5 Effect of Concentration on Activation Energy of Permeation 151
7.6 Mixed Gas Diffusivity 153
7.7 Effect Concentration on Activation Energy of Diffusion 159
7.8 Dual Mode Permeability Model 160
7.8.1 Pure Gas 160
7.8.2 Mixed Gas 161
7.9 Selectivity 167
7.9.1 Permeability Selectivity 167
7.9.2 Diffusivity Selectivity 168
7.9.3 Solubility Selectivity 169
7.10 Conclusions 174

7.11 References....174

Chapter 8: Conclusions and Recommendations....177

8.1 Conclusions....177

8.1.1 Poly(dimethylsiloxane) (PDMS)....178

8.1.2 Poly(1-trimethylsilyl-1-propyne) (PTMSP)....179

8.2 Recommendations....180

8.2.1 Other Gas Mixtures....180

8.2.2 Conventional Glassy Polymers....181

8.2.3 New Model for PTMSP....181

8.3 References....182

Appendix A: Fugacity Calculations....184

References....185

Appendix B: Calculations of Effective Diffusion Coefficients in Mixtures....187

Reference....188

Appendix C: Maxwell-Stefan Equations....189

References....192

Appendix D: Supplementary Figures....193

Bibliography....197

Vita….....206

List of Tables

Table 4.1 Pure gas CH_4 solubility, *n*-C_4H_{10} solubility, and *n*-C_4H_{10}/CH_4 solubility selectivity in PDMS 37

Table 4.2 Average partial molar volumes of CH_4 and *n*-C_4H_{10} in PDMS as a function of temperature 40

Table 5.1 Pure gas CH_4 and *n*-C_4H_{10} permeability and diffusivity in PDMS 69

Table 5.2 Activated state model parameters for permeability data 92

Table 5.3 $\langle D_A \rangle_o$ and $\langle D_B \rangle_o$ in PDMS at various temperatures 94

Table 5.4 Effect of temperature on pure and mixed gas *n*-C_4H_{10}/CH_4 permeability, solubility, and diffusivity selectivities 98

Table 6.1 CH_4 and *n*-C_4H_{10} dual mode parameters in PTMSP determined from pure gas sorption isotherms 109

Table 6.2 CH_4 and *n*-C_4H_{10} dual mode parameters in PTMSP determined from both pure and mixed gas sorption isotherms 118

Table 6.3 Best fit V_D of CH_4 and *n*-C_4H_{10} in PTMSP at various temperatures 135

Table 6.4 Best fit V_D of various penetrants at 35°C 137

Table 7.1 Dual mode diffusion coefficients, permeability and concentration-averaged diffusion coefficients at infinite dilution in PTMSP 146

Table 7.2 CH_4 dual mode diffusion coefficient parameters based on Eq. (7.9) using pure and mixed gas data 165

Table 7.3 Effect of temperature on pure and mixed gas *n*-C_4H_{10}/CH_4 permeability, solubility, and diffusivity selectivities 173

List of Figures

Figure 1.1 CO_2/CH_4 selectivity in cellulose acetate at 23°C; permeate pressure: atmospheric [6]. 2

Figure 1.2 Effect of relative propane pressure in propane/hydrogen mixtures on permeation properties of PTMSP membranes: (a) propane and hydrogen permeabilities, and (b) propane/hydrogen selectivity. Total feed pressure: 200 psig; permeate pressure: atmospheric; temperature: 25°C [7].....4

Figure 2.1 Fugacities of (a) CH_4 and (b) *n*-C_4H_{10} in *n*-C_4H_{10}/CH_4 mixtures estimated using the Soave-Redlich-Kwong (SRK) equation of state and the virial equation of state. The composition of *n*-C_4H_{10} in the mixtures is up to 50 mol%: (●) pure *n*-C_4H_{10}, (○) 2 mol% *n*-C_4H_{10}, (+) 3 mol% *n*-C_4H_{10} (■) 4 mol% *n*-C_4H_{10}, (□) 6 mol% *n*-C_4H_{10}, (▲) 8 mol% *n*-C_4H_{10}, (◊) 10 mol% *n*-C_4H_{10}, (▵) 20 mol% *n*-C_4H_{10}, and (▼) 50 mol% *n*-C_4H_{10}. The pressure and temperature ranges from 0.2 to 20 atm, and from -20 to 50°C, respectively. The straight line represents the case where the fugacity values estimated by SRK equation of state are the same as those estimated by virial equation of state.....17

Figure 2.2 Fugacity coefficients of CH_4 and *n*-C_4H_{10} in a 2 mol% *n*-C_4H_{10}/CH_4 mixture at 35°C. The dashed line represents the fugacity coefficient of an ideal gas. The curves labeled CH_4 and *n*-C_4H_{10} are the fugacity

coefficients of CH_4 and *n*-C_4H_{10}, respectively, in a 2 mol% *n*-C_4H_{10}/CH_4 mixture at 35°C estimated using the Soave-Redlich-Kwong (SRK) equation of state. 18

Figure 3.1 Chemical structure of poly(dimethylsiloxane) (PDMS). 22

Figure 3.2 Chemical structure of poly(1-trimethylsilyl-1-propyne) (PTMSP). 23

Figure 3.3 Schematic of pure and mixed gas permeation system. 25

Figure 3.4 Gas sorption system schematic. 28

Figure 3.5 Dilation equipment schematic....32

Figure 4.1 CH_4 pure gas sorption isotherms in PDMS from -20 to 50°C. 36

Figure 4.2 *n*-C_4H_{10} pure gas sorption isotherms in PDMS from -20 to 50°C as a function of (a) fugacity and (b) activity (f/f_{sat})....38

Figure 4.3 Thermal expansion of PDMS at 0 atm pressure (*i.e.,* under vacuum). The thermal expansion coefficient, α, is determined using Eq. (4.4)....42

Figure 4.4 (a) Pure gas CH_4 induced-dilation of PDMS as a function of fugacity from -20 to 50°C. (b) Pure gas *n*-C_4H_{10} induced-dilation of PDMS as a function of fugacity from -20 to 50°C....44

Figure 4.5 Effect of gas concentration on CH_4 and *n*-C_4H_{10} pure gas partial molar volumes in PDMS at 35°C. The error bars are estimated using the propagation of errors method [7]. 47

Figure 4.6 Pure and mixed gas sorption isotherms of CH_4 in PDMS at (a) 50°C, (b) 35°C, (c) 25 °C, (d) 0 °C, (e) -10 °C, (f) -20 °C. The solid lines and the data points correspond to mixture data, and the dashed lines represent pure gas sorption results (*cf.,* Figure 4.1). The reported *n*-C_4H_{10} fugacity, $f_{n-C_4H_{10}}$, is the average *n*-C_4H_{10} fugacities over the course of each mixture sorption isotherm. The uncertainty represents

the standard deviation of the average value. The corresponding activity, $a_{n-C_4H_{10}}$, for each mixture sorption isotherm is indicated in the figures and was calculated as described in Appendix A. 49

Figure 4.7 Mixed gas CH_4 solubility in PDMS at various temperatures as a function of (a) *n*-C_4H_{10} fugacity and (b) *n*-C_4H_{10} concentration in the polymer. The lines represent least squares fits to the data. 51

Figure 4.8 Solubility of CH_4 in liquid *n*-C_4H_{10} and in PDMS as a function of temperature. The lines represent least squares. [1]Reference [22]. [2]Reference [23]. [3]Reference [24]. 53

Figure 4.9 CH_4 mixed gas solubility in PDMS as a function of *n*-C_4H_{10} volume fraction in the polymer. The lines are estimated from pure gas CH_4 solubility in PDMS and liquid *n*-C_4H_{10} using Eq. (4.9) [22-24]. 54

Figure 4.10 Pure and mixed gas *n*-C_4H_{10} solubility in PDMS at various temperatures. The lines represent pure gas solubility values calculated from the sorption data in Figure 4.2. The points are measured solubility data in *n*-C_4H_{10}/CH_4 mixtures. The error bars are determined using the propagation of errors method [7]. The CH_4 fugacity in the mixture experiments is up to 16 atm. 55

Figure 4.11 Enthalpy of sorption of (a) CH_4 and (b) *n*-C_4H_{10} in PDMS as a function of *n*-C_4H_{10} concentration in the polymer. The enthalpy of sorption of CH_4 in liquid *n*-C_4H_{10} is calculated from Eq. (4.12) at 8 atm CH_4 fugacity, using CH_4 solubility data in liquid *n*-C_4H_{10} from the literature [22-24]. The error bars are determined using the propagation of errors method [7]. 58

Figure 4.12 n-C_4H_{10}/CH_4 mixture dilation behavior in PDMS at 35°C, based on (a) total pressure and (b) total fugacity of the mixture. The gas mixture is 2 mol% n-C_4H_{10}, and the balance is CH_4.....61

Figure 4.13 PDMS mixture dilation behavior at (a) 50°C, (b) 35°C, (c) 25°C, (d) 0°C, (e) -10°C, and (f) -20°C, as a function of total mixture fugacity. The dashed lines are additive dilation lines estimated using Eq. (4.13) based on fugacity.....62

Figure 5.1 Pure gas permeability of (a) CH_4 and (b) n-C_4H_{10} in PDMS as a function of upstream fugacity and temperature. 69

Figure 5.2 Pure gas (a) CH_4 and (b) n-C_4H_{10} concentration-averaged diffusion coefficients in PDMS as a function of upstream fugacity and temperature. 72

Figure 5.3 Pure and mixed gas CH_4 permeability in PDMS. Gases are pure CH_4 and mixtures containing 2, 4, 6, and 8 mol% n-C_4H_{10} in CH_4 at (a) 50°C, (b) 35°C, (c) 25°C, (d) 0°C, (e) -10°C, (f) -20°C.....75

Figure 5.4 The permeability of CH_4 in PDMS as a function of (a) n-C_4H_{10} upstream activity (f/f_{sat}) in the mixtures and (b) n-C_4H_{10} concentration at the upstream side of the membrane. The feed gas compositions are 2, 4, 6, and 8 mol% n-C_4H_{10} in CH_4. The total feed pressure was from 1.7 – 14.6 atm. The permeate pressure was a helium sweep at 1 atm, so the permeate partial pressure of CH_4 and n-C_4H_{10} was negligible. The lines represent model fits to the experimental data using Eq. (5.17) and the adjustable parameters in Table 5.2. 76

Figure 5.5 The permeability of n-C_4H_{10} in PDMS as a function of n-C_4H_{10} upstream fugacity. The feed gas compositions are 2, 4, 6, and 8 mol% n-C_4H_{10} in CH_4. The total feed pressure was from 1.7 – 14.6 atm. The permeate pressure was a helium sweep at 1 atm, so the permeate partial pressure of CH_4 and n-C_4H_{10} was negligible. The lines represent the model fits to the experimental data using Eq. (5.15) and the adjustable parameters in Table 5.2. 77

Figure 5.6 (a) CH_4 and (b) n-C_4H_{10} permeability coefficients in PDMS at 0^oC as a function of n-C_4H_{10} downstream activity. The feed was 6 mol% n-C_4H_{10}/CH_4 mixture. The total upstream pressure was 11.2 atm. 78

Figure 5.7 The average effective diffusion coefficient of: (a) CH_4 and (b) n-C_4H_{10} as a function of n-C_4H_{10} activity in the feed mixtures. 80

Figure 5.8 Local diffusion coefficient as a function of n-C_4H_{10} concentration in the polymer: (a) n-C_4H_{10} and (b) CH_4. The lines represent a best fit of Eq. (5.16) using the parameters in Table 5.2. 82

Figure 5.9 Activation energy of permeation of (a) CH_4 and (b) n-C_4H_{10} in PDMS as a function of n-C_4H_{10} concentration in the polymer at the upstream face of the film. The error bars are determined using the propagation of errors method [2]. 84

Figure 5.10 Activation energy of diffusion of (a) CH_4 and (b) n-C_4H_{10} in PDMS as a function of n-C_4H_{10} concentration in the polymer. 85

Figure 5.11 Correlation between fractional free volume of the polymer/penetrant mixtures and effective diffusion coefficients of: (a) n-C_4H_{10} and (b) CH_4, in PDMS at various penetrant concentrations and temperatures. The temperature ranges from -20 to 50^oC: (□) -20^oC, (■) -10^oC, (○)

0°C, (▲) 25°C, (△) 35°C, and (♦) 50°C. The lines represent best fits to Eq. (5.8). 89

Figure 5.12 The mixed gas permeability of (a) *n*-C_4H_{10} and (b) CH_4 in PDMS at 35°C as a function of *n*-C_4H_{10} upstream activity. The filled symbols (●) represent the experimental data. The solid line represents the predictions from the Maxwell-Stefan equations with the best fit $\langle D_{BA} \rangle_o$ of 3.3x10^{-6} cm^2/s. The dashed line is prediction from the Maxwell-Stefan equations without coupling effects (*i.e.,* $\varepsilon_A=\varepsilon_B=0$).....95

Figure 5.13 The fraction of convective flow contribution to the overall flux in *n*-C_4H_{10}/CH_4 mixture permeation in PDMS estimated from the Maxwell-Stefan model. 95

Figure 5.14 Mixed gas permeability selectivity of *n*-C_4H_{10}/CH_4 in PDMS as a function of *n*-C_4H_{10} upstream fugacity in the mixtures and temperature. The lines are estimates from pure gas data. 96

Figure 5.15 Mixed gas diffusivity selectivity of *n*-C_4H_{10}/CH_4 in PDMS as a function of *n*-C_4H_{10} concentration in the polymer and temperature. The lines represent linear regression fits to the data. 99

Figure 5.16 The ratio of permeability, solubility, and diffusivity selectivities at 0°C to infinite dilution values of these selectivities at 50°C as a function of *n*-C_4H_{10} activity. 101

Figure 6.1 CH_4 pure gas sorption isotherm as a function of CH_4 fugacity and temperature. The dashed line represents the CH_4 pure gas isotherm in PTMSP at 35°C reported by Merkel *et al*.[1] The solid lines are from the dual mode sorption model using parameters from Table 6.1. 106

Figure 6.2 n-C_4H_{10} pure gas sorption isotherm as a function of (a) n-C_4H_{10} fugacity and (b) n-C_4H_{10} activity (f/f_{sat}). The dashed line represents the n-C_4H_{10} pure gas sorption isotherm in PTMSP at 35°C reported by Morisato *et al.*.[6] The solid lines are from the dual mode sorption equation using parameters from Table 6.1. For n-C_4H_{10}, f_{sat} values are 3.00, 2.26, 0.99, and 0.44 atm at 35, 25, 0, and -20°C, respectively [5].....107

Figure 6.3 The ratio of pure gas (a) CH_4 and (b) n-C_4H_{10} solubility coefficient to their infinite dilution pure gas solubility coefficients as a function of $1/(1+bf)$ at various temperatures: (○) 35°C, (▲) 25°C, (□) 0°C, and (●) -20°C. S is calculated from the pure gas sorption data in Figures 1 and 2 using Eq. (2.7). S_∞ is calculated from Eq. (6.1) using the dual mode parameters in Table 6.2. The lines are fits to Eq. (6.3) with best fit $C_H'b/k_D$ values of 5.2 ± 1.6 and 30 ± 2 for CH_4 and n-C_4H_{10}, respectively.....110

Figure 6.4 Pure and mixed gas sorption isotherms of (a) CH_4 and (b) n-C_4H_{10} as a function of CH_4 fugacity at 35°C. Each isotherm is determined at a nominally fixed n-C_4H_{10} fugacity, whose value (in atm) is given by the numbers in the figures. These n-C_4H_{10} fugacities are averages over the course of each sorption isotherm. The average n-C_4H_{10} activities (f/f_{sat}) in these isotherms are: (○) 0 (*i.e.,* pure CH_4), (●) 0.017 ± 0.003, (△) 0.08 ± 0.01, (▲) 0.15 ± 0.01, (□) 0.24 ± 0.01, and (■) 0.54 ± 0.01. f_{sat} of n-C_4H_{10} at 35°C is 3.00 atm [5]. The uncertainties in the n-C_4H_{10} activity values represent the standard deviation of the average values over the course of the sorption

experiment. The lines represent the dual mode sorption model fits using the parameters in Table 6.2. 112

Figure 6.5 Pure and mixed gas sorption isotherms of (a) CH_4 and (b) n-C_4H_{10} as a function of CH_4 fugacity at -20°C. Each isotherm is determined at a nominally fixed n-C_4H_{10} fugacity, whose value (in atm) is given by the numbers in the figures. These n-C_4H_{10} fugacities are averages over the course of each sorption isotherm. The average n-C_4H_{10} activities (f/f_{sat}) in these isotherms are: (○) 0 (*i.e.,* pure CH_4), (●) 0.09 ± 0.01, (△) 0.22 ± 0.02, (▲) 0.34 ± 0.02, and (□) 0.61 ± 0.02. The f_{sat} of n-C_4H_{10} at -20°C is 0.44 atm. The uncertainties represent the standard deviation of the average values. The lines represent the dual mode sorption model fits using the parameters in Table 6.2. 113

Figure 6.6 CH_4 mixed gas solubility (in the limit of zero CH_4 fugacity) in PTMSP at (a) 35 and 0°C and (b) 25 and -20°C as a function of n-C_4H_{10} activity. The dashed lines are the dual mode sorption model predictions using pure gas parameters from Table 6.1. The solid lines are the dual mode sorption model prediction using mixed gas parameters from Table 6.2. 115

Figure 6.7 Pure and mixed gas n-C_4H_{10} solubility in PTMSP as a function of n-C_4H_{10} activity and temperature. The closed symbols represent pure gas data. The open symbols represent mixed gas data at various CH_4 fugacities. The solid lines represent prediction of the dual mode sorption model using parameters from Table 6.2. 116

Figure 6.8 The effect of temperature on k_D of CH_4 and n-C_4H_{10} in PTMSP. The dashed lines are fits from Eq. (6.6) with $k_{Do} = 6.3 \pm 0.5 \times 10^{-2}$

cm^3(STP)/(cm^3 atm) and ΔH_D = -5.8 ± 0.5 kJ/mol for CH_4, and k_{Do} = 0.27 ± 0.02 x10^{-2} cm^3(STP)/(cm^3 atm) and ΔH_D = -24 ± 2 kJ/mol for *n*-C_4H_{10}.....120

Figure 6.9 The effect of temperature on *b* of CH_4 and *n*-C_4H_{10} in PTMSP. The dashed lines are fits from Eq. (6.7) with b_o = 6.4 ± 0.5 x 10^{-4} atm^{-1} and ΔH_b = -11 ± 1 kJ/mol for CH_4, and k_{Do} = 2.0 ± 0.2 x10^{-4} atm^{-1} and ΔH_b = -29 ± 2 kJ/mol for *n*-C_4H_{10}. 121

Figure 6.10 The effect of concentration on CH_4 (pure and mixed gas) and *n*-C_4H_{10} isosteric enthalpy of sorption in PTMSP. The error bars are estimated using the propagation of errors method [7]. 124

Figure 6.11 (a) Mixed gas *n*-C_4H_{10}/CH_4 solubility selectivity in PTMSP as a function of *n*-C_4H_{10} activity in the mixture. (b) Ratio of *n*-C_4H_{10}/CH_4 mixed gas to pure gas solubility selectivity in PTMSP. The pure gas solubility selectivity is calculated from *n*-C_4H_{10} pure gas solubility at different *n*-C_4H_{10} activity values and CH_4 pure gas solubility in the limit of zero CH_4 fugacity. The lines represent predictions of the dual mode sorption model using parameters from Table 6.2.....125

Figure 6.12 Pure gas (a) CH_4 and (b) *n*-C_4H_{10} induced length (*i.e.,* x-direction) dilation of PTMSP at 35°C as a function of fugacity. The open symbols represent the data obtained as gas pressure was increased. The filled symbols are the data obtained as gas pressure was decreased.....127

Figure 6.13 Length (*i.e.,* x-direction) and width (*i.e.,* y-direction) dilation of PTMSP films in liquid methanol. The closed symbols are the length dilation data. The open symbols are the width dilation data. The

dimensions of sample 1 were 6.59 cm x 6.61 cm x 300 μm and those of sample 2 were 4.74 cm x 4.72 cm x 300 μm. 127

Figure 6.14 Pure gas *n*-C_4H_{10} induced length (*i.e.,* x-direction) and thickness (*i.e.,* z-direction) dilation of PTMSP at (a) 25^oC and (b) 0^oC. The open symbols represent the thickness dilation data. The filled symbols are the length dilation data.....128

Figure 6.15 The change in polymer volume during pure gas *n*-C_4H_{10} sorption in PTMSP at (a) 25^oC and (b) 0^oC. The data points are volume dilation estimated from the length and thickness dilation data using Eq. (6.8). The lines are calculated from Eq. (4.5) using the length dilation data and assuming isotropic expansion. 130

Figure 6.16 Pure gas (a) CH_4 and (b) *n*-C_4H_{10} induced-dilation of PTMSP as a function of fugacity from -20 to 35^oC. The solid lines are predictions from Eq. (6.11) with the best-fit V_D recorded in Table 6.3. The dashed line represents the estimated volume dilation at 25^oC using Eq. (6.11) with (a) V_D = 53 cm^3/mol for CH_4, and V_D = 100 cm^3/mol for *n*-C_4H_{10}. 131

Figure 6.17 Pure gas partial molar volumes of (a) CH_4 as a function of CH_4 concentration and (b) *n*-C_4H_{10} as a function of *n*-C_4H_{10} concentration in the polymer. The various symbols represent values at different temperatures: (●) 35^oC, (○) 25^oC, (▲) 0^oC, and (△) -20^oC.....133

Figure 6.18 *n*-C_4H_{10}/CH_4 mixture dilation in PTMSP at (a) 35^oC, (b) 25^oC, (c) 0^oC, and (d) -20^oC, as a function of total mixture fugacity. The solid lines are predictions from Eq. (6.12) using k_D values from Table 6.2

and V_D values from Table 6.3. The numbers beside the data points represent the mole percent *n*-C_4H_{10} in the gas mixture.....138

Figure 7.1 (a) Pure gas permeability of CH_4 in PTMSP as a function of upstream fugacity and temperature. The dashed line represents pure CH_4 permeability values at 35°C reported by Merkel *et al.* [2] (b) Pure gas permeability of *n*-C_4H_{10} in PTMSP as a function of upstream activity and temperature. The solid lines represent a nonlinear least squares fit of Eq. (2.17) to the experimental data. The pure gas *n*-C_4H_{10} permeability value in PTMSP reported by Pinnau and Toy [4] is presented as a reference.....145

Figure 7.2 (a) Effect of upstream fugacity and temperature on pure gas CH_4 concentration-averaged diffusion coefficients in PTMSP. The dashed lines are pure gas values at 35°C determined by Merkel *et al.* [2] (b) Pure gas *n*-C_4H_{10} concentration-averaged diffusion coefficients in PTMSP as a function of upstream activity and temperature. The solid lines represent Eq. (7.4) and (7.5) using parameters in Table 7.1. 148

Figure 7.3 CH_4 permeability in PTMSP as a function of (a) *n*-C_4H_{10} upstream fugacity and (b) *n*-C_4H_{10} upstream activity in the feed at 35°C (○), 25°C (■), 0°C (□), and -20°C (▲). The feed gas compositions are 2, 4, 6, and 8 mol% *n*-C_4H_{10} in CH_4. The total feed pressure was from 1.1 – 14.6 atm. The permeate was swept with helium at 1 atm, so the permeate partial pressures of CH_4 and *n*-C_4H_{10} were negligible. The lines represent model fits to the experimental data using Eq. (7.9) and the parameters in Table 7.2. 149

Figure 7.4 n-C_4H_{10} permeability in PTMSP as a function of n-C_4H_{10} upstream activity. The feed gas compositions are 2, 4, 6, and 8 mol% n-C_4H_{10} in CH_4. The total feed pressure was from 1.1 – 14.6 atm. The permeate was swept with helium at 1 atm, so the permeate partial pressures of CH_4 and n-C_4H_{10} were negligible. The lines represent model fits to the experimental data using Eq. (2.20) and the parameters in Table 7.1. For comparison, pure gas n-C_4H_{10} permeation data are also presented. 150

Figure 7.5 Activation energies of permeation of CH_4 and n-C_4H_{10} as a function of penetrant concentration at the upstream face of the film. The n-C_4H_{10} activation energies of permeation are estimated based on mixed gas data, while both pure and mixed gas estimates of the CH_4 activation energies are provided. There is essentially no difference between the pure and mixed gas n-C_4H_{10} permeability data in PTMSP, so the activation energies of permeation for n-C_4H_{10} are the same, within the uncertainty in the measurements, in both pure and mixed gas cases.....153

Figure 7.6 The average effective diffusion coefficient of: (a) CH_4 and (b) n-C_4H_{10} as a function of n-C_4H_{10} activity in the feed mixtures. The solid lines in (a) are predictions from Eq. (7.10) using the parameters in Table 7.2. The lines in (b) are predictions from Eq. (7.5) using the parameters in Table 7.1.....154

Figure 7.7 The ratio of CH_4 mixed gas permeability (P), solubility (S), and diffusivity ($\overline{D}$) coefficients to those of pure gas at infinite dilution as a function of n-C_4H_{10} activity at (a) 35°C, (b) 25°C, (c) 0°C, and (d)

-20°C. The total feed pressure was from 1.1 – 14.6 atm. The solid lines are predictions of the dual mode models (*i.e.,* Eqs. (2.17), (7.9), (7.4), (7.10), and (2.18)). 156

Figure 7.8 Local diffusion coefficients as a function of *n*-C_4H_{10} concentration in the polymer: (a) *n*-C_4H_{10} and (b) CH_4. For comparison, pure gas *n*-C_4H_{10} data (*i.e.,* the data points in the box) are presented along with the mixed gas data. The solid lines in (a) are predictions of the dual mode permeability model (*i.e.,* Eq. (7.6)). The pure gas CH_4 local diffusion coefficients are reported at 4.4 atm upstream pressure....158

Figure 7.9 Pure and mixed gas activation energy of diffusion for CH_4 and *n*-C_4H_{10} as a function of penetrant concentration in the polymer at the upstream face of the film. The *n*-C_4H_{10} activation energies of diffusion are estimated based on mixed gas data. There is essentially no difference between the pure and mixed gas *n*-C_4H_{10} diffusivity data in PTMSP, so the activation energies of diffusion of *n*-C_4H_{10} are the same, within the uncertainty in the measurements, in both pure and mixed gas cases. The error bars were determined using the propagation of errors method [11]. 160

Figure 7.10 Correlation between fractional free volume of the polymer/penetrant mixtures and effective diffusion coefficients of CH_4 in PTMSP at various penetrant concentrations and temperatures. The FFV was estimated based on penetrant concentrations at the upstream face of the film as described in Chapter 5.....167

Figure 7.11 (a) Mixed gas *n*-C_4H_{10}/CH_4 permeability selectivity in PTMSP as a function of *n*-C_4H_{10} upstream activity. (b) Ratio of *n*-C_4H_{10}/CH_4

mixed gas to pure gas permeability selectivity in PTMSP. The pure gas permeability selectivity is calculated from *n*-C_4H_{10} permeability at different *n*-C_4H_{10} upstream activity values and CH_4 pure gas permeability at infinite dilution. The lines are predictions of the dual mode mixture permeability model (*i.e.,* Eqs.(2.17) and (7.9))…. 170

Figure 7.12 (a) Mixed gas *n*-C_4H_{10}/CH_4 diffusivity selectivity in PTMSP as a function of *n*-C_4H_{10} upstream activity. (b) Ratio of *n*-C_4H_{10}/CH_4 mixed gas to pure gas diffusivity selectivity in PTMSP. The pure gas diffusivity selectivity is calculated from *n*-C_4H_{10} diffusivity values at the indicated *n*-C_4H_{10} upstream activity values and CH_4 pure gas diffusivity at infinite dilution. 171

Figure 7.13 (a) Mixed gas *n*-C_4H_{10}/CH_4 solubility selectivity in PTMSP as a function of *n*-C_4H_{10} activity in the mixture. (b) Ratio of *n*-C_4H_{10}/CH_4 mixed gas to pure gas solubility selectivity in PTMSP. The pure gas solubility selectivity is calculated from *n*-C_4H_{10} pure gas solubility at the indicated *n*-C_4H_{10} activity values and CH_4 pure gas solubility in the limit of zero CH_4 fugacity. The lines represent predictions of the dual mode sorption model (*i.e.,* Eqs. (2.18) and (2.19)). 172

Chapter 1: Introduction

1.1 Membrane Separation for Higher Hydrocarbon Removal from Natural Gas

Raw natural gas contains primarily methane with minor constituents such as ethane, propane, butane, nitrogen, carbon dioxide, hydrogen sulfide, and water vapor [1]. Higher hydrocarbon removal from raw natural gas is always required before delivery to the pipeline to reduce the dewpoint and heating value of natural gas to pipeline specification, prevent condensation during transport, and recover valuable higher hydrocarbons as chemical feedstock [2]. The current technology for this separation is condensation [2]. However, this method is capital-intensive and requires large amounts of energy.

Membrane separation technology has recently emerged as a potential alternative technique to remove higher hydrocarbons from natural gas [2]. For economic reasons, membranes for this application should be organic vapor selective materials such as poly(dimethylsiloxane) (PDMS) or ultra-high free volume polymers such as poly(1-trimethylsilyl-1-propyne) (PTMSP). These polymers, often called solubility selective polymers, sieve penetrant molecules based primarily on relative penetrant solubility in the polymer [3-5]. Larger, more condensable higher hydrocarbons are much more soluble than smaller, less condensable gases such as methane. As a result, methane, the major constituent in natural gas, can be kept at high pressure, which eliminates the cost of recompression that would be incurred if a methane-selective membrane were used for this separation.

1.2 PURE VS. MIXED GAS PERMEATION PROPERTY MEASUREMENTS

Traditionally, membrane separation performance is estimated from pure gas permeation measurements. However, this approach has been shown to be inaccurate in certain cases. For example, Figure 1.1 presents the overall CO_2/CH_4 selectivity in cellulose acetate estimated from pure gas permeability measurements compared to that determined from mixed gas experiments [6]. Based on pure gas measurements, the CO_2/CH_4 selectivity increases as the pressure difference across the membrane increases. However, completely opposite behavior is observed in mixtures. The presence of CO_2 induces membrane plasticization, which presumably decreases CO_2/CH_4 diffusivity selectivity, and consequently, overall selectivity, as CO_2 partial pressure difference increases.

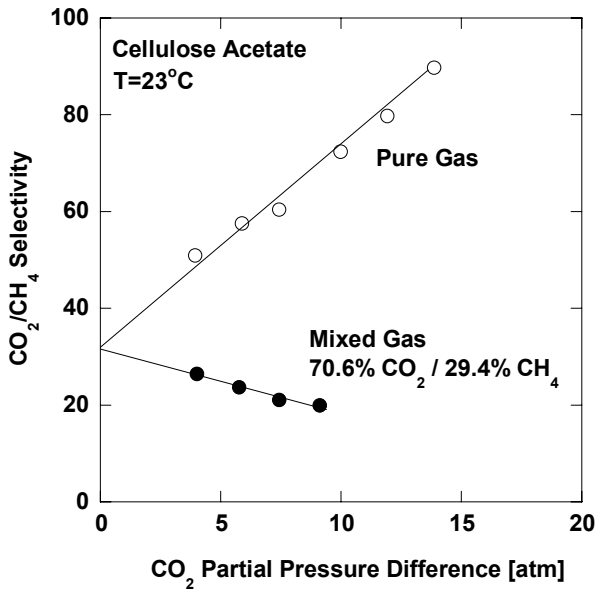

Figure 1.1 CO_2/CH_4 selectivity in cellulose acetate at 23°C; permeate pressure: atmospheric [6].

In some cases, the selectivity of a vapor over a permanent gas in a mixture is actually higher than that obtained from pure gas measurements. For example, Pinnau *et al.* [7] observed a significant decrease in hydrogen permeability in poly(1-trimethylsilyl-1-propyne) (PTMSP) in the presence of propane in gas mixtures, which increased the selectivity of propane over hydrogen (see Figure 1.2). Hydrogen permeability decreased from 20,000 x 10^{-10} cm^3(STP).cm/(cm^2 s cmHg) for pure gas to 1,000 x 10^{-10} cm^3(STP) cm/(cm^2 s cmHg) in a mixture with a relative propane pressure of 0.8 [7]. The propane permeability doubled as the relative propane pressure increased from 0 to 1. Consequently, the propane/hydrogen selectivity increased from about 1, based on pure gas measurements, to approximately 25 in a mixture with high relative propane pressure [7]. In a similar study, Pinnau and Toy [8] reported an increase in *n*-butane/methane selectivity in PTMSP, from 5 in pure gas to 30 in a mixture of 2 mol% *n*-butane in methane at 250 psig feed pressure and 23°C. In mixture permeation measurements, methane permeability was only 1,800 x 10^{-10} cm^3(STP) cm/(cm^2 s cmHg), almost 10 times less than the pure gas value (15,400 x 10^{-10} cm^3(STP) cm/(cm^2 s cmHg)) [8]. The larger, more soluble, *n*-butane, the authors speculated, partially blocked the methane permeation pathway, decreasing its diffusion coefficient [8]. Neither study, however, provided mixture solubility or mixture diffusion data. Without such data, it is impossible to evaluate these assumptions.

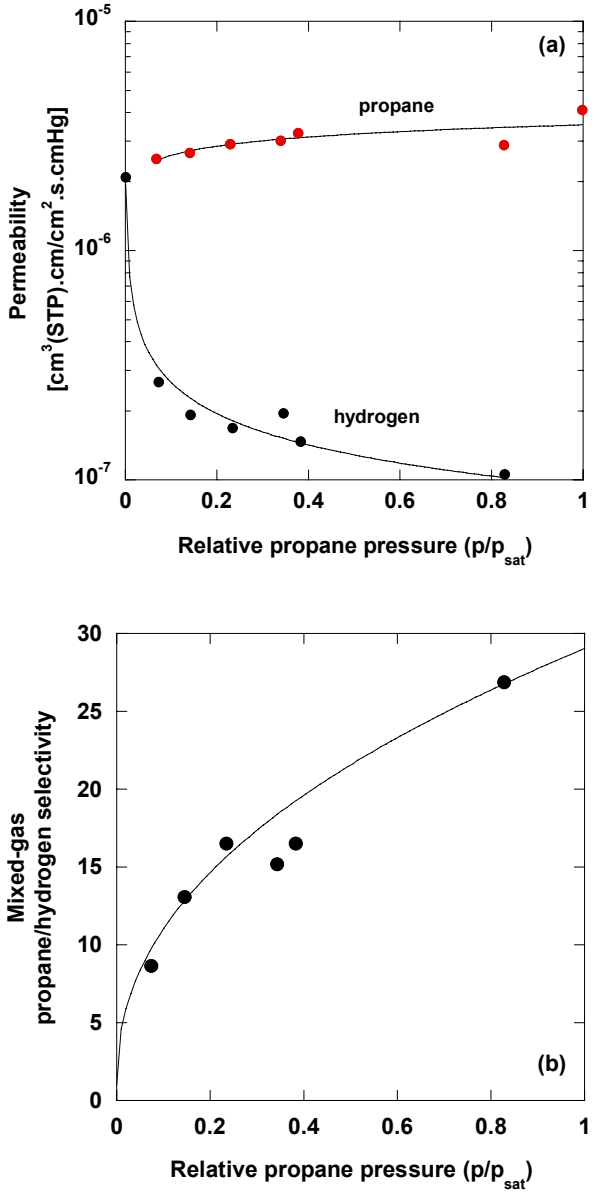

Figure 1.2 Effect of relative propane pressure in propane/hydrogen mixtures on permeation properties of PTMSP membranes: (a) propane and hydrogen permeabilities, and (b) propane/hydrogen selectivity. Total feed pressure: 200 psig; permeate pressure: atmospheric; temperature: 25°C [7].

Differences between pure and mixed gas permeation properties in rubbery polymers have also been reported [9-11]. For example, Jordan and Koros [9] reported an increase in CH_4 permeability in PDMS with increasing CO_2 fugacity in the feed mixture. In a 50/50 CO_2/CH_4 mixture, CH_4 permeability in PDMS increased from 1,700 x 10^{-10} cm^3(STP) cm/(cm^2 s cmHg) (pure gas) to 2,500 x 10^{-10} cm^3(STP) cm/(cm^2 s cmHg) in the presence of 27 atm of CO_2 fugacity at 35°C. On the other hand, CO_2 permeability in the mixture at partial pressure below 250 psia was slightly lower than that observed in pure gas measurements. Based on diffusion coefficients estimated from free volume analysis, they concluded that CO_2 plasticization increased CH_4 diffusion and, in turn, CH_4 permeability coefficients [9]. They further speculated that high pressure CH_4 could compress the polymer, which was then supposed to reduce polymer fractional free volume (FFV), and, therefore, CO_2 diffusion and permeability coefficients at lower pressures (*i.e.,* below 250 psia) [9]. In a different study, Pinnau and He [10] observed an increase in CH_4 permeability in PDMS in the presence of *n*-C_4H_{10}. For instance, at 35°C, CH_4 permeability increased from 1,300 x 10^{-10} cm^3(STP) cm/(cm^2 s cmHg) (pure gas) to 1,450 x 10^{-10} cm^3(STP) cm/(cm^2 s cmHg) when the polymer was exposed to an *n*-C_4H_{10}/CH_4 mixture having an *n*-C_4H_{10} relative pressure (p/p_{sat}) to 0.38. They speculated that this behavior was due to an increase in CH_4 diffusion coefficients as a result of polymer swelling (*i.e.,* plasticization) [10]. However, in both of these studies, no mixture solubility or diffusion data were measured. Both studies speculate that volumetric changes in the polymer due to contact with the gases contribute to observed transport property changes. However, without mixture solubility, diffusivity, and dilation data, it is impossible to evaluate these assumptions, and such data were not in the literature for PDMS, to the best of our knowledge, prior to the studies described in this thesis.

1.3 GOALS AND ORGANIZATION OF THE DISSERTATION

While there are many reports of pure gas sorption and transport properties in vapor selective materials [4,5,12-17], gas mixture separation properties, which are required for estimating membrane separation performance, are less often reported [7,9,10,18]. And, to the best of our knowledge, there were no published reports of gas mixture solubility in such polymers. The objective of this study was to develop a fundamental database of mixture sorption, diffusion, and permeation in solubility selective polymers such as poly(dimethylsiloxane) (PDMS) and poly(1-trimethylsilyl-1-propyne) (PTMSP). Pure and mixed gas *n*-butane/methane permeability and solubility in PDMS and PTMSP were determined experimentally. *n*-butane/methane mixtures were selected as the model vapor/gas mixture due to interest in using membranes for higher hydrocarbons removal from natural gas [2]. Methane is the primary product in the natural gas stream, and *n*-butane is used as a model marker for higher hydrocarbons. The temperature range explored in this study was from -20 to 50^{o}C. The lower limit, -20^{o}C, is representative of the dewpoint requirement of pipeline-grade natural gas [2]. Some condensation processes used to remove higher hydrocarbons operate in this temperature range [1]. The upper limit, 50^{o}C, is in the range of common operating temperatures for membrane gas separation processes [2].

This dissertation is comprised of eight chapters including this introductory chapter. Chapter 2 outlines the background and theories on gas sorption and transport in polymeric membranes. Chapter 3 describes materials preparation and experimental methods.

Chapter 4 presents pure and mixed gas *n*-butane/methane solubility and dilation properties of PDMS. This study explored the influence of *n*-butane on methane mixture solubility. The next chapter, Chapter 5, presents pure and mixed gas *n*-butane/methane

permeability and diffusion coefficients in PDMS. The effects of *n*-butane on methane permeability and *n*-butane/methane permeability selectivity are discussed in this study.

Chapter 6 presents pure and mixed gas *n*-butane/methane solubility and dilation properties of PTMSP. Competitive sorption between *n*-butane and methane in PTMSP are observed. Chapter 7 presents pure and mixed gas *n*-butane/methane permeability and diffusion coefficients in PTMSP. The influence of *n*-butane on methane transport properties in PTMSP is investigated. This study also discusses the solubility- and diffusivity-related contributions to the deviations between pure and mixed gas permeation properties in PTMSP.

Finally, Chapter 8 presents the conclusions and recommendations for future work.

1.4 REFERENCES

[1] A. Rojey, C. Jaffret, S. Cornot-Gandolphe, B. Durand, S. Jullian, and M. Valais, Natural Gas Production Processing Transport, Editions Technip, Paris, 1997.

[2] R. W. Baker, Membrane Technology and Applications, 2nd ed., John Wiley & Sons, New York, 2004.

[3] J. Schultz and K.-V. Peinemann, "Membranes for separation of higher hydrocarbons from methane", Journal of Membrane Science, 110 (1996) 37-45.

[4] T. C. Merkel, V. I. Bondar, K. Nagai, B. D. Freeman, and I. Pinnau, "Gas sorption, diffusion, and permeation in poly(dimethylsiloxane)", Journal of Polymer Science: Part B: Polymer Physics, 38 (2000) 415-34.

[5] T. C. Merkel, V. Bondar, K. Nagai, and B. D. Freeman, "Sorption and transport of hydrocarbon and perfluorocarbon gases in poly(1-trimethylsilyl-1-propyne)", Journal of Polymer Science: Part B: Polymer Physics, 38 (2000) 273-96.

[6] S. Y. Lee and B. S. Minhas, "Effect of gas composition and pressure on permeation through cellulose acetate membrane", AICHE Symposium Series, 84 (1970) 93-101.

[7] I. Pinnau, C. G. Casillas, A. Morisato, and B. D. Freeman, "Hydrocarbon/hydrogen mixed gas permeation in poly(1-trimethylsilyl-1-propyne) (PTMSP), poly(1-phenyl-1-propyne) (PPP), and PTMSP/PPP blends", Journal of Polymer Science: Part B: Polymer Physics, 34 (1996) 2613-21.

[8] I. Pinnau and L. G. Toy, "Transport of organic vapors through poly(1-trimethylsilyl-1-propyne)", Journal of Membrane Science, 116 (1996) 199-209.

[9] S. M. Jordan and W. J. Koros, "Permeability of pure and mixed gases in silicone rubber at elevated pressures", Journal of Polymer Science: Part B: Polymer Physics, 28 (1990) 795-809.

[10] I. Pinnau and Z. He, "Pure- and mixed-gas permeation properties of polydimethylsiloxane for hydrocarbon/methane and hydrocarbon/hydrogen separation", Journal of Membrane Science, 244 (2004) 227-33.

[11] H. Lin and B. D. Freeman, "Gas permeation and diffusion in cross-linked poly(ethylene glycol diacrylate)", Macromolecules, 39 (2006) 3568-80.

[12] Y. Kamiya, Y. Naito, K. Terada, K. Mizoguchi, and A. Tsuboi, "Volumetric properties and interaction parameters of dissolved gases in poly(dimethylsiloxane) and polyethylene", Macromolecules, 33 (2000) 3111-9.

[13] R. M. Barrer, J. A. Barrie, and N. K. Raman, "Solution and diffusion in silicone rubber I - A comparison with natural rubber", Polymer, 3 (1962) 595-603.

[14] A. Morisato, B. D. Freeman, I. Pinnau, and C. G. Casillas, "Pure hydrocarbon sorption properties of poly(1-trimethylsilyl-1-propyne) (PTMSP), poly(1-phenyl-1-propyne) (PPP), and PTMSP/PPP blends", Journal of Polymer Science: Part B: Polymer Physics, 34 (1996) 1925-34.

[15] D. S. Pope, W. J. Koros, and H. B. Hopfenberg, "Sorption and dilation of poly(1-(trimethylsilyl)-1-propyne) by carbon dioxide and methane", Macromolecules, 27 (1994) 5839-44.

[16] L. C. Witchey-Lakshmanan, H. B. Hopfenberg, and R. T. Chern, "Sorption and transport of organic vapors in poly(1-trimethylsilyl-1-propyne)", Journal of Membrane Science, 48 (1990) 321-31.

[17] M. Ghisellini, M. Quinzi, M. Giacinti Baschetti, F. Doghieri, G. Costa, and G. C. Sarti, "Sorption and diffusion of vapors in PTMSP and PTMSP/PTMSE copolymers", Desalination, 149 (2002) 441-5.

[18] S. S. Dhingra and E. Marand, "Mixed gas transport study through polymeric membranes", Journal of Membrane Science, 141 (1998) 45-63.

Chapter 2: Background

2.1 FUNDAMENTALS OF PERMEATION IN POLYMER MEMBRANES

Penetrant transport in polymer membranes is often described by the solution-diffusion mechanism and is expressed by a permeability coefficient, P_A, defined as follows [1]:

$$P_A = \frac{N_A l}{f_{A,2} - f_{A,1}} \tag{2.1}$$

where P_A is the gas permeability coefficient (cm^3(STP) cm/(cm^2 s cmHg)), N_A is the steady state penetrant flux through the membrane (cm^3(STP)/(cm^2 s)), l is the membrane or film thickness (cm), $f_{A,2}$ is the upstream fugacity (cmHg), and $f_{A,1}$ is the downstream fugacity (cmHg). Often, fugacity is replaced by partial pressure in Eq. (2.1) if the experimental conditions are such that the gas is effectively ideal. In this study, fugacity is used to account for gas phase nonidealities because they are significant in the mixtures considered [2]. This issue is discussed in greater detail later in this chapter.

Penetrant transport through a non porous polymer film can be modeled using Fick's Law. In the simplest case (*i.e.,* one dimensional transport of one penetrant), the steady state flux is [3]:

$$N_A = -\frac{D_{loc,A}}{1 - w_A}\frac{dC_A}{dx} = -D_A \frac{dC_A}{dx} \tag{2.2}$$

where C_A is the penetrant concentration, w_A is the penetrant mass fraction in the polymer, x is the spatial coordinate, $D_{loc,A}$ is the binary mutual diffusion coefficient, and D_A is the effective diffusion coefficient in the polymer. Combining Eqs. (2.1) and (2.2) and integrating across the film thickness yields [3]:

$$P_A = \frac{1}{f_{A,2} - f_{A,1}} \int_{C_{A,1}}^{C_{A,2}} D_A \, dC_A \tag{2.3}$$

where $C_{A,2}$ and $C_{A,1}$ are the penetrant concentrations at the upstream and downstream faces, respectively, of the film. Eq. (2.3) can also be written as [3]:

$$P_A = \bar{D}_A \cdot \left(\frac{C_{A,2} - C_{A,1}}{f_{A,2} - f_{A,1}} \right) \tag{2.4}$$

where $\bar{D}_A$ is the concentration averaged effective diffusion coefficient defined as follows:

$$\bar{D}_A = \frac{1}{C_{A,2} - C_{A,1}} \int_{C_{A,1}}^{C_{A,2}} D_A \, dC_A \tag{2.5}$$

When the downstream fugacity is much less than the upstream fugacity (*i.e.,* $C_{A,2} >> C_{A,1}$ and $f_{A,2} >> f_{A,1}$), Eq. (2.4) can be simplified as follows:

$$P_A = \bar{D}_A \cdot S_A \tag{2.6}$$

and

$$S_A = \frac{C_{A,2}}{f_{A,2}} \tag{2.7}$$

S_A is the solubility coefficient of A evaluated at the upstream face of the film.

The selectivity of a polymer for penetrant A relative to penetrant B is the ratio of the permeability coefficients of the two penetrants [3]:

$$\alpha_{A/B} = \frac{P_A}{P_B} = \left[\frac{\bar{D}_A}{\bar{D}_B} \right] \left[\frac{S_A}{S_B} \right] \tag{2.8}$$

where $\bar{D}_A / \bar{D}_B$ is the diffusivity selectivity, and S_A/S_B is the solubility selectivity. Diffusivity selectivity is strongly influenced by the size difference between A and B and by the size-sieving ability of the polymer matrix [3]. Solubility selectivity is controlled by the relative penetrant condensability and the affinity between the penetrants and the

polymer matrix [3]. In a weakly size sieving rubbery polymer, such as PDMS, the overall selectivity depends significantly on solubility selectivity [3].

The temperature dependence of permeability, diffusivity, and solubility at temperatures far removed from polymer thermal transitions is described as follows [4]:

$$P_A = P_o \exp\left(\frac{-E_P}{RT}\right) \tag{2.9}$$

$$S_A = S_o \exp\left(\frac{-\Delta H_S}{RT}\right) \tag{2.10}$$

$$\overline{D}_A = \overline{D}_o \exp\left(\frac{-E_D}{RT}\right) \tag{2.11}$$

where P_o, S_o, and D_o are pre-exponential factors, R is the universal gas constant, T is the absolute temperature, and E_P, ΔH_S, and E_D are the activation energy of permeation, the enthalpy of sorption, and the activation energy of diffusion, respectively. Combining Eqs. (2.6), (2.9), (2.10), and (2.11), the following expression can be obtained:

$$E_P = E_D + \Delta H_S \tag{2.12}$$

This formalism is straightforward and self-consistent when permeability, solubility, and diffusivity are independent of pressure. If this is not the case, then care must be exercised in applying this model [5].

2.2 SORPTION AND TRANSPORT IN RUBBERY POLYMERS

2.2.1 Pure Gas

Gas sorption in rubbery polymers often obeys Henry's law [6]:

$$C = k_D f \tag{2.13}$$

where C is the gas concentration in the polymer, k_D is the Henry's law constant, and f is the gas fugacity in contact with the polymer. For highly sorbing penetrants, deviations

from Henry's law are observed [6]. In such cases, penetrant concentration in the polymer is often represented by the Flory-Huggins equation [7]:

$$\ln \frac{f}{f_{sat}} = \ln \phi + (1-\phi) + \chi (1-\phi)^2 \tag{2.14}$$

where f_{sat} is the saturation fugacity at the temperature of the measurement. χ is the Flory-Huggins interaction parameter, and ϕ is the volume fraction of the penetrant in the polymer, which is given by:

$$\phi = \frac{C\overline{V}}{22,414 + C\overline{V}} \tag{2.15}$$

where $\overline{V}$ is the penetrant partial molar volume.

Gas diffusion coefficients are generally independent of concentration at low concentrations [6]. However, when a large amount of penetrant sorbs into a polymer, the diffusion coefficient may become concentration dependent [6]. This effect is often observed with condensable vapors, and diffusion coefficients usually increase with increasing penetrant concentration [1].

2.2.2 Mixed Gas

For rubbery polymers, in the absence of plasticization, it is generally believed that, in a multicomponent gas mixture, one component sorbs, diffuses, and permeates independently of the others [8]. That is, the solubility and diffusivity parameters obtained from pure gas measurements are often used directly for mixed gas calculations [8]. The validity of this hypothesis, however, depends on the total amount of sorption in the polymer. For mixtures of light gases where the total amount of gas sorption in the polymer is low (*e.g.,* < 1 wt.%), the hypothesis of independent sorption and diffusion of various gas species may be reasonable. However, when there are high levels of sorption in the polymer, deviations in mixture solubility and diffusivity values from those based

on pure gas measurements could be observed. For instance, in pervaporation, where typical sorption levels are 2-20 wt.%, sorption of one component is known to alter the sorption properties of the second component [9,10]. Differences between pure and mixed gas permeation properties in rubbery polymers have been reported in the literature [11-13]. However, prior to this study, there were no definitive data to understand if such differences were due mainly to solubility or diffusivity effects.

2.3 SORPTION AND TRANSPORT IN GLASSY POLYMERS

2.3.1 Pure Gas

Sorption in a glassy polymer is often described using the dual mode sorption model, where penetrant molecules are viewed as being partitioned between the dense equilibrium structure of the polymer (Henry's law region) and the non-equilibrium excess volume (Langmuir region). The model for pure gas sorption is given by [14]:

$$C = C_D + C_H = k_D f + \frac{C_H' b f}{1 + b f} \tag{2.16}$$

where C_D and C_H are the concentrations of penetrant sorbed in the Henry's law and Langmuir regions, respectively; k_D is the Henry's law constant, C_H' is the Langmuir sorption capacity, and b is the Langmuir affinity constant.

Similarly, gas permeability in glassy polymers is often modeled using the dual mode transport model. In this model, pure gas permeability at a negligible downstream fugacity can be written as follows: [8]

$$P = k_D \bar{D}_D + \frac{C_H' b \bar{D}_H}{1 + b f_2} \tag{2.17}$$

where $\bar{D}_D$ and $\bar{D}_H$ are the average effective diffusion coefficient of penetrant molecules in the Henry's law and Langmuir regions, respectively, and f_2 is the upstream fugacity.

2.3.2 Mixed Gas

Competitive effects have been observed during gas mixture sorption in glassy polymers [15,16]. Penetrant molecules compete for the limited number of sorption sites available in the non-equilibrium excess volume (*i.e.,* Langmuir sites), which leads to lower gas solubilities in mixtures than in pure gas studies [16]. Within the context of the dual mode model, the fraction of unrelaxed free volume that each penetrant can occupy depends on the penetrant affinity constant (b) and the fugacities of individual components [16]. Sanders, in his Ph.D. dissertation, extended the dual mode model to binary mixtures [15]. Based on this model, sorption of a binary mixture of gases A and B in a polymer will result in concentrations of A and B in the glassy polymer, C_A and C_B, respectively, given by the following equations [15]:

$$C_A = k_{D_A} f_A + \frac{C'_{H_A} b_A f_A}{1 + b_A f_A + b_B f_B} \tag{2.18}$$

$$C_B = k_{D_B} f_B + \frac{C'_{H_B} b_B f_B}{1 + b_A f_A + b_B f_B} \tag{2.19}$$

where f_A and f_B are the fugacities of A and B, respectively, in the gas phase in contact with the polymer.

The dual mode transport model was extended to mixtures by Koros *et al.* [8] by introducing the competitive sorption effect in Eq. (2.17). The mixed gas permeability of component A in the presence of component B is written as follows [8]:

$$P_A = k_{D_A} \bar{D}_{D_A} + \frac{C'_{H_A} b_A \bar{D}_{H_A}}{1 + b_A f_{A,2} + b_B f_{B,2}} \tag{2.20}$$

where b_B and $f_{B,2}$ are the Langmuir affinity parameter of component B and the upstream fugacity of B, respectively. A similar expression for the permeability of component B in a binary mixture may be written as follows [8]:

$$P_B = k_{D_B}\bar{D}_{D_B} + \frac{C'_{H_B} b_B \bar{D}_{H_B}}{1 + b_A f_{A,2} + b_B f_{B,2}} \tag{2.21}$$

2.4 GAS PHASE NONIDEALITIES

The Soave-Redlich-Kwong (SRK) equation of state was used to estimate fugacity [17,18]. For mixtures, the SRK equation requires only pure gas parameters and one additional interaction for the particular mixture of interest. For CH_4 and *n*-C_4H_{10}, this interaction parameter is available in the literature over the entire composition, pressure, and temperature range considered [19]. Details concerning the calculation of fugacity using the SRK equation are presented in Appendix A. Figures 2.1(a) and (b) compare fugacities of CH_4 and *n*-C_4H_{10}, respectively, estimated using the SRK equation of state with those estimated using the virial equation of state for various mixtures of *n*-C_4H_{10} and CH_4 at -20°C to 50°C. The SRK equation of state parameters were obtained from Poling *et al.* [17] and Knapp *et al.* [19]. The virial coefficients for pure CH_4, *n*-C_4H_{10}, and their mixtures are from Dymond *et al.* [20]. Within the composition, pressure, and temperature range of this study, there is no significant difference between fugacity values determined using the SRK equation and those determined using the virial equation of state.

Figure 2.2 presents the fugacity coefficients of CH_4 and *n*-C_4H_{10} in an *n*-C_4H_{10}/CH_4 mixture containing 2 mol% *n*-C_4H_{10} as a function of CH_4 and *n*-C_4H_{10} partial pressures at 35°C. The fugacity coefficient, which is the ratio of fugacity to partial pressure, of an ideal gas is unity [21]. The CH_4 fugacity coefficient in the mixture does not deviate much from unity and is similar to that estimated for pure CH_4 at the same partial pressure. On the other hand, the *n*-C_4H_{10} fugacity coefficient decreases significantly as the total mixture pressure increases. For example, at 25 atm total pressure, which corresponds to an *n*-C_4H_{10} partial pressure of 0.5 atm, the *n*-C_4H_{10} fugacity coefficient is only 0.75. This value is low, especially considering the low partial

pressure of *n*-C_4H_{10}. For comparison, the fugacity coefficient of pure *n*-C_4H_{10} at 0.5 atm is 0.98, which is very close to ideal. The nonideality of *n*-C_4H_{10} in the mixture is even greater at lower temperature. For example, at -20^{o}C and the same total pressure (*i.e.,* 25 atm), the *n*-C_4H_{10} fugacity coefficient is as low as 0.56. Due to the strong non-ideality of *n*-C_4H_{10} in *n*-C_4H_{10}/CH_4 mixtures, the use of fugacity, instead of pressure, is required to properly account for these gas phase nonidealities when analyzing sorption and dilation properties.

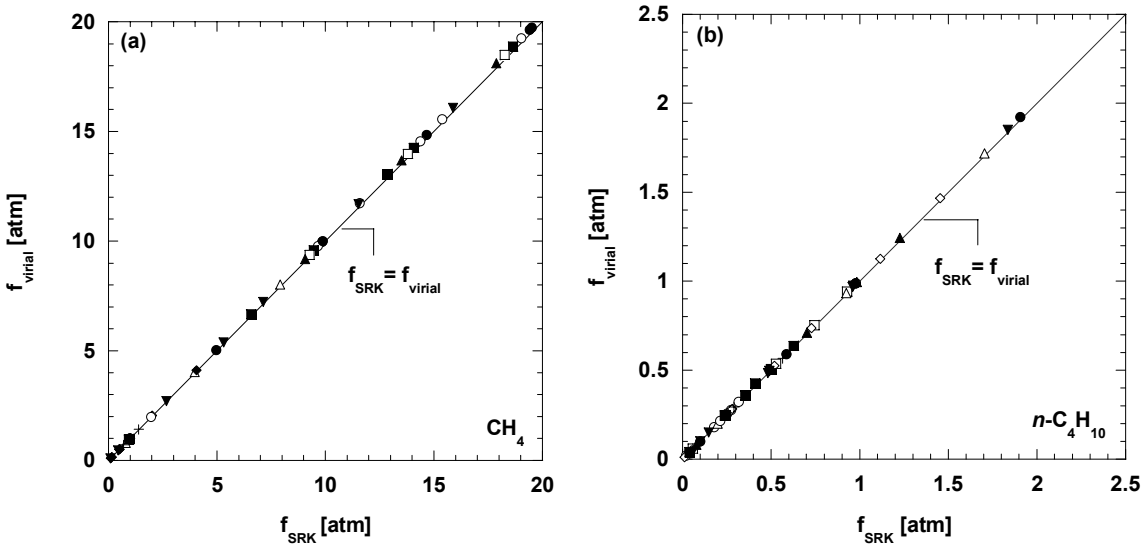

Figure 2.1 Fugacities of (a) CH_4 and (b) n-C_4H_{10} in n-C_4H_{10}/CH_4 mixtures estimated using the Soave-Redlich-Kwong (SRK) equation of state and the virial equation of state. The composition of n-C_4H_{10} in the mixtures is up to 50 mol%: (●) pure n-C_4H_{10}, (○) 2 mol% n-C_4H_{10}, (+) 3 mol% n-C_4H_{10} (■) 4 mol% n-C_4H_{10}, (□) 6 mol% n-C_4H_{10}, (▲) 8 mol% n-C_4H_{10}, (◊) 10 mol% n-C_4H_{10}, (△) 20 mol% n-C_4H_{10}, and (▼) 50 mol% n-C_4H_{10}. The pressure and temperature ranges from 0.2 to 20 atm, and from -20 to 50°C, respectively. The straight line represents the case where the fugacity values estimated by SRK equation of state are the same as those estimated by virial equation of state.

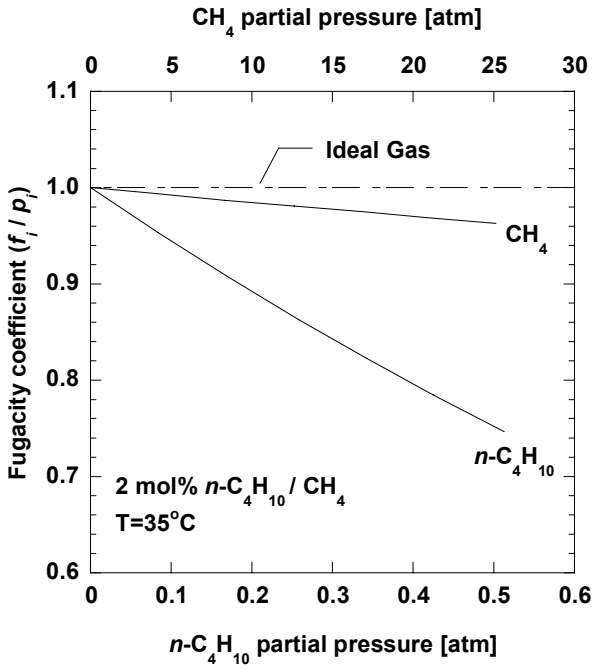

Figure 2.2 Fugacity coefficients of CH_4 and *n*-C_4H_{10} in a 2 mol% *n*-C_4H_{10}/CH_4 mixture at 35°C. The dashed line represents the fugacity coefficient of an ideal gas. The curves labeled CH_4 and *n*-C_4H_{10} are the fugacity coefficients of CH_4 and *n*-C_4H_{10}, respectively, in a 2 mol% *n*-C_4H_{10}/CH_4 mixture at 35°C estimated using the Soave-Redlich-Kwong (SRK) equation of state.

2.5 REFERENCES

[1] K. Ghosal and B. D. Freeman, "Gas separation using polymer membranes: an overview", Polymers for Advanced Technologies, 5 (1994) 673-97.

[2] R. D. Raharjo, B. D. Freeman, and E. S. Sanders, "Pure and mixed gas CH_4 and *n*-C_4H_{10} sorption and dilation in poly(dimethylsiloxane)", Journal of Membrane Science, 292 (2007) 45-61.

[3] S. Matteucci, Y. Yampolskii, B. D. Freeman, and I. Pinnau, "Transport of gases and vapors in glassy and rubbery polymers", in Y. Yampolskii, I. Pinnau and B. D. Freeman (Eds.), Materials Science of Membranes, John Wiley & Sons, Ltd., Chichester, 2006.

[4] S. V. Dixon-Garrett, K. Nagai, and B. D. Freeman, "Ethylbenzene solubility, diffusivity, and permeability in poly(dimethylsiloxane)", Journal of Polymer Science: Part B: Polymer Physics, 38 (2000) 1461-73.

[5] R. S. Prabhakar, R. Raharjo, L. G. Toy, H. Lin, and B. D. Freeman, "Self-consistent model of concentration and temperature dependence of permeability in rubbery polymers", Industrial & Engineering Chemistry Research, 44 (2005) 1547-56.

[6] G. J. van Amerongen, "The permeability of different rubber to gases and its relation to diffusivity and solubility", Journal of Applied Physics, 17 (1946) 972-85.

[7] P. J. Flory, Principles of Polymer Chemistry, Cornell University Press, Ithaca, NY, 1953.

[8] W. J. Koros, R. T. Chern, V. Stannett, and H. B. Hopfenberg, "A model for permeation of mixed gases and vapors in glassy polymers", Journal of Polymer Science: Part B: Polymer Physics, 19 (1981) 1513-30.

[9] M. H. V. Mulder, T. Franken, and C. A. Smolders, "Preferential sorption versus preferential permeability in pervaporation", Journal of Membrane Science, 22 (1985) 155-73.

[10] H. Okuno, T. Nishida, and T. Uragami, "Preferential sorption and permeation of binary liquid mixtures in poly(vinyl chloride) membrane by pervaporation", Journal of Polymer Science: Part B: Polymer Physics, 33 (1995) 299-307.

[11] S. M. Jordan and W. J. Koros, "Permeability of pure and mixed gases in silicone rubber at elevated pressures", Journal of Polymer Science: Part B: Polymer Physics, 28 (1990) 795-809.

[12] I. Pinnau and Z. He, "Pure- and mixed-gas permeation properties of polydimethylsiloxane for hydrocarbon/methane and hydrocarbon/hydrogen separation", Journal of Membrane Science, 244 (2004) 227-33.

[13] H. Lin and B. D. Freeman, "Gas permeation and diffusion in cross-linked poly(ethylene glycol diacrylate)", Macromolecules, 39 (2006) 3568-80.

[14] W. J. Koros, A. H. Chan, and D. R. Paul, "Sorption and transport of various gases in polycarbonate", Journal of Membrane Science, 2 (1977) 165-90.

[15] E. S. Sanders, High-pressure sorption of pure and mixed gases in glassy polymers, Ph.D. Dissertation, North Carolina State University, Raleigh, N.C., 1983.

[16] E. S. Sanders, W. J. Koros, H. B. Hopfenberg, and V. Stannett, "Pure and mixed gas sorption of carbon dioxide and ethylene in poly(methyl methacrylate)", Journal of Membrane Science, 18 (1984) 53-74.

[17] B. E. Poling, J. M. Prausnitz, and J. P. O'Connell, The Properties of Gases and Liquids, 5th ed., McGraw-Hill, New York, NY, 2001.

[18] J. M. Prausnitz, R. N. Lichtenthaler, and E. G. de Azevedo, Molecular Thermodynamics of Fluid-Phase Equilibria, 3rd ed., Prentice-Hall, Inc., Upper Saddle River, NJ, 1999.

[19] H. Knapp, R. Doring, L. Oellrich, U. Plocker, and J. M. Prausnitz, Vapor-liquid equilibria for mixtures of low boiling substances, Chemistry Data Series, Vol. 6, DECHEMA, Great Neck, NY, 1989.

[20] J. H. Dymond, K. N. Marsh, R. C. Wilhoit, and K. C. Wong, The Virial Coefficients of Pure Gases and Mixtures, Vol. 21, Springer, Darmstadt, Germany, 2002.

[21] J. M. Smith, H. C. V. Ness, and M. M. Abbott, Introduction to Chemical Engineering Thermodynamics, McGraw-Hill, New York, NY, 2001.

Chapter 3: Materials and Experimental Methods

3.1 MATERIALS

3.1.1 Poly(dimethylsiloxane) (PDMS)

The repeat unit of poly(dimethylsiloxane) (PDMS) is shown in Figure 3.1. PDMS is a highly permeable, vapor selective, rubbery polymer with a flexible polymer chain backbone, as reflected in its very low glass transition temperature (T_g ~ -120^{o}C) [1]. PDMS has been used in a number of vapor separation applications [2,3]. Currently, it is being considered for the removal of higher hydrocarbons (C_{3+}) from raw natural gas streams [2,3].

PDMS dense films were prepared from cyclohexane solution containing 40 wt.% Dehesive 940A silicone (Wacker Silicones Corporation, Adrian, MI). As supplied by manufacturer, Dehesive 940A is a viscous 30 wt.% silicone gum in naphtha solvent. Before casting, a proprietary crosslinker (V24) and catalyst (OL) system provided by Wacker were added to the polymer solution. Films were prepared by pouring the polymer solution into a casting ring on a Teflon-coated glass plate. The cast films were dried slowly under ambient conditions for 4 days. They were then placed in an oven at 110^{o}C for 30 min to remove residual solvent and to fully crosslink the polymer. Afterwards, they were cooled to room temperature, and the crosslinked films were easily removed from the casting ring and glass plate. Finally, the films were washed with *n*-heptane in a Soxhlet extractor for 3 days to remove any unreacted crosslinker, catalyst, and any polymer not bound to the network. The resulting PDMS films were transparent and not tacky. Film thicknesses were determined with a digital micrometer (Mitutoyo) readable to ±1 μm. Samples were 300 μm for the permeation, sorption, and dilation measurements.

The density of the PDMS films at 25°C was 0.98 ± 0.01 g/cm^3, which was determined by measuring the difference in weight of the film in a salt/water solution containing 20 wt.% NaCl and in air. The crosslink density was approximately 3.15 ± 0.03 x 10^{-4} mol/cm^3, which corresponds to approximately 42 repeat units between crosslinks. The crosslink density was estimated as describe previously [4].

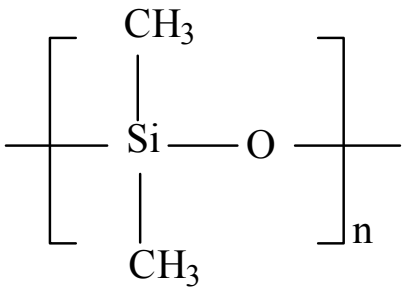

Figure 3.1 Chemical structure of poly(dimethylsiloxane) (PDMS).

3.1.2 Poly(1-trimethylsilyl-1-propyne) (PTMSP)

Poly(1-trimethylsilyl-1-propyne) (PTMSP) is a glassy, disubstituted polyacetylene with extremely high gas permeabilities [5,6]. The repeat unit of PTMSP is shown in Figure 3.2. Its glass transition temperature is greater than 250°C [7]. PTMSP was selected for this study because of its unusually high gas permeability, high vapor/gas mixed gas selectivities, and unusual gas transport mechanism [5,6]. The rigid C=C double bond in the backbone, coupled with its bulky side groups, hinders chain segmental motion and restrains polymer chains from packing efficiently, creating large and possibly interconnected free volume elements in the polymer matrix that provide very efficient permeation pathway for penetrants [5,8]. In addition, this very open structure attenuates the polymer's ability to discriminate between large and small molecules. Therefore,

unlike conventional glassy polymers (*e.g.,* polycarbonate), PTMSP is more permeable to larger, more condensable organic vapors than to smaller, less condensable permanent gases [5-7].

PTMSP was kindly supplied by Air Products, Inc. (St. Louis, MO). Dense films of PTMSP were prepared by casting a polymer solution in a flat bottomed glass dish at ambient conditions. The polymer solution contained 2 wt.% PTMSP in toluene. After drying, which generally required about 24 hrs at ambient conditions, the samples were stored in liquid methanol at ambient conditions to inhibit physical aging [9]. The films were removed from methanol and dried at ambient conditions for 24 hrs before being used in experiments. Film thicknesses were determined with a digital micrometer (Mitutoyo) readable to ±1 μm. Samples for the sorption and dilation measurements were approximately 100 μm thick. Those for the permeation measurements were approximately 250 μm thick. The density of the PTMSP films at 25°C was approximately 0.73 ± 0.01 g/cm^3, and it was determined by measuring the difference in the weight of a film in water and in air.

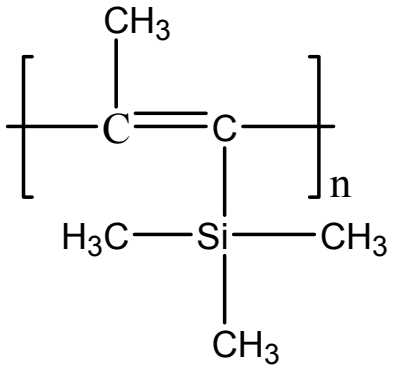

Figure 3.2 Chemical structure of poly(1-trimethylsilyl-1-propyne) (PTMSP).

3.1.3 Gases

Chemical-grade CH_4 and *n*-C_4H_{10} (99% purity) were purchased from Air Gas Southwest Inc. (Corpus Christi, TX). Certified 2, 4, 6, and 8 mol% *n*-C_4H_{10}/CH_4 gas mixtures were purchased from Air Liquide America Corporation (Houston, TX). All gases were used as received.

3.2 PURE AND MIXED GAS PERMEABILITY MEASUREMENTS

The CH_4 and *n*-C_4H_{10} pure and mixed gas permeabilities were determined using a constant pressure/variable volume apparatus [10,11]. A schematic of the apparatus is presented in Figure 3.3. The system is equipped with a mass flow controller (MKS Model# 1179A23CSIBV, Wilmington, MA) on the upstream side to regulate residue flow rate. Helium was used to sweep the downstream side of the membrane and carry the permeate (*i.e.,* CH_4 and *n*-C_4H_{10}) to a gas chromatograph (GC). The total flowrate on the downstream side (*i.e.,* helium + permeate) was measured with a soap film flowmeter. The system temperature was controlled to $\pm 0.1^oC$ using a constant temperature circulator. For temperatures below 0^oC, a water/methanol mixture was used.

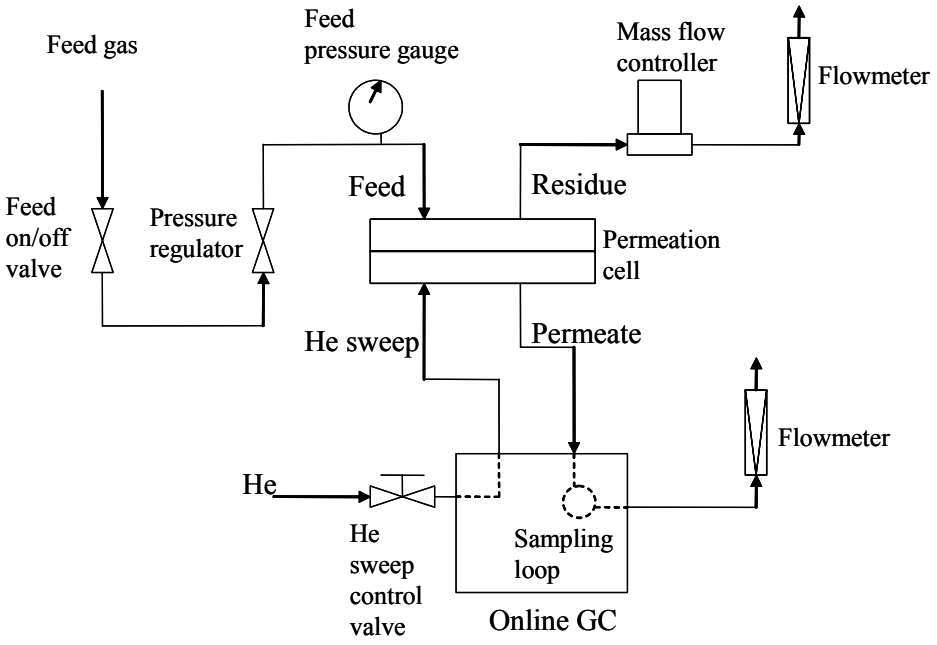

Figure 3.3 Schematic of pure and mixed gas permeation system.

For CH_4 pure gas permeability measurements, the feed pressure was varied from 4.4 to 14.6 atm. The temperature ranged from -20 to 50°C. For *n*-C_4H_{10} pure gas permeability measurements, the feed pressure was varied from 1.1 to 1.8 atm. The *n*-C_4H_{10} pure gas permeability was determined at 25, 35, and 50°C. The permeation apparatus only permits measurement at total upstream pressures greater than atmospheric pressure. Pure gas *n*-C_4H_{10} permeability coefficients at low temperatures (*e.g.,* 0, -10, and -20°C) could not be determined since the saturation pressure of *n*-C_4H_{10} at these temperatures is lower than 1 atm [12]. A constant residue flowrate of 20 cm^3/min was maintained during the pure gas permeability measurement to remove any helium that might permeate to the upstream side of the film from the downstream side. The flow rate of helium that could back permeate to the upstream side of the permeation cell is estimated to be, at most, 0.02 cm^3/min for PDMS at 35°C (*i.e.,* based on the helium

permeability coefficient in PDMS at 35°C reported by Stern *et al.* [1] and a downstream partial pressure of 1 atm) and 0.04 cm^3/min for PTMSP at 25°C (*i.e.,* based on the helium permeability coefficient in PTMSP at 25°C reported by Srinivasan *et al*. [8] and a downstream partial pressure of 1 atm). These values are far below the retentate flow rate of 20 cm^3/min.

In the mixture measurements, a sufficient residue flowrate was maintained (*i.e.,* a stage cut of less than 1%) to prevent concentration polarization. That is, the residue flowrate was set high enough so that the results reported in this study were independent of residue flowrate. The feed pressure was varied from 1.1 to 14.6 atm. For most experiments, the partial pressures of CH_4 and *n*-C_4H_{10} on the downstream side of the film were maintained at practically zero (<0.05 atm) by adjusting the helium flowrate. In this way, the downstream *n*-C_4H_{10} activity, which is the ratio of fugacity to the saturation fugacity at a given temperature (f/f_{sat}), was always less than 0.01. The saturation fugacity was the fugacity at the saturation pressure (p_{sat}), and p_{sat} was estimated using the Wagner equation [12]. One experiment (described in Figures 5.6(a) and (b)) was directed towards determining the influence of downstream partial pressure on permeability, but all other results are reported at very low downstream partial pressures of CH_4 and *n*-C_4H_{10}. Unless indicated otherwise, the permeability experiments were performed at *n*-C_4H_{10} downstream activities of less than 0.01 and CH_4 downstream fugacities of less than 0.05 atm.

The steady state gas permeability was calculated as follows [5]:

$$P_A = \frac{1}{f_{A,2} - f_{A,1}} \frac{273}{TA} \frac{p_{atm}}{76} \left(y_{A,1} \frac{dV}{dt} \right) \tag{3.1}$$

where $f_{A,2}$ and $f_{A,1}$ are the upstream and downsteam fugacities of gas A (cmHg), respectively. These fugacities were determined as described in Appendix A. $y_{A,1}$ is the

mole fraction of gas A on the downstream side of the film determined using the GC, p_{atm} is the atmospheric pressure (cmHg), A is the membrane area (cm^2), T is temperature (K), l is membrane thickness (cm), and dV/dt is the steady state volumetric displacement rate of a soap film in the bubble flowmeter (cm^3/s). The permeability coefficients are commonly expressed in Barrers, where 1 Barrer = 1 x 10^{-10} cm^3(STP) cm/(cm^2 s cmHg).

3.3 PURE AND MIXED GAS SORPTION MEASUREMENTS

Pure and mixed gas solubility coefficients were determined using an apparatus based on the barometric, pressure-decay method [13]. The system consists of three interconnected cells, V_A, V_B, and V_C, as shown in Figure 3.4. V_A is the polymer-containing volume, V_B is the charge volume, and V_C is the sample volume. V_C contains the gas sample mixture from V_A in a mixture measurement before it is sent to a gas chromatograph (GC) for compositional analysis. Each cell is equipped with a Super TJE pressure transducer from Honeywell Sensotec (Columbus, OH) which has an accuracy of 0.05% of full scale. The full scale readings of transducers A, B, and C are 500, 500, and 100 psia, respectively. The cell volumes were determined using the method described by Burnett [14]. They are 15.00, 11.41, and 11.40 cm^3 for V_A, V_B, and V_C, respectively. The GC is a type 6890 from Agilent Technology (Santa Clara, CA), which is equipped with two columns: (1) 15 m x 530 μm, 5% phenyl/methyl siloxane, 3.0 μm film thickness, and (2) 30 m x 530 μm, CarboPLOT, 1.5 μm film thickness. A flame ionization detector (FID) connected to the first column is used to determine the composition of CH_4 and n-C_4H_{10} in the mixtures.

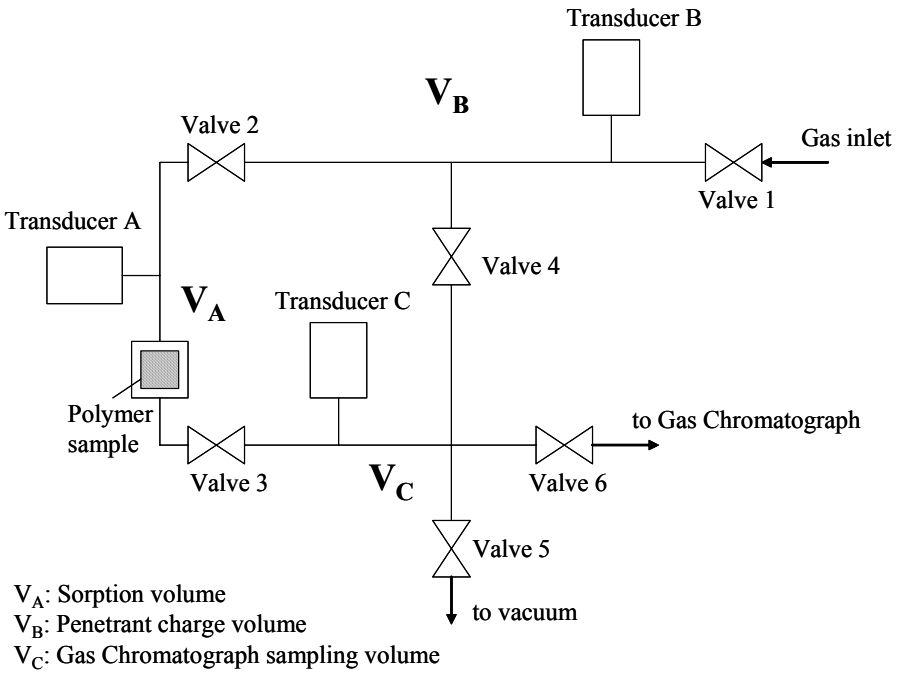

Figure 3.4 Gas sorption system schematic.

For pure gas sorption measurements, only two volumes, V_A and V_B, are utilized. The sample was degassed by maintaining the sorption system under vacuum overnight before each measurement. Initially, a desired amount of penetrant gas was added to V_B, the charge volume. After a steady pressure reading was obtained, the penetrant gas was expanded into the sample chamber containing the polymer sample (*i.e.,* V_A) and allowed to equilibrate (*i.e.,* until the pressure in V_A was no longer changing with time). Once the pressure in V_A was constant, additional penetrant was admitted into V_B, then expanded to V_A, and equilibrium was reestablished. In this incremental manner, the amount of gas sorbed in the polymer as a function of penetrant fugacity/pressure was determined using mass balance calculations. For the pure gas *n*-C_4H_{10} sorption measurements at 0, -10, and -20°C, V_B and V_C were used as a single penetrant charge volume by leaving valve 4 open and using only transducer C to monitor pressure decay. The *n*-C_4H_{10} saturation pressure

at these temperatures is relatively low (<1 atm) [12]. Thus utilizing the transducer in V_C that has the smallest uncertainty (*i.e.,* ± 0.05 psia) improves the accuracy of the measurement.

The mixed gas experiments followed the method described by Sanders *et al.* [13,15], which involves adding only pure gases to the polymer-containing volume. This method allows the partial pressure of one component to be held relatively constant during the experiment. Pure *n*-C_4H_{10} was first added to V_B and then expanded into the polymer-containing volume, V_A. This step was repeated until a desired pressure of *n*-C_4H_{10} in V_A was achieved. After evacuating *n*-C_4H_{10} from V_B, pure CH_4 was charged to V_B and then expanded into V_A. A sufficient pressure difference between V_A and V_B was maintained to avoid backflow of *n*-C_4H_{10} into V_B. During the expansion of CH_4 from V_B to V_A, valve 2 was opened only slightly, so that CH_4 leaving V_B had a high enough velocity to overcome any *n*-C_4H_{10} diffusion back into V_B. To confirm that this was the case, after the expansion, a sample of gas in V_B was sent to the GC through V_C to test for traces of *n*-C_4H_{10}, and no traces of *n*-C_4H_{10} were observed. After equilibrium in V_A was established between the polymer and gas mixture, a small amount of the gas mixture from V_A was expanded into V_C and injected into the GC. Once the pressure in V_A was stable, additional CH_4 was added to V_A. Equilibrium was reestablished, and a small amount of the gas mixture in V_A was again injected into the GC through V_C. The gas sample size withdrawn from V_A was small, less than 1% of the material in the gas phase, and it was accounted for in the material balance.

In most cases, the ternary mixtures (CH_4-*n*-C_4H_{10}-polymer) in V_A were allowed to equilibrate for 24 hrs to ensure complete mixing of CH_4 and *n*-C_4H_{10} in the gas phase. Some were allowed to equilibrate for 48-72 hrs. There was no noticeable influence of equilibration time (*i.e.,* 24 hrs as opposed to 48 or 72 hrs) on the composition of gas in

equilibrium with the polymer, indicating that equilibrium has been attained after 24 hrs. Moreover, to ensure that the composition was uniform throughout the volume, metering the equilibrium mixture from V_A to the GC was done through valves 2 and 3. There was essentially no measurable difference in composition if the mixture was withdrawn through valve 2 or 3, suggesting that a uniform composition in V_A was achieved after 24 hrs.

3.4 PURE AND MIXED GAS DILATION MEASUREMENTS

Pure and mixed gas dilation measurements were performed using an apparatus based on the design by Fleming and Koros [16]. Figure 3.5 presents a diagram of the system. The device monitors one coordinate dimension of a polymer film during sorption. A strip of polymer was placed in the Jerguson gauge, where it was unconstrained in its ability to elongate but was guided by a wire track so that the polymer could dilate freely in its length dimension but was precluded from curling. The length of the polymer strip (*i.e.,* x-direction) was monitored by a COHU (model 4915-2000) CCD camera (San Diego, CA) which takes digital images of the sample as a function of time. The minimum length change that can be detected with this device is 0.017 mm. The samples used for the length (*i.e.,* x-direction) dilation measurements were approximately 100 and 90 mm long, for PDMS and PTMSP, respectively. More detailed information regarding the digital image capture and analysis protocols was reported by McDowell *et al.* [17]. A water jacketed glass vessel connected to a temperature controller (Thermo Neslab) was used to control temperature. For most of the measurements, a pressure gauge (model CM) from Heise (Stratford, CT) with a full scale reading of 700 psia and an accuracy of 0.1% of full scale values was utilized. For pure gas *n*-C_4H_{10} dilation measurements, a digital pressure gauge (model PM, also from Heise) with higher accuracy (0.025% of full scale, where full scale was 300 psig) was used. The overall dimensions of PDMS dilation

samples were 100 mm x 5 mm x 300 μm, in the x-, y-, and z-direction, respectively. The overall dimensions of PTMSP dilation samples were 90 mm x 5 mm x 120 μm.

Polymer dilation measurements in mixtures were used to complement the mixed gas sorption isotherms. As described in Chapter 4 and 6, PDMS and PTMSP swell upon sorbing CH_4 and *n*-C_4H_{10}, particularly at low temperature. The increase in polymer volume reduces the volume occupied by the gas phase in the polymer-containing cell (*i.e.,* V_A) of the sorption apparatus. This reduction in the gas phase volume of the polymer-containing cell was introduced into the mass balance calculations used to calculate sorption coefficients of the gases in the polymer. The swelling effect, especially for PDMS, can be significant. For example, in the mixed gas sorption measurement at -20^{o}C and in the presence of 0.23 atm (fugacity) of *n*-C_4H_{10}, PDMS swelling results in an approximately 0.6 cm^3 reduction in gas phase volume in V_A. When this reduction in the gas phase volume in V_A is appropriately introduced in the mass balance calculations, the resulting CH_4 mixed gas solubility value is 1.04 cm^3(STP)/(cm^3 polymer atm) which is approximately 10% higher than that calculated by neglecting the influence of polymer swelling on the reported sorption levels.

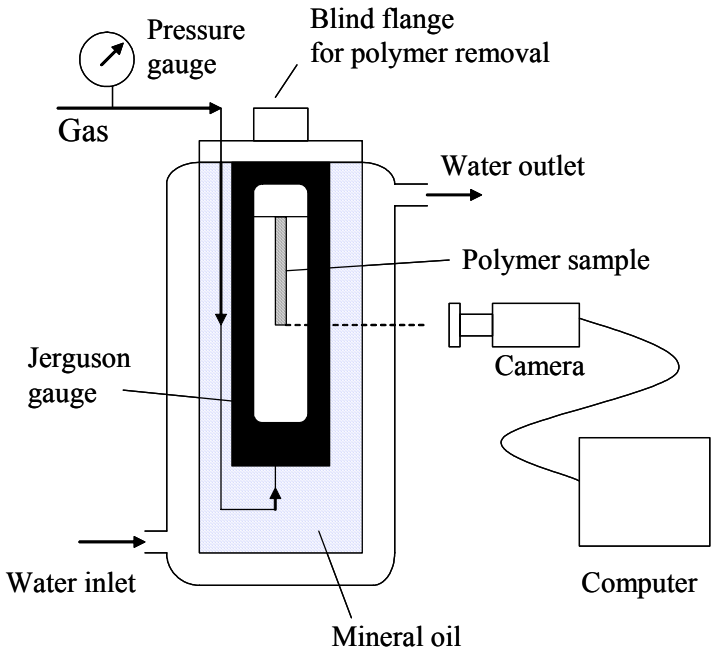

Figure 3.5 Dilation equipment schematic.

For the mixture dilation measurements, a certified gas mixture was fed directly into the dilatometer. Due to the high ratio of the dilation chamber volume to the polymer sample volume (~700), the amount of gas sorbed in the polymer is very small compared to the amount of gas in the chamber, so any changes in gas mixture composition during the experiment should be negligible. This assumption was confirmed by using the GC to analyze the gas mixture in equilibrium with the polymer. The gas mixtures contained 2, 4, 6, and 8 mol% *n*-C_4H_{10}, and the balance was CH_4. Dilation measurements were performed at temperatures ranging from -20 to 50^{o}C. At low temperatures, a constant flow rate of dry nitrogen was maintained in the enclosed are surrounding the system to prevent moisture from condensing on the glass surface of the dilatometer through which experimental measurements were made.

3.5 REFERENCES

[1] S. A. Stern, V. M. Shah, and B. J. Hardy, "Structure-permeability relationships in silicone polymers", Journal of Polymer Science: Part B: Polymer Physics, 25 (1987) 1263-98.

[2] V. Nitsche, K. Ohlrogge, and K. Sturken, "Separation of organic vapors by means of membranes", Chemical Engineering Technology, 21 (1998) 925-35.

[3] R. W. Baker, Membrane Technology and Applications, 2nd ed., John Wiley & Sons, New York, 2004.

[4] A. Singh, B. D. Freeman, and I. Pinnau, "Pure and mixed gas acetone/nitrogen permeation properties of polydimethylsiloxane [PDMS]", Journal of Polymer Science: Part B: Polymer Physics, 36 (1998) 289-301.

[5] T. C. Merkel, V. Bondar, K. Nagai, and B. D. Freeman, "Sorption and transport of hydrocarbon and perfluorocarbon gases in poly(1-trimethylsilyl-1-propyne)", Journal of Polymer Science: Part B: Polymer Physics, 38 (2000) 273-96.

[6] I. Pinnau and L. G. Toy, "Transport of organic vapors through poly(1-trimethylsilyl-1-propyne)", Journal of Membrane Science, 116 (1996) 199-209.

[7] K. Nagai, T. Masuda, T. Nakagawa, B. D. Freeman, and I. Pinnau, "Poly[1-(trimethylsilyl)-1-propyne] and related polymers: synthesis, properties and functions", Progress in Polymer Science, 26 (2001) 721-98.

[8] R. Srinivasan, S. R. Auvil, and P. M. Burban, "Elucidating the mechanism(s) of gas transport in poly[1-(trimethylsilyl)-1-propyne] (PTMSP) membranes", Journal of Membrane Science, 86 (1994) 67-86.

[9] K. Nagai and T. Nakagawa, "Effects of aging on the gas permeability and solubility in poly(1-trimethylsilyl-1-propyne) membranes synthesized with various catalysts", Journal of Membrane Science, 105 (1995) 261-72.

[10] S. A. Stern, P. J. Gareis, T. F. Sinclair, and P. H. Mohr, "Performance of a versatile variable-volume permeability cell. Comparison of gas permeabiltiy measurements by the variable-volume and variable-pressure methods", Journal of Applied Polymer Science, 7 (1963) 2035-51.

[11] K. C. O'Brien, W. J. Koros, and T. A. Barbari, "A new technique for the measurement of multicomponent gas transport through polymeric films", Journal of Membrane Science, 29 (1986) 229-38.

[12] B. E. Poling, J. M. Prausnitz, and J. P. O'Connell, The Properties of Gases and Liquids, 5th ed., McGraw-Hill, New York, NY, 2001.

[13] E. S. Sanders, W. J. Koros, H. B. Hopfenberg, and V. Stannett, "Mixed gas sorption in glassy polymers: equipment design considerations and preliminary results", Journal of Membrane Science, 13 (1983) 161-74.

[14] E. S. Burnett, "Compressibility determinations without volume measurements", Journal of Applied Mechanics, 3 (1936) 136-40.

[15] E. S. Sanders, High-pressure sorption of pure and mixed gases in glassy polymers, Ph.D. Dissertation, North Carolina State University, Raleigh, N.C., 1983.

[16] G. K. Fleming and W. J. Koros, "Dilation of polymers by sorption of carbon dioxide at elevated pressures. 1. Silicone rubber and unconditioned polycarbonate", Macromolecules, 19 (1986) 2285-91.

[17] C. C. McDowell, B. D. Freeman, and G. W. McNeely, "Acetone sorption and uptake kinetic in poly(ethylene terephtalate)", Polymer, 40 (1999) 3487-99.

Chapter 4: Pure and Mixed CH_4 and *n*-C_4H_{10} Sorption and Dilation in Poly(dimethylsiloxane)

This chapter presents the pure and mixed gas *n*-C_4H_{10} and CH_4 sorption and dilation properties in poly(dimethylsiloxane) (PDMS) at temperatures ranging from -20 to 50°C. The influence of *n*-C_4H_{10} on CH_4 mixture solubility in PDMS is investigated. This chapter also discusses the increase in *n*-C_4H_{10}/CH_4 mixture solubility selectivity in PDMS with increasing *n*-C_4H_{10} activity (f/f_{sat}) and decreasing temperature.

4.1 PURE GAS SOLUBILITY

Figure 4.1 presents CH_4 pure gas sorption isotherms in PDMS as a function of temperature. The isotherms are linear, which is consistent with previously reported CH_4 sorption isotherms in PDMS [1] and is common for sorption of permanent gases in rubbery polymers [2,3]. Consequently, the CH_4 pure gas solubility is independent of fugacity, and its value is constant at a given temperature. Table 4.1 records the average solubility coefficients as a function of temperature. These solubility values are reasonably close to those in the literature. Merkel *et al.* [1] and Shah *et al.* [4] report pure gas CH_4 solubility in PDMS at 35°C and infinite dilution to be 0.42 and 0.45 cm^3(STP)/(cm^3 polymer atm), respectively. Kamiya *et al.* [1] reported CH_4 infinite dilution solubility at 25°C of 0.44 cm^3(STP)/(cm^3 polymer atm). Based on our study, CH_4 average solubility coefficients in PDMS at 35 and 25°C are 0.47 and 0.50 cm^3(STP)/(cm^3 polymer atm), respectively.

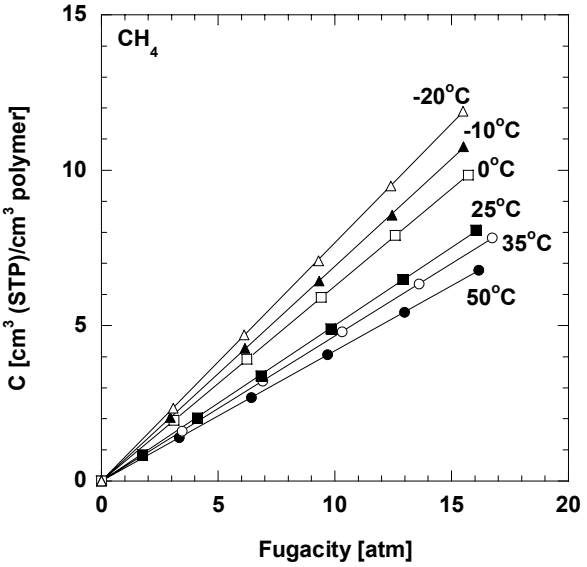

Figure 4.1 CH_4 pure gas sorption isotherms in PDMS from -20 to 50°C.

Pure gas sorption isotherms of *n*-C_4H_{10} in PDMS for each temperature studied are presented as a function of fugacity in Figure 4.2(a). Being more condensable than CH_4, the *n*-C_4H_{10} sorption isotherm is nonlinear and convex to the fugacity axis. This trend is typically observed when highly soluble penetrants sorb into rubbery polymers at high activity [1]. Figure 4.2(b) presents the *n*-C_4H_{10} pure gas sorption isotherms as a function of activity, which is defined as the ratio of fugacity to the saturation fugacity at a given temperature (f/f_{sat}) [5]. The saturation fugacity is the fugacity at the saturation pressure (p_{sat}), and p_{sat} is estimated using the Wagner equation (Eq. (A.10)) [6]. Details regarding the calculation of the saturation fugacity are presented in the Appendix A. When the sorption data are reported as a function of *n*-C_4H_{10} activity, the data fall on a single master curve. In other words, at the same activity, regardless of the temperature or *n*-C_4H_{10} fugacity, the *n*-C_4H_{10} concentration sorbed in the polymer is the same. The pure

gas solubility of *n*-C_4H_{10} increases as *n*-C_4H_{10} fugacity and activity increases. The solubility coefficient in the limit of zero fugacity is the infinite dilution solubility:

$$S^{\infty} = \lim_{f \to 0} \frac{C}{f} \tag{4.1}$$

Table 4.1 Pure gas CH_4 solubility, *n*-C_4H_{10} solubility, and *n*-C_4H_{10}/CH_4 solubility selectivity in PDMS

T (^oC)	S^{∞} (cm^3 (STP)/ (cm^3 atm)][c]		$S^{\infty}_{n-C_4H_{10}} / S^{\infty}_{CH_4}$
	CH_4[a]	*n*-C_4H_{10}[b]	
-20	0.77 ± 0.02	135 ± 4	175 ± 9
-10	0.69 ± 0.02	86 ± 3	125 ± 7
0	0.63 ± 0.02	61 ± 2	97 ± 4
25	0.50 ± 0.02	26 ± 1	52 ± 3
35	0.47 ± 0.02	18.6 ± 0.6	40 ± 2
50	0.42 ± 0.02	12.5 ± 0.4	30 ± 2

[a]Average value. The uncertainty is determined using the propagation of errors method [7].
[b]Infinite dilution value is estimated from a second order polynomial fit of the Solubility vs. *f* data determined from *C* vs. *f* data (Figure 4.2(a)) using Eq. (2.7). The uncertainty is determined using the propagation of errors method [7].
[c]Solubility calculated based on fugacity (Eq. (4.1)).

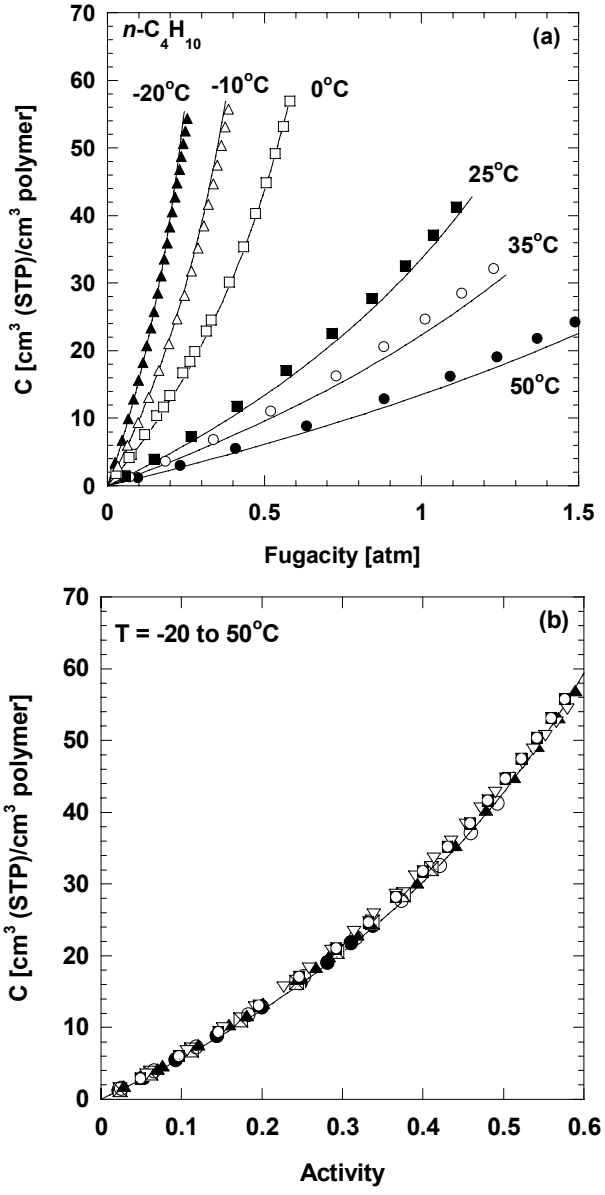

Figure 4.2 n-C_4H_{10} pure gas sorption isotherms in PDMS from -20 to 50°C as a function of (a) fugacity and (b) activity (f/f_{sat}).

The pure gas n-C_4H_{10} infinite dilution solubility coefficients at each temperature are recorded in Table 4.1. These data are in good agreement with the literature. Kamiya *et al.* [8] reported n-C_4H_{10} infinite dilution solubility in PDMS of 24 cm^3(STP)/(cm^3 polymer atm) at 25°C, which is in an excellent agreement with our value (24 cm^3(STP)/(cm^3 polymer atm). The n-C_4H_{10} solubility coefficients determined in this study also agree, within the uncertainty of the measurement, with those reported by Barrer *et al.* [9]. Based on their measurement, the n-C_4H_{10} solubility coefficients at 30 and 50°C are 21 and 12.5 cm^3(STP)/(cm^3 polymer atm), respectively.

The sorption of n-C_4H_{10} in PDMS can be described by the Flory-Huggins model [5], as shown in Eq. (2.14). The partial molar volume of n-C_4H_{10} is estimated from the pure gas sorption and dilation measurements. The lines in Figure 4.2(a) and (b) represent the best fit of Eq. (2.14) to the data, and a χ value of 0.34 ± 0.04 is obtained. The Flory-Huggins equation estimates the sorption of n-C_4H_{10} in the polymer reasonably well with only one adjustable parameter, χ, which is independent of concentration and temperature. The n-C_4H_{10} partial molar volume in the polymer decreases somewhat with decreasing temperature, as shown in Table 4.2, and this observation will be discussed in more detail below. The fit in Figure 4.2(a) employs the temperature-dependent partial molar volumes from Table 4.2 to calculate the volume fraction of n-C_4H_{10} in the polymer (see Eq. (2.15)) at each temperature and composition. In Figure 4.2(b), an average partial molar volume (110 cm^3/mol) was used to obtain a single fit for all temperatures. For our study, there is no significant difference between the sorption isotherm estimated using the Flory-Huggins equation and that estimated using Flory-Rehner equation, which accounts for the polymer crosslink density [5]. The χ parameter value of 0.34 obtained in this study is somewhat lower than Kamiya *et al.*'s [8] previously reported value of 0.45 based on measurements at 25°C. Since the n-C_4H_{10} infinite dilution solubility determined in this

study is similar to that reported by Kamiya *et al.* [8], the difference in the χ parameter value presumably originates from the difference in the *n*-C_4H_{10} partial molar volume used in Eq. (2.15) (*i.e.,* 110 in this study versus 101 cm^3/mol in Kamiya *et al.*'s study).

Table 4.2 Average partial molar volumes of CH_4 and *n*-C_4H_{10} in PDMS as a function of temperature

T (^oC)	CH_4 (cm^3/mol)	*n*-C_4H_{10} (cm^3/mol)
-20	54 ±3	104 ± 2
-10	57 ± 3	102 ± 2
0	56 ± 3	106 ± 2
25	61 ± 3	110 ± 2
35	59 ± 3	116 ± 2
50	63 ± 3	127 ± 2

4.2 EFFECT OF TEMPERATURE ON PURE GAS SOLUBILITY

The temperature dependence of solubility is usually described using the Van't Hoff-Arrhenius approach, as shown in Eq. (2.10). The ΔH_s values for CH_4 and *n*-C_4H_{10} at infinite dilution are -5.8 ± 0.3 and -23.0 ± 0.5 kJ/mol, respectively. The ΔH_s value for CH_4 reported by Shah *et al.* [4] using data at 10, 35, and 55^{o}C is slightly lower (-7.7 kJ/mol). Our ΔH_s value for *n*-C_4H_{10} is reasonably close to the value reported by Barrer *et al.* [9] (-22.1 kJ/mol), which was based on solubility data measured at temperatures ranging from 30 to 70^{o}C. The negative ΔH_s values indicate that the sorption process is exothermic. Since sorption in polymer is typically viewed as a two-step process involving

penetrant condensation from a gas like density to a liquid like density followed by mixing condensed penetrant molecules with polymer segments, the enthalpy of sorption can be viewed as a sum of the enthalpy changes for these two steps [10]:

$$\Delta H_s = \Delta H_{cond} + \Delta H_m \tag{4.2}$$

where ΔH_{cond} and ΔH_m are the enthalpy changes associated with penetrant condensation and mixing, respectively [10]. ΔH_{cond} values depend on temperature for a given penetrant. In this study, the ΔH_{cond} value of *n*-C_4H_{10} at 15°C (*i.e.,* the median of the temperature range explored in this study), -21.6 kJ/mol, was used to estimate the ΔH_m of *n*-C_4H_{10} in PDMS [11]. On this basis, the infinite dilution ΔH_m of *n*-C_4H_{10} in PDMS is -1.3 kJ/mol, which is small relative to $|\Delta H_s|$. For comparison, ΔH_m of C_3H_8 in PDMS at infinite dilution is -2.8 kJ/mol [12]. The dependence of ΔH_m on *n*-C_4H_{10} concentration in the polymer is discussed later in this paper. The analysis in Eq. (4.2) is not applicable for CH_4 since CH_4 is a supercritical gas over the temperature of study, and does not, therefore, have a defined ΔH_{cond}.

4.3 PURE GAS DILATION

The thermal expansion coefficient of PDMS can be determined from the data presented in Figure 4.3, which presents the change in polymer volume (when the sample is held under vacuum in the dilatometer) as temperature changes. PDMS dilation has been reported to be isotropic [13], so the change in polymer volume, ΔV, was calculated as follows [8]:

$$\Delta V = V_{o(25^oC)}\left(\frac{L_x}{L_{x,o(25^oC)}}\right)^3 - V_{o(25^oC)} \tag{4.3}$$

where $L_{x,o(25^oC)}$ is the measured polymer length (*i.e,* x-direction) at 25°C, and L_x is the measured polymer length at temperature *T*. $V_{o(25^oC)}$ is the polymer volume at 25°C, and it

is calculated using the known sample mass and density. The volumetric thermal expansion coefficient is defined as follows [14]:

$$\alpha = -\frac{1}{\rho}\left(\frac{\partial \rho}{\partial T}\right)_p = \frac{1}{V}\left(\frac{\partial V}{\partial T}\right)_p \tag{4.4}$$

where ρ is polymer density, V is polymer volume, and T is temperature. This property provides a measure of the density change with temperature at constant pressure. The thermal expansion coefficient of PDMS obtained in this study is $(9.1\pm0.3)\text{x}10^{-4}\ ^{o}C^{-1}$. This value is in excellent agreement with Zoller and Walsh's [15] estimated value of $9.4\text{x}10^{-4}$ oC^{-1} using a very different experimental technique. Kamiya *et al.* [8] report a value of $7.8\text{x}10^{-4}\ ^{o}C^{-1}$, which is somewhat lower than that determined in this study.

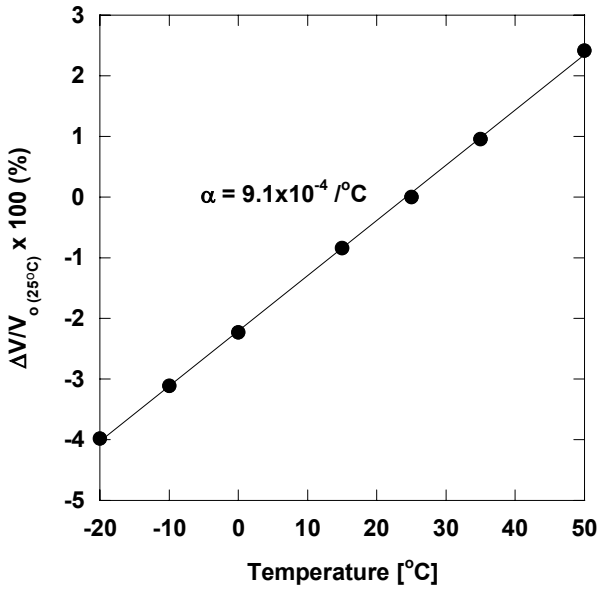

Figure 4.3 Thermal expansion of PDMS at 0 atm pressure (*i.e.,* under vacuum). The thermal expansion coefficient, α, is determined using Eq. (4.4).

Figure 4.4(a) presents pure gas CH_4 induced-dilation of PDMS as a function of fugacity at temperatures ranging from -20 to 50°C. V_o is the initial penetrant-free pure polymer volume at the temperature of the experiment, which is calculated from the polymer sample mass and density. V_o increases with increasing temperature, as shown in Figure 4.3. The polymer density at various temperatures can be estimated using the thermal expansion coefficient. When exposed to the gas mixtures explored in this study, the polymer swells. Since PDMS dilation is isotropic [13], the change in the polymer volume relative to the initial pure polymer volume, $\Delta V/V_o$, is calculated as follows [8]:

$$\frac{\Delta V}{V_o} = \left(\frac{L_x}{L_{x,o}} \right)^3 - 1 \tag{4.5}$$

where $L_{x,o}$ is the initial length of the pure polymer at the temperature of the experiment, and L_x is the polymer length when exposed to gas. At all temperatures, polymer volume increases linearly as CH_4 fugacity increases. The presence of high pressure CH_4 surrounding the PDMS does not compress the polymer, as has been suggested [16]. Figure 4.4(b) presents pure gas *n*-C_4H_{10} induced-dilation of PDMS as a function of fugacity at temperatures ranging from -20 to 50°C. The *n*-C_4H_{10} dilation isotherms are convex to the fugacity axis, similar to the *n*-C_4H_{10} sorption isotherms (*cf.,* Figure 4.2(a)). The polymer dilates more at lower temperature, which is consistent with the higher *n*-C_4H_{10} sorption at lower temperatures.

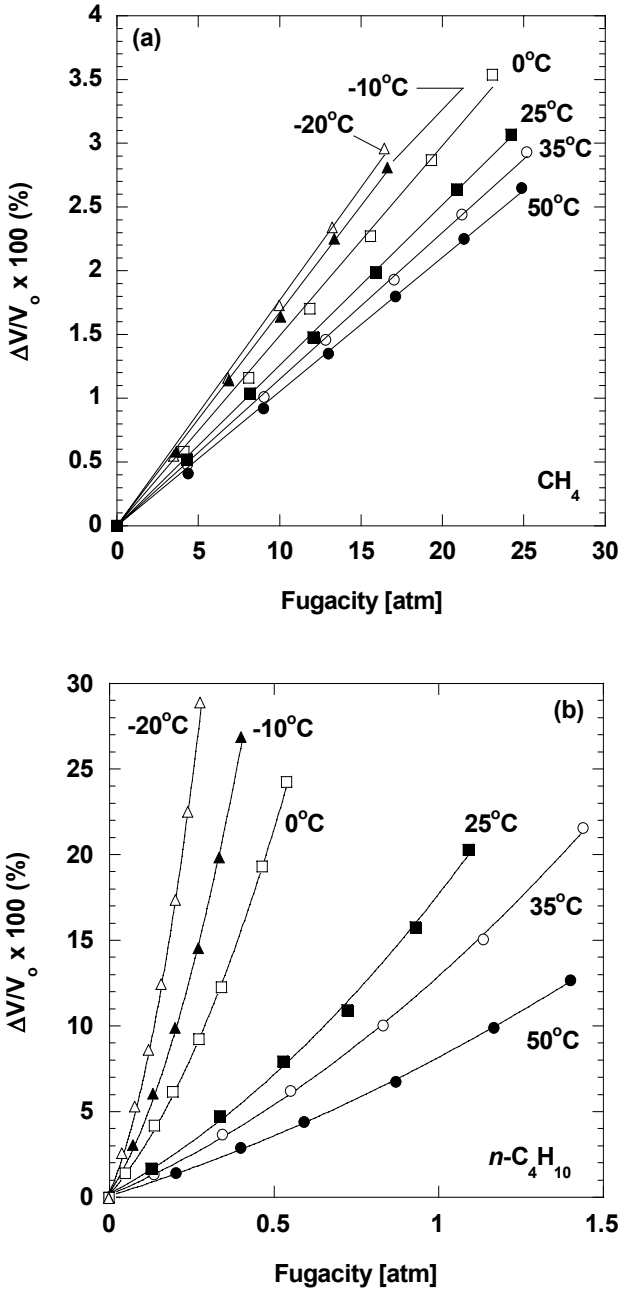

Figure 4.4 (a) Pure gas CH_4 induced-dilation of PDMS as a function of fugacity from -20 to 50°C. (b) Pure gas *n*-C_4H_{10} induced-dilation of PDMS as a function of fugacity from -20 to 50°C.

The experimental sorption and dilation data can be combined to determine the penetrant partial molar volume in the polymer. The partial molar volume of a component in a mixture is defined as [17]:

$$\bar{V}_i \equiv \left(\frac{\partial V}{\partial n_i} \right)_{T,p,n_j \neq i} \tag{4.6}$$

where n_i is the number of moles of component i in the mixture, and V is the total mixture volume. For a gas-polymer mixture, the partial molar volume of the penetrant is estimated from dilation data as follows [18]:

$$\bar{V}_i = 22414 \left[\frac{d}{dp} \left(\frac{\Delta V}{V_o} \right) + \beta \right] \frac{dp}{dC} \tag{4.7}$$

where p is pressure, and β is the isothermal compressibility of the polymer, which is defined as follows [10]:

$$\beta \equiv -\frac{1}{V_o} \left(\frac{\partial V}{\partial p} \right)_{T,n_1,n_2} \tag{4.8}$$

This study uses the previously reported temperature dependence of the isothermal compressibility of PDMS from the work of Kamiya *et al.* [8], which is consistent with data reported by Zoller and Walsh [15]. For most permanent gases, the polymer compressibility contribution to Eq. (4.7) is fairly small [13]. For more soluble penetrants, such as *n*-C_4H_{10}, this term is negligible. For example, based on the pure gas CH_4 dilation measurement at 35°C, the value of $\frac{d}{dp}\left(\frac{\Delta V}{V_o} \right)$ in Eq. (4.7) is 1.11×10^{-3} atm^{-1}. The β value of PDMS at this temperature is 1.06×10^{-4} atm^{-1}, which is an order of magnitude smaller [8]. In pure gas *n*-C_4H_{10} dilation, where $\frac{d}{dp}\left(\frac{\Delta V}{V_o} \right)$ is 1.02×10^{-1} atm^{-1} (at p = 0.20 atm), the contribution of β (*i.e.,* 1.06×10^{-4} atm^{-1}) to Eq. (4.7) is negligible.

There is no significant dependence of gas concentration on the partial molar volumes of CH_4 and *n*-C_4H_{10} in PDMS, as illustrated in Figure 4.5. The average partial molar volumes of CH_4 and *n*-C_4H_{10} in PDMS at all temperatures studied are summarized in Table 4.2. The partial molar volumes determined in this study are reasonably close to the values reported in the literature. De Angelis *et al.* [13] reported that the CH_4 pure gas infinite dilution partial molar volume in PDMS was 57 cm^3/mol at 35°C, which is in a good agreement with the value determined in this study (59 cm^3/mol). Kamiya *et al.* [8] reported CH_4 and *n*-C_4H_{10} partial molar volumes of 54 and 101 cm^3/mol, respectively, at 25°C. Based on our measurement, the CH_4 and *n*-C_4H_{10} partial molar volumes in PDMS at 25°C are 61 and 110 cm^3/mol, respectively. These values are similar to the partial molar volumes of CH_4 and *n*-C_4H_{10} in liquids. The average partial molar volume of CH_4 in five organic solvents at 25°C is 53 cm^3/mol [19]. The pure liquid molar volume of *n*-C_4H_{10} at its saturation pressure and 20°C is 100 cm^3/mol [6]. This observation is consistent with results from previous studies in rubbery polymers [8,13,20].

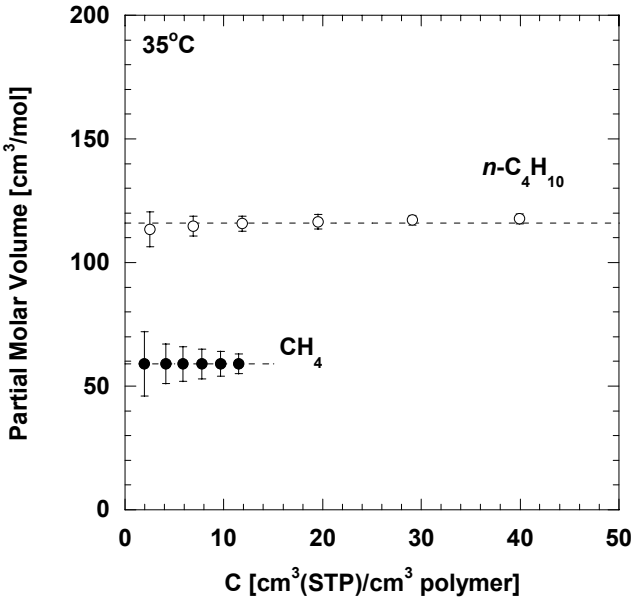

Figure 4.5 Effect of gas concentration on CH_4 and *n*-C_4H_{10} pure gas partial molar volumes in PDMS at 35°C. The error bars are estimated using the propagation of errors method [7].

4.4 MIXED GAS SOLUBILITY

Similar to the pure gas case (*i.e.,* Figure 4.1), CH_4 sorption isotherms in *n*-C_4H_{10}/CH_4 mixtures are linear (*i.e.,* they obey Henry's law), as illustrated in Figures 4.6(a)-(f). These figures present CH_4 isotherms in PDMS in the presence of a fixed *n*-C_4H_{10} fugacity at temperatures ranging from -20 to 50°C. The CH_4 mixed gas sorption isotherms at different *n*-C_4H_{10} fugacities are also linear, but they are not shown here for brevity. The *n*-C_4H_{10} fugacity values reported in Figures 4.6(a)-(f) is a nominal value, as there is actually a slight variation in the *n*-C_4H_{10} fugacity over the course of each sorption isotherm. As pure CH_4 is added to the gas mixture in contact with the polymer sample during the measurement of the isotherm, the total pressure of the mixture increases, which leads to a slight decrease in *n*-C_4H_{10} fugacity, as calculated from the SRK equation of state (see Figure 2.2). This decrease in *n*-C_4H_{10} fugacity could result in a slight

desorption of *n*-C_4H_{10} from the polymer, which increases *n*-C_4H_{10} fugacity in the gas phase. These two effects that follow the addition of pure CH_4 in the mixture contribute to the slight variation of *n*-C_4H_{10} fugacity observed during the isotherm. For example, in Figure 4.6(a) (50^oC), the *n*-C_4H_{10} fugacity during the isotherm decreases slightly from 0.94 in pure *n*-C_4H_{10} (zero CH_4 fugacity) to 0.90 at 15 atm CH_4 fugacity. In Figure 4.6(f) (-20^oC), the *n*-C_4H_{10} fugacity in the isotherm decreases slightly from 0.26 in pure *n*-C_4H_{10} (zero CH_4 fugacity) to 0.22 at 15 atm CH_4 fugacity. The *n*-C_4H_{10} fugacities reported in Figures 4.6(a)-(f) are average values for each mixture isotherm. The uncertainties shown in these figures are the standard deviations of the average values.

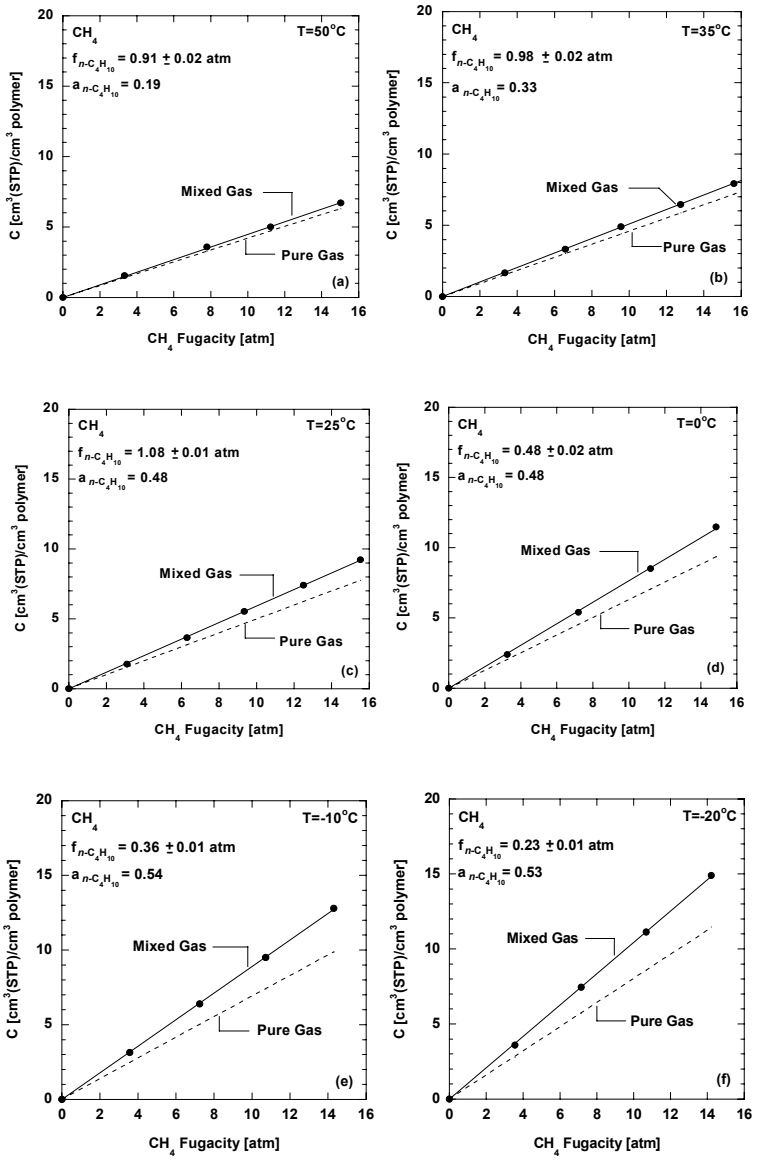

Figure 4.6 Pure and mixed gas sorption isotherms of CH_4 in PDMS at (a) 50°C, (b) 35°C, (c) 25 °C, (d) 0 °C, (e) -10 °C, (f) -20 °C. The solid lines and the data points correspond to mixture data, and the dashed lines represent pure gas sorption results (*cf.,* Figure 4.1). The reported *n*-C_4H_{10} fugacity, $f_{n-C_4H_{10}}$, is the average *n*-C_4H_{10} fugacities over the course of each mixture sorption isotherm. The uncertainty represents the standard deviation of the average value. The corresponding activity, $a_{n-C_4H_{10}}$, for each mixture sorption isotherm is indicated in the figures and was calculated as described in Appendix A.

Due to the linearity of the mixture sorption isotherms, the calculated CH_4 solubility coefficients are independent of CH_4 fugacity. The average CH_4 solubility coefficients obtained from the mixture isotherms in

Figure 4.6 at various *n*-C_4H_{10} fugacities and temperatures are displayed in Figures 4.7(a) and (b). Figure 4.7(a) presents mixed gas CH_4 solubility as a function of *n*-C_4H_{10} fugacity and temperature. In general, CH_4 solubility in the polymer increases as *n*-C_4H_{10} fugacity increases. This solubility enhancement is more pronounced at lower temperatures. That is, the presence of *n*-C_4H_{10} increases the solubility of CH_4 in PDMS, which is contrary to the typical assumption that each gas sorbs independently in rubbery polymers [21]. For instance, at 25^oC, only a 10% increase in CH_4 solubility is observed, from 0.50 cm^3(STP)/(cm^3 polymer atm) in pure gas to 0.55 cm^3(STP)/(cm^3 polymer atm) in the presence of 0.66 atm (fugacity) of *n*-C_4H_{10} (~ 0.29 *n*-C_4H_{10} activity). At 0^oC, in the presence of a slightly lower *n*-C_4H_{10} fugacity of 0.56 atm (~ 0.57 *n*-C_4H_{10} activity), CH_4 solubility increases nearly 30%, from 0.63 (pure gas) to 0.81 cm^3(STP)/(cm^3 polymer atm).

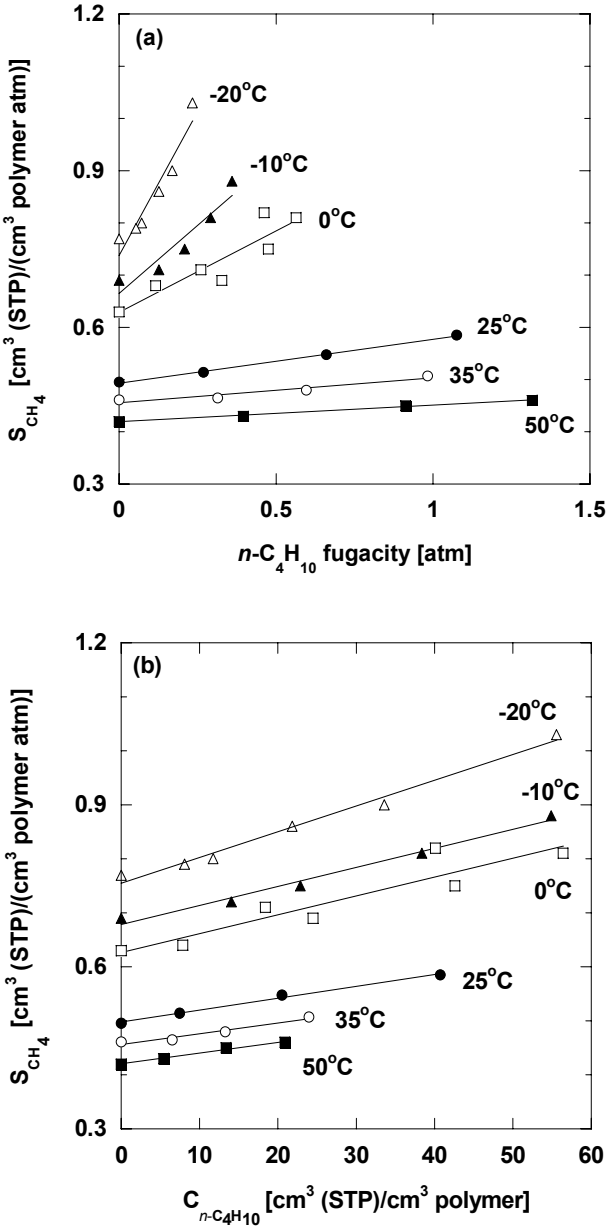

Figure 4.7 Mixed gas CH_4 solubility in PDMS at various temperatures as a function of (a) *n*-C_4H_{10} fugacity and (b) *n*-C_4H_{10} concentration in the polymer. The lines represent least squares fits to the data.

The increase in CH_4 solubility is related to the *n*-C_4H_{10} concentration in the polymer. To illustrate this point, Figure 4.7(b) presents CH_4 solubility in mixtures as a function of *n*-C_4H_{10} concentration in the polymer. As shown in Figure 4.7(b), the amount of *n*-C_4H_{10} sorbed in the polymer during the mixture sorption measurement can be substantial. For example, at 0^oC, the *n*-C_4H_{10} concentration in the polymer during the mixture measurement is as high as 56 cm^3(STP)/(cm^3 polymer), which corresponds to 22 vol.% or 13 wt.% of *n*-C_4H_{10}. Such a large amount of one penetrant in the polymer could presumably affect the solubility of other penetrants. The high concentration of *n*-C_4H_{10} in the polymer renders the environment in the dense polymer matrix more similar to that of *n*-C_4H_{10}, in which CH_4 is more soluble, as shown in Figure 4.8. In this sense, the presence of *n*-C_4H_{10} in the polymer might create a more favorable environment for CH_4 sorption, which leads to an enhancement in CH_4 solubility. Data from the literature shows that CH_4 solubility in liquid *n*-C_4H_{10} increases with increasing CH_4 fugacity [22-24]. The measurements in the literature studies were at CH_4 fugacity values as high as 120 atm. Within the CH_4 fugacity range in our study (*i.e.,* up to 16 atm), the increase in CH_4 solubility in liquid *n*-C_4H_{10} with increasing CH_4 fugacity is minimal. For example, at 35^oC, the CH_4 solubilities in liquid *n*-C_4H_{10} at CH_4 fugacities of 5 and 20 atm are 0.92 and 1.06 cm^3(STP)/(cm^3 atm), respectively. The CH_4 solubility data in liquid *n*-C_4H_{10} reported in Figure 4.8 are solubility values at 8 atm CH_4 fugacity, which is approximately the median of the CH_4 fugacity range of our study.

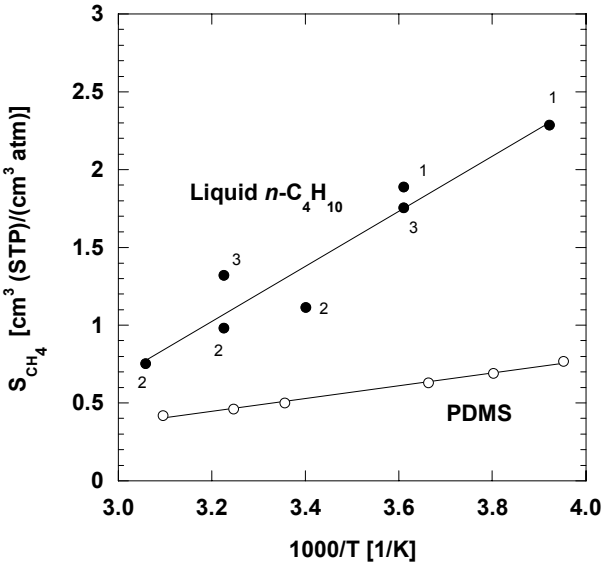

Figure 4.8 Solubility of CH_4 in liquid n-C_4H_{10} and in PDMS as a function of temperature. The lines represent least squares.
[1]Reference [22].
[2]Reference [23].
[3]Reference [24].

The increase in CH_4 solubility in PDMS in the presence of n-C_4H_{10} can be described using the following model [25-28]:

$$\ln S_{A,mix} = \phi_B \ln S_{A,B} + \phi_P \ln S_{A,P} \tag{4.9}$$

The subscripts A, B, and P refer to CH_4, n-C_4H_{10}, and PDMS, respectively. Therefore, $S_{A,mix}$ is the mixed gas CH_4 solubility in PDMS; $S_{A,B}$ and $S_{A,P}$ are the CH_4 pure gas solubility in liquid n-C_4H_{10} and in PDMS, respectively. ϕ_B is the volume fraction of n-C_4H_{10} in the mixture, and this value was estimated from pure gas n-C_4H_{10} sorption isotherms using Eq. (2.15), since n-C_4H_{10} mixed gas solubility in PDMS is essentially unaffected by CH_4, as shown later in this paper. ϕ_P is the volume fraction of PDMS in the mixture. Assuming that the volume fraction of CH_4 in the mixture, ϕ_A, is small, ϕ_P can be determined from ϕ_B (*i.e.*, $\phi_P = 1 - \phi_B$). This assumption is reasonable since ϕ_A in the

mixture never exceeds 5%. For instance, at -20°C, at the highest CH_4 mixture solubility observed (at 0.23 *n*-C_4H_{10} fugacity or 0.53 *n*-C_4H_{10} activity), ϕ_A, at a CH_4 fugacity of 14.2 atm, is only 0.03. This model requires only pure gas parameters to predict mixture solubility coefficients. It assumes that there is no specific interaction between *n*-C_4H_{10} and PDMS [25,27]. Figure 4.9 presents CH_4 mixture solubility in PDMS as a function of the volume fraction of *n*-C_4H_{10} sorbed in the polymer. The solid lines are predictions from Eq. (4.9), which represents the experimental data reasonably well considering that there are no adjustable parameters. In general, Eq. (4.9) could be used to estimate the solubility of a supercritical gas (A) in a rubbery polymer (P) in the presence of a solvent or a condensable vapor (B). However, the model requires that the sorption isotherms of the gas in the pure polymer and the pure solvent obey Henry's law. Therefore, $S_{A,mix}$, $S_{A,B}$, and $S_{A,P}$ in Eq. (4.9) should be independent of CH_4 fugacity, which they are in this case. If

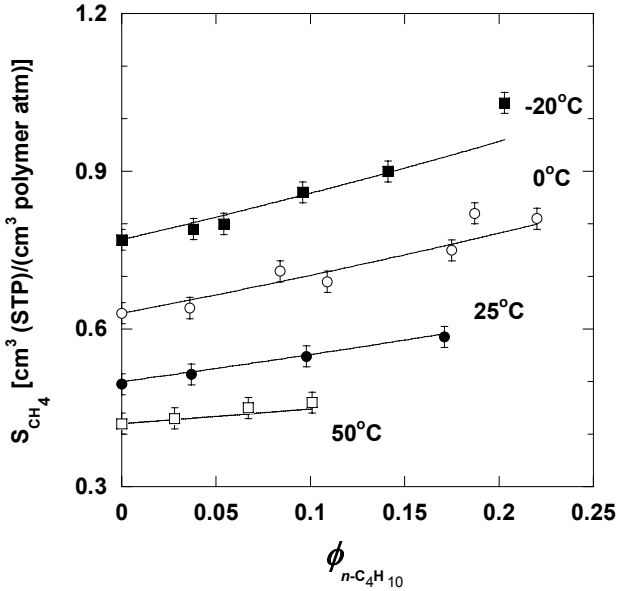

Figure 4.9 CH_4 mixed gas solubility in PDMS as a function of *n*-C_4H_{10} volume fraction in the polymer. The lines are estimated from pure gas CH_4 solubility in PDMS and liquid *n*-C_4H_{10} using Eq. (4.9) [22-24].

the interaction between the solvent and polymer is significant, Eq. (4.9) may be extended by introducing an adjustable interaction parameter, a_{BP}, as follows [27]:

$$\ln S_{A,mix} = \phi_B \ln S_{A,B} + \phi_P \ln S_{A,P} - a_{B,P}\phi_B\phi_P \tag{4.10}$$

Figure 4.10 presents pure and mixed gas n-C_4H_{10} solubility in PDMS as a function of n-C_4H_{10} activity (f/f_{sat}) at various temperatures. The lines are from pure gas measurements; and the symbols are data points from mixture measurements. The mixture solubilities of n-C_4H_{10} in PDMS are close to the pure gas values. There is, at most, a weak influence of CH_4 on n-C_4H_{10} solubility.

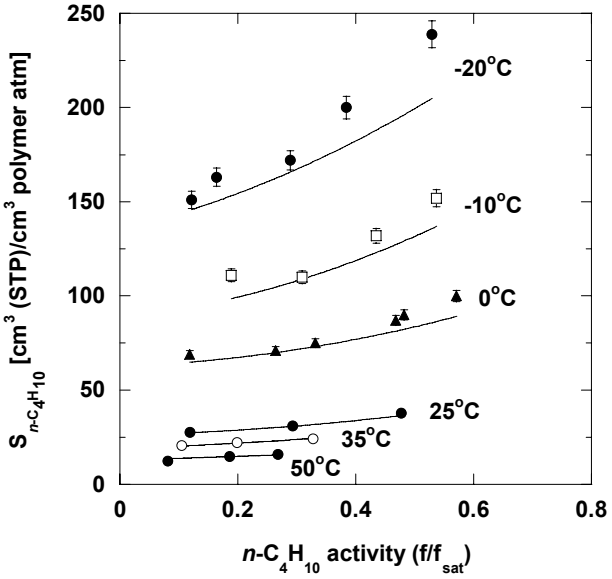

Figure 4.10 Pure and mixed gas n-C_4H_{10} solubility in PDMS at various temperatures. The lines represent pure gas solubility values calculated from the sorption data in Figure 4.. The points are measured solubility data in n-C_4H_{10}/CH_4 mixtures. The error bars are determined using the propagation of errors method [7]. The CH_4 fugacity in the mixture experiments is up to 16 atm.

4.5 EFFECT OF CONCENTRATION ON ENTHALPY OF SORPTION

The temperature dependence of gas solubility in mixtures can be described using Eq. (2.10), which is the same equation used for pure gas solubility. The enthalpy of sorption of CH_4 at a particular *n*-C_4H_{10} concentration in the polymer (*i.e.,* the isosteric enthalpy of sorption) can be calculated from the data in Figure 4.7(b) as follows [12]:

$$\Delta H_S^C = -R\left(\frac{d\ln S_A}{d\left(1/T\right)}\right)_C \tag{4.11}$$

where ΔH_s^C is the enthalpy of sorption at a particular *n*-C_4H_{10} concentration in the polymer. Figure 4.11(a) presents CH_4 enthalpy of sorption as a function *n*-C_4H_{10} concentration in PDMS. The CH_4 enthalpy of sorption decreases slightly as *n*-C_4H_{10} concentration in the polymer increases. For example, the enthalpy of sorption of CH_4 decreases from -5.8 ± 0.3 kJ/mol in pure gas to -6.9 ± 0.3 kJ/mol in the presence of 60 cm^3(STP)/(cm^3 polymer) of *n*-C_4H_{10} in the polymer. This trend suggests that the CH_4 sorption process in PDMS is more favorable when *n*-C_4H_{10} is present in the polymer. Figure 4.(a) also shows the enthalpy of sorption of CH_4 in liquid *n*-C_4H_{10} at 8 atm CH_4 fugacity (*i.e.,* the median of the CH_4 fugacity range explored in this study), which is determined using the following equation [12]:

$$\Delta H_s^f = -R\left(\frac{d\ln S_A}{d\left(1/T\right)}\right)_f \tag{4.12}$$

where ΔH_s^f is the enthalpy of sorption at fixed fugacity. The enthalpy of sorption of CH_4 in liquid *n*-C_4H_{10} (at 8 atm CH_4 fugacity), -9.7 kJ/mol, is lower than the enthalpy of sorption of CH_4 in pure PDMS (-5.9 ± 0.3 kJ/mol). Therefore, the interaction between CH_4 and *n*-C_4H_{10} molecules is somewhat more favorable than that between CH_4 molecules and PDMS polymer chains. As *n*-C_4H_{10} concentration in the polymer

increases, the environment into which CH_4 is sorbed becomes more like that of *n*-C_4H_{10}, and, therefore, CH_4 enthalpy of sorption decreases with increasing *n*-C_4H_{10} concentration in the polymer. Figure 4.11(b) presents pure and mixed gas *n*-C_4H_{10} enthalpy of sorption in PDMS as a function of *n*-C_4H_{10} concentration. There should be very little difference in the *n*-C_4H_{10} enthalpy of sorption estimated based on pure and mixed gas measurements since the pure and mixed gas *n*-C_4H_{10} solubility coefficients in PDMS are similar. The enthalpy of sorption in Figure 4.11(b) is estimated from the pure gas data because they are more comprehensive (*i.e.,* there are more pure gas data points than mixture data points) than the mixed gas data in this study. There is no significant dependence of *n*-C_4H_{10} enthalpy of sorption on *n*-C_4H_{10} concentration in the polymer. And, since ΔH_{cond} is not concentration dependent, the *n*-C_4H_{10} enthalpy of mixing is also independent of *n*-C_4H_{10} concentration in the polymer. The average *n*-C_4H_{10} enthalpy of mixing over the *n*-C_4H_{10} concentration range of study is -1.3 ± 0.3 kJ/mol. ΔH_{cond} at 15°C (-21.6 kJ/mol) is used in Eq. (4.2) to estimate the *n*-C_4H_{10} enthalpy of mixing as a function of *n*-C_4H_{10} concentration.

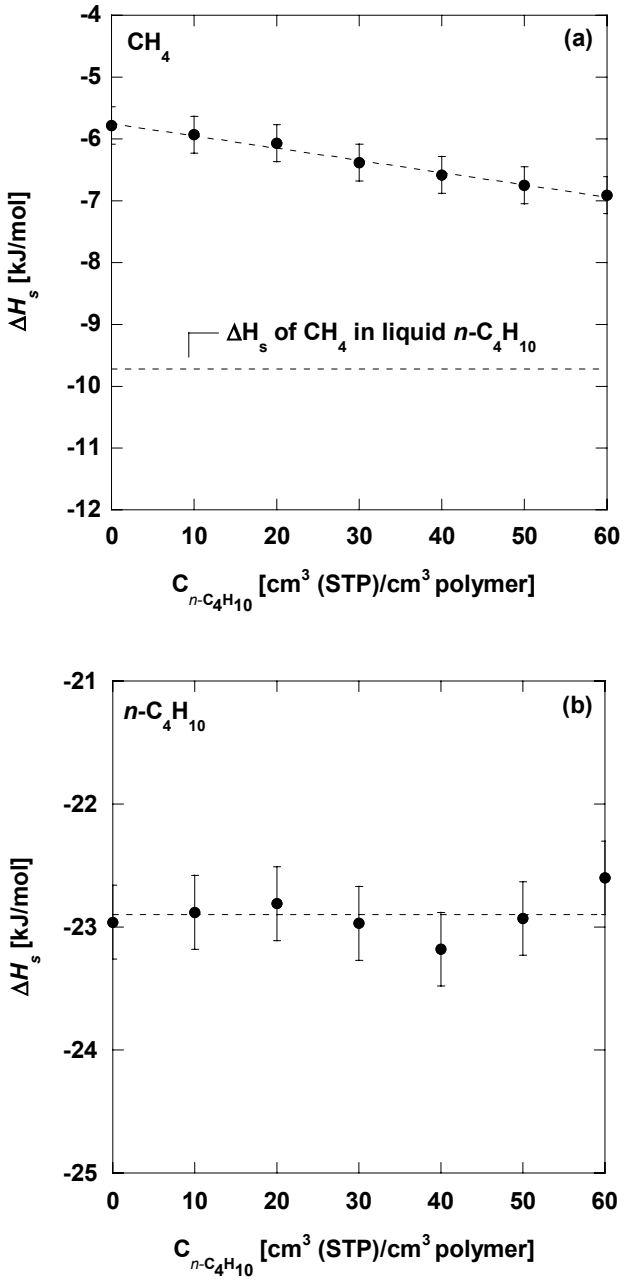

Figure 4.11 Enthalpy of sorption of (a) CH_4 and (b) n-C_4H_{10} in PDMS as a function of n-C_4H_{10} concentration in the polymer. The enthalpy of sorption of CH_4 in liquid n-C_4H_{10} is calculated from Eq. (4.12) at 8 atm CH_4 fugacity, using CH_4 solubility data in liquid n-C_4H_{10} from the literature [22-24]. The error bars are determined using the propagation of errors method [7].

4.6 MIXED GAS DILATION

Figure 4.12(a) presents PDMS dilation as a function of the total pressure of a 2 mol% *n*-C_4H_{10}/ 98 mol% CH_4 mixture at 35°C. The mixture experimental data are represented by the symbols and connected by the solid line. The dashed curve is constructed based on pure gas sorption and dilation measurement assuming that sorption is additive. This line is computed as follows:

$$\frac{\Delta V}{V_o} = \frac{C_A \bar{V}_A + C_B \bar{V}_B}{V_o} \tag{4.13}$$

where ΔV is the change in the polymer volume due to penetrant sorption, V_o is the initial penetrant-free polymer volume, and $\bar{V}_A$ and $\bar{V}_B$ are the pure gas partial molar volumes of CH_4 and *n*-C_4H_{10}, respectively (from Table 2). C_A and C_B are the concentrations of CH_4 and *n*-C_4H_{10} at the mixture partial pressure determined from the pure gas sorption measurements in Figure 4.1 and Figure 4.2, respectively. There is a deviation between the mixture data and the additive dilation line, as shown in Figure 4.12(a). Figure 4.12(b) presents the mixture dilation data and the additive dilation line calculated based on fugacity as a function of the total fugacity of the mixture. The fugacity-based additive dilation line in Figure 4.12(b) is also computed from Eq. (4.13) and uses the same pure gas values of $\bar{V}_A$ and $\bar{V}_B$ from Table 4.2. However, C_A and C_B are estimated based on the pure gas values at the mixture fugacity rather than at the mixture partial pressure of each gas. As shown in Figure 4.12(b), this fugacity-based additive dilation line agrees well with the mixture data. The fugacity coefficient of *n*-C_4H_{10} in the *n*-C_4H_{10}/CH_4 mixture is relatively low compared to that in pure gas, which means that the *n*-C_4H_{10} fugacity is considerably lower than its partial pressure. Consequently, the slope of the additive dilation line estimated based on fugacity (Figure 4.12(b)) is lower than that estimated based on pressure (Figure 4.12(a)).

PDMS dilation isotherms as a function of fugacity for different n-C_4H_{10}/CH_4 mixtures at various temperatures are presented in Figures 4.13(a)-(f). The mixture data in these figures are in good agreement with the additive dilation model. Although the additive lines are based on constant CH_4 solubility at every temperature, this agreement does not, in any way, contradict the mixture sorption result, which shows an increase in CH_4 solubility with increasing n-C_4H_{10} fugacity. Due to the much higher n-C_4H_{10} solubility in PDMS relative to that of CH_4, the n-C_4H_{10}/CH_4 mixture dilation measurement is essentially insensitive to n-C_4H_{10}-induced changes in CH_4 solubility, even if they are rather large. When the additive dilation model is applied using mixture sorption data (*i.e.,* when C_A in Eq. (4.13) is the actual CH_4 concentration in PDMS), there is still very good agreement between the mixture dilation data and the additive dilation model. There is essentially no noticeable change in the additive dilation model estimated based on pure gas or mixed gas sorption measurements. For this reason, the pure and mixed gas partial molar volumes of CH_4 and n-C_4H_{10} in PDMS are similar.

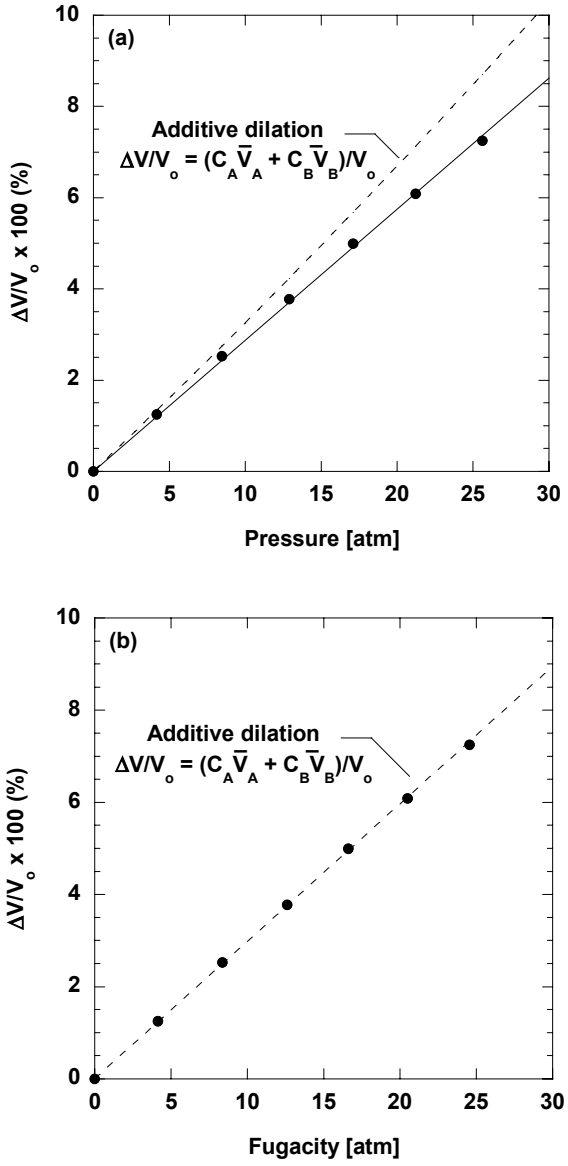

Figure 4.12 *n*-C_4H_{10}/CH_4 mixture dilation behavior in PDMS at 35°C, based on (a) total pressure and (b) total fugacity of the mixture. The gas mixture is 2 mol% *n*-C_4H_{10}, and the balance is CH_4.

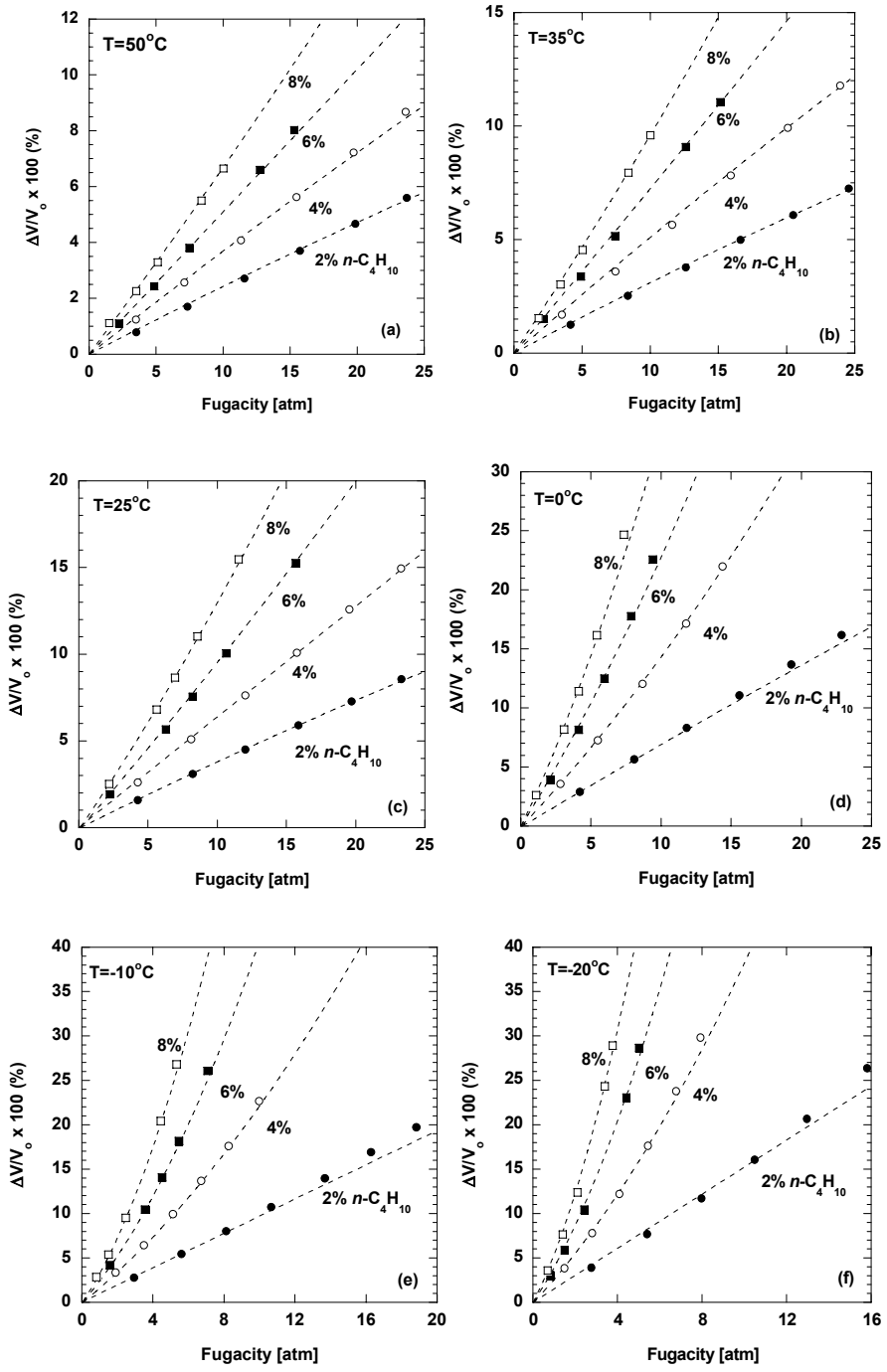

Figure 4.13 PDMS mixture dilation behavior at (a) 50°C, (b) 35°C, (c) 25°C, (d) 0°C, (e) -10°C, and (f) -20°C, as a function of total mixture fugacity. The dashed lines are additive dilation lines estimated using Eq. (4.13) based on fugacity.

4.7 SOLUBILITY SELECTIVITY

Figure 4.14 shows the mixed gas solubility selectivity of n-C_4H_{10}/CH_4 in PDMS as a function of n-C_4H_{10} activity (f/f_{sat}) in the mixture at various temperatures. These values were calculated based on the n-C_4H_{10}/CH_4 mixture solubility data. The solubility selectivity increases as n-C_4H_{10} activity increases and temperature decreases, and the solubility selectivity is a stronger function of temperature than n-C_4H_{10} activity. n-C_4H_{10}/CH_4 solubility selectivity increases by almost an order of magnitude as temperature decreases from 50 to -20^oC. On the other hand, the increase in solubility selectivity with n-C_4H_{10} activity is less than 50% at any given temperature. Figure 4.14 also compares the n-C_4H_{10}/CH_4 solubility selectivity values in mixtures to those estimated from pure gas solubility measurements which are illustrated by the dashed lines. Due to the increase in CH_4 solubility with increasing n-C_4H_{10} activity, the solubility selectivities determined from the mixture data are always lower than those estimated from pure gas measurements. At lower temperatures, where higher n-C_4H_{10} activity values are more accessible experimentally, the deviations between mixture and pure gas solubility selectivity values are larger. The reduced mixed gas solubility selectivity relative to pure gas solubility selectivity should contribute directly to lower mixed gas permeability selectivity, which has been reported in the literature for this gas pair in PDMS [29].

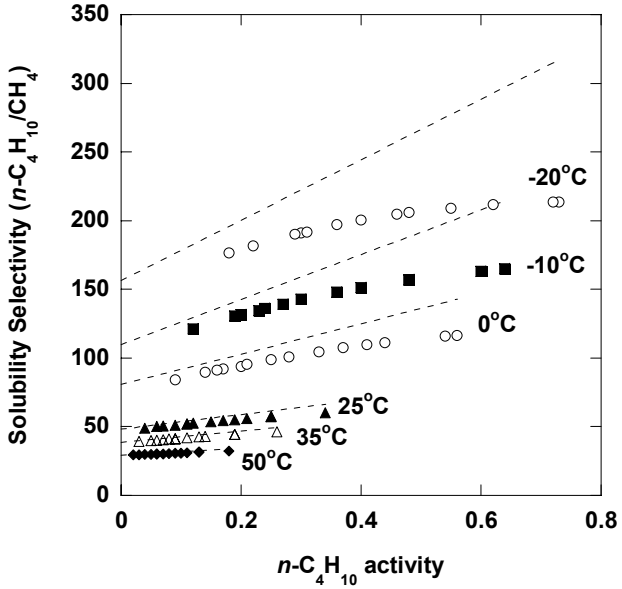

Figure 4.14 Mixed gas n-C_4H_{10}/CH_4 solubility selectivity in PDMS as a function of n-C_4H_{10} activity in the mixture. The dashed lines are estimates from the pure gas data.

4.8 CONCLUSIONS

It is generally accepted that different penetrants sorb independently of one another in rubbery polymers [21]. However, this model can only be even approximately obeyed when the total penetrant sorption in the polymer is low (*e.g.,* <1 wt.%) [30]. In this study, the presence of n-C_4H_{10} in PDMS creates a more favorable environment for CH_4 sorption and, consequently, CH_4 solubility is enhanced. The increase in CH_4 mixture solubility in PDMS can be described accurately using a model requiring only pure gas solubility data and containing no adjustable parameters. On the other hand, there is essentially no change in n-C_4H_{10} solubility in the presence of CH_4. n-C_4H_{10} mixed gas solubility is similar to the pure gas n-C_4H_{10} solubility. The amount of CH_4 sorbed in the polymer is presumably too low to measurably influence n-C_4H_{10} solubility. The mixture dilation data are in a good agreement with the additive dilation model. The partial molar volumes of CH_4 and n-C_4H_{10} in PDMS do not change significantly in pure or mixed gas

environments. The n-C_4H_{10}/CH_4 mixed gas solubility selectivity increases as n-C_4H_{10} activity increases and temperature decreases, and it is lower than the value estimated from pure gas measurements.

4.9 REFERENCES

[1] T. C. Merkel, V. I. Bondar, K. Nagai, B. D. Freeman, and I. Pinnau, "Gas sorption, diffusion, and permeation in poly(dimethylsiloxane)", Journal of Polymer Science: Part B: Polymer Physics, 38 (2000) 415-34.

[2] H. Lin and B. D. Freeman, "Gas solubility, diffusivity and permeability in poly(ethylene oxide)", Journal of Membrane Science, 239 (2004) 105-17.

[3] K. Ghosal and B. D. Freeman, "Gas separation using polymer membranes: an overview", Polymers for Advanced Technologies, 5 (1994) 673-97.

[4] V. M. Shah, B. J. Hardy, and S. A. Stern, "Solubility of carbon dioxide, methane, and propane in silicone polymers: effect of polymer side chains", Journal of Polymer Science: Part B: Polymer Physics, 24 (1986) 2033-47.

[5] P. J. Flory, Principles of Polymer Chemistry, Cornell University Press, Ithaca, NY, 1953.

[6] B. E. Poling, J. M. Prausnitz, and J. P. O'Connell, The Properties of Gases and Liquids, 5th ed., McGraw-Hill, New York, NY, 2001.

[7] P. R. Bevington, Data reduction and error analysis for the physical sciences, 2nd ed., McGraw-Hill, New York, NY, 1992.

[8] Y. Kamiya, Y. Naito, K. Terada, K. Mizoguchi, and A. Tsuboi, "Volumetric properties and interaction parameters of dissolved gases in poly(dimethylsiloxane) and polyethylene", Macromolecules, 33 (2000) 3111-9.

[9] R. M. Barrer, J. A. Barrie, and N. K. Raman, "Solution and diffusion in silicone rubber I - A comparison with natural rubber", Polymer, 3 (1962) 595-603.

[10] J. M. Prausnitz, R. N. Lichtenthaler, and E. G. de Azevedo, Molecular Thermodynamics of Fluid-Phase Equilibria, 3rd ed., Prentice-Hall, Inc., Upper Saddle River, NJ, 1999.

[11] DIPPR Physical and Thermodynamic Properties, http://dippr.byu.edu/public/chemsearch.asp.

[12] R. S. Prabhakar, T. C. Merkel, B. D. Freeman, T. Imizu, and A. Higuchi, "Sorption and transport properties of propane and perfluoropropane in poly(dimethylsiloxane) and poly(1-trimethylsilyl-1-propyne)", Macromolecules, 38 (2005) 1899-910.

[13] M. G. De Angelis, T. C. Merkel, V. I. Bondar, B. D. Freeman, F. Doghieri, and G. C. Sarti, "Hydrocarbon and fluorocarbon solubility and dilation in poly(dimethylsiloxane): comparison of experimental data with predictions of the Sanchez-Lacombe equation of state", Journal of Polymer Science: Part B: Polymer Physics, 37 (1999) 3011-26.

[14] F. P. Incropera and D. P. DeWitt, Fundamentals of Heat and Mass Transfer, John Wiley & Sons, New York, NY, 1996.

[15] P. Zoller and D. Walsh, Standard Pressure-Volume-Temperature Data for Polymers, Technomic, Lancaster, PA, 1995.

[16] S. M. Jordan and W. J. Koros, "Permeability of pure and mixed gases in silicone rubber at elevated pressures", Journal of Polymer Science: Part B: Polymer Physics, 28 (1990) 795-809.

[17] J. M. Smith, H. C. V. Ness, and M. M. Abbott, Introduction to Chemical Engineering Thermodynamics, McGraw-Hill, New York, NY, 2001.

[18] Y. Kamiya, Y. Naito, T. Hirose, and K. Mizoguchi, "Sorption and partial molar volume of gases in poly(dimethylsiloxane)", Journal of Polymer Science: Part B: Polymer Physics, 28 (1990) 1297-308.

[19] J. Horiuti, "The solubility of gas and coefficient of dilatation by absorption", Scientific Papers of the Institute of Physical and Chemical Research, 17 (1931) 125-256.

[20] G. K. Fleming and W. J. Koros, "Dilation of polymers by sorption of carbon dioxide at elevated pressures. 1. Silicone rubber and unconditioned polycarbonate", Macromolecules, 19 (1986) 2285-91.

[21] W. J. Koros, R. T. Chern, V. Stannett, and H. B. Hopfenberg, "A model for permeation of mixed gases and vapors in glassy polymers", Journal of Polymer Science: Polymer Physics Edition, 19 (1981) 1513-30.

[22] D. G. Elliot, R. J. J. Chen, P. S. Chappelear, and R. Kobayashi, "Vapor-liquid equilibrium of methane-*n*-butane system at low temperatures and high pressures", Journal of Chemical and Engineering Data, 19 (1974) 71-7.

[23] B. H. Sage, B. L. Hicks, and W. N. Lacey, "Phase equilibria in hydrocarbon systems. The methane-butane system in two-phase region", Journal of Industrial and Engineering Chemistry, 32 (1940) 1085-92.

[24] H. C. Wiese, J. Jacobs, and B. H. Sage, "Phase equilibria in the hydrocarbon systems. Phase behavior in the methane-propane-*n*-butane system", Journal of Chemical and Engineering Data, 15 (1970) 82-91.

[25] I. Shulgin and E. Ruckenstein, "Prediction of gas solubility in binary polymer + solvent mixtures", Polymer, 44 (2003) 901-7.

[26] I. R. Krichevsky, "Thermodynamics of an infinitely dilute solution in mixed solvents. I. The Henry's coefficient in a mixed solvent behaving as an ideal solvent", Zhournal Fizicheskoi Khimii, 9 (1937) 41-7.

[27] J. P. O'Connell and J. M. Prausnitz, "Thermodynamics of gas solubility in mixed solvents", AIChE Journal, 3 (1964) 347-51.

[28] M. Catte, C. Achard, C.-G. Dussap, and J.-B. Gros, "Prediction of gas solubilities in pure and mixed solvents using a group contribution method", Industrial & Engineering Chemistry Research, 32 (1993) 2193-8.

[29] I. Pinnau and Z. He, "Pure- and mixed-gas permeation properties of polydimethylsiloxane for hydrocarbon/methane and hydrocarbon/hydrogen separation", Journal of Membrane Science, 244 (2004) 227-33.

[30] R. W. Baker, Membrane Technology and Applications, 2nd ed., John Wiley & Sons, New York, 2004.

Chapter 5: Pure and Mixed Gas CH_4 and *n*-C_4H_{10} Permeability and Diffusivity in Poly(dimethylsiloxane)

This chapter presents the pure and mixed gas CH_4 and *n*-C_4H_{10} permeability coefficients in poly(dimethylsiloxane) (PDMS) at temperatures from -20 to 50°C. Diffusion coefficients of CH_4 and *n*-C_4H_{10} in the mixtures are determined from the mixture permeability data and the mixture solubility data presented in the previous chapter. The influence of *n*-C_4H_{10} on CH_4 transport properties is investigated. Several theoretical models are evaluated for their ability to describe the experimental pure and mixed gas data. In addition, this chapter discusses the effect of *n*-C_4H_{10} and temperature on *n*-C_4H_{10}/CH_4 mixture permeability, solubility, and diffusivity selectivity in PDMS.

5.1 PURE GAS PERMEABILITY

Figures 5.1(a) and (b) present CH_4 and *n*-C_4H_{10} pure gas permeability coefficients in PDMS as a function of upstream fugacity at temperatures ranging from -20 to 50°C. CH_4 permeability is independent of upstream fugacity, which is typical for permeation of light gases in rubbery polymers [1]. The average CH_4 pure gas permeability values at each temperature are presented in Table 5.1. The uncertainty was determined using the propagation of errors method [2]. The CH_4 permeability values are in good agreement with previously reported values. Merkel *et al.* [3] and Stern *et al.* [4] reported infinite dilution CH_4 permeability at 35°C of 1,200 and 1,350 Barrer, respectively. Pinnau and He [5] reported CH_4 permeability of 710, 930, 1200, and 1300 Barrer, at -20, 0, 25, and 35°C, respectively.

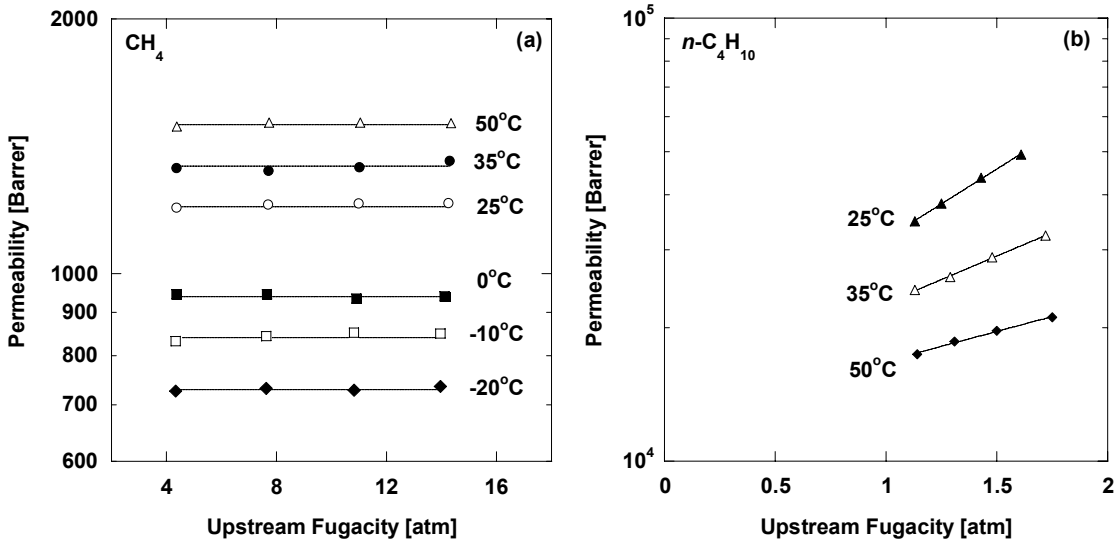

Figure 5.1 Pure gas permeability of (a) CH_4 and (b) *n*-C_4H_{10} in PDMS as a function of upstream fugacity and temperature.

Table 5.1 Pure gas CH_4 and *n*-C_4H_{10} permeability and diffusivity in PDMS

T (°C)	P (Barrer)		$\overline{D}$ x 10^6 (cm^2/s)	
	CH_4[a]	*n*-C_4H_{10}[b]	CH_4[a]	*n*-C_4H_{10}[b]
-20	730 ± 40	-	7.3 ± 0.5	-
-10	840 ± 40	-	9.2 ± 0.6	-
0	940 ± 50	-	11 ± 0.8	-
25	1200 ± 60	16000 ± 800	18 ± 1	4.4 ± 0.3
35	1300 ± 70	14000 ± 700	22 ± 2	5.6 ± 0.4
50	1500 ± 80	12000 ± 600	27 ± 2	7.5 ± 0.5

[a]Average value
[b]Infinite dilution estimated using Eq. (5.1) or (5.3).

Unlike CH_4, the permeability of more condensable *n*-C_4H_{10} increases as upstream fugacity increases. As discussed later, this trend is partly due to plasticization. Plasticization refers to an increase in penetrant diffusivity resulting from increased polymer local segmental motion or fractional free volume (FFV) caused by the presence of penetrant molecules in the polymer matrix [6]. Highly sorbing penetrants, like *n*-C_4H_{10}, plasticize the polymer matrix due to their high concentration in the polymer. In addition, *n*-C_4H_{10} solubility increases with increasing fugacity, and this factor increases permeability as well [7,8]. Gas permeability is often empirically related to fugacity as follows [4]:

$$P_A = P_{A,o} \exp\left(m\Delta f_A\right) \tag{5.1}$$

where $P_{A,,o}$ is the permeability coefficient when $\Delta f_A = 0$ and is referred to as the infinite dilution permeability, m is an adjustable parameter which is taken to be constant at a given temperature, and Δf_A is the difference between the upstream and downstream fugacity values ($\Delta f_A = f_{A,2} - f_{A,1}$). For most experiments considered in this study, $f_{A,1}$ is practically 0, so Δf_A can be replaced by $f_{A,2}$. The experimental data were fit to this equation, and the resulting infinite dilution *n*-C_4H_{10} pure gas permeabilities at 25, 35, and 50^{o}C in PDMS are presented in Table 5.1. They are in a reasonable agreement with the literature. For example, Barrer *et al.* [7] reported *n*-C_4H_{10} infinite dilution permeability of 15,300 and 14,000 Barrer, at 30 and 50^{o}C, respectively.

5.2 PURE GAS DIFFUSIVITY

Concentration-averaged diffusion coefficients were estimated from the permeability and sorption data using the following rearranged form of Eq. (2.4) [1]:

$$\bar{D}_A = P_A \left(\frac{f_{A,2} - f_{A,1}}{C_{A,2} - C_{A,1}} \right) \tag{5.2}$$

Figures 5.2(a) and (b) present pure gas CH_4 and *n*-C_4H_{10} concentration-averaged diffusion coefficients in PDMS as a function of upstream fugacity (*i.e.,* $f_{A,2}$). Pure gas CH_4 diffusion coefficients in PDMS are essentially independent of fugacity, which is consistent with the results of Merkel *et al.* [3]. The average CH_4 pure gas concentration-averaged diffusion coefficients at each temperature are presented in Table 5.1. CH_4 diffusion coefficients determined from this study are in excellent agreement with literature values. For example, CH_4 diffusion coefficients at 35°C are reported to be 2.2×10^{-5} and 2.45×10^{-5} cm^2/s in the work of Merkel *et al.* [3] and Stern *et al.* [4], respectively.

Pure gas *n*-C_4H_{10} diffusion coefficients increase as total upstream fugacity increases. The high concentration of *n*-C_4H_{10} in the polymer apparently induces plasticization [3,9]. The fugacity dependence of the diffusion coefficients can be described by the following linear relation [4]:

$$\bar{D}_A = \bar{D}_{A,o} \left(1 + q \Delta f_A \right) \tag{5.3}$$

where $\bar{D}_{A,o}$ is the diffusion coefficient at $\Delta f_A = 0$ and q is a parameter characterizing the pressure dependence of diffusion coefficients. The infinite dilution diffusion coefficients, $\bar{D}_{A,o}$, of *n*-C_4H_{10} at each temperature are presented in Table 5.1. These results are in reasonable agreement with those of Barrer *et al.* [7], who reported values of 5.44×10^{-6} and 8.49×10^{-6} cm^2/s at 30 and 50°C, respectively.

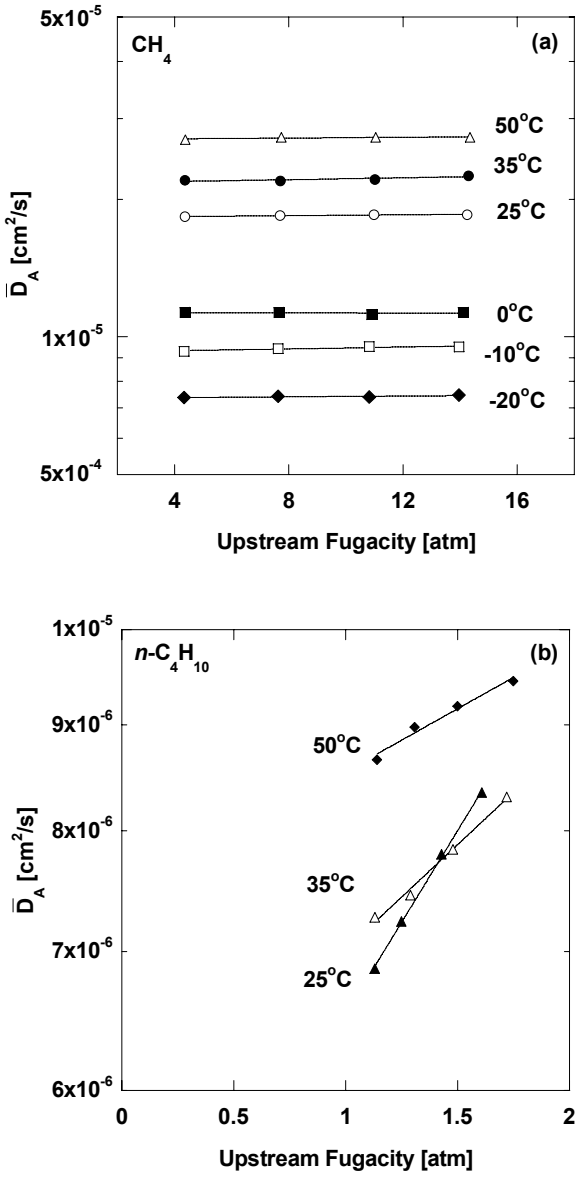

Figure 5.2 Pure gas (a) CH_4 and (b) n-C_4H_{10} concentration-averaged diffusion coefficients in PDMS as a function of upstream fugacity and temperature.

5.3 EFFECT OF TEMPERATURE ON PURE GAS PERMEABILITY AND DIFFUSIVITY

The temperature dependence of permeability can be described using Eq. (2.9). The E_P values at infinite dilution are 6.8 ± 0.6 and -7 ± 2 kJ/mol for CH_4 and *n*-C_4H_{10}, respectively. A positive E_P value indicates that permeability decreases as temperature decreases, and a negative E_P means that permeability increases as temperature decreases. The E_p value of CH_4 is in good agreement with the value reported by Pinnau and He, which is 7.1 kJ/mol [10]. The E_p value for *n*-C_4H_{10} agrees, within experimental uncertainty, with the value reported by Barrer *et al.*, which is -5.3 kJ/mol [7].

Using known E_P and ΔH_S values [8], the activation energy of diffusion, E_D, for CH_4 and *n*-C_4H_{10} at infinite dilution can be determined using Eq. (2.12). The E_D values for CH_4 and *n*-C_4H_{10} are 12.6 ± 0.7 and 17 ± 3 kJ/mol, respectively. These results are in good agreement with literature values. For example, Stern *et al.* [4] reported a value of 12 kJ/mol as the E_D value of CH_4. Barrer *et al.* [7] reported a value of 18 kJ/mol as the E_D value of *n*-C_4H_{10}.

5.4 MIXED GAS PERMEABILITY

Figures 5.3(a)-(f) presents the influence of upstream pressure on CH_4 permeability in PDMS in pure gas and in mixtures containing 2, 4, 6, and 8 mol% *n*-C_4H_{10} in CH_4 from -20 to 50°C. CH_4 permeability in the mixtures increases as total upstream pressure and, therefore, *n*-C_4H_{10} concentration in the feed increases. The increase in CH_4 permeability with increasing total feed pressure is greater at lower temperature. For example, at 35°C, CH_4 permeability increases by only 8%, from 1,300 Barrer in pure gas to 1,400 Barrer in the 8 mol% *n*-C_4H_{10} mixture at 4.4 atm total feed pressure. However, at -20°C and similar upstream fugacity of the same feed mixture (*i.e.,* similar *n*-C_4H_{10} upstream fugacity), CH_4 permeability increases more than 100%, from 730 in pure gas to 1,500 Barrer in the 8 mol% *n*-C_4H_{10} mixture. *n*-C_4H_{10} is more

condensable at lower temperature, as reflected by the decrease in n-C_4H_{10} saturation fugacity as temperature decreases. As a result, at similar n-C_4H_{10} fugacity value, the activity (f/f_{sat}) of n-C_4H_{10} in the mixture and, consequently, the concentration of n-C_4H_{10} in the polymer are higher at lower temperature [8], which presumably explains the greater increase in CH_4 mixture permeability with pressure as temperature decreases.

The CH_4 permeability coefficients at various temperatures from Figures 5.3(a)-(f) are plotted as a function of n-C_4H_{10} activity (f/f_{sat}) in the feed in Figure 5.4(a). CH_4 permeability increases with increasing n-C_4H_{10} activity at each temperature. Using experimental mixed gas sorption data obtained previously [8], n-C_4H_{10} concentration in the polymer at a particular n-C_4H_{10} activity can be calculated. Figure 5.4(b) presents CH_4 permeability in mixtures as a function of n-C_4H_{10} concentration at the upstream side of the membrane. Similar to Figure 5.4(a), CH_4 permeability increases systematically with increasing upstream n-C_4H_{10} concentration.

While n-C_4H_{10} increases CH_4 permeability, the presence of CH_4 does not noticeably change n-C_4H_{10} permeability. Figure 5.5 presents n-C_4H_{10} permeability in PDMS as a function of n-C_4H_{10} feed fugacity for both pure gas and mixed gas conditions. As the pure gas data are extrapolated to lower n-C_4H_{10} fugacity, they coincide well with the mixture permeability data, which suggests that n-C_4H_{10} permeation is not influenced by the presence of CH_4. There is no measurable difference between pure gas and mixed gas n-C_4H_{10} permeability coefficients in PDMS. The amount of CH_4 in the polymer is presumably too low to influence n-C_4H_{10} permeability.

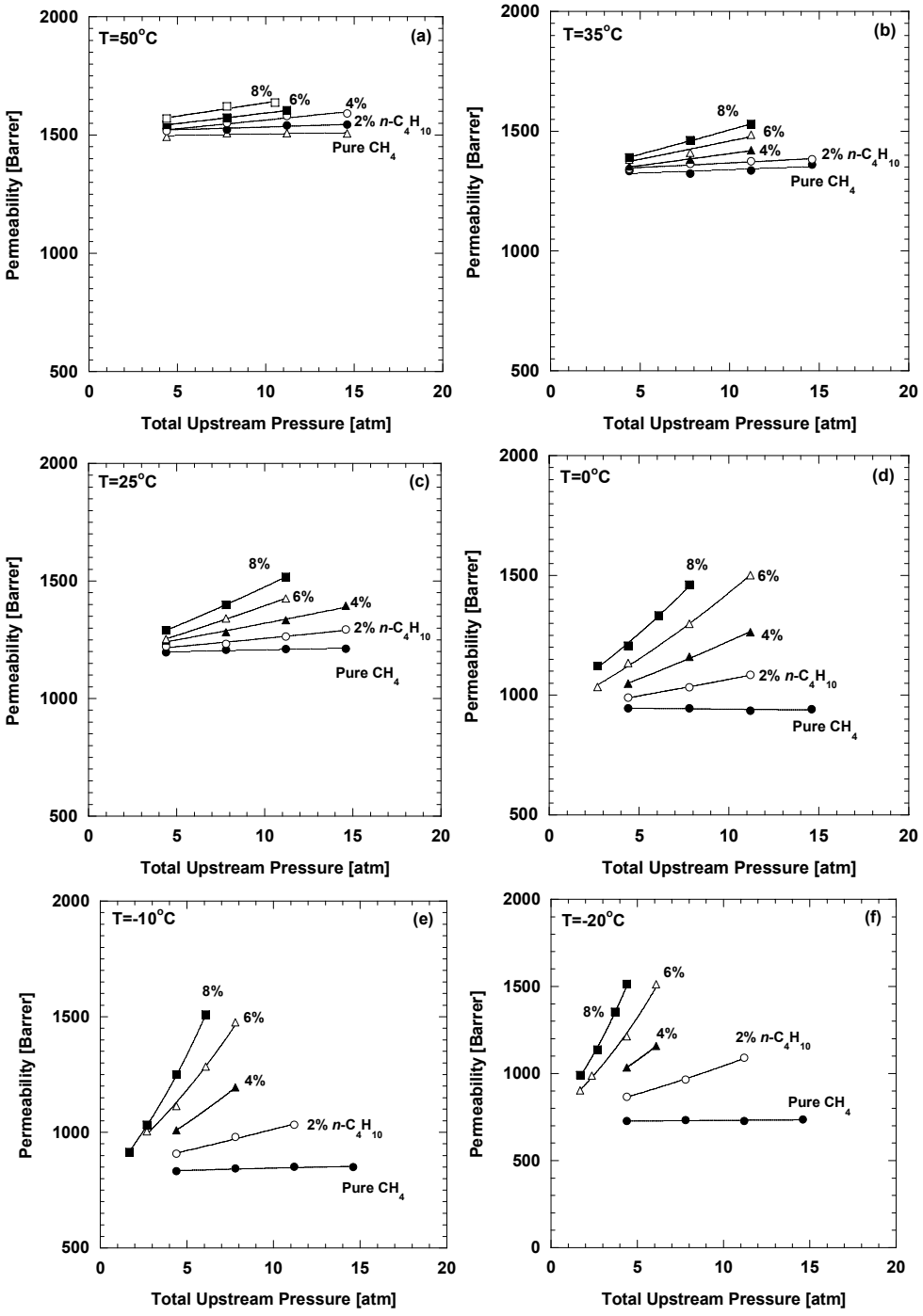

Figure 5.3 Pure and mixed gas CH_4 permeability in PDMS. Gases are pure CH_4 and mixtures containing 2, 4, 6, and 8 mol% n-C_4H_{10} in CH_4 at (a) 50°C, (b) 35°C, (c) 25°C, (d) 0°C, (e) -10°C, (f) -20°C.

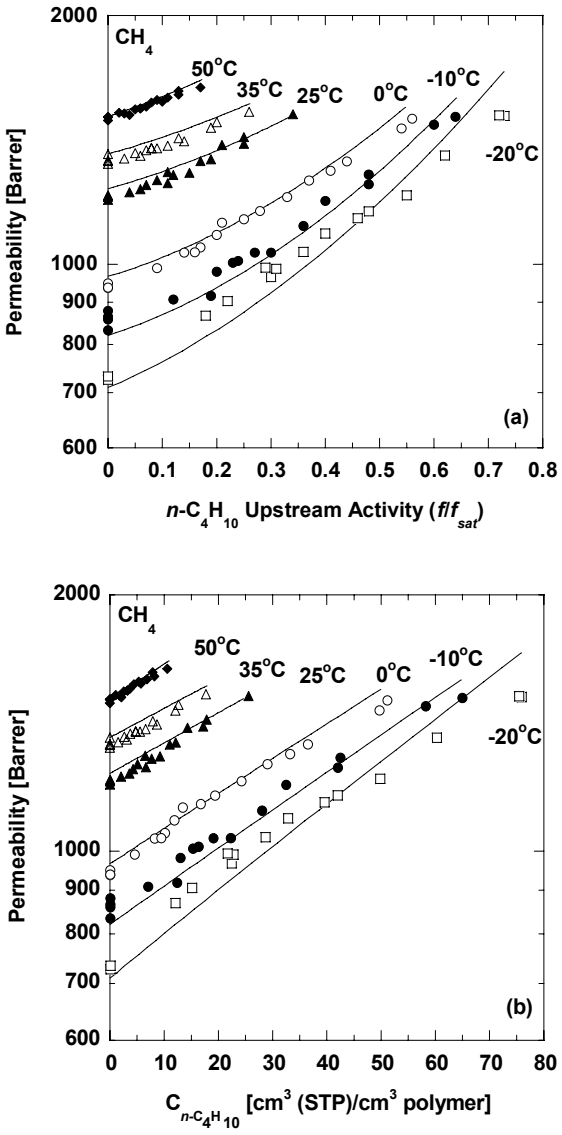

Figure 5.4 The permeability of CH_4 in PDMS as a function of (a) *n*-C_4H_{10} upstream activity (f/f_{sat}) in the mixtures and (b) *n*-C_4H_{10} concentration at the upstream side of the membrane. The feed gas compositions are 2, 4, 6, and 8 mol% *n*-C_4H_{10} in CH_4. The total feed pressure was from 1.7 – 14.6 atm. The permeate pressure was a helium sweep at 1 atm, so the permeate partial pressure of CH_4 and *n*-C_4H_{10} was negligible. The lines represent model fits to the experimental data using Eq. (5.17) and the adjustable parameters in Table 5.2.

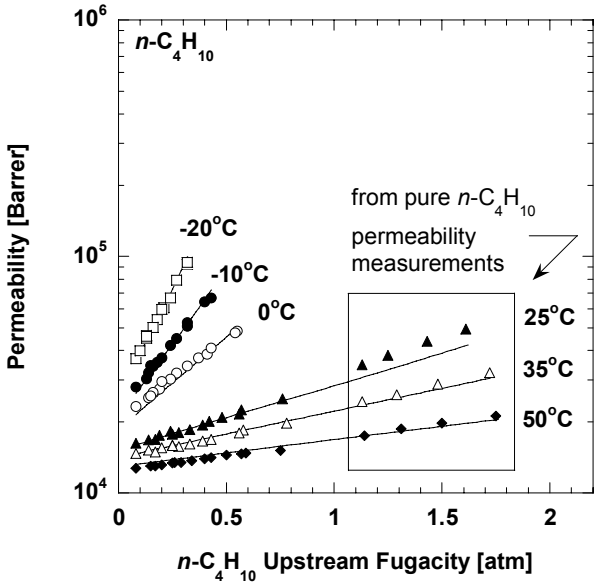

Figure 5.5 The permeability of n-C_4H_{10} in PDMS as a function of n-C_4H_{10} upstream fugacity. The feed gas compositions are 2, 4, 6, and 8 mol% n-C_4H_{10} in CH_4. The total feed pressure was from 1.7 – 14.6 atm. The permeate pressure was a helium sweep at 1 atm, so the permeate partial pressure of CH_4 and n-C_4H_{10} was negligible. The lines represent the model fits to the experimental data using Eq. (5.15) and the adjustable parameters in Table 5.2.

Pinnau and He reported CH_4/n-C_4H_{10} mixed gas permeability in PDMS and observed an increase in CH_4 permeability in the presence of n-C_4H_{10} [10]. Their permeability values are in reasonable agreement with ours. For example, the CH_4 and n-C_4H_{10} permeabilities in a 2 mol% n-C_4H_{10} mixture at 11 atm of feed pressure and 0°C were 1,410 and 23,000 Barrer, respectively [10]. In the present study, the values at similar conditions are 1,100 and 28,000 Barrer, for CH_4 and n-C_4H_{10}, respectively. The permeate pressure in our permeability measurement was essentially 0 atm; while in their study, the permeate pressure was 1 atm.

The effect of permeate pressure on permeability could be significant, particularly with condensable vapors (*e.g.,* C_3H_8, *n*-C_4H_{10}) [11]. For example, propane permeability in PDMS at -10°C increases approximately 24% as the downstream pressure increases from 0 to 1 atm [11]. Figures 5.6(a) and (b) present the permeability of CH_4 and *n*-C_4H_{10} in PDMS, respectively, at 0°C as a function of *n*-C_4H_{10} downstream activity. The feed mixture was 6 mol% *n*-C_4H_{10} in CH_4, and the total upstream pressure was 11.2 atm. The variation in *n*-C_4H_{10} downstream activity was achieved by adjusting the downstream helium sweep flowrate. From Figure 5.6(a), there is essentially no variation in CH_4 permeability with *n*-C_4H_{10} downstream activity. On the other hand, as illustrated in Figure 5.6(b), *n*-C_4H_{10} permeability increases as downstream *n*-C_4H_{10} activity increases. The permeability of *n*-C_4H_{10} increases from 48,000 to 65,000 Barrer as the *n*-C_4H_{10} downstream fugacity increases from 0.01 to 0.14 atm or as the downstream *n*-C_4H_{10} activity increases from 0.01 to 0.14 (the *n*-C_4H_{10} saturation fugacity at 0°C is 0.99 atm) [12].

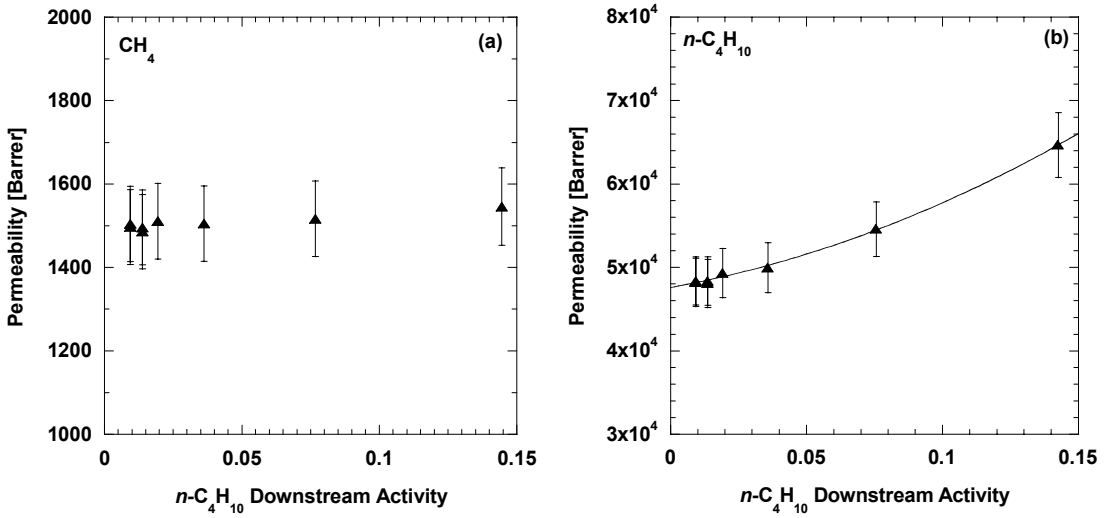

Figure 5.6 (a) CH_4 and (b) *n*-C_4H_{10} permeability coefficients in PDMS at 0°C as a function of *n*-C_4H_{10} downstream activity. The feed was 6 mol% *n*-C_4H_{10}/CH_4 mixture. The total upstream pressure was 11.2 atm.

Increases in the permeability of one penetrant in the presence of a second penetrant in a rubbery polymer has been reported previously [13]. Jordan and Koros [13] reported an increase in CH_4 and N_2 permeability in PDMS in CO_2/CH_4 and CO_2/N_2 mixtures. Based on free volume analysis, they hypothesized that highly sorbing CO_2 plasticized the polymer matrix, which resulted in an increase in light gas diffusivity and, consequently, permeability. In addition, a slight depression (from pure gas) in CO_2 permeability at low partial pressure (< 17 atm) was observed [13]. The presence of these light gases (*i.e.,* N_2 and CH_4) was speculated to compress the polymer, reducing its fractional free volume (FFV), and, consequently, lowering CO_2 diffusivity and permeability. In our study, this hypothesized compression effect by CH_4 was not observed. In fact, CH_4 swells PDMS at all pressures and temperatures considered [8]. Using Eq. (5.9) and the pure gas CH_4 sorption and dilation data reported in the previous chapter, the FFV of the penetrant and polymer mixture was estimated. The FFV of the PDMS/penetrant system increased monotonically with increasing CH_4 fugacity (up to 25 atm), so there is no compression effect exerted by CH_4 on the polymer. In contrast to the behavior reported by Jordan and Koros for CO_2, *n*-C_4H_{10} permeability in mixtures is similar to the pure gas value and is unaffected by the presence of CH_4.

5.5 MIXED GAS DIFFUSIVITY

The concentration-averaged CH_4 and *n*-C_4H_{10} diffusion coefficients in mixtures were estimated using Eq. (5.2) and are presented in Figures 5.7(a) and (b), respectively, as a function of *n*-C_4H_{10} activity in the feed mixtures. As shown in Figure 5.2(a), CH_4 diffusion coefficients are independent of methane fugacity (or concentration). In mixtures, *n*-C_4H_{10} swells the polymer matrix, thereby increasing the FFV, which increases CH_4 diffusivity in the polymer. At each temperature, the CH_4 diffusion coefficients increase systematically as *n*-C_4H_{10} activity in the feed mixture increases, as

illustrated in Figure 5.7(a). Plasticization increases n-C_4H_{10} diffusion coefficients in the polymer, as shown in Figure 5.7(b). However, there is no measurable difference between the pure gas and mixed gas diffusivity values. That is, the effect of CH_4 on n-C_4H_{10} diffusion coefficients is negligible.

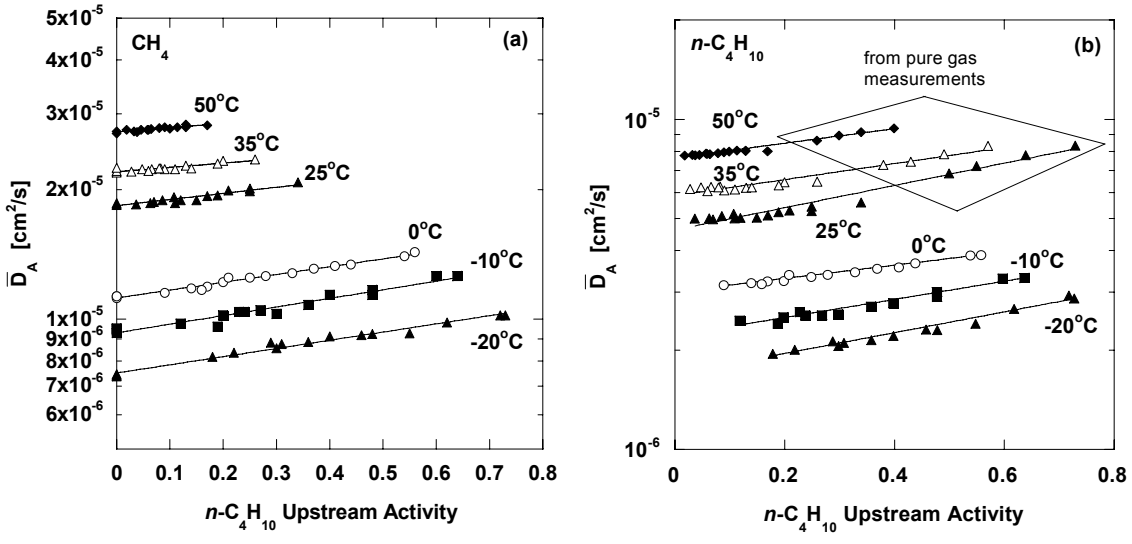

Figure 5.7 The average effective diffusion coefficient of: (a) CH_4 and (b) n-C_4H_{10} as a function of n-C_4H_{10} activity in the feed mixtures.

The local effective diffusion coefficient, D_A, is a measure of the ability of a penetrant to migrate through a polymer at a particular, well-defined penetrant concentration [6]. Pure gas D_A values were calculated from the slope of the sorption isotherm [8] and the pressure dependence of permeability as follows [14]:

$$D_A\left(C_{A,2}\right)=\left[P_A+f_{A,2}\frac{dP_A}{df_{A,2}}\right]_{f_{A,2}}\left(\frac{df_A}{dC_A}\right)_{f_{A,2}} \tag{5.4}$$

The local effective diffusion coefficients of n-C_4H_{10} in n-C_4H_{10}/CH_4 mixtures were also calculated using Eq. (5.4) because n-C_4H_{10} permeability, diffusivity, and solubility in

these mixtures are essentially unaffected by the presence of CH_4. In Eq. (5.4), $dP_A/df_{A,2}$ is estimated from the *n*-C_4H_{10} fugacity dependence of *n*-C_4H_{10} mixture permeability in the polymer (*i.e.,* the slopes in Figure 5.5), and df_A/dC_A is estimated from the pure gas sorption isotherms of *n*-C_4H_{10} in PDMS [8]. Figure 5.8(a) presents D_A values for *n*-C_4H_{10} in mixtures as a function of *n*-C_4H_{10} concentration. The trend is similar to that in Figure 5.7(b). High levels of *n*-C_4H_{10} sorption plasticize the membrane, which increases the *n*-C_4H_{10} diffusion coefficient.

The local effective diffusion coefficients of CH_4 in mixtures, which depend on *n*-C_4H_{10} concentration in the polymer, are estimated using Eq. (B.6). The ratio of the local effective diffusion coefficient of *n*-C_4H_{10}, D_A, to the local effective diffusion coefficient of CH_4, D_B, is obtained by taking the derivative of Eq. (B.6) with respect to $f_{A,2}$:

$$\frac{D_A\left(C_{A,2}\right)}{D_B\left(C_{A,2}\right)} = \left[\frac{d}{dC_A}\left(\frac{P_A f_{A,2} S_B}{P_B}\right)\right]_{f_{A,2}} \tag{5.5}$$

In Eqs. (5.5) and (5.6), the subscripts A and B refer to *n*-C_4H_{10} and CH_4, respectively. D_A was determined using Eq. (5.4). The following expression for D_B can be derived from Eq. (5.5):

$$D_B\left(C_{A,2}\right) = \frac{D_A P_B^{\,2}}{S_B P_B D_A + P_A f_{A,2}\left[\frac{dS_B}{dC_A} P_B - S_B \frac{dP_B}{dC_A}\right]} \tag{5.6}$$

where dP_B/dC_A is estimated from the *n*-C_4H_{10} concentration dependence of the CH_4 mixture permeability data (*i.e.,* the slopes in Figure 5.4(b)), and dS_B/dC_A is determined from the *n*-C_4H_{10} concentration dependence of the CH_4 mixture solubility data (see Figure 4.7(b)). Figure 5.8(b) presents calculated values of D_A for CH_4 in mixtures as a function of *n*-C_4H_{10} concentration at the upstream side of the membrane. Similar to the

data reported in Figure 5.7(a), the local effective diffusion coefficient of CH_4 increases as n-C_4H_{10} concentration increases.

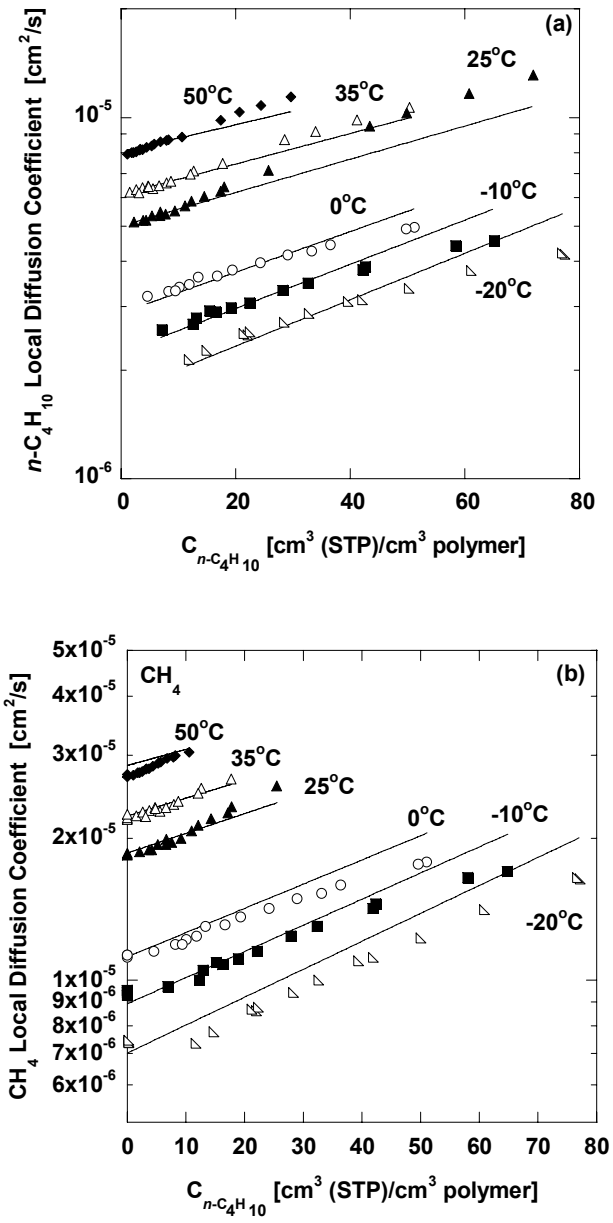

Figure 5.8 Local diffusion coefficient as a function of n-C_4H_{10} concentration in the polymer: (a) n-C_4H_{10} and (b) CH_4. The lines represent a best fit of Eq. (5.16) using the parameters in Table 5.2.

5.6 EFFECT OF CONCENTRATION ON ACTIVATION ENERGY OF PERMEATION AND DIFFUSION

The temperature dependence of gas permeability in mixtures can be described using Eq. (2.9), which is the same equation used for pure gas permeability. The activation energy of permeation, E_P, of CH_4 at a particular *n*-C_4H_{10} upstream concentration in the polymer can be calculated from the data in Figure 5.4(b) as follows:

$$E_P^C = -R\left(\frac{d\ln P_A}{d\left(1/T\right)}\right)_C \tag{5.7}$$

where $E_P{}^C$ is the activation energy of permeation at a particular *n*-C_4H_{10} upstream concentration in the polymer. Figure 5.9(a) presents CH_4 activation energy of permeation as a function *n*-C_4H_{10} concentration at the upstream face of the PDMS film. The error bars are determined using the propagation of errors method [2]. The CH_4 activation energy of permeation decreases as *n*-C_4H_{10} concentration in the polymer increases. For example, it decreases from 6.8 ± 0.5 kJ/mol in pure gas to 5.1 ± 0.5 kJ/mol in the presence of 60 cm^3(STP) *n*-C_4H_{10} /(cm^3 polymer). Figure 5.9(b) presents *n*-C_4H_{10} activation energy of permeation as a function *n*-C_4H_{10} concentration in PDMS, and it is nearly constant or perhaps decreases slightly with increasing upstream *n*-C_4H_{10} concentration, going from -8.2 ± 0.5 kJ/mol in pure gas to -8.9 ± 0.5 kJ/mol in the presence of 60 cm^3(STP) *n*-C_4H_{10} /(cm^3 polymer). The change in E_P with *n*-C_4H_{10} concentration is near the uncertainty in the E_P values. The infinite dilution *n*-C_4H_{10} activation energy of permeation in Figure 5.9(b) (*i.e.,* -8.2 kJ/mol) is slightly different from that reported earlier in the pure gas section (*i.e.,* -7 kJ/mol). The value in Figure 5.9(b) is estimated from mixture data from -20 to 50°C, while that reported in the pure gas section is determined from pure gas data at 25, 35, and 50°C.

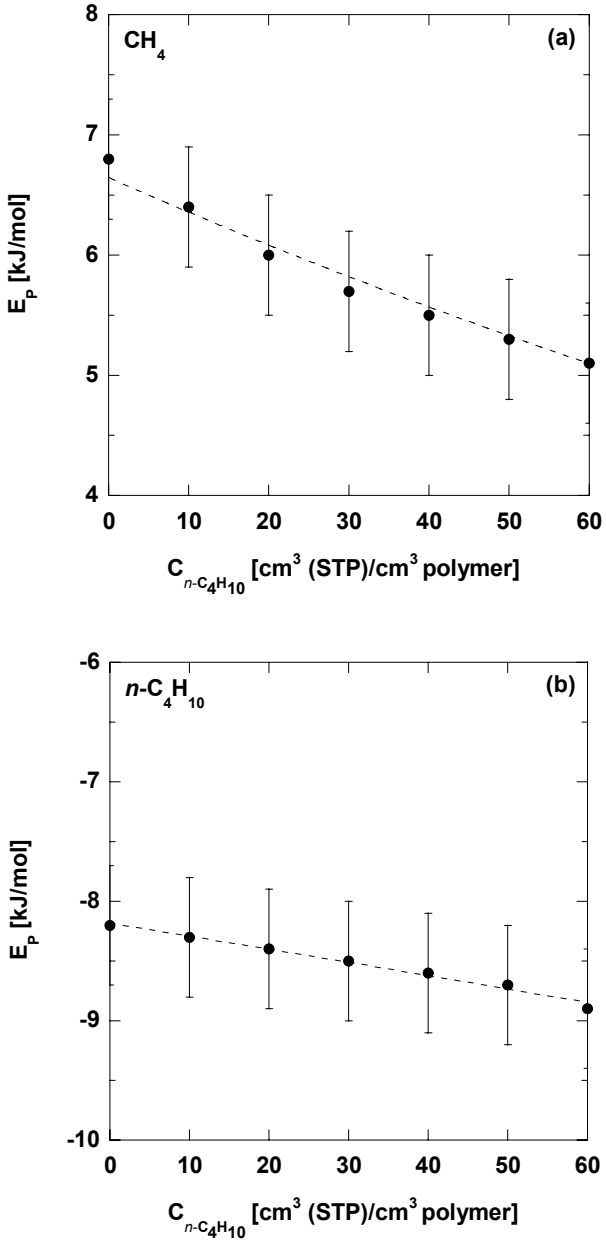

Figure 5.9 Activation energy of permeation of (a) CH_4 and (b) n-C_4H_{10} in PDMS as a function of n-C_4H_{10} concentration in the polymer at the upstream face of the film. The error bars are determined using the propagation of errors method [2].

The activation energy of diffusion, E_D, as a function n-C_4H_{10} concentration can be determined using Eq. (2.11) and the known values of E_P and ΔH_S values recorded in the previous chapter. Figures 5.10(a) and (b) present CH_4 and n-C_4H_{10} E_D values as a function of n-C_4H_{10} concentration in the polymer. The activation energy of diffusion of CH_4 in mixtures is similar to that in pure gas. The n-C_4H_{10} E_D decreases only very slightly, if at all, with increasing n-C_4H_{10} concentration in the polymer. The infinite dilution n-C_4H_{10} activation energy of diffusion in Figure 5.10(b) (*i.e.,* 14.7 kJ/mol) is slightly different from the value reported earlier in the pure gas section (*i.e.,* 17 kJ/mol). The value in Figure 5.10(b) is estimated from mixture data from -20 to 50°C, while that reported in the pure gas section is determined from pure gas data at 25, 35, and 50°C.

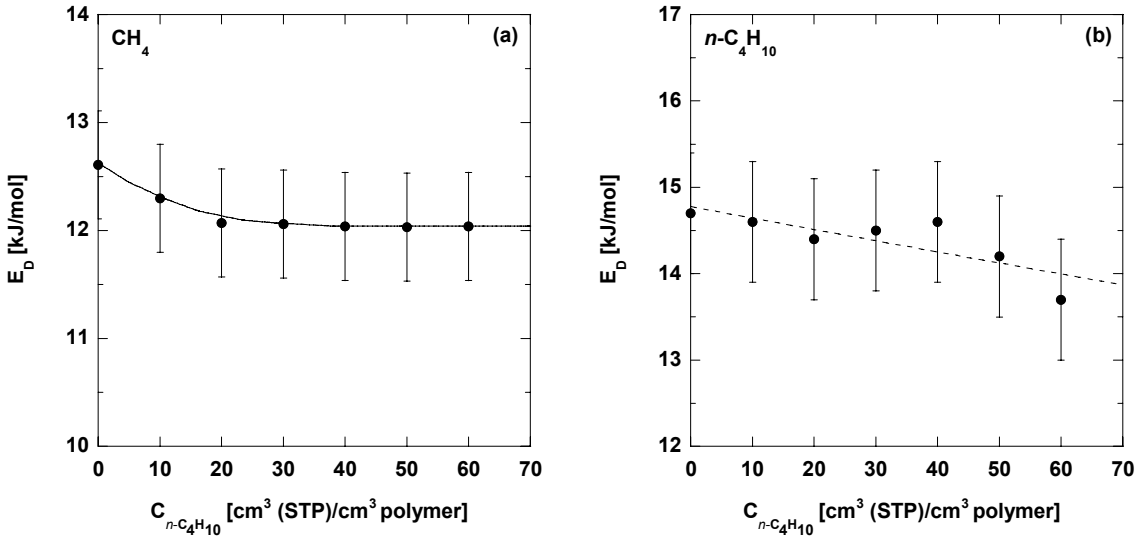

Figure 5.10 Activation energy of diffusion of (a) CH_4 and (b) n-C_4H_{10} in PDMS as a function of n-C_4H_{10} concentration in the polymer.

5.7 MODELING

Several theoretical models were evaluated for their ability to describe the experimental pure and mixed gas data. Two models, based on free volume theory and activated state theory, were used to describe the diffusion coefficient data, and the results from these models were compared. Also, the pure and mixed gas permeability data were described using a Maxwell-Stefan model, which allows one to rationally and consistently account for coupling between the transport of one component and another in a mixture. The use of the experimental data, particularly the mixture diffusion and permeability data, provides a more rigorous test of these models than one could obtain with pure gas data alone.

5.7.1 FFV Model

The free volume of a polymer/penetrant mixture is often used to correlate penetrant diffusivity as shown below [9]:

$$D_A = A\exp\left(\frac{-B}{FFV}\right) \tag{5.8}$$

where FFV is the fractional free volume of a polymer/penetrant mixture, and A and B are adjustable constants. Strictly speaking, Eq. (5.8) applies to the penetrant self-diffusion coefficients rather than mutual diffusion coefficients [9]. However, in most cases, the local effective mutual diffusion coefficient is not more than 15% lower than the self diffusion coefficient in this study, which is within the uncertainty in the diffusion coefficients, so Eq. (5.8) can be used to describe the effect of free volume on local, effective mutual diffusion coefficients. This model can be extended to describe the influence of temperature and penetrant concentration on diffusion coefficients as described below.

The n-C_4H_{10}/CH_4 mixture sorption and dilation data in PDMS, presented in the previous chapter, can be used to estimate the local fractional free volume (FFV) of the polymer/gas system at a particular n-C_4H_{10} and CH_4 fugacity in the mixture. For these calculations, FFV is calculated as follows [15]:

$$FFV = \frac{v_{mix} - v_{o,mix}}{v_{o,mix}} \tag{5.9}$$

where v_{mix} is the specific volume of the polymer/gas mixture, which is computed from experimental sorption and dilation data:

$$v_{mix} = w_p \frac{1+\alpha(T-25)-\beta p}{\rho_{25}} + w_A \frac{\overline{V}_A}{MW_A} + w_B \frac{\overline{V}_B}{MW_B} \tag{5.10}$$

w_p, w_A and w_B are the weight fractions of polymer, n-C_4H_{10}, and CH_4, respectively, in the polymer/penetrant mixture. $\overline{V}_A$ and $\overline{V}_B$ are the penetrant partial molar volumes of n-C_4H_{10} and CH_4, respectively, determined from pure gas dilation measurements [8]. MW_A and MW_B are the molecular weights of n-C_4H_{10} and CH_4, respectively. ρ_{25} is the density of penetrant-free polymer at 25°C (in g/cm^3), α is the thermal expansion coefficient of the polymer determined from dilation measurements (9.1x10^{-3} /°C) [8], β is the isothermal compressibility of the polymer [16], p is the total pressure of the mixture, and T is the temperature of the system (°C). $v_{o,mix}$ in Eq. (5.10) is the occupied volume of the polymer/penetrant mixture, which is calculated as follows:

$$v_{o,mix} = w_p v_{o,p} + w_A v_{o,A} + w_B v_{o,B} \tag{5.11}$$

where w_p, w_A and w_B are the weight fractions of the polymer, n-C_4H_{10}, and CH_4, respectively, in the polymer/penetrant mixture. $v_{o,p}$, $v_{o,A}$, and $v_{o,B}$ are the specific occupied volume of pure polymer, n-C_4H_{10}, and CH_4, respectively. These occupied volumes are estimated as 1.3 times the van der Waals volume, which are determined from Bondi's

group contribution method [17]. The factor of 1.3 is an approximation typically used for the packing density (at 0 Kelvin) of infinitely long cylindrical molecules, such as polymers [17,18]. For smaller molecules, Bondi suggested using the factors of 1.5 and 1.4 for CH_4 and *n*-C_4H_{10}, respectively, rather than 1.3, which is used ubiquitously in calculation of polymer FFV [17]. However, there is only a slight difference between the FFV values estimated using these factors (*i.e.,* 1.5 and 1.4 for CH_4 and *n*-C_4H_{10}) and those estimated using 1.3 for CH_4 and *n*-C_4H_{10}. For instance, at -20°C, when the CH_4 and *n*-C_4H_{10} concentrations are 3.5 and 61 cm^3(STP)/cm^3 in the polymer, respectively, the FFV calculated using the factors 1.5 and 1.4 for CH_4 and *n*-C_4H_{10}, respectively, is 0.19, and that estimated using 1.3 for CH_4 and *n*-C_4H_{10} is 0.20. The difference between these two FFVs is only 5%, which is within the experimental uncertainty. Since the factor 1.3 is essentially universally known and familiar to the readers, it is used to estimate the occupied volumes of the pure polymer, *n*-C_4H_{10}, and CH_4 in this study [18].

Based on Eq. (5.9) and the experimental data, FFV always increases with increasing CH_4 and *n*-C_4H_{10} concentration in the polymer. Figures 5.11(a) and (b) present the local effective diffusion coefficients of *n*-C_4H_{10} and CH_4, respectively, at various *n*-C_4H_{10} and CH_4 concentrations and temperatures, as a function of inverse FFV in the polymer/penetrant mixture. Clearly, the FFV, as estimated in this work, does not provide a parameter that perfectly collapses all of the diffusivity data to a single master curve. However, to a rough approximation, the experimental data obey the model. The best-fit values for *A* are 1.67 ± 0.01 x10^{-4} and 2.76 ± 0.01 x10^{-4} cm^2/s for *n*-C_4H_{10} and CH_4, respectively. The best-fit values for *B* are 0.697 ± 0.001 and 0.540 ± 0.001 for *n*-C_4H_{10} and CH_4, respectively. There is usually a correlation between *B* in Eq. (5.8) and penetrant size [1]. In general, *B* increases as penetrant size increases [1], which is consistent with the result in this study.

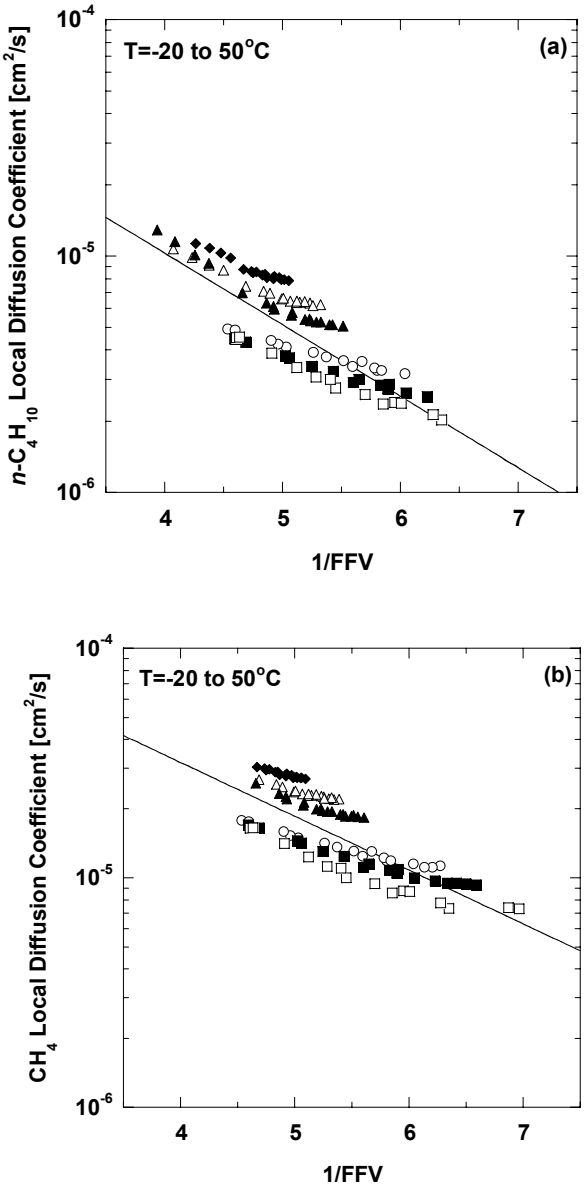

Figure 5.11 Correlation between fractional free volume of the polymer/penetrant mixtures and effective diffusion coefficients of: (a) *n*-C_4H_{10} and (b) CH_4, in PDMS at various penetrant concentrations and temperatures. The temperature ranges from -20 to 50°C: (□) -20°C, (■) -10°C, (○) 0°C, (▲) 25°C, (△) 35°C, and (♦) 50°C. The lines represent best fits to Eq. (5.8).

5.7.2 Activated Diffusion Model

Another approach for describing the concentration and temperature dependence of diffusion coefficients is based on activated state diffusion theory. Prabhakar and co-workers have included the concentration dependence of diffusivity based on a concentration dependence of E_D, which is modeled empirically as follows [11]:

$$E_D = E_D^o\left(1 - kC\right) \tag{5.12}$$

where E_D^o is the activation energy of diffusion at infinite dilution, and k is an adjustable constant, which is independent of temperature. The linear free energy relationship correlates D_o and E_D in Eq. (2.11) as follows:

$$\ln D_o = a'\frac{E_D}{R} - b' \tag{5.13}$$

where a' and b' are adjustable parameters. Based on diffusivity data for light gases in several rubbery polymers, van Amerongen reported an a' value of 0.0023 K^{-1} and a b' value of 9.7, when D_o has units of cm^2/s [19]. More recent a' and b' values, based on the original diffusivity data from van Amerongen as well as other reports of D_o and E_D values for rubbery polymers, are 0.002 K^{-1} and 8.3, respectively [11]. Substituting Eq. (5.13) into Eq. (2.11) yields [11]:

$$D_A\left(C_A\right) = e^{-b'}\exp\left[\lambda E_D^o\left(1 - kC_A\right)\right] \tag{5.14}$$

where

$$\lambda = \frac{1}{R}\left(a' - \frac{1}{T}\right)$$

From Eqs. (2.4), (2.5), and (5.14), the pure gas permeability can be written as follows ($f_{B,1} = 0$, $C_{A,1} = 0$) [11]:

$$P_A = \frac{e^{-b'}}{f_{A,2}} \frac{\exp\left[\lambda E_D^o \left(1 - kC_{A,2}\right)\right] - \exp\left[\lambda E_D^o\right]}{\left(-\lambda E_D^o k\right)} \tag{5.15}$$

This approach has been successfully used to model pure gas permeability in rubbery polymers such as PDMS, polyethylene (PE), and crosslinked poly(ethylene glycol diacrylate) (XLPEGDA) as a function of temperature and pressure [9,11].

This model can be applied to the mixture *n*-C_4H_{10} permeability data in PDMS since *n*-C_4H_{10} permeability is essentially unaffected by the presence of CH_4. The concentration of *n*-C_4H_{10} at the upstream face of the film, $C_{A,2}$, is determined from experimental mixture sorption data reported in Chapter 4. The value of a' is set to 0.002 K^{-1}, as suggested by Prabhakar *et al.* [11]. b', k, and E_D^o are treated as adjustable parameters. The best-fit of the model is represented by the lines in Figure 5.5, which describes the experimental data well. The best-fit values of E_D^o, b', and k are recorded in Table 5.2. The best fit value of E_D^o is 14.8 ± 0.1 kJ/mol which agrees, within the uncertainty, with the E_D value at infinite dilution estimated using Eq. (2.11) and mixture diffusivity data from -20 to 50°C (*i.e.,* 14.7 kJ/mol), and it is close to Barrer *et al.*'s reported E_D value (*i.e.,* 18 kJ/mol). The best fit value for b', 9.79 ± 0.01, is similar to that reported in the literature. Van Krevelen [18] reported a value of 9.2 for b', van Amerongen [19] reported a value of 9.7, and Prabhakar *et al.* [11] reported a value of 8.3. The best fit value of k is 4.1 ± 0.1 x 10^{-3} cm^3/cm^3(STP), which is similar to the value of k reported by Prabhakar *et al.* [11] for C_3H_8 in PDMS, which was 5.35 x 10^{-3} cm^3/cm^3(STP).

Table 5.2 Activated state model parameters for permeability data

Penetrant	b'	k x10^3 (cm^3/cm^3(STP))	E_D^o (kJ/mol)
n-C_4H_{10}	9.79 ± 0.01	4.1 ± 0.1	14.8 ± 0.1
CH_4	8.69 ± 0.01	4.1 ± 0.1	13.5 ± 0.1

This model has been extended to describe CH_4 mixture permeability in PDMS in the presence of n-C_4H_{10} in the polymer. As illustrated in Figure 5.8(a), CH_4 diffusion coefficients increase with increasing n-C_4H_{10} concentration, but they are independent of CH_4 concentration (as shown in the pure gas results). Therefore, the effective diffusion coefficient of CH_4 in the mixture, D_B, is written as follows:

$$D_B\left(C_A\right) = e^{-b'} \exp\left[\lambda E_D^o\left(1 - k_B C_A\right)\right] \tag{5.16}$$

where C_A is the concentration of n-C_4H_{10} in the polymer. By substituting Eq. (5.14) and (5.16) into Eq. (B.6), CH_4 mixture permeability in PDMS in the presence of n-C_4H_{10} can be written as follows:

$$P_B = P_A f_{A,2} S_B \frac{e^{-b'_B}}{e^{-b'_A}} \frac{e^{\lambda E^o_{D_B}}}{e^{\lambda E^o_{D_A}}} \frac{\lambda E^o_{D_B} k_B - \lambda E^o_{D_A} k_A}{\exp\left[\lambda\left(E^o_{D_B} k_B - E^o_{D_A} k_A\right) C_{A,2}\right] - 1} \tag{5.17}$$

where the subscripts A and B represent n-C_4H_{10} and CH_4, respectively. P_A is the experimental mixture permeability coefficients of n-C_4H_{10}, and $f_{A,2}$ is the upstream fugacity of n-C_4H_{10} in the mixture. S_B is the solubility coefficient of CH_4 at the upstream face of the membrane, which is determined from mixture sorption data [8]. The value of a is set to 0.002 K^{-1}, as suggested by Prabhakar *et al.* [11]. The values of b'_A, k_A, and $E^o_{D_A}$ were previously determined by independently fitting the mixture n-C_4H_{10} permeability data to Eq. (5.15). For simplicity, plasticization in PDMS induced by

n-C_4H_{10} sorption is presumed to have the same effect on CH_4 and n-C_4H_{10} diffusion coefficients (*i.e.,* $k_B = k_A = 4.1 \times 10^{-3}$ cm^3/cm^3(STP)). Therefore, the only adjustable parameters in Eq. (5.17) are b'_B and $E^o_{D_B}$. The best-fit of the model is presented in Figures 5.4(a) and (b), and it describes the experimental data reasonably well. The best-fit values of the adjustable constants for CH_4, b'_B and $E^o_{D_B}$, are recorded in Table 2. $E^o_{D_B}$ is 13.5 ± 0.1 kJ/mol, which is similar to the estimated E_D value at infinite dilution based on pure and mixed gas CH_4 diffusivity data (*i.e.,* 12.6 kJ/mol). The best fit value for b'_B is 8.69 ± 0.01, which is similar to values reported in the literature [11,18,19].

Using the best fit parameters in Table 5.2 along with Eqs. (5.14) and (5.16), the effective diffusion coefficients of n-C_4H_{10} and CH_4 in PDMS can be predicted. The model fit, which is represented by the lines in Figures 5.8(a) and (b), provides a reasonable estimation for n-C_4H_{10} and CH_4 effective diffusion coefficient in PDMS.

5.7.3 Maxwell-Stefan Model

The mixed gas permeability data were fit to the ternary Maxwell-Stefan model to explore the importance of coupling effects in n-C_4H_{10}/CH_4 mixture permeation in PDMS [20]. The Maxwell-Stefan equations for a ternary system (2 penetrants, 1 polymer) are presented in Appendix C. Pure gas data at 25, 35, and 50°C were used to determine $\langle D_A \rangle_o$, $\langle D_B \rangle_o$, and β. $\langle D_A \rangle_o$ and $\langle D_B \rangle_o$ are the infinite dilution diffusion coefficients of n-C_4H_{10} and CH_4, respectively. β is an adjustable parameter that describes the effect of penetrant weight fraction in the polymer on penetrant diffusion. The best fit value of β is 7.6 ± 0.1. The values of $\langle D_A \rangle_o$ and $\langle D_B \rangle_o$ at various temperatures are recorded in Table 5.3.

The mixture data were fit using Eqs. (C.17) and (C.18) by treating $\langle D_{BA} \rangle_o$ as an adjustable parameter. Figures 5.12(a) and (b) present the permeability of n-C_4H_{10} and CH_4, respectively, in n-C_4H_{10}/CH_4 mixtures at 35°C as a function of n-C_4H_{10} activity. The

figures show the predictions of the Maxwell-Stefan model using the best-fit $\langle D_{BA} \rangle_o$ value at this temperature (3.3±0.3 x10^{-6}cm^2/s). For reference, the mutual diffusion coefficient of CH_4 in liquid *n*-C_4H_{10} at 35°C, determined using the Wilke-Chang equation, is 1.4x10^{-4} cm^2/s. The best-fit $\langle D_{BA} \rangle_o$ values at 25 and 50°C are 7.9±0.8 x10^{-6} and 7.7±0.8 x10^{-6} cm^2/s, respectively. The frictional coupling terms estimated using Eqs. (C.19) and (C.20), which indicate the fraction of convective flow contribution to the overall flux (*i.e.,* diffusion + convective) in mixture permeation experiments, are small in this study (*i.e.,* $\varphi_A < 0.05$ and $\varphi_B < 0.15$), as shown in Figure 5.13. Since the uncertainty in the mixture permeability coefficients are of the same magnitude as the coupling terms, these terms represent an essentially negligible contribution to the penetrant flux in the film. The ternary Maxwell-Stefan equations without coupling effects (*i.e.,* Eqs. (C.21) and (C.22)) describe the experimental data reasonably well (see Figures 5.12(a) and (b)). Those equations are identical to the Fick's law flux expression for binary mixture transport through a polymer membrane (*c.f.,* Eqs. (B.1), (B.2), and (2.2)). In this regard, the binary transport model adequately describes the permeation of *n*-C_4H_{10}/CH_4 mixtures in PDMS.

Table 5.3 $\langle D_A \rangle_o$ and $\langle D_B \rangle_o$ in PDMS at various temperatures

T (°C)	$\langle D_A \rangle_o$ x 10^6 (cm^2/s)	$\langle D_B \rangle_o$ x 10^6 (cm^2/s)
25	5.8 ± 0.4	18 ± 1
35	5.8 ± 0.4	22 ± 2
50	7.6 ± 0.5	27 ± 2

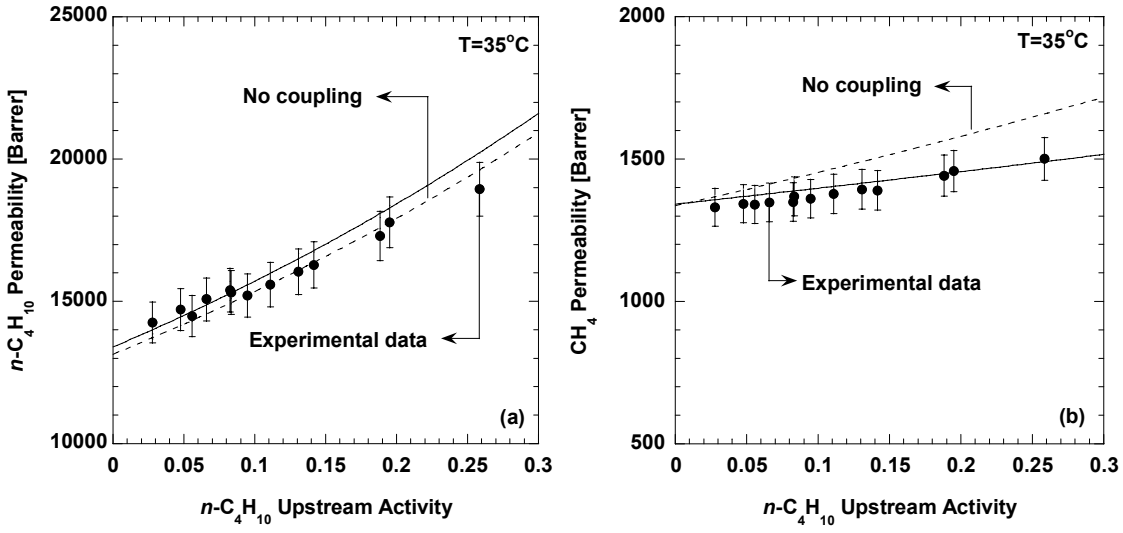

Figure 5.12 The mixed gas permeability of (a) n-C_4H_{10} and (b) CH_4 in PDMS at 35°C as a function of n-C_4H_{10} upstream activity. The filled symbols (●) represent the experimental data. The solid line represents the predictions from the Maxwell-Stefan equations with the best fit $\left\langle D_{BA} \right\rangle_o$ of 3.3x10^{-6} cm^2/s. The dashed line is prediction from the Maxwell-Stefan equations without coupling effects (*i.e.*, $\varepsilon_A=\varepsilon_B=0$).

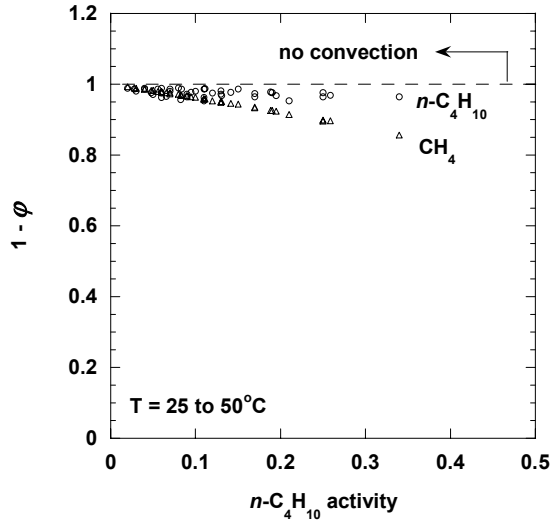

Figure 5.13 The fraction of convective flow contribution to the overall flux in n-C_4H_{10}/CH_4 mixture permeation in PDMS estimated from the Maxwell-Stefan model.

5.8 SELECTIVITY

5.8.1 Permeability Selectivity

Mixed gas *n*-C_4H_{10}/CH_4 permeability selectivity in PDMS as a function of *n*-C_4H_{10} fugacity is presented in Figure 5.14. The permeability selectivity increases as *n*-C_4H_{10} fugacity increases and temperature decreases. For example, at 25°C, the mixed gas selectivity increases from 13 to 16 as *n*-C_4H_{10} fugacity increases from 0.08 to 0.76 atm (activity increases from 0.04 to 0.34). At -20°C, the selectivity increases from 43 to 62 as *n*-C_4H_{10} fugacity increases from 0.08 to 0.32 atm (activity increases from 0.18 to 0.72). The effect of temperature on mixed gas permeability selectivity is greater than that of *n*-C_4H_{10} fugacity. The permeability selectivity increases by almost an order of magnitude as temperature decreases from 50 to -20°C. The lines in Figure 5.14 represent *n*-C_4H_{10}/CH_4 permeability selectivities in PDMS estimated from pure gas measurements.

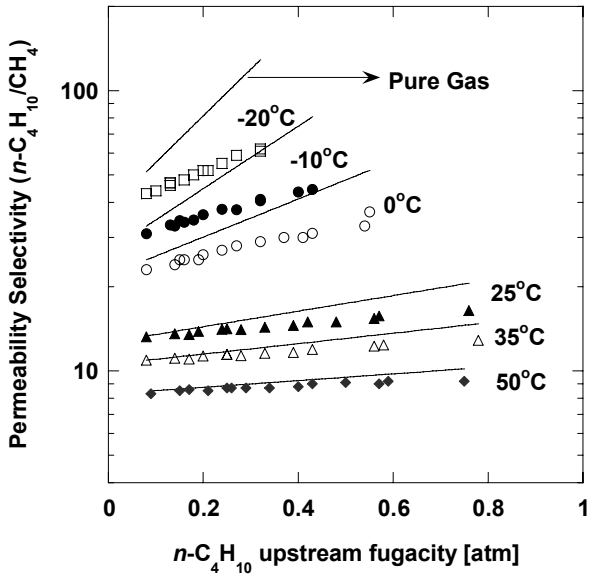

Figure 5.14 Mixed gas permeability selectivity of *n*-C_4H_{10}/CH_4 in PDMS as a function of *n*-C_4H_{10} upstream fugacity in the mixtures and temperature. The lines are estimates from pure gas data.

In general, the pure gas permeability selectivities agree with those determined from the mixed gas data at higher temperatures and lower *n*-C_4H_{10} fugacity. In these cases, the concentration of *n*-C_4H_{10} in the polymer is low. However, as temperature decreases and *n*-C_4H_{10} fugacity increases, conditions favoring high *n*-C_4H_{10} sorption, the pure and mixed gas selectivities become different, and the mixed gas selectivity is always lower than the pure gas selectivity.

Table 5.4 compares pure and mixed gas *n*-C_4H_{10}/CH_4 permeability, solubility, and diffusivity selectivities at various temperatures. At higher temperatures (*i.e.,* 25, 35, and 50^oC), permeability selectivities estimated from pure gas measurements are similar to those determined from the mixture data. However, as temperature decreases, the deviation between pure and mixed gas permeability selectivities becomes more significant. For instance, at -20^oC, the selectivity of a 6 mol% *n*-C_4H_{10} mixture at 4.4 atm feed pressure is 40% lower than that estimated from pure gas data. The *n*-C_4H_{10} permeability, solubility, and diffusivity in mixtures are similar to the pure gas values. In the pure gas case, CH_4 permeability, solubility, and diffusivity are independent of fugacity, while in mixtures, they increase as *n*-C_4H_{10} fugacity (or activity) increases. For this reason, the mixture permeability, solubility, and diffusivity selectivities are less than those estimated from pure gas measurements. As shown in Table 5.4, the deviation between pure and mixed gas permeability selectivities is a result of both lower solubility and diffusivity selectivities in mixtures relative to those in pure gas.

Table 5.4 Effect of temperature on pure and mixed gas *n*-C_4H_{10}/CH_4 permeability, solubility, and diffusivity selectivities

T (^oC)	Permeability Selectivity			Solubility Selectivity			Diffusivity Selectivity		
	Mixed[a]	Pure[b]	Mixed/Pure	Mixed[a]	Pure[b]	Mixed/Pure	Mixed[a]	Pure[b]	Mixed/Pure
50	8.7 ± 0.3	8.9 ± 0.3	0.98 ± 0.05	30 ± 1	31 ± 1	0.98 ± 0.05	0.29 ± 0.02	0.29 ± 0.02	1.0 ± 0.1
35	11.5 ± 0.5	11.8 ± 0.5	0.97 ± 0.06	41 ± 2	42 ± 2	0.97 ± 0.07	0.28 ± 0.02	0.28 ± 0.02	1.0 ± 0.1
25	14.1 ± 0.6	14.8 ± 0.6	0.95 ± 0.06	52 ± 3	54 ± 3	0.97 ± 0.08	0.27 ± 0.02	0.28 ± 0.02	0.98 ± 0.09
0	27 ± 1	32 ± 2	0.84 ± 0.06	99 ± 5	107 ± 5	0.93 ± 0.07	0.27 ± 0.02	0.30 ± 0.02	0.89 ± 0.09
-10	38 ± 2	51 ± 2	0.75 ± 0.06	148 ± 7	167 ± 8	0.88 ± 0.06	0.25 ± 0.02	0.30 ± 0.02	0.85 ± 0.09
-20	55 ± 4	93 ± 5	0.59 ± 0.08	209 ± 10	277 ± 14	0.75 ± 0.06	0.26 ± 0.02	0.33 ± 0.02	0.79 ± 0.09

[a]Feed composition: 6 mol% *n*-C_4H_{10}; feed pressure: 4.4 atm. The permeate side of the film was swept with Helium.
[b]Estimated using *n*-C_4H_{10} mixture properties at the same upstream condition as specified above[a] and CH_4 pure gas properties recorded in Table 5.1 and [8].

5.8.2 Diffusivity Selectivity

Figure 5.15 presents n-C_4H_{10}/CH_4 mixture diffusivity selectivity as a function of n-C_4H_{10} concentration in the polymer at each temperature. Relative to solubility selectivity (shown in the previous chapter), n-C_4H_{10}/CH_4 diffusivity selectivity changes much less with n-C_4H_{10} concentration and temperature. Intuitively, the swelling of the polymer matrix should increase the diffusion of the larger molecules (*e.g.,* n-C_4H_{10}) more than that of the smaller molecules (*e.g.,* CH_4), as suggested by Pinnau and He [10]. However, this effect is not significant in a weakly size-sieving material like PDMS. Plasticization increases the diffusivity of both penetrants by similar amount, so it has little influence on diffusivity selectivity.

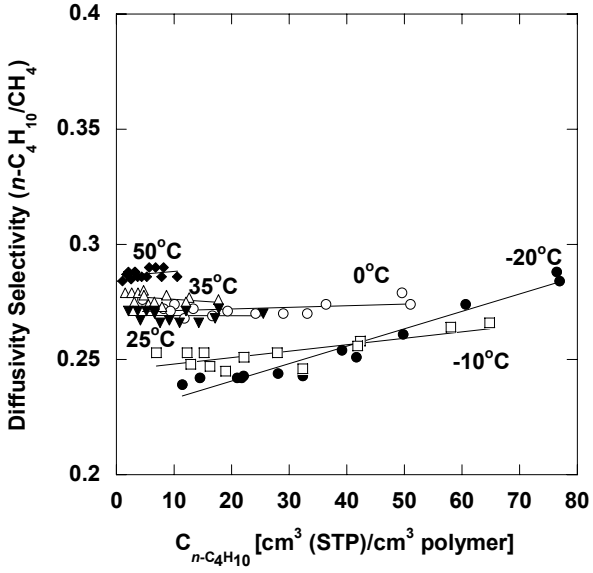

Figure 5.15 Mixed gas diffusivity selectivity of n-C_4H_{10}/CH_4 in PDMS as a function of n-C_4H_{10} concentration in the polymer and temperature. The lines represent linear regression fits to the data.

Figure 5.16 presents the ratio of overall, solubility, and diffusivity selectivities at 0^oC to those in the limit of 0 atm of *n*-C_4H_{10} fugacity at 50^oC, which is the highest temperature studied. At 50^oC, *n*-C_4H_{10} is least condensable and has little influence on *n*-C_4H_{10}/CH_4 selectivities. Solubility selectivity increases by almost a factor of three as temperature decreases from 50 to 0^oC. However, the increase in solubility selectivity as *n*-C_4H_{10} activity increases from 0.09 to 0.56 is less than 40%. On the other hand, diffusivity selectivity is practically independent of temperature and *n*-C_4H_{10} activity. Based on Figure 5.16, the increase in mixed gas *n*-C_4H_{10}/CH_4 permeability selectivity with increasing *n*-C_4H_{10} activity is due to the increase in solubility selectivity, not diffusivity selectivity as had been previously speculated [10].

5.9 CONCLUSIONS

The presence of high concentrations of *n*-C_4H_{10} in PDMS enhances CH_4 and *n*-C_4H_{10} diffusivity, solubility and, consequently, permeability. High sorption of *n*-C_4H_{10} swells the polymer, leading to increases in CH_4 and *n*-C_4H_{10} diffusivity. CH_4 solubility increases with increasing *n*-C_4H_{10} concentration due to the thermodynamically more favorable environment created by *n*-C_4H_{10} in the polymer [8]. The enhancement in CH_4 permeability in *n*-C_4H_{10}/CH_4 mixtures in PDMS is not only due to the increase in CH_4 diffusivity, as suggested previously [10], but also due to the increase in CH_4 solubility in the mixture, as shown in Chapter 4. In contrast, the presence of CH_4 does not measurably affect *n*-C_4H_{10} solubility, diffusivity, or permeability.

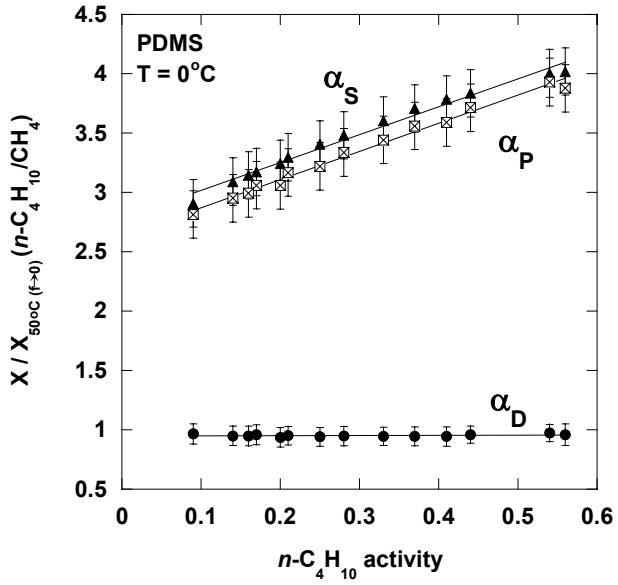

Figure 5.16 The ratio of permeability, solubility, and diffusivity selectivities at 0°C to infinite dilution values of these selectivities at 50°C as a function of n-C_4H_{10} activity.

While the diffusion coefficients of both CH_4 and n-C_4H_{10} increase with increasing n-C_4H_{10} activity, the n-C_4H_{10}/CH_4 diffusivity selectivity in PDMS remains relatively constant. It hardly changes with temperature as well. The solubility selectivity is mainly responsible for increases in overall selectivity with increasing n-C_4H_{10} activity and decreasing temperature.

5.10 REFERENCES

[1] S. Matteucci, Y. Yampolskii, B. D. Freeman, and I. Pinnau, "Transport of gases and vapors in glassy and rubbery polymers", in B. D. Freeman (Ed.), Materials Science of Membranes, John Wiley & Sons, Ltd., Chichester, 2006.

[2] P. R. Bevington and D. K. Robinson, Data Reduction and Error Analysis for the Physical Sciences, 3rd ed., McGraw-Hill, New York, NY, 2002.

[3] T. C. Merkel, V. I. Bondar, K. Nagai, B. D. Freeman, and I. Pinnau, "Gas sorption, diffusion, and permeation in poly(dimethylsiloxane)", Journal of Polymer Science: Part B: Polymer Physics, 38 (2000) 415-34.

[4] S. A. Stern, V. M. Shah, and B. J. Hardy, "Structure-permeability relationships in silicone polymers", Journal of Polymer Science: Part B: Polymer Physics, 25 (1987) 1263-98.

[5] I. Pinnau, C. G. Casillas, A. Morisato, and B. D. Freeman, "Hydrocarbon/hydrogen mixed gas permeation in poly(1-trimethylsilyl-1-propyne) (PTMSP), poly(1-phenyl-1-propyne) (PPP), and PTMSP/PPP blends", Journal of Polymer Science: Part B: Polymer Physics, 34 (1996) 2613-21.

[6] W. J. Koros and M. W. Hellums, "Transport properties", in J. I. Kroschwitz (Ed.), Encyclopedia of Polymer Science and Technology, Wiley, New York, 1990, pp. 724-802.

[7] R. M. Barrer, J. A. Barrie, and N. K. Raman, "Solution and diffusion in silicone rubber I - A comparison with natural rubber", Polymer, 3 (1962) 595-603.

[8] R. D. Raharjo, B. D. Freeman, and E. S. Sanders, "Pure and mixed gas CH_4 and *n*-C_4H_{10} sorption and dilation in poly(dimethylsiloxane)", Journal of Membrane Science, 292 (2007) 45-61.

[9] H. Lin and B. D. Freeman, "Gas permeation and diffusion in cross-linked poly(ethylene glycol diacrylate)", Macromolecules, 39 (2006) 3568-80.

[10] I. Pinnau and Z. He, "Pure- and mixed-gas permeation properties of polydimethylsiloxane for hydrocarbon/methane and hydrocarbon/hydrogen separation", Journal of Membrane Science, 244 (2004) 227-33.

[11] R. S. Prabhakar, R. Raharjo, L. G. Toy, H. Lin, and B. D. Freeman, "Self-consistent model of concentration and temperature dependence of permeability in rubbery polymers", Industrial & Engineering Chemistry Research, 44 (2005) 1547-56.

[12] B. E. Poling, J. M. Prausnitz, and J. P. O'Connell, The Properties of Gases and Liquids, 5th ed., McGraw-Hill, New York, NY, 2001.

[13] S. M. Jordan and W. J. Koros, "Permeability of pure and mixed gases in silicone rubber at elevated pressures", Journal of Polymer Science: Part B: Polymer Physics, 28 (1990) 795-809.

[14] W. J. Koros and D. R. Paul, "Transient and steady-state permeation in poly(ethylene terephthalate) above and below the glass transition", Journal of Polymer Science, Polymer Physics Edition, 16 (1978) 2171-87.

[15] W. M. Lee, "Selection of barrier materials from molecular structure", Polymer Engineering and Science, 20 (1980) 65-9.

[16] Y. Kamiya, Y. Naito, K. Terada, K. Mizoguchi, and A. Tsuboi, "Volumetric properties and interaction parameters of dissolved gases in poly(dimethylsiloxane) and polyethylene", Macromolecules, 33 (2000) 3111-9.

[17] A. Bondi, Physical Properties of Molecular Crystals, Liquids, and Glasses, John Wiley and Sons, New York, 1968, pp. 25-52, 3-97.

[18] D. W. van Krevelen, Properties of Polymers: Their Correlation with Chemical Structures; Their Numerical Estimation and Prediction from Additive Group Contribution, 3rd ed., Elsevier Science, Amsterdam, 1990, pp. 71-107.

[19] G. J. van Amerongen, "The permeability of different rubber to gases and its relation to diffusivity and solubility", Journal of Applied Physics, 17 (1946) 972-85.

[20] D. R. Paul, "Reformulation of the solution-diffusion theory of reverse osmosis", Journal of Membrane Science, 241 (2004) 371-86.

Chapter 6: Pure and Mixed Gas CH_4 and *n*-C_4H_{10} Sorption and Dilation in Poly(1-trimethylsilyl-1-propyne)

This chapter provides the pure and mixed gas *n*-C_4H_{10} and CH_4 sorption and dilation in poly(1-trimethylsilyl-1-propyne) (PTMSP) at temperatures ranging from -20 to 35^oC. The competitive sorption effect between *n*-C_4H_{10} and CH_4 in the polymer is investigated. The dual mode sorption model is used to describe the experimental data. The dilations of PTMSP during pure and mixed gas *n*-C_4H_{10} and CH_4 sorption are determined and studied as well.

6.1 EXPERIMENTAL

6.1.1 Hysteresis Effects

No hysteresis effects were observed during the sorption measurements. Pure gas CH_4 sorption isotherms determined before and after pure gas sorption studies of *n*-C_4H_{10} were essentially the same, consistent with previous findings for PTMSP by Merkel *et al.* [1] Because physical aging can decrease the penetrant solubility values in the polymer over time [2], pure gas sorption isotherms of CH_4 and *n*-C_4H_{10} were determined before every mixture sorption measurement. If significant physical aging effects were found, the polymer sample was rejuvenated by immersing them in liquid methanol for 24 hrs, then drying at ambient 24 hrs before measurements were taken.

Unlike the sorption measurements, a small hysteresis effect was observed during the dilation measurements. The polymer sample tends to dilate more following dilation studies involving pure gas *n*-C_4H_{10} or mixtures containing *n*-C_4H_{10}. To eliminate hysteresis effects, between dilation measurements, polymer films were immersed in liquid methanol for 24 hrs and then dried at ambient conditions for 24 hrs before the next dilation measurement.

6.1.2 Checking for Isotropic Expansion

Unlike in rubbery polymers (*e.g.,* PDMS), dilations in glassy polymers, such as PTMSP are not necessarily isotropic. In addition to the length (*i.e.,* x-direction) dilation measurements, the width (*i.e.,* y-direction) and thickness (*i.e.,* z-direction) dilations of PTMSP are determined to check for isotropic expansion of the sample.

The thickness (*i.e.,* z-direction) dilation measurements were performed using a similar setup described in Chapter 3. However, for these measurements, the polymer sample in the Jerguson gauge was repositioned so that the camera monitored the cross section of the film [3]. A smaller but thicker PTMPS film (100 mm x 100 mm x 200 μm) was used to reduce the chance of sample curling, and a longer focal length lens was used to improve accuracy. The minimum detectable thickness change using this setup was 0.008 mm.

Two large sheets of PTMSP films (6.59 cm x 6.61 cm x 300 μm and 4.74 cm x 4.72 cm x 300 μm) were dilated in liquid methanol solution for 24 hrs to investigate the magnitude of the polymer width (*i.e.,* y-direction) dilation relative to that of the length (*i.e.,* x-direction) dilation. The initial (dry) and dilated (in pure liquid methanol) length and width of the films were determined using a Vernier caliper with ±0.01 cm accuracy.

6.2 PURE GAS SOLUBILITY

Figure 6.1 presents pure gas CH_4 sorption isotherms in PTMSP as a function of fugacity and temperature. The sorption isotherms are slightly concave to the pressure axis, which is common for sorption in glassy polymers [1]. The dashed line is the pure gas CH_4 sorption isotherm in PTMSP at 35^{o}C previously reported by Merkel *et al.* [1]. It is in good agreement with the pure gas CH_4 sorption isotherm at 35^{o}C in this study.

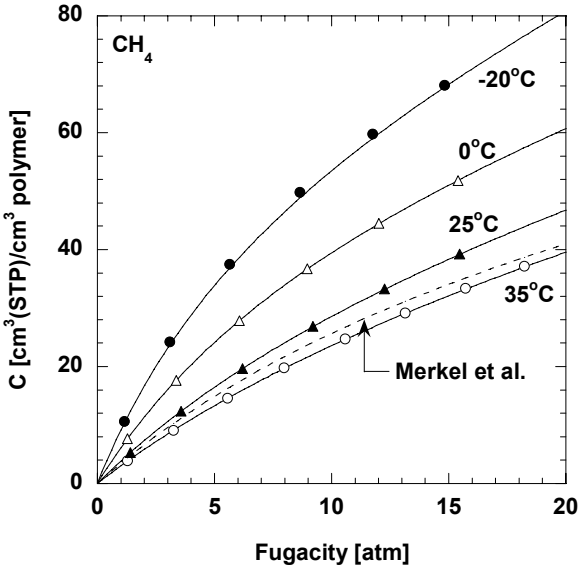

Figure 6.1 CH_4 pure gas sorption isotherm as a function of CH_4 fugacity and temperature. The dashed line represents the CH_4 pure gas isotherm in PTMSP at 35°C reported by Merkel *et al.*[1] The solid lines are from the dual mode sorption model using parameters from Table 6.1.

Figure 6.2(a) presents pure gas *n*-C_4H_{10} sorption isotherms in PTMSP as a function of fugacity and temperature. The sorption isotherms are concave to the pressure axis at low pressure. At high pressure, the isotherms are linear, indicating saturation of the Langmuir sites. The isotherm at 35°C is in good agreement with that previously reported by Morisato *et al.* [1]. Figure 6.2(b) presents the pure gas *n*-C_4H_{10} sorption isotherms as a function of activity, which is defined as the ratio of fugacity to the saturation fugacity at a given temperature (f/f_{sat}) [4]. The saturation fugacity is the fugacity at the saturation pressure (p_{sat}), and p_{sat} is estimated using the Wagner equation [4,5]. When plotted as a function of activity, the isotherms at high activity exhibit similar slopes (*i.e.,* activity-normalized k_D values are essentially independent of temperatures).

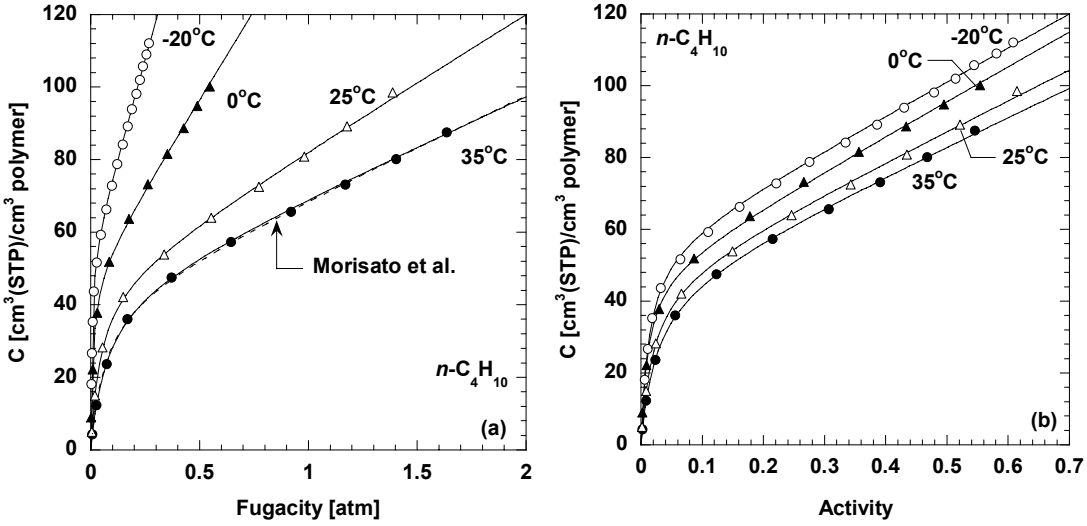

Figure 6.2 n-C_4H_{10} pure gas sorption isotherm as a function of (a) n-C_4H_{10} fugacity and (b) n-C_4H_{10} activity (f/f_{sat}). The dashed line represents the n-C_4H_{10} pure gas sorption isotherm in PTMSP at 35°C reported by Morisato *et al.*.[6] The solid lines are from the dual mode sorption equation using parameters from Table 6.1. For n-C_4H_{10}, f_{sat} values are 3.00, 2.26, 0.99, and 0.44 atm at 35, 25, 0, and -20°C, respectively [5].

The pure gas sorption isotherms can be described by the dual mode sorption model, as described in Eq. (2.16). Table 6.1 presents the dual mode parameters obtained by a nonlinear least squares fit of Eq. (2.16) to the experimental data. The uncertainties were estimated according to the propagation of errors method [7]. Although the b value for CH_4 at 35°C in this study (0.051 ± 0.005 atm^{-1}) agrees with that reported by Merkel *et al.* (0.05 atm^{-1}) [1], our k_D value (0.86 ± 0.05 cm^3(STP)/(cm^3 atm)) is higher than theirs (0.50 cm^3(STP)/(cm^3 atm)), and our C_H' value (44 ± 5 cm^3(STP)/cm^3) is lower than Merkel *et al.*'s value (62 cm^3(STP)/cm^3) [1]. These discrepancies are probably due to the difficulty of obtaining a unique set of dual mode parameters for light gas sorption in glassy polymers when a limited pressure range is explored [1]. The maximum pressure in

the present study is 18 atm. Merkel *et al.* measured the CH_4 isotherm at pressures up to 25 atm [1]. In these pressure ranges, the Langmuir sites in PTMSP are not saturated (*i.e., bf* is not much greater than unity). Due to the lack of curvature in the CH_4 sorption isotherms, the estimated dual mode parameters are less reliable than those for *n*-C_4H_{10}, where the more strongly curve isotherms permits a more reliable estimate of a unique set of dual mode parameters. The *n*-C_4H_{10} parameters in this study are similar to those previously reported by Morisato *et al.* [6]. Their k_D, C_H', and b values of *n*-C_4H_{10} in PTMSP at 35°C are 28 cm^3(STP)/(cm^3 atm), 43 cm^3(STP)/cm^3, and 15 atm^{-1}, respectively [6]; our values at the same temperature are 27 ± 2 cm^3(STP)/(cm^3 atm), 45 ± 2 cm^3(STP)/cm^3, and 13 ± 1 atm^{-1}. In general, k_D, C_H', and b values increase as temperature decreases. k_D increases mainly because the penetrant condensability increases with decreasing temperature. For example, k_D of *n*-C_4H_{10} increases from 27 to 211 cm^3(STP)/(cm^3 atm) as temperature decreases from 35 to -20°C. However, when corrected for the influence of penetrant condensability, the k_D values are essentially independent of temperature, which is also apparent from the slopes of the isotherms at higher activity in Figure 2(b). Activity-based k_D values (*i.e.,* k_Df_{sat}) for *n*-C_4H_{10} at 35, 25, 0, and -20°C are 80 ± 7, 84 ± 7, 96 ± 8, 93 ± 8 cm^3(STP)/cm^3, respectively. C_H' increases as temperature decreases, which is consistent with the fact that non-equilibrium excess volume in a glass polymer should increase as temperature decreases or as the difference between the temperature of the experiment and the glass transition temperature ($T-T_g$) increases [1]. In general, activity-based b values (*i.e.,* bf_{sat}) of *n*-C_4H_{10} increase with decreasing temperature. The values at 35, 25, 0, and -20°C are 40 ± 3, 51 ± 4, 89 ± 8, and 77 ± 8, respectively.

Table 6.1 CH_4 and *n*-C_4H_{10} dual mode parameters in PTMSP determined from pure gas sorption isotherms

T (°C)	CH_4			*n*-C_4H_{10}		
	k_D [a]	C'_H [b]	b [c]	k_D [a]	C'_H [b]	b [c]
-20	1.7 ± 0.2	66 ± 6	0.13 ± 0.01	211 ± 17	56 ± 2	175 ± 19
0	1.2 ± 0.1	58 ± 5	0.09 ± 0.01	97 ± 8	49 ± 2	90 ± 8
25	1.0 ± 0.1	46 ± 5	0.06 ± 0.01	37 ± 3	47 ± 2	22 ± 2
35	0.86 ± 0.05	44 ± 5	0.05 ± 0.01	27 ± 2	45 ± 2	13 ± 1

[a] $cm^3(STP)/(cm^3\ atm)$
[b] $cm^3(STP)/cm^3$
[c] atm^{-1}

The pure gas sorption data at various temperature and fugacity (*cf.* Figures 6.1 and 6.2) can be collapsed onto a single master curve for each penetrant by plotting the ratio of the pure gas solubility data (*i.e.,* calculated using Eq. (2.7)) to that at infinite dilution as a function of 1/(1+*bf*), as shown in Figures 6.3(a) and (b). The pure gas infinite dilution solubility coefficient is calculated using the dual mode sorption model as follows [1]:

$$S_\infty = k_D + C'_H b \tag{6.1}$$

The dual mode parameters from Table 6.2, whose significance will be discussed shortly, are used to calculate S_∞ according to Eq. (6.1) and 1/(1+*bf*). The best fit line in Figures 6.3(a) and (b) was estimated using the dual mode sorption model as follows:

$$\frac{S}{S_\infty} = \frac{k_D + \dfrac{C'_H b}{1+bf}}{k_D + C'_H b} \tag{6.2}$$

Rearrangement of Eq. (6.2) then yields:

$$\frac{S}{S_\infty} = \frac{1}{1+C_H^{'}b/k_D} + \frac{1}{1+k_D/\left(C_H^{'}b\right)}\frac{1}{1+bf} \tag{6.3}$$

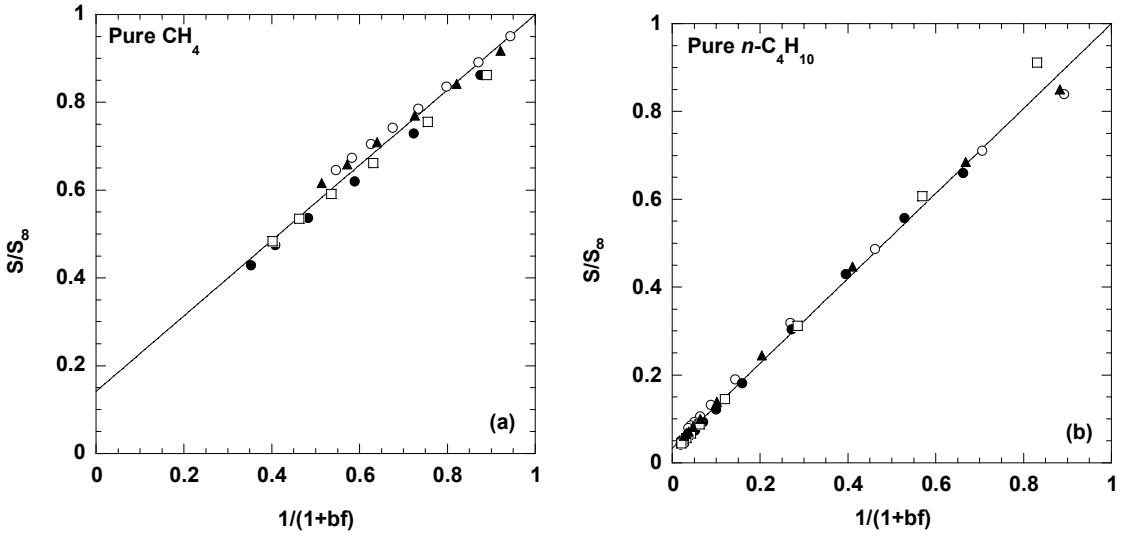

Figure 6.3 The ratio of pure gas (a) CH_4 and (b) *n*-C_4H_{10} solubility coefficient to their infinite dilution pure gas solubility coefficients as a function of 1/(1+*bf*) at various temperatures: (○) 35°C, (▲) 25°C, (□) 0°C, and (●) -20°C. *S* is calculated from the pure gas sorption data in Figures 1 and 2 using Eq. (2.7). S_∞ is calculated from Eq. (6.1) using the dual mode parameters in Table 6.2. The lines are fits to Eq. (6.3) with best fit $C_H^{'}b/k_D$ values of 5.2 ± 1.6 and 30 ± 2 for CH_4 and *n*-C_4H_{10}, respectively.

The best fit of the data in Figures 6.3(a) and (b) to Eq. (6.3) yields a straight line whose slope and intercept depend only on a single parameter, $C_H^{'}b/k_D$. If this grouping is independent of temperature, then the data will lie on a straight line, as they do in this case. A least squares fit of the data in Figure 6.3 to Eq. (6.3) determines the best effective values of $C_H^{'}b/k_D$ to describe data. The $C_H^{'}b/k_D$ obtained from these master curves are 6.0 ± 1.6 and 29 ± 2 for CH_4 and *n*-C_4H_{10}, respectively. These values agree, within

experimental uncertainty, with the average $C_H' b / k_D$ values from all temperatures calculated using the dual mode parameters in Table 6.2, which are 6.6 ± 1.0 and 35 ± 5 for CH_4 and *n*-C_4H_{10}, respectively.

6.3 MIXED GAS SOLUBILITY

Figures 6.4(a) and (b) present pure and mixed gas sorption isotherms for CH_4 and *n*-C_4H_{10} in PTMSP at 35°C as a function of CH_4 fugacity. Each mixture isotherm is determined at a nominally fixed *n*-C_4H_{10} fugacity. Due to the experimental methodology, the *n*-C_4H_{10} fugacity varies slightly over the course of each sorption isotherm, as discussed previously [4]. The *n*-C_4H_{10} fugacities reported in Figures 6.4(a) and (b) are average values for each mixture isotherm. The uncertainties shown are standard deviations from the average values. Figure 6.4(a) shows that, at similar CH_4 fugacity, CH_4 concentration sorbed in the polymer decreases as *n*-C_4H_{10} fugacity increases. For example, the CH_4 concentration in the polymer at 8.0 atm CH_4 fugacity is 19.8 cm^3(STP)/cm^3 when no *n*-C_4H_{10} is present. At similar CH_4 fugacity, CH_4 concentrations in the presence of 0.23 atm *n*-C_4H_{10} fugacity (~0.08 activity) and 1.62 atm *n*-C_4H_{10} fugacity (~0.54 activity) are 8.7 and 5.5 cm^3(STP)/cm^3, respectively. Competitive sorption effects have been observed previously during gas mixture sorption in glassy polymers [8]. Penetrant molecules compete for the limited number of sorption sites in the non-equilibrium excess volume (*i.e.,* Langmuir sites), resulting in lower gas solubilities in mixtures than in pure gases [8]. In this study, *n*-C_4H_{10}, which is much more soluble than CH_4 in the polymer, presumably occupies more of the sorption sites in the Langmuir region. Thus, the presence of *n*-C_4H_{10} reduces CH_4 sorption significantly, and consequently, decreases CH_4 mixture solubility in the polymer. On the other hand, *n*-C_4H_{10} solubility is not significantly affected by the presence of CH_4 in the mixture. Figure 6.4(b) shows that the *n*-C_4H_{10} concentration is essentially unchanged as CH_4

fugacity increases. That is, methane is not condensable enough to effectively compete with n-C_4H_{10} for the limited number of Langmuir sites.

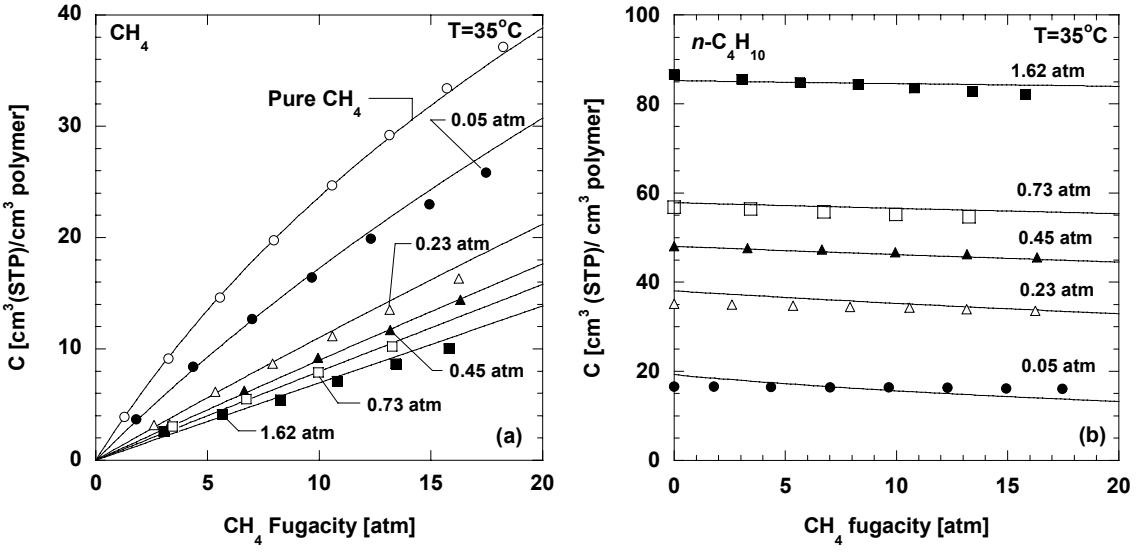

Figure 6.4 Pure and mixed gas sorption isotherms of (a) CH_4 and (b) n-C_4H_{10} as a function of CH_4 fugacity at 35°C. Each isotherm is determined at a nominally fixed n-C_4H_{10} fugacity, whose value (in atm) is given by the numbers in the figures. These n-C_4H_{10} fugacities are averages over the course of each sorption isotherm. The average n-C_4H_{10} activities (f/f_{sat}) in these isotherms are: (○) 0 (*i.e.,* pure CH_4), (●) 0.017 ± 0.003, (△) 0.08 ± 0.01, (▲) 0.15 ± 0.01, (□) 0.24 ± 0.01, and (■) 0.54 ± 0.01. f_{sat} of n-C_4H_{10} at 35°C is 3.00 atm [5]. The uncertainties in the n-C_4H_{10} activity values represent the standard deviation of the average values over the course of the sorption experiment. The lines represent the dual mode sorption model fits using the parameters in Table 6.2.

Competitive effects are observed at all temperatures studied. Figures 6.5(a) and (b) present pure and mixed gas sorption isotherms of CH_4 and n-C_4H_{10} in PTMSP at -20°C as a function of CH_4 fugacity. The CH_4 concentration in the polymer is considerably reduced in the presence of n-C_4H_{10}, while the n-C_4H_{10} concentration remains relatively unchanged in the presence of CH_4. Mixture sorption isotherms of CH_4 and n-C_4H_{10} at 25 and 0°C, presented in the Appendix D, exhibit similar trends.

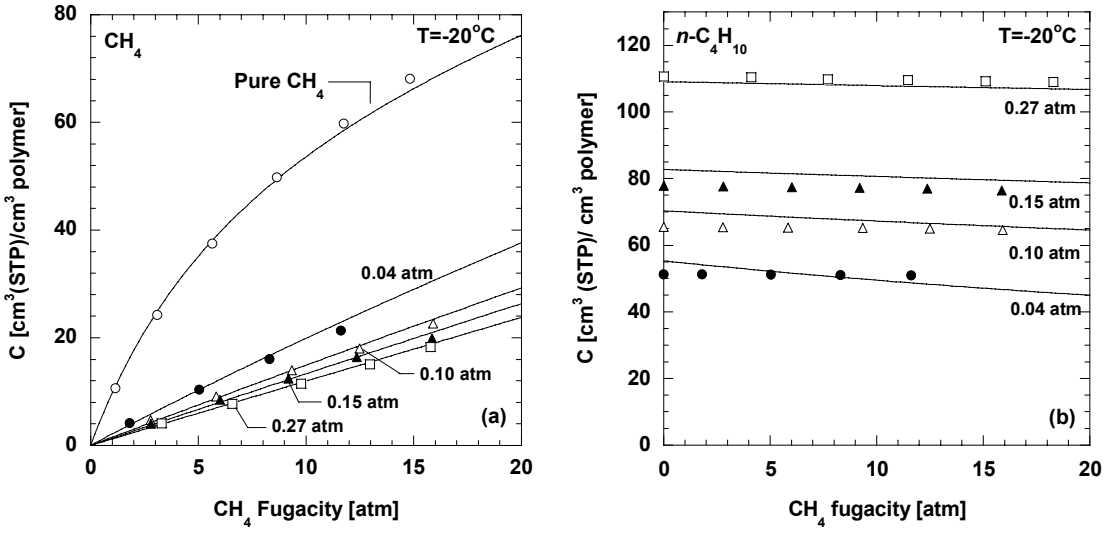

Figure 6.5 Pure and mixed gas sorption isotherms of (a) CH_4 and (b) n-C_4H_{10} as a function of CH_4 fugacity at -20°C. Each isotherm is determined at a nominally fixed n-C_4H_{10} fugacity, whose value (in atm) is given by the numbers in the figures. These n-C_4H_{10} fugacities are averages over the course of each sorption isotherm. The average n-C_4H_{10} activities (f/f_{sat}) in these isotherms are: (○) 0 (*i.e.,* pure CH_4), (●) 0.09 ± 0.01, (△) 0.22 ± 0.02, (▲) 0.34 ± 0.02, and (□) 0.61 ± 0.02. The f_{sat} of n-C_4H_{10} at -20°C is 0.44 atm. The uncertainties represent the standard deviation of the average values. The lines represent the dual mode sorption model fits using the parameters in Table 6.2.

Figures 6.6(a) and (b) present mixed gas solubility of CH_4 in PTMSP, in the limit of 0 atm of CH_4 fugacity, as a function of *n*-C_4H_{10} activity. The mixed gas CH_4 solubility in the limit of 0 atm CH_4 fugacity is calculated from Eq. (2.7) and (2.18) as follows:

$$\lim_{f_A \to 0} S_A = S_{A,\inf} = k_{D_A} + \frac{C'_{H_A} b_A}{1 + b_B f_B} \tag{6.4}$$

where the subscripts *A* and *B* refer to CH_4 and *n*-C_4H_{10}, respectively. The symbols are calculated from the best-fit dual mode parameters for each individual mixture isotherm. The dashed lines and solid lines in Figures 6.6(a) and (b) are determined using the dual mode parameters in Tables 6.1 and 6.2, respectively, which represent fits to all pure gas data and all pure and mixed gas data, respectfully. The mixed gas CH_4 solubility is considerably lower than the pure gas solubility due to the competitive sorption effects discussed earlier. For example, CH_4 infinite dilution pure gas solubility in PTMSP at 25°C is 4.0 cm^3(STP)/(cm^3 atm). In the presence of *n*-C_4H_{10} at an activity of 0.21, CH_4 solubility decreases by a factor of four, to 1.0 cm^3(STP)/(cm^3 atm). At higher *n*-C_4H_{10} activity, CH_4 mixture solubility in the polymer apparently reaches a plateau that, consistent with the dual mode sorption model (*cf.* Eq. (6.4)), is the CH_4 k_D value at that temperature.

Figure 6.7 presents pure and mixed gas solubility of *n*-C_4H_{10} in PTMSP as a function of *n*-C_4H_{10} activity and temperature. The closed symbols are from pure gas measurements, and the open symbols are data points from mixture measurements. The mixture solubilities of *n*-C_4H_{10} in PTMSP are close to the pure gas values. The influence of CH_4 on *n*-C_4H_{10} solubility is too weak to be measured in these experiments.

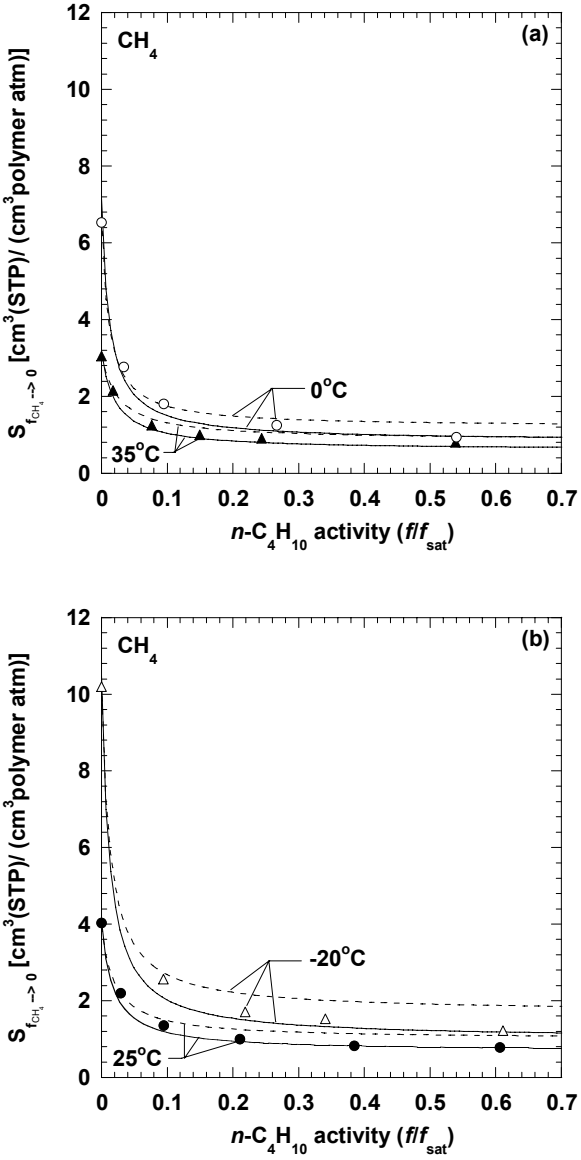

Figure 6.6 CH_4 mixed gas solubility (in the limit of zero CH_4 fugacity) in PTMSP at (a) 35 and 0°C and (b) 25 and -20°C as a function of *n*-C_4H_{10} activity. The dashed lines are the dual mode sorption model predictions using pure gas parameters from Table 6.1. The solid lines are the dual mode sorption model prediction using mixed gas parameters from Table 6.2.

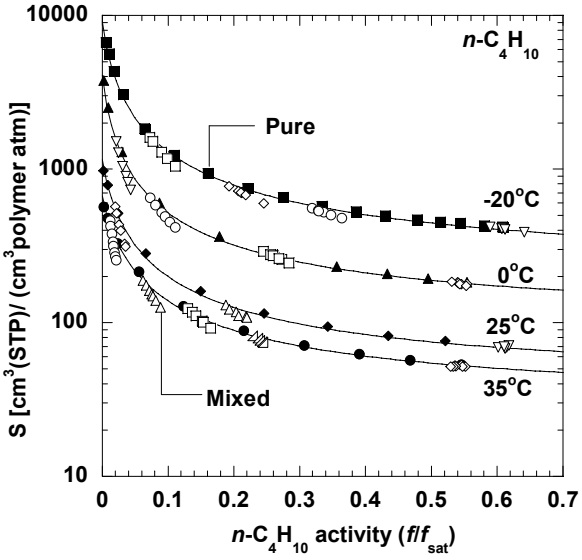

Figure 6.7 Pure and mixed gas n-C_4H_{10} solubility in PTMSP as a function of n-C_4H_{10} activity and temperature. The closed symbols represent pure gas data. The open symbols represent mixed gas data at various CH_4 fugacities. The solid lines represent prediction of the dual mode sorption model using parameters from Table 6.2.

6.4 DUAL MODE MIXTURE SORPTION MODEL

The mixed gas sorption isotherms can be described using the dual model sorption model for binary mixtures (*i.e.,* Eq. (2.18) and (2.19)). The pure gas dual mode parameters recorded in Table 6.1 were initially used to predict mixture sorption behavior in PTMSP. The predictions from the pure gas parameters, shown as dashed lines in Figures 6.6(a) and (b), overestimate the mixed gas CH_4 solubility somewhat at higher n-C_4H_{10} activity. The source of the discrepancy is the CH_4 pure gas dual mode parameters calculated from pure gas sorption measurements; these values are not completely reliable due to the lack of curvature in the CH_4 pure gas sorption isotherms. Table 6.2 records the best-fit CH_4 and n-C_4H_{10} dual mode parameters determined by simultaneously fitting the pure and mixed gas CH_4 and n-C_4H_{10} sorption data to Eq. (2.18) and (2.19). The model

predictions using these parameters, presented in Figures 6.4-6.7, describe the experimental data well. There is some disagreement between the CH_4 dual mode parameters in Table 6.1 and those in Table 6.2. The k_D values of CH_4 estimated from the pure gas data (*e.g.,* 0.86 ± 0.05 cm^3(STP)/(cm^3 atm at 35°C) are higher than those estimated from the pure and mixed gas data (0.60 ± 0.05 cm^3(STP)/(cm^3 atm) at 35°C). The C_H' values for CH_4 obtained from the pure gas data are, in general, slightly lower than those determined from the pure and mixed gas data. The *b* values estimated from the pure gas data and the mixed gas data, however, are similar. The CH_4 dual mode parameters estimated simultaneously from the pure and mixed gas data (*i.e.,* the values in Table 6.2) are presumably more reliable than those estimated only from pure gas sorption isotherms (*i.e.,* the values in Table 6.1). As shown in Figures 6.6(a) and (b), CH_4 solubility reaches a plateau at higher *n*-C_4H_{10} activity, which indicates saturation of the Langmuir sites. In this plateau region, penetrant sorption occurs mostly in the dense equilibrium Henry's law region, and, according to the dual mode sorption model, the CH_4 solubility approaches k_D. Therefore, the mixture data provide a more accurate and reliable approximation of k_D, because, by using *n*-C_4H_{10} to saturate the Langmuir sites, one obtains CH_4 solubility values that are more consistent with sorption only in the Henry's law sites. The CH_4 dual mode parameters in Table 6.2 agree with CH_4 pure gas parameters in the literature [1]. Our values at 35°C are 0.60 cm^3(STP)/(cm^3 atm), 56 cm^3(STP)/cm^3, and 0.051 atm^{-1} for k_D, C_H', and *b*, respectively. Merkel *et al.* reported values of 0.50 cm^3(STP)/cm^3 atm, 62 cm^3(STP)/cm^3, and 0.05 atm^{-1} at this temperature for k_D, C_H', and *b*, respectively [1]. Srinivasan *et al.* [9] reported k_D, C_H', and *b* values at 25°C of 0.63 cm^3(STP)/cm^3 atm, 59 cm^3(STP)/cm^3, and 0.058 atm^{-1}, respectively, in good agreement with the parameters obtained in this study (0.68 cm^3(STP)/cm^3 atm, 56 cm^3(STP)/cm^3, and 0.061 atm^{-1}). The *n*-C_4H_{10} dual mode parameters estimated

simultaneously from the pure and mixture data (Table 6.2) are essentially the same as those determined from pure gas data alone (Table 6.1).

Table 6.2 CH_4 and *n*-C_4H_{10} dual mode parameters in PTMSP determined from both pure and mixed gas sorption isotherms

T (°C)	CH_4			*n*-C_4H_{10}		
	k_D [a]	C'_H [b]	b [c]	k_D [a]	C'_H [b]	b [c]
-20	1.00 ± 0.07	79 ± 7	0.12 ± 0.01	213 ± 17	53 ± 3	188 ± 20
0	0.83 ± 0.05	63 ± 5	0.10 ± 0.01	96 ± 7	47 ± 2	85 ± 9
25	0.68 ± 0.05	56 ± 5	0.06 ± 0.01	38 ± 3	43 ± 2	26 ± 3
35	0.60 ± 0.05	56 ± 5	0.05 ± 0.01	29 ± 2	40 ± 2	16 ± 2

[a] $cm^3(STP)/(cm^3\ atm)$
[b] $cm^3(STP)/cm^3$
[c] atm^{-1}

The Langmuir capacity parameter, C'_H, can be used to estimate the amount of non-equilibrium excess free volume in a glassy polymer using the following expression [10]:

$$C'_H\left(\frac{MW}{22,414}\right)=\frac{v_p-v_l}{v_p}\rho^*=\varepsilon\times\rho^* \tag{6.5}$$

where C'_H has units of $cm^3(STP)/cm^3$, MW is the molecular weight of the penetrant, v_p is the specific volume of the polymer, v_l is the specific volume of the densified polymer matrix, ε is the accessible non-equilibrium excess free volume fraction, ρ^* is the condensed penetrant density, and 22,414 $cm^3(STP)$/mole is a conversion factor. ρ^* has been estimated as the liquid density of the pure penetrant at the experimental temperature

[1]. The saturated liquid densities of *n*-C_4H_{10} at 35, 25, 0, and -20°C are 0.56, 0.57, 0.60, and 0.62 g/cm^3 [11]. Based on these values and C_H' from Table 6.2, the excess free volume fraction in PTMSP (*i.e.,* ε) from *n*-C_4H_{10} data is 0.18, 0.19, 0.20, and 0.22, at 35, 25, 0, and -20°C, respectively. These values are unusually high compared to those estimated in conventional, low free volume glassy polymers, such as polycarbonate (0.04) and poly(phenylene oxide) (0.06) [10,12]. However, the excess free volume fraction estimated in this study is slightly lower than that previously reported for PTMSP: Merkel *et al.* reported an ε value in PTMSP of 0.25 based on C_3H_8 sorption data at 35°C [1], and Srinivasan *et al.* reported an ε value of 0.24 based on CO_2 sorption data at 25°C [9].

The temperature dependence of k_D can be described using a van't Hoff expression, as follows [13]:

$$k_D = k_{Do} \exp\left(\frac{-\Delta H_D}{RT}\right) \tag{6.6}$$

where k_{Do} is a constant, ΔH_D is the enthalpy change of sorption in the Henry's law region, R is the gas constant, and T is absolute temperature. The k_D values of CH_4 and *n*-C_4H_{10} recorded in Table 6.2 are plotted against $1/T$ in Figure 6.8. Fitting these k_D values to Eq. (6.6) yields k_{Do} values of 6.3 ± 0.5 x10^{-2} and 0.27 ± 0.02 x10^{-2} cm^3(STP)/(cm^3 atm) for CH_4 and *n*-C_4H_{10}, respectively. The ΔH_D of CH_4 and *n*-C_4H_{10} are -5.8 ± 0.5 and -24 ± 2 kJ/mol, respectively. Interestingly, these ΔH_D values are very similar to the pure gas enthalpies of sorption of CH_4 and *n*-C_4H_{10} (-5.8 and -23.0 kJ/mol, respectively) at infinite dilution in poly(dimethylsiloxane) (PDMS) [4]. In addition, the ΔH_D of *n*-C_4H_{10} in PTMSP is very close to the enthalpy of condensation, ΔH_{cond}, of *n*-C_4H_{10}. In this regard, the ΔH_{cond} of *n*-C_4H_{10} at 15°C (*i.e.,* the median of the temperature range explored in this study) is -21.6 kJ/mol [11]. That is, ΔH_D is essentially given by the enthalpy of

condensation, and its value is sensibly equal to the enthalpy of sorption in a nonpolar, rubbery polymer (*i.e.,* PDMS).

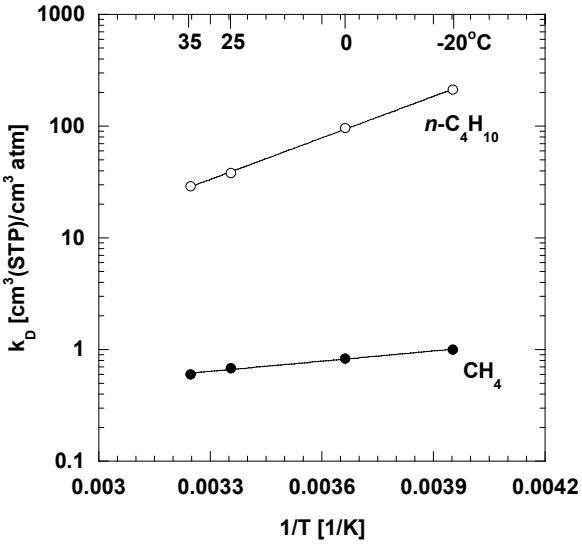

Figure 6.8 The effect of temperature on k_D of CH_4 and n-C_4H_{10} in PTMSP. The dashed lines are fits from Eq. (6.6) with k_{Do} = 6.3 ± 0.5 x10^{-2} cm^3(STP)/(cm^3 atm) and ΔH_D = -5.8 ± 0.5 kJ/mol for CH_4, and k_{Do} = 0.27 ± 0.02 x10^{-2} cm^3(STP)/(cm^3 atm) and ΔH_D = -24 ± 2 kJ/mol for n-C_4H_{10}.

The temperature dependence of b is typically given by: [13]

$$b = b_o \exp\left(\frac{-\Delta H_b}{RT}\right) \tag{6.7}$$

where b_o is a constant and ΔH_b is the corresponding enthalpy change. The temperature dependence of b values for CH_4 and n-C_4H_{10} in PTMSP (Table 6.2) are presented in Figure 6.9. The b_o values of CH_4 and n-C_4H_{10} are 6.4 ± 0.5 x 10^{-4} and 2.0 ± 0.2 x 10^{-4} atm^{-1}, respectively. The ΔH_b of CH_4 and n-C_4H_{10} are -11 ± 1 and -29 ± 2 kJ/mol, respectively. These ΔH_b values are lower (*i.e.,* more negative) than the ΔH_D values determined earlier. Similar observations have been reported in the literature [14,15].

Sorption in the Henry's law region involves separation of polymer chain segments to accommodate penetrant molecules [13]. In the Langmuir region, since the microvoids supposedly already exist, no extra energy is required to separate chains to accommodate sorption in this region [13]. As a result, sorption in the Langmuir region is less energetic than that in the Henry's law region [13], so, for the same penetrant, ΔH_b is more negative than ΔH_D. The ΔH_b of CH_4 in PTMSP is slightly higher (*i.e.,* less negative) than the CH_4 enthalpy of adsorption in porous materials (*e.g.,* zeolite, carbon membranes), which is typically between -15 to -25 kJ/mol [16-18]. Nevertheless, they are quite close to these values, which suggests a similarity between the hole-filling sorption mechanism in the Langmuir region of PTMSP and the adsorption mechanism in porous materials. For instance, the enthalpy of adsorption of CH_4 in β-zeolite with pore size of 6-7 Å is -16 kJ/mol [19].

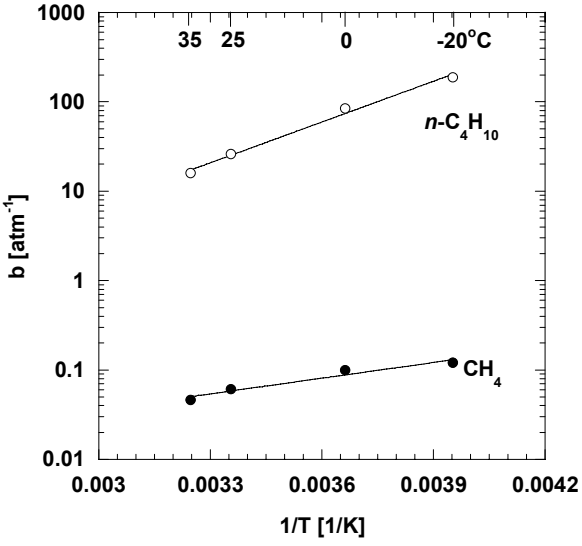

Figure 6.9 The effect of temperature on b of CH_4 and n-C_4H_{10} in PTMSP. The dashed lines are fits from Eq. (6.7) with $b_o = 6.4 \pm 0.5 \times 10^{-4}$ atm^{-1} and $\Delta H_b = -11 \pm 1$ kJ/mol for CH_4, and $k_{Do} = 2.0 \pm 0.2 \times 10^{-4}$ atm^{-1} and $\Delta H_b = -29 \pm 2$ kJ/mol for n-C_4H_{10}.

6.5 EFFECT OF CONCENTRATION ON ENTHALPY OF SORPTION

The isosteric enthalpy of sorption, ΔH_S^C, at a fixed penetrant concentration, C, can be calculated using Eq. (4.11) [13]. Figure 6.10 presents pure gas enthalpy of sorption as a function of penetrant concentration in the polymer. The ΔH_S of CH_4 is essentially independent of CH_4 concentration. The average ΔH_S^C of CH_4 over the concentration range is -14 ± 1 kJ/mol, which is lower than the enthalpy of sorption of CH_4 in liquid *n*-C_4H_{10} (-9.7 kJ/mol) [4] and in PDMS (-5.8 kJ/mol) [4] due to the pre-existing voids that are readily available for sorption in the Langmuir region. The ΔH_S^C of *n*-C_4H_{10} initially decreases with increasing *n*-C_4H_{10} concentration, reaches a minimum at approximately 40 cm^3(STP)/cm^3, and then increases with increasing *n*-C_4H_{10} concentration at *n*-C_4H_{10} concentration greater than 40 cm^3(STP)/cm^3. A similar trend has been reported in other glassy polymers and is consistent with the dual mode interpretation of penetrant sorption [13,20,21]. At low *n*-C_4H_{10} concentration, sorption occurs predominantly in the Langmuir region, in which sorption sites are readily accessible. As *n*-C_4H_{10} concentration increases, the Langmuir region becomes progressively more saturated, resulting in a larger fraction of the sorption occurring in the Henry's law region, in which penetrant dissolution is more energetically demanding than that in the Langmuir region since it involves the separation of polymer chain segments to accommodate penetrant molecules [21]. Consequently, the ΔH_S^C of *n*-C_4H_{10} increases with *n*-C_4H_{10} concentration (for C > 40 cm^3(STP)/cm^3) and appears to approach the ΔH_{cond} of *n*-C_4H_{10} at higher *n*-C_4H_{10} concentration. In this study, the ΔH_S^C of *n*-C_4H_{10} is always lower than the ΔH_{cond} of *n*-C_4H_{10} throughout the concentration range explored, which means that the enthalpy of mixing of *n*-C_4H_{10} is exothermic. The trend in ΔH_{mix} should exhibit the same functional dependence on concentration as ΔH_S^C since ΔH_{cond} is independent of concentration. Figure 6.10 also presents the ΔH_S^C of CH_4 in mixtures as a

function of *n*-C_4H_{10} concentration in the polymer. The trend is similar to that observed for *n*-C_4H_{10}. As *n*-C_4H_{10} concentration increases, a greater fraction of CH_4 molecules partitions into the Henry's law region. As a result, CH_4 sorption in the polymer becomes energetically more difficult. The ΔH_S^C of CH_4 increases with increasing *n*-C_4H_{10} concentration at *n*-C_4H_{10} concentration greater than 30 cm^3(STP)/cm^3. Interestingly, the minimum in ΔH_S^C for both CH_4 and *n*-C_4H_{10} occurs at a similar *n*-C_4H_{10} concentration (around 30-40 cm^3(STP)/cm^3). At *n*-C_4H_{10} concentrations greater than 60 cm^3(STP)/cm^3, the ΔH_S^C of CH_4 in mixtures is somewhat higher than the ΔH_S^C of CH_4 in liquid *n*-C_4H_{10}. The ΔH_S^C of CH_4 seems to reach an asymptotic value at higher *n*-C_4H_{10} concentration. At the highest *n*-C_4H_{10} concentration studied (110 cm^3(STP)/cm^3), the ΔH_S^C of CH_4 is -6.8 ± 0.6 kJ/mol which is close to the ΔH_S^C of CH_4 in rubbery PDMS. For reference, the ΔH_S^C of CH_4 in PDMS decreases from -5.8 kJ/mol in pure gas to -6.9 kJ/mol in the presence of 60 cm^3(STP)/cm^3 of *n*-C_4H_{10} in the polymer [4]. The difference in the trends between the pure and mixed gas ΔH_S^C of CH_4 in PTMSP is shown in Figure 6.10. The weak concentration dependence of ΔH_S^C for pure gas CH_4 indicates that the Langmuir region is below saturation point during the measurement, which is consistent with our previous observation on this issue.

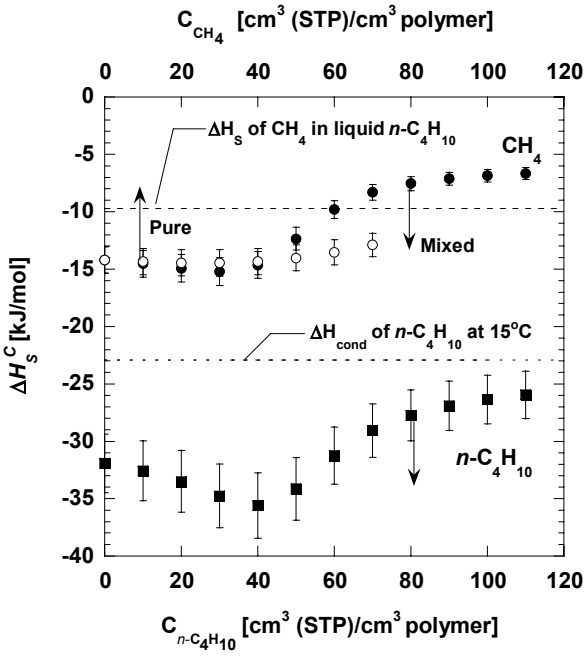

Figure 6.10 The effect of concentration on CH_4 (pure and mixed gas) and n-C_4H_{10} isosteric enthalpy of sorption in PTMSP. The error bars are estimated using the propagation of errors method [7].

6.6 SOLUBILITY SELECTIVITY

Figure 6.11(a) presents the mixed gas n-C_4H_{10}/CH_4 solubility selectivity in PTMSP as a function of n-C_4H_{10} activity in the mixture at various temperatures. The solubility selectivity decreases as n-C_4H_{10} activity and temperature increase. For example, at -20°C, the n-C_4H_{10}/CH_4 mixed gas solubility selectivity in PTMSP decreases from 690 to 480 as n-C_4H_{10} activity increases from 0.05 to 0.24. At 35°C, the solubility selectivity decreases from 175 to 96 as n-C_4H_{10} activity increases from 0.03 to 0.26. Basically, the n-C_4H_{10} solubility decreases more than that of CH_4 as temperature increases or as n-C_4H_{10} activity increases. Similar to the mixed gas data, the pure gas solubility selectivity also decreases with increasing n-C_4H_{10} activity and temperature. The dual mode model adequately captures these trends.

Figure 6.11(b) presents the ratio of n-C_4H_{10}/CH_4 mixed gas to pure gas solubility selectivity at various temperatures. Due to the CH_4 solubility decrease in the mixture as a result of competitive sorption, the n-C_4H_{10}/CH_4 solubility selectivities determined from the mixture measurements are substantially higher than those estimated from pure gas data. These differences between pure and mixed gas solubility selectivities are even greater at higher n-C_4H_{10} activity and lower temperature. For example, at -20°C and an n-C_4H_{10} activity of 0.73, the mixed gas solubility selectivity is approximately 9 times higher than the pure gas solubility selectivity.

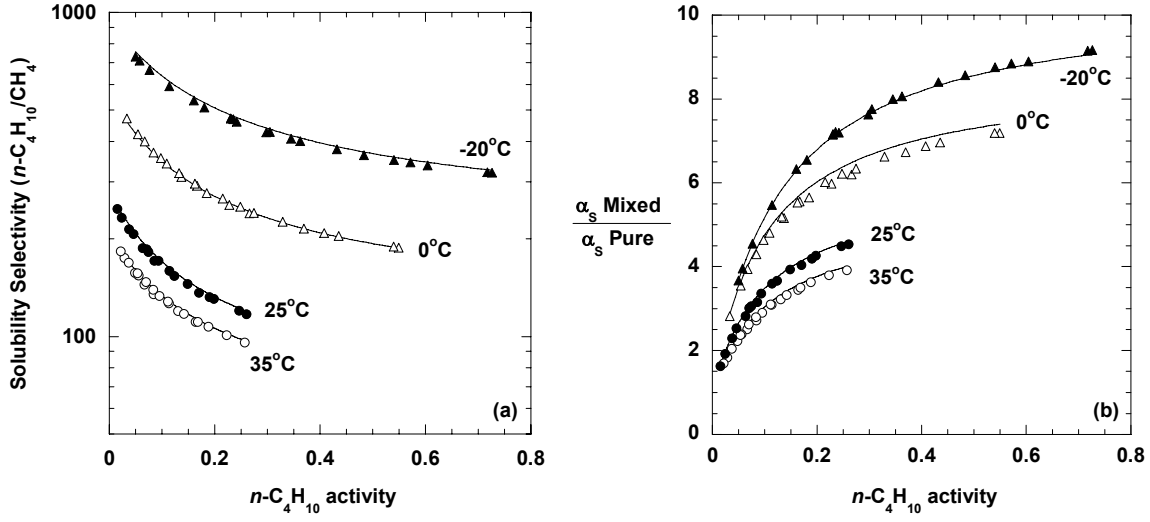

Figure 6.11 (a) Mixed gas n-C_4H_{10}/CH_4 solubility selectivity in PTMSP as a function of n-C_4H_{10} activity in the mixture. (b) Ratio of n-C_4H_{10}/CH_4 mixed gas to pure gas solubility selectivity in PTMSP. The pure gas solubility selectivity is calculated from n-C_4H_{10} pure gas solubility at different n-C_4H_{10} activity values and CH_4 pure gas solubility in the limit of zero CH_4 fugacity. The lines represent predictions of the dual mode sorption model using parameters from Table 6.2.

6.7 PURE GAS DILATION

Figures 6.12(a) and (b) present pure gas CH_4 and *n*-C_4H_{10} induced length (*i.e.,* x-direction) dilation of PTMSP at 35°C as a function of fugacity. ΔL_x is the change in polymer length during the measurements: $\Delta L_x = L_x - L_{x,o}$. $L_{x,o}$ is the initial penetrant-free pure polymer sample length at the experimental temperature, and L_x is the polymer sample length when exposed to gas. Similarities between the sorption and desorption cycles in the dilation isotherms indicate only very slight hysteresis during the measurements. The error bars were determined using the propagation of errors method [7].

Figure 6.13 presents the length and width (*i.e.,* y-direction) dilation of two sheets of PTMSP in liquid methanol (at unit activity) at 25°C. The initial (*i.e.,* dry) films are approximately square. Figure 6.13 shows that the polymer dilation in the x and y-direction is essentially the same during methanol swelling. Based on this observation, it is reasonable to assume that, during *n*-C_4H_{10} sorption, where the activity is always lower than unit activity, the polymer dilations similarly in the x and y-direction.

The thickness (*i.e.,* z-direction) and length (*i.e.,* x-direction) dilation of the polymer during *n*-C_4H_{10} sorption at 25 and 0°C are shown in Figures 6.14(a) and (b). At similar *n*-C_4H_{10} fugacity, the thickness dilation is perhaps slightly higher than that of the length. However, due to limitation of our apparatus, the uncertainty in the thickness measurements is considerably higher than that in the length dilation measurements. In any event, the dilation is, at least, approximately isotropic.

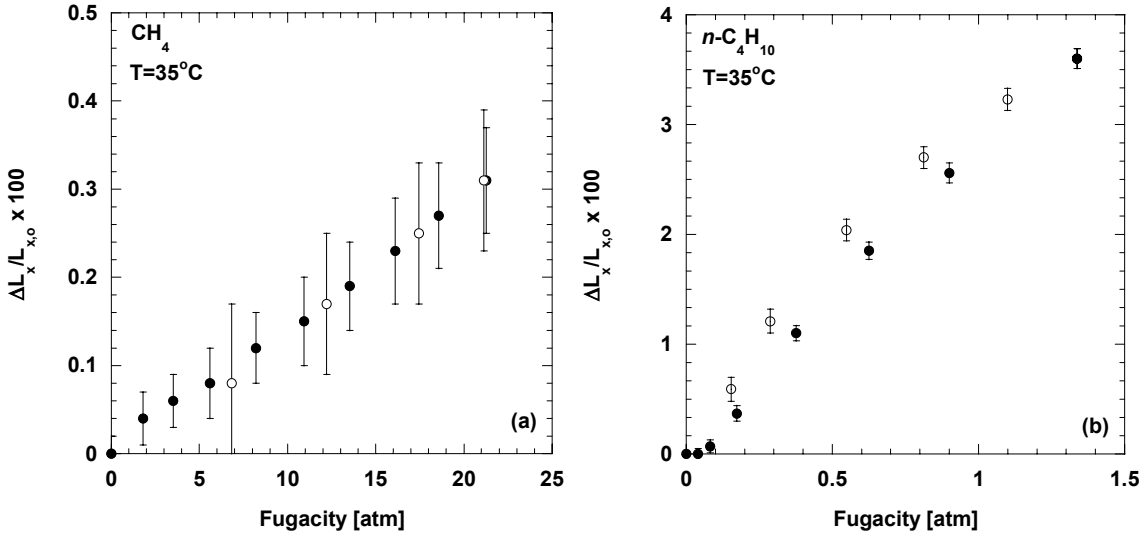

Figure 6.12 Pure gas (a) CH_4 and (b) n-C_4H_{10} induced length (*i.e.,* x-direction) dilation of PTMSP at 35°C as a function of fugacity. The open symbols represent the data obtained as gas pressure was increased. The filled symbols are the data obtained as gas pressure was decreased.

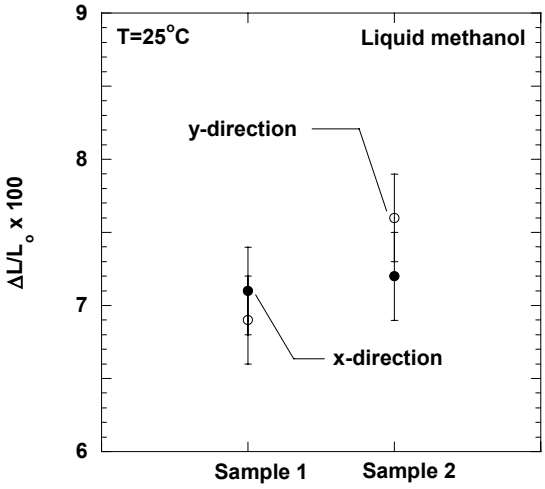

Figure 6.13 Length (*i.e.,* x-direction) and width (*i.e.,* y-direction) dilation of PTMSP films in liquid methanol. The closed symbols are the length dilation data. The open symbols are the width dilation data. The dimensions of sample 1 were 6.59 cm x 6.61 cm x 300 μm and those of sample 2 were 4.74 cm x 4.72 cm x 300 μm.

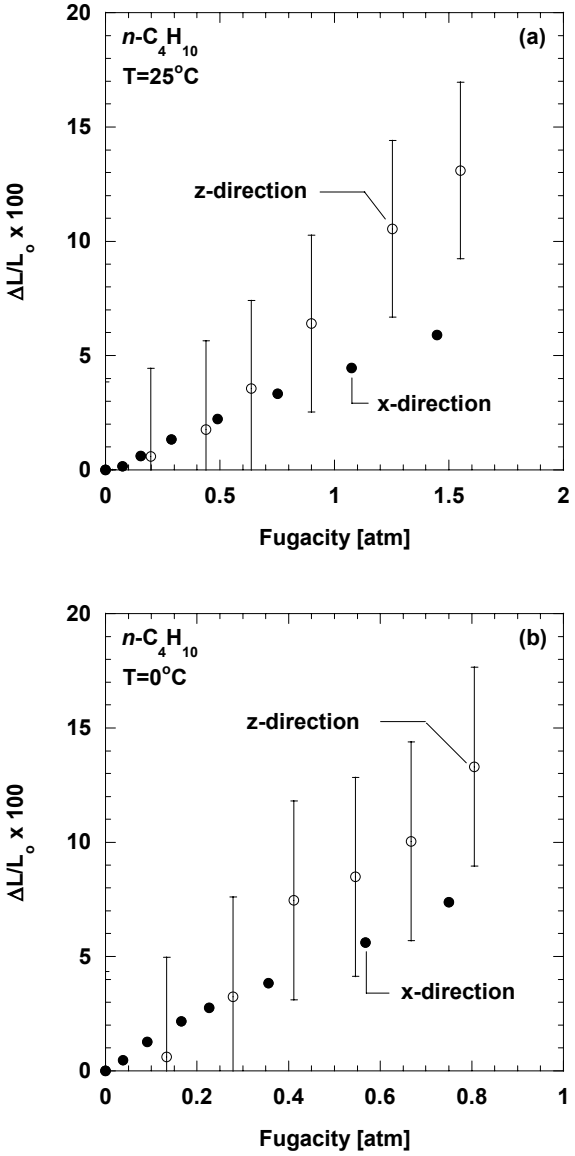

Figure 6.14 Pure gas n-C_4H_{10} induced length (*i.e.,* x-direction) and thickness (*i.e.,* z-direction) dilation of PTMSP at (a) 25°C and (b) 0°C. The open symbols represent the thickness dilation data. The filled symbols are the length dilation data.

By assuming that dilation is isotropic in the x and y (*i.e.,* length and width) directions, the change in polymer volume relative to the initial pure polymer volume, $\Delta V/V_o$, can be calculated as follows [4]:

$$\frac{\Delta V}{V_o} = \left(\frac{L_x}{L_{x,o}}\right)^2 \left(\frac{L_z}{L_{z,o}}\right) - 1 \tag{6.8}$$

where $L_{z,o}$ is the initial penetrant-free pure polymer sample length at the temperature of the experiment, and L_z is the polymer sample length when exposed to gas. $\Delta V/V_o$ can also be estimated using only the length dilation data and assuming isotropic expansion, as shown in Eq. (4.5) [4].

The change in polymer volume during dilation, estimated using the length and thickness dilation data (Eq. (6.8)), is compared to that estimated only using the length dilation (Eq. (4.5)) in Figures 6.15(a) and (b). They agree well within the experimental uncertainty. Consequently, the change in the polymer volume can be reasonably estimated using only the length dilation data, which have significantly lower uncertainty than the thickness dilation data, and by assuming isotropic expansion. The remaining polymer volume dilation data have been calculated in this way. Pure gas dilation isotherms for CH_4 and *n*-C_4H_{10} are presented in Figures 6.16(a) and (b).

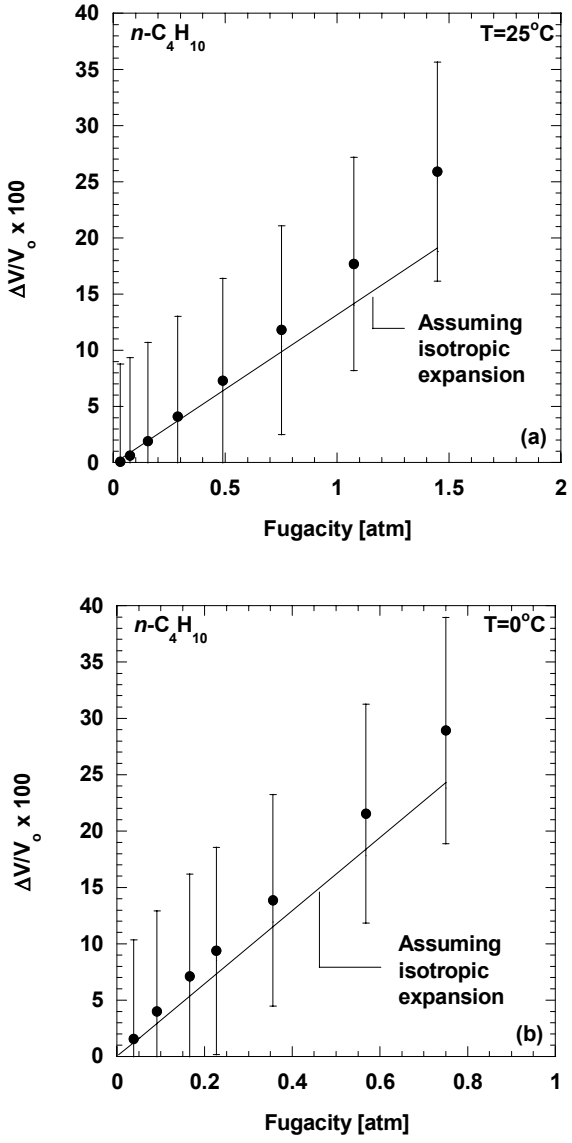

Figure 6.15 The change in polymer volume during pure gas n-C_4H_{10} sorption in PTMSP at (a) 25°C and (b) 0°C. The data points are volume dilation estimated from the length and thickness dilation data using Eq. (6.8). The lines are calculated from Eq. (4.5) using the length dilation data and assuming isotropic expansion.

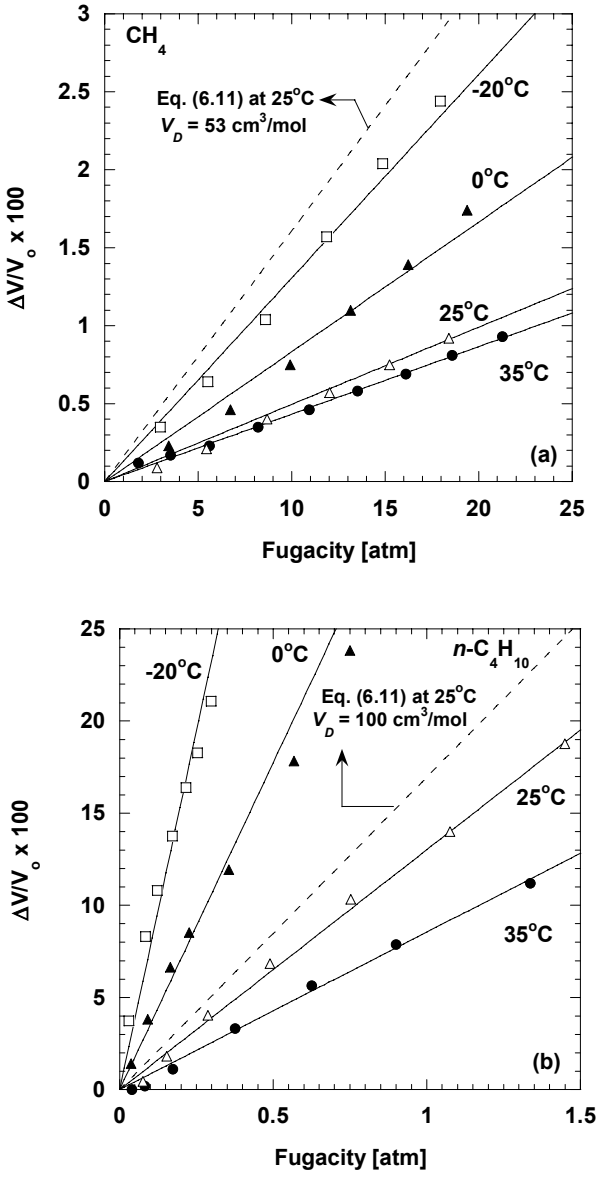

Figure 6.16 Pure gas (a) CH_4 and (b) n-C_4H_{10} induced-dilation of PTMSP as a function of fugacity from -20 to 35°C. The solid lines are predictions from Eq. (6.11) with the best-fit V_D recorded in Table 6.3. The dashed line represents the estimated volume dilation at 25°C using Eq. (6.11) with (a) V_D = 53 cm^3/mol for CH_4, and V_D = 100 cm^3/mol for n-C_4H_{10}.

The partial molar volume of the penetrant is estimated from dilation data using Eq. (4.7). β, which is the isothermal compressibility of the polymer, is usually small enough, especially for glassy polymers, to be neglected [22]. Figures 6.17(a) and (b) present the pure gas partial molar volumes of CH_4 and *n*-C_4H_{10} in PTMSP as functions of concentration at temperatures from -20 to 35^oC. The concentrations of CH_4 and *n*-C_4H_{10} in PTMSP are determined from the pure gas sorption data. In general, CH_4 pure gas partial molar volume slightly increases with increasing CH_4 concentration. *n*-C_4H_{10} pure gas partial molar volume increases, to a greater extent than CH_4, with increasing *n*-C_4H_{10} concentration. The partial molar volumes of CH_4 and *n*-C_4H_{10} in PTMSP are much lower than those in liquids. For comparison, the average partial molar volume of CH_4 in five organic solvents at 25^oC is 53 cm^3/mol [23]. The pure liquid molar volume of *n*-C_4H_{10} at 20^oC is 100 cm^3/mol [5]. The extraordinarily low penetrant partial molar volumes in glassy PTMSP has been explained by a hole-filling sorption mechanism implicitly expressed in the dual mode sorption model [24]. Fleming and Koros suggested that, ideally, only the fraction of the total sorption associated with the actual separation of chain segments to accommodate the penetrant would cause volume dilation [24]. If the sorption in the Langmuir sites corresponds to a true hole-filling process, the polymer volume dilation should arise only from sorption in the Henry's law region (*i.e.,* C_D). This idea can qualitatively explain the low partial molar volume values in glassy PTMSP compared to low molecular weight systems, in which no such hole-filling mechanism occurs.

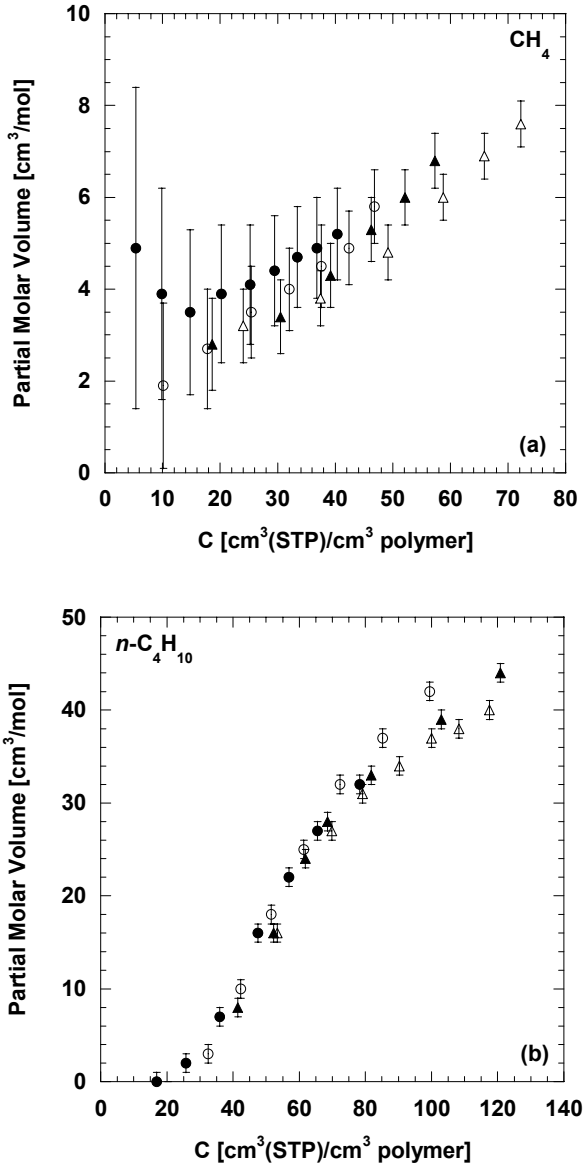

Figure 6.17 Pure gas partial molar volumes of (a) CH_4 as a function of CH_4 concentration and (b) *n*-C_4H_{10} as a function of *n*-C_4H_{10} concentration in the polymer. The various symbols represent values at different temperatures: (●) 35°C, (○) 25°C, (▲) 0°C, and (△) -20°C.

The small lag in PTMSP dilation at a very low *n*-C_4H_{10} fugacity (Figure 6.12(b)) and the near-zero partial molar volume of *n*-C_4H_{10} at low *n*-C_4H_{10} concentration (Figure 6.17(b)) can be rationalized using the same hole-filling concept. Based on the dual mode sorption model, the relative penetrant populations in the Henry's law and Langmuir regions can be estimated, using the dual mode parameter in Table 6.2, as follows:

$$\frac{C_H}{C_D} = \frac{C_H' b}{k_D (1 + bf)} \tag{6.9}$$

In the limit of zero fugacity, Eq. (6.9) can be written as follows:

$$\lim_{f \to 0} \frac{C_H}{C_D} = \frac{C_H' b}{k_D} \tag{6.10}$$

Penetrant sorption in glassy polymers, especially for condensable vapors, always favors sorption in the Langmuir region over the Henry's law region at the limit of low fugacity. For example, at 35°C and in the limit of zero fugacity, the *n*-C_4H_{10} concentration sorbed in the Langmuir region is approximately 22 times that sorbed in the Henry's law region. Since most *n*-C_4H_{10} sorption at low *n*-C_4H_{10} fugacity in PTMSP takes place in the Langmuir region, there should be no significant dilation observed at this *n*-C_4H_{10} fugacity range, as shown in Figure 6.12(b). And, as a result, the estimated *n*-C_4H_{10} partial molar volume is practically zero at low *n*-C_4H_{10} concentrations, as shown in Figure 6.17(b)). As fugacity increases, the ratio C_H/C_D calculated using Eq. (6.9) decreases. In other words, the fraction of penetrant sorption in the Henry's law region increases with fugacity. This trend is consistent with the dilation data in Figures 6.17(a) and (b), where the partial molar volumes of CH_4 and *n*-C_4H_{10} increase with increasing concentration (or fugacity).

Fleming and Koros suggested that the pure gas dilation data can be predicted from the concentration of penetrant sorbed in the Henry's law region [24]:

$$\frac{\Delta V}{V_o} = \frac{C_D}{22414} V_D = \frac{k_D f}{22414} V_D \tag{6.11}$$

where V_D is the penetrant partial molar volume in the Henry's law region. Ideally, V_D should be similar to the penetrant partial molar volume in low molecular weight systems [24]. The dashed lines in Figures 6.16(a) and (b) represent pure gas volume dilation of CH_4 and *n*-C_4H_{10} at 25°C calculated from Eq. (6.11), using the k_D values of CH_4 and *n*-C_4H_{10} at 25°C from in Table 6.2, the average partial molar volume of CH_4 in five organic solvents at 25°C (53 cm^3/mol) [23] as V_D of CH_4, and the pure liquid molar volume of *n*-C_4H_{10} at 20°C (100 cm^3/mol) [5] as V_D of *n*-C_4H_{10}. These values of V_D substantially overestimate the polymer volume dilation at 25°C. The solid lines in Figure 16(a) and (b) are predictions from Eq. (6.11) using best fit V_D values at each temperature recorded in Table 6.3. The best fit V_D values are still considerably lower than the partial molar volumes of CH_4 and *n*-C_4H_{10} in low molecular weight systems.

Table 6.3 Best fit V_D of CH_4 and *n*-C_4H_{10} in PTMSP at various temperatures

T (°C)	V_D (cm^3/mol)	
	CH_4	*n*-C_4H_{10}
-20	29 ± 3	82 ± 6
0	22 ± 3	83 ± 5
25	16 ± 3	77 ± 6
35	16 ± 3	66 ± 5

The same results are also observed when Eq. (6.11) is used to fit other PTMSP dilation data in the literature [22,25]. The best fit V_D values of CO_2 in PTMSP at 35°C (6.2 cm^3/mol) is well below the CO_2 partial molar volume in liquids (46 cm^3/mol) [22]. The best fit V_D values of *n*-C_9H_{20} in PTMSP at 35°C is 17% lower than the liquid molar volume of *n*-C_9H_{20} at the same temperature [25]. These values are presented in Table 6.4 which also compares the V_D values in poly(2,2-bistrifluoromethyl-4,5-difluoro-1,3-dioxole-*co*-tetrafluoroethylene) (AF2400), a glassy polymer with very high fractional free volume (~0.32) [21] similar to PTMSP, and in polycarbonate, a conventional, low free volume glassy polymer. Similar to PTMSP, the best fit V_D of CO_2 in AF2400 (16 cm^3/mol) is considerably lower than the CO_2 partial molar volume in liquid [26]. In contrast, the best fit V_D values for CO_2 and CH_4 in low free volume polycarbonate are practically the same as their molar volumes in liquids [24,27]. The dense Henry's law region in high free volume glassy polymers, such as PTMSP and AF2400 could contain free volume elements that are large enough for some penetrant molecules to fill without introducing as much swelling as in a dense material such as a liquid, a low free volume glassy polymer, or a rubbery polymer. As penetrant size increases, this effect presumably diminishes, and V_D becomes more similar to the partial molar volume in liquids. For example, the V_D of CO_2, CH_4, *n*-C_4H_{10} and *n*-C_9H_{20} (*i.e.,* increasing penetrant critical volume) in PTMSP are 13, 30, 66 and 83%, respectively, of their partial molar volumes in liquids. Although using Eq. (6.11) with the penetrant partial molar volume in liquids as V_D provides reasonable dilation prediction in conventional, low free volume glassy polymers, there are also cases where this method underestimates the dilation in such polymers [15]. This effect has been ascribed to swelling of the polymer by penetrants in the Langmuir as well as Henry's law sites. In this case, the best fit V_D values are greater

than the partial molar volumes in liquids. In summary, more theoretical and experimental studies are needed to better understand the swelling of glassy polymers.

Table 6.4 Best fit V_D of various penetrants at 35°C

	V_D (cm^3/mol)			
	CO_2	CH_4	*n*-C_4H_{10}	*n*-C_9H_{20}
PTMSP	6.2[a]	16	66	148[b]
AF2400[c]	14	-	-	-
Polycarbonate[d]	46	48	-	-
Liquid	46[e]	53[e]	100[f]	179[f]

[a]Pope *et al.* [22]
[b]Witchey-Lakshmanan *et al.* [25]
[c]De Angelis, *et al.* [26]
[d]Fleming [27]
[e]Partial molar volumes in organic liquids at 25°C [23]
[f]Pure liquid molar volume at 20°C [5]

6.8 MIXED GAS DILATION

PTMSP dilation isotherms as a function of fugacity for different *n*-C_4H_{10}/CH_4 mixtures at various temperatures are presented in Figures 6.18(a)-(d). These mixture isotherms can be estimated reasonably well from the pure gas sorption and dilation data, using the following extension of Eq.(6.11):

$$\frac{\Delta V}{V_o} = \frac{k_{D_A} f_A}{22414} V_{D_A} + \frac{k_{D_B} f_B}{22414} V_{D_B} \tag{6.12}$$

where the subscripts *A* and *B* represent CH_4 and *n*-C_4H_{10}, respectively. V_{D_A} and V_{D_B} are the partial molar volumes of CH_4 and *n*-C_4H_{10}, respectively, in the Henry's law region, determined from pure gas measurements (*cf.,* Table 6.3). The solid lines in Figures

6.18(a)-(d), which represent predictions of Eq. (6.12), describe the experimental mixture dilation data reasonably well.

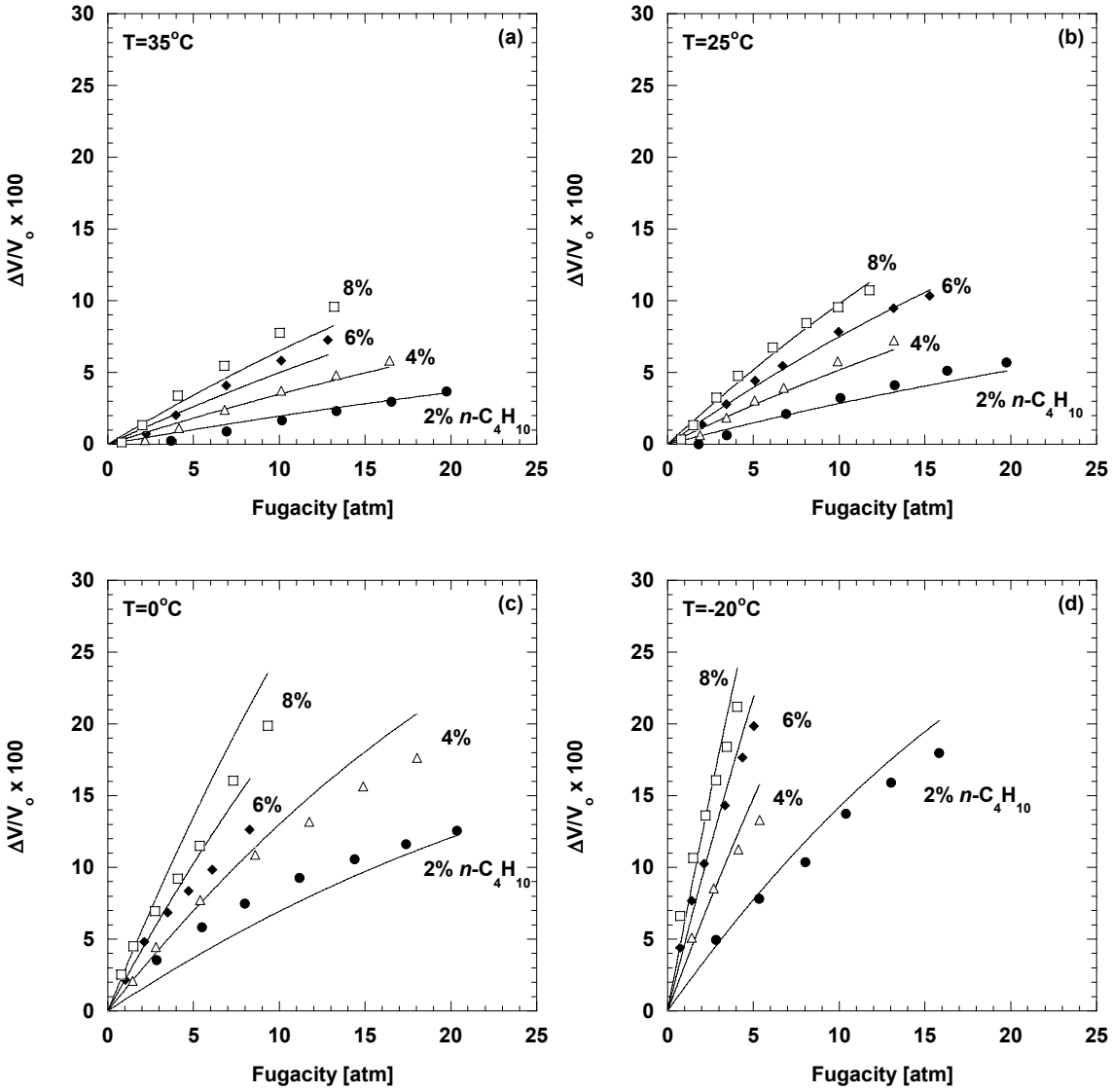

Figure 6.18 n-C_4H_{10}/CH_4 mixture dilation in PTMSP at (a) 35°C, (b) 25°C, (c) 0°C, and (d) -20°C, as a function of total mixture fugacity. The solid lines are predictions from Eq. (6.12) using k_D values from Table 6.2 and V_D values from Table 6.3. The numbers beside the data points represent the mole percent n-C_4H_{10} in the gas mixture.

6.9 CONCLUSIONS

Competitive sorption effects in PTMSP considerably reduce CH_4 solubility in mixtures with *n*-C_4H_{10}. *n*-C_4H_{10}, which is more condensable than CH_4 and preferentially sorbed in the polymer, occupies many of the Langmuir sorption sites, thereby reducing the CH_4 sorption capacity, and, consequently, decreases CH_4 mixture solubility. On the other hand, *n*-C_4H_{10} solubility is not significantly affected by the presence of CH_4 in the mixture. The dual mode mixture sorption model captures this competitive effect and is able to satisfactorily describe the experimental mixture sorption data. The *n*-C_4H_{10}/CH_4 mixture solubility selectivity decreases as *n*-C_4H_{10} decreases and temperature increases. The solubility selectivities determined from the mixed gas measurements are significantly higher than those estimated from the pure gas measurements due to the presence of *n*-C_4H_{10} reducing the concentration of CH_4 dissolved in the polymer.

As suggested previously, the pure and mixed gas volume dilation in glassy PTMSP is attributed only to the swelling in the Henry's law region. The penetrant partial molar volumes of CH_4 and *n*-C_4H_{10} in the Henry's law region do not change significantly in pure or mixed gas environments. The mixed gas dilation in PTMSP can be described reasonably using an additive model that ascribes polymer dilation only to those penetrant molecules sorbed in the Henry's Law regions of the polymer. However, the effective partial molar volumes of CH_4 and *n*-C_4H_{10} required to describe the data are markedly lower than the values expected based on the partial molar volumes of these penetrants in liquids or rubbery polymers, suggesting that these molecules sorb into even the Henry's law regions of the polymer with relatively little polymer swelling.

6.10 REFERENCES

[1] T. C. Merkel, V. Bondar, K. Nagai, and B. D. Freeman, "Sorption and transport of hydrocarbon and perfluorocarbon gases in poly(1-trimethylsilyl-1-propyne)", Journal of Polymer Science: Part B: Polymer Physics, 38 (2000) 273-96.

[2] K. Nagai and T. Nakagawa, "Effects of aging on the gas permeability and solubility in poly(1-trimethylsilyl-1-propyne) membranes synthesized with various catalysts", Journal of Membrane Science, 105 (1995) 261-72.

[3] D. S. Pope, W. J. Koros, and G. K. Fleming, "Measurement of thickness dilation in polymer films", Journal of Polymer Science: Part B: Polymer Physics, 27 (1989).

[4] R. D. Raharjo, B. D. Freeman, and E. S. Sanders, "Pure and mixed gas CH_4 and *n*-C_4H_{10} sorption and dilation in poly(dimethylsiloxane)", Journal of Membrane Science, 292 (2007) 45-61.

[5] B. E. Poling, J. M. Prausnitz, and J. P. O'Connell, The Properties of Gases and Liquids, 5th ed., McGraw-Hill, New York, NY, 2001.

[6] I. Pinnau, C. G. Casillas, A. Morisato, and B. D. Freeman, "Hydrocarbon/hydrogen mixed gas permeation in poly(1-trimethylsilyl-1-propyne) (PTMSP), poly(1-phenyl-1-propyne) (PPP), and PTMSP/PPP blends", Journal of Polymer Science: Part B: Polymer Physics, 34 (1996) 2613-21.

[7] P. R. Bevington, Data Reduction and Error Analysis for the Physical Sciences, 3rd ed., McGraw-Hill, New York, NY, 2002.

[8] E. S. Sanders, W. J. Koros, H. B. Hopfenberg, and V. Stannett, "Pure and mixed gas sorption of carbon dioxide and ethylene in poly(methyl methacrylate)", Journal of Membrane Science, 18 (1984) 53-74.

[9] R. Srinivasan, S. R. Auvil, and P. M. Burban, "Elucidating the mechanism(s) of gas transport in poly[1-(trimethylsilyl)-1-propyne] (PTMSP) membranes", Journal of Membrane Science, 86 (1994) 67-86.

[10] W. J. Koros, A. H. Chan, and D. R. Paul, "Sorption and transport of various gases in polycarbonate", Journal of Membrane Science, 2 (1977) 165-90.

[11] K. C. O'Brien, W. J. Koros, and T. A. Barbari, "A new technique for the measurement of multicomponent gas transport through polymeric films", Journal of Membrane Science, 29 (1986) 229-38.

[12] K. Toi, G. Morel, and D. R. Paul, "Gas sorption and transport in poly(phenylene oxide) and comparisons with other glassy polymers", Journal of Applied Polymer Science, 27 (1982) 2997-3005.

[13] W. J. Koros, D. R. Paul, and G. S. Huvard, "Energetics of gas sorption in glassy polymers", Polymer, 20 (1979) 956-60.

[14] A. S. Michaels, W. R. Vieth, and J. A. Barrie, "Diffusion of gases in poly(ethylene terephthalate)", Journal of Applied Physics, 34 (1963) 13-20.

[15] J.-S. Wang and Y. Kamiya, "Concurrent measurements of sorption and dilation isotherms and diffusivity for polysulfone membrane/carbon dioxide system", Journal of Membrane Science, 98 (1995) 69-76.

[16] E. Buss, "Gravimetric measurement of binary gas adsorption equilibria of methane-carbon dioxide mixtures on activated carbon", Gas Separation and Purification, 9 (1995) 189-97.

[17] F. Vigne-Maeder and A. Auroux, "Potential maps of methane, water, and methanol in silicalite", Journal of Physical Chemistry, 94 (1990) 316-22.

[18] N. A. Al-Baghli and K. F. Loughlin, "Adsorption of methane, ethane, and ethylene on titanosilicate ETS-10 zeolite", Journal of Chemincal Engineering Data, 50 (2005) 843-8.

[19] P. Li and H. Tezel, "Adsorption separation of N_2, O_2, CO_2, and CH_4 gases by β-zeolite", Microporous and Mesoporous Materials, 98 (2007) 94-101.

[20] J. A. Barrie, K. Munday, and M. Williams, "Sorption and diffusion of hydrocarbon vapors in glassy polymers", Organic Coatings and Plastics Chemistry, 39 (1978) 187-91.

[21] T. C. Merkel, V. Bondar, K. Nagai, B. D. Freeman, and Y. Yampolskii, "Gas sorption, diffusion, and permeation in poly(2,2-bis(trifluoromethyl)-4,5-difluoro-1,3-dioxole-*co*-tetrafluoroethylene)", Macromolecules, 32 (1999) 8427-40.

[22] D. S. Pope, W. J. Koros, and H. B. Hopfenberg, "Sorption and dilation of poly(1-(trimethylsilyl)-1-propyne) by carbon dioxide and methane", Macromolecules, 27 (1994) 5839-44.

[23] J. Horiuti, "The solubility of gas and coefficient of dilatation by absorption", Scientific Papers of the Institute of Physical and Chemical Research, 17 (1931) 125-256.

[24] G. K. Fleming and W. J. Koros, "Dilation of polymers by sorption of carbon dioxide at elevated pressures. 1. Silicone rubber and unconditioned polycarbonate", Macromolecules, 19 (1986) 2285-91.

[25] L. C. Witchey-Lakshmanan, H. B. Hopfenberg, and R. T. Chern, "Dilation of poly[1-(trimethylsilyl)-1-propyne] during sorption of *n*-nonane", Journal of Polymer Science: Part B: Polymer Physics, 31 (1993) 1545-53.

[26] M. G. De Angelis, T. C. Merkel, V. I. Bondar, B. D. Freeman, F. Doghieri, and G. C. Sarti, "Gas sorption and dilation in poly(2,2-bis(trifluoromethyl)-4,5-difluoro-1,3-dioxole-*co*-tetrafluoroethylene): Comparison of experimental data with predictions of the nonequilibrium lattice fluid model", Macromolecules, 35 (2002) 1276-88.

[27] G. K. Fleming, Dilation of silicone rubber and glassy polycarbonates due to high pressure gas sorption, Ph.D Dissertation, University of Texas at Austin, Austin, TX, 1988.

Chapter 7: Pure and Mixed Gas CH_4 and *n*-C_4H_{10} Permeability and Diffusivity in Poly(1-trimethylsilyl-1-propyne)

This chapter provides the pure and mixed gas *n*-C_4H_{10} and CH_4 permeability and diffusivity in poly(1-trimethylsilyl-1-propyne) (PTMSP) at temperatures ranging from -20 to 35°C. The blocking effect by *n*-C_4H_{10} that hinders CH_4 transport through the polymer is investigated. This chapter also quantifies the extent to which deviations between pure and mixed gas permeation properties in PTMSP depend on differences between pure and mixed gas solubility and diffusivity. In addition, the effects of *n*-C_4H_{10} and temperature on *n*-C_4H_{10}/CH_4 mixture permeability, solubility, and diffusivity selectivities in PTMSP are discussed. The dual mode permeability model is used to describe the experimental data.

7.1 Physical Aging and Hysteresis During Measurements

The pure and mixed gas permeability measurements for each sample (*i.e.,* fresh) were completed in 8 hours at most. The pure gas CH_4 and *n*-C_4H_{10} permeabilities in PTMSP were essentially constant over this time period, indicating that the physical aging of the film was minimal during the time of measurement. The pure gas CH_4 permeability decreased after exposing the film to *n*-C_4H_{10} (*i.e.,* after mixture measurements). For example, the pure gas CH_4 permeability at 4.4 atm feed pressure and 35°C decreased by approximately 22%, from 24000 to 19000 Barrer, after exposing the film to a 2 mol% *n*-C_4H_{10}/CH_4 mixture up to 14.6 atm. This behavior can be related to penetrant-induced hysteresis, which has been observed previously in another high free volume glassy polymer [1]. To avoid such hysteresis effect, fresh PTMSP films were used for each mixture permeability measurement.

7.2 PURE GAS PERMEABILITY

Figures 7.1(a) and (b) present CH_4 and *n*-C_4H_{10} pure gas permeability coefficients in PTMSP as a function of upstream fugacity, or upstream activity for *n*-C_4H_{10}, at temperatures from -20 to 35°C. In general, CH_4 and *n*-C_4H_{10} permeabilities decrease with increasing upstream fugacity and temperature. The infinite dilution permeability values at each temperature presented in Table 7.1 are calculated as follows:

$$P_o = k_D \bar{D}_D + C'_H b \bar{D}_H \tag{7.1}$$

The CH_4 and *n*-C_4H_{10} permeability values are somewhat higher than some reported literature values for PTMSP [2-4]. Merkel *et al.* reported CH_4 pure gas infinite dilution permeability of 15000 Barrer at 35°C [2]. Srinivasan *et al.* reported a value of 17000 Barrer at 25°C [3]. For comparison, the CH_4 pure gas infinite dilution permeability coefficients in this study are 28000 and 31000 Barrer at 35 and 25°C, respectively. Pinnau and Toy reported *n*-C_4H_{10} permeability of 78000 Barrer at 23°C and 0.63 *n*-C_4H_{10} upstream activity (p/p_{sat}), about 30% lower than the value determined in this study under similar upstream conditions (112000 Barrer at 25°C and 0.61 *n*-C_4H_{10} upstream activity). Gas transport properties in PTMSP are quite sensitive to film preparation conditions and processing history [5,6]. As a result, PTMSP permeability values in the literature vary widely [3]. Our PTMSP film density (0.73 g/cm^3) is slightly lower than that reported by Merkel *et al.*, Srinivasan *et al.*, and Pinnau and Toy (0.75 g/cm^3) [2-4], and this lower density translates to a higher fractional free volume (FFV), which may explain the higher permeability values in this study. Recently, Hu *et al.* reported CH_4 permeability at 25°C to be 30,000 Barrer in PTMSP, which is quite similar to our value [7]. However, *n*-C_4H_{10} permeability and polymer density were not reported in this study, so one cannot comment further on the reason for the good agreement between our CH_4 permeability and theirs.

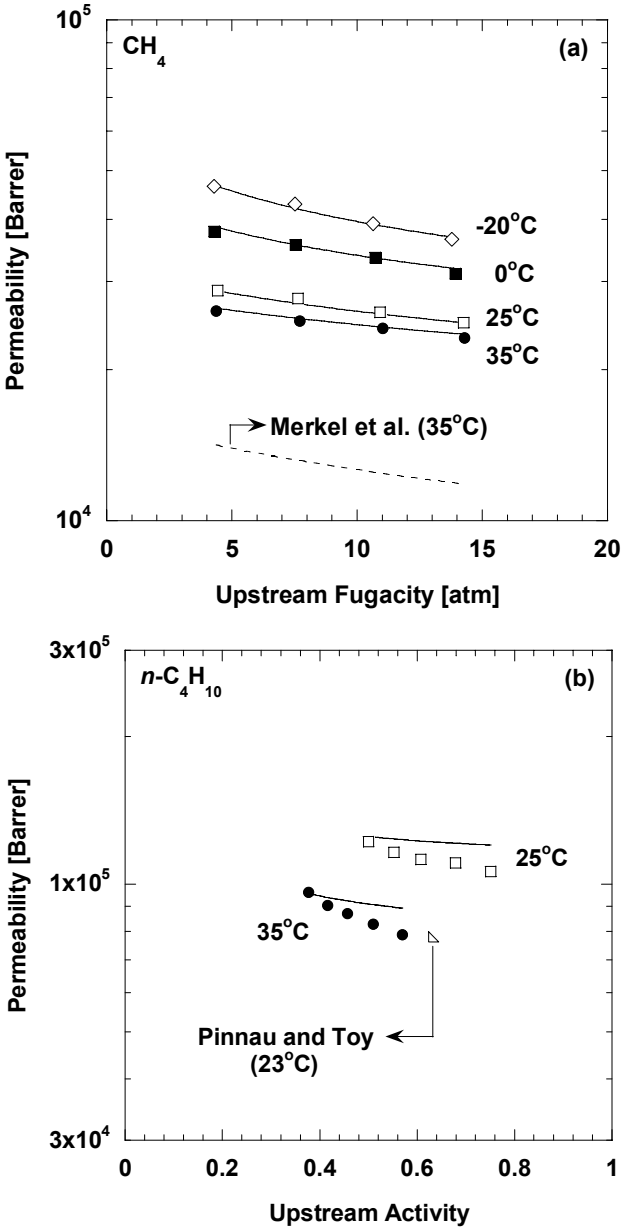

Figure 7.1 (a) Pure gas permeability of CH_4 in PTMSP as a function of upstream fugacity and temperature. The dashed line represents pure CH_4 permeability values at 35°C reported by Merkel *et al.* [2] (b) Pure gas permeability of *n*-C_4H_{10} in PTMSP as a function of upstream activity and temperature. The solid lines represent a nonlinear least squares fit of Eq. (2.17) to the experimental data. The pure gas *n*-C_4H_{10} permeability value in PTMSP reported by Pinnau and Toy [4] is presented as a reference.

Table 7.1 Dual mode diffusion coefficients, permeability and concentration-averaged diffusion coefficients at infinite dilution in PTMSP

T (^{o}C)	CH_4[a]				n-C_4H_{10}[b]			
	$\bar{D}_D$ x 10^6 (cm^2/s)	$\bar{D}_H$ x 10^6 (cm^2/s)	$\bar{D}_o$ x 10^6 (cm^2/s)	P_o x 10^{-3} (Barrer)	$\bar{D}_D$ x 10^6 (cm^2/s)	$\bar{D}_H$ x 10^6 (cm^2/s)	$\bar{D}_o$ x 10^6 (cm^2/s)	P_o x 10^{-3} (Barrer)
-20	180 ± 20	28 ± 3	44 ± 4	52 ± 3	9 ± 1	1.6 ± 0.2	1.7 ± 0.2	2300 ± 150
0	200 ± 20	29 ± 3	52 ± 5	41 ± 2	14 ± 1	2.3 ± 0.2	2.5 ± 0.2	1400 ± 80
25	180 ± 20	35 ± 3	61 ± 6	31 ± 2	21 ± 2	3.3 ± 0.3	3.8 ± 0.3	580 ± 40
35	200 ± 20	39 ± 4	70 ± 7	28 ± 2	20 ± 2	4.4 ± 0.4	5.1 ± 0.5	450 ± 30

[a]Based on pure gas measurements

[b]Based on pure and mixed gas measurements

1 Barrer = 1 x 10^{-10} cm^3(STP) cm/(cm^2 s cmHg)

7.3 PURE GAS DIFFUSIVITY

Concentration-averaged diffusion coefficients were estimated from the permeability and sorption data using the following rearranged form of Eq. (2.4) [8]:

$$\bar{D}_A = P_A \left(\frac{f_{A,2}}{C_{A,2}} \right) \tag{7.2}$$

Figures 7.2(a) and (b) present pure gas CH_4 and *n*-C_4H_{10} concentration-averaged diffusion coefficients in PTMSP as a function of upstream fugacity, or upstream activity for *n*-C_4H_{10}. The pure gas diffusion coefficient of CH_4 increases with increasing upstream fugacity and temperature, consistent with the results of Merkel *et al.* [2], although our values are somewhat higher than theirs, consistent with the higher permeability coefficients reported in Figure 7.1. Merkel *et al.* reported that the pure gas CH_4 diffusion coefficient at 35°C and infinite dilution was 3.6×10^{-6} cm^2/s [2]. As discussed earlier, this discrepancy is most likely due to the lower film density in our study. The diffusion coefficients in PTMSP are about 10^3 to 10^6 times higher than those observed in conventional, low free volume, glassy polymers (*e.g.,* polycarbonate) [9].

7.4 MIXED GAS PERMEABILITY

Figure 7.3(a) presents CH_4 mixed gas permeability in PTMSP as a function of *n*-C_4H_{10} feed fugacity. The presence of *n*-C_4H_{10} significantly decreases CH_4 mixture permeability in PTMSP. For example, at 35°C, CH_4 permeability decreases by more than a factor of 10, from 28000 Barrer in pure gas at infinite dilution, to 2200 Barrer in the presence of 0.77 atm *n*-C_4H_{10} fugacity (~0.26 *n*-C_4H_{10} activity). At -20°C, CH_4 permeability decreases from 52000 Barrer in pure gas at infinite dilution, to 1700 Barrer in the presence of 0.32 atm *n*-C_4H_{10} fugacity (~0.73 *n*-C_4H_{10} activity), a more than 30-fold decrease. The CH_4 mixture permeability data at various temperatures collapse

slightly when plotted as a function of *n*-C_4H_{10} upstream activity, rather than fugacity, as shown in Figure 7.3(b). The CH_4 permeability appears to approach a plateau value at high *n*-C_4H_{10} upstream activity.

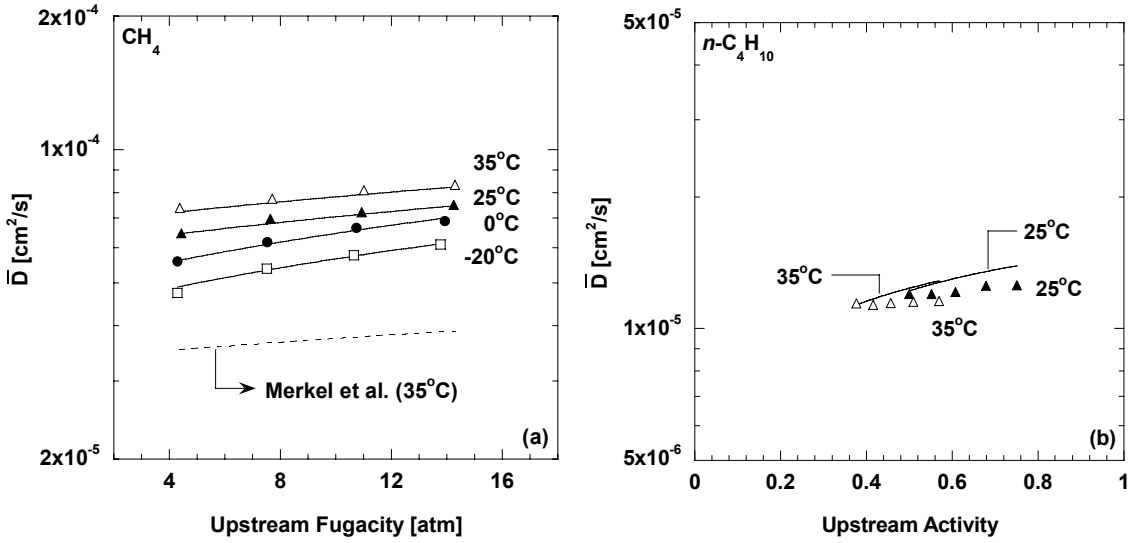

Figure 7.2 (a) Effect of upstream fugacity and temperature on pure gas CH_4 concentration-averaged diffusion coefficients in PTMSP. The dashed lines are pure gas values at 35°C determined by Merkel *et al.* [2] (b) Pure gas *n*-C_4H_{10} concentration-averaged diffusion coefficients in PTMSP as a function of upstream activity and temperature. The solid lines represent Eq. (7.4) and (7.5) using parameters in Table 7.1.

As will be described in more detail later, this decrease in mixture CH_4 permeability is partly due to the decrease in the CH_4 solubility coefficient in the mixtures due to competitive sorption effects described in the previous chapter. *n*-C_4H_{10}, which is much more condensable than CH_4, preferentially occupies the Langmuir sorption sites, thereby reducing CH_4 sorption capacity in this region, which decreases CH_4 solubility in the polymer. Additionally, the reduction in the CH_4 diffusion coefficient in mixtures due to *n*-C_4H_{10} blocking effects also contributes to the decrease in CH_4 mixture permeability in PTMSP.

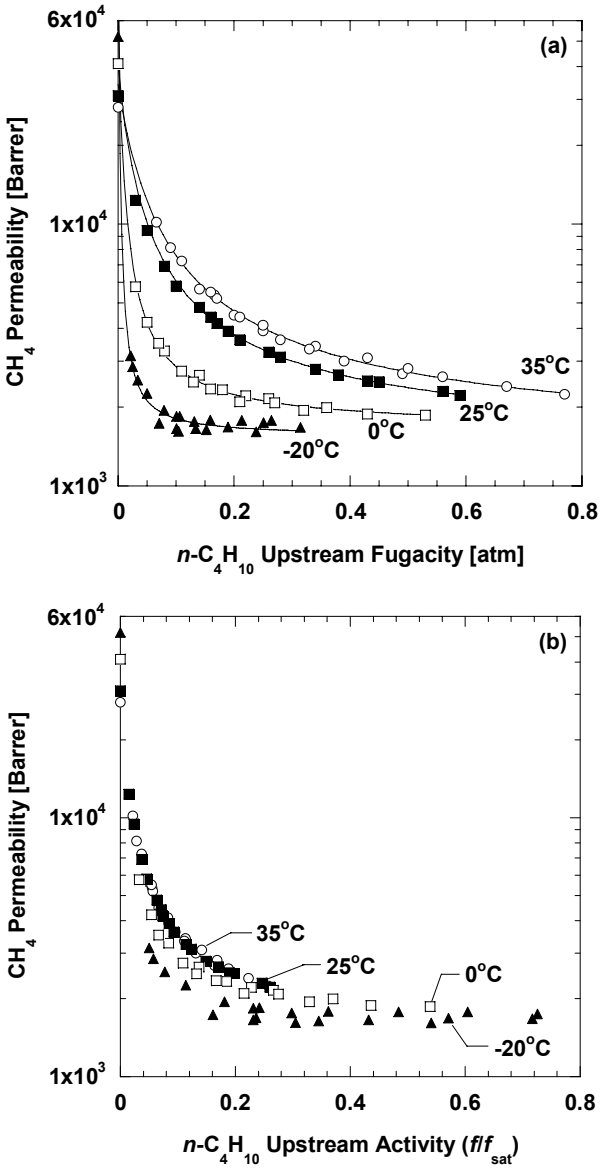

Figure 7.3 CH_4 permeability in PTMSP as a function of (a) *n*-C_4H_{10} upstream fugacity and (b) *n*-C_4H_{10} upstream activity in the feed at 35°C (○), 25°C (■), 0°C (□), and -20°C (▲). The feed gas compositions are 2, 4, 6, and 8 mol% *n*-C_4H_{10} in CH_4. The total feed pressure was from 1.1 – 14.6 atm. The permeate was swept with helium at 1 atm, so the permeate partial pressures of CH_4 and *n*-C_4H_{10} were negligible. The lines represent model fits to the experimental data using Eq. (7.9) and the parameters in Table 7.2.

The presence of CH_4 does not noticeably change n-C_4H_{10} permeability in PTMSP. Figure 7.4 presents n-C_4H_{10} permeability in PTMSP as a function of n-C_4H_{10} feed activity for pure gas and mixed gas conditions. The n-C_4H_{10} permeability coefficients decrease with increasing n-C_4H_{10} activity, which is qualitatively consistent with expectations of the dual mode model (*i.e.,* Eq.(2.17)). The pure gas data agree with the mixture permeability data, suggesting that n-C_4H_{10} permeation is not influenced by the presence of CH_4.

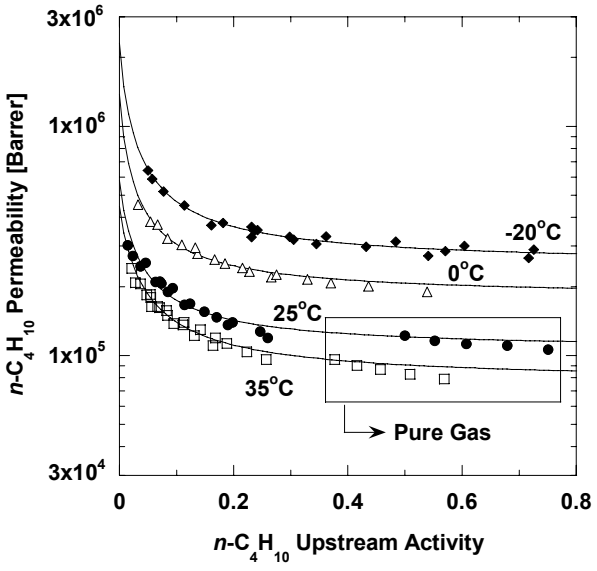

Figure 7.4 n-C_4H_{10} permeability in PTMSP as a function of n-C_4H_{10} upstream activity. The feed gas compositions are 2, 4, 6, and 8 mol% n-C_4H_{10} in CH_4. The total feed pressure was from 1.1 – 14.6 atm. The permeate was swept with helium at 1 atm, so the permeate partial pressures of CH_4 and n-C_4H_{10} were negligible. The lines represent model fits to the experimental data using Eq. (2.20) and the parameters in Table 7.1. For comparison, pure gas n-C_4H_{10} permeation data are also presented.

7.5 EFFECT OF CONCENTRATION ON ACTIVATION ENERGY OF PERMEATION

The temperature dependence of gas permeability in pure gas and mixtures can be described using Eq. (2.9) provided one restricts its use to a given upstream gas concentration. In this case, the activation energy of permeation, E_P, at a fixed penetrant concentration in the polymer can be calculated using Eq. (5.7). The permeability coefficients are estimated from the dual mode permeability models (*i.e.,* Eqs. (2.20) and (7.9)) using parameters determined based on experimental data (Tables 7.1 and 7.2). The upstream gas concentrations were calculated using the dual mode sorption model (*i.e.,* Eqs. (2.18) and (2.19)) and the parameters from Table 6.2.

Figure 7.5 presents pure and mixed gas E_P^C values for CH_4 and *n*-C_4H_{10}. The CH_4 pure gas E_P^C values (open symbols) are presented as a function of upstream CH_4 concentration. The error bars are determined using the propagation of errors method [11]. These pure gas E_P^C values for CH_4 in PTMSP are negative (*i.e.,* exothermic), which is unusual for permanent gas permeation in polymers [12]. That is, CH_4 permeability in PTMSP increases with decreasing temperature. The pure gas E_P^C of CH_4 in PTMSP (*i.e.,* at infinite dilution) is -7.3 ± 1.5 kJ/mol, which is consistent with literature values of -6.3 and -7.6 kJ/mol reported by Masuda *et al.* [13] and Merkel *et al.* [14], respectively. In conventional glassy and even rubbery polymers, E_P^C values for permanent gases (*e.g.,* H_2, N_2, CH_4) are usually positive [12]. Negative E_P^C values for such light gases are commonly observed for microporous solids in which the pore dimensions are larger than the kinetic diameter of the diffusing gas molecules [3]. In contrast to the pure gas behavior, where E_P^C of CH_4 is practically independent of concentration, the E_P^C for CH_4 in *n*-C_4H_{10}/CH_4 mixtures initially increases, from -7.3 ± 1.5 kJ/mol for pure gas, with increasing *n*-C_4H_{10} concentration before reaching a plateau, at approximately 1.1 ± 1.5 kJ/mol, at higher *n*-C_4H_{10} concentrations, as shown in Figure 7.5. The increase in the E_P^C

of CH_4 with increasing *n*-C_4H_{10} concentration is presumably related to the combination of blocking and competitive sorption effects [10], which reduce CH_4 diffusivity and solubility, respectively, in mixtures with *n*-C_4H_{10}. Positive E_P^C values are typical for permanent gas permeation in conventional glassy and rubbery polymers [12]. For example, the E_P^C of pure gas CH_4 in poly(vinly chloride) (PVC), a glassy polymer, is 66.2 kJ/mol [15]. The E_P^C of CH_4 in rubbery PDMS is 6.8 kJ/mol in the pure gas case and 5.1 kJ/mol in the presence of 60 cm^3(STP)/cm^3 of *n*-C_4H_{10} at the upstream face of the film [16]. The pure and mixed gas E_P^C values of *n*-C_4H_{10} with *n*-C_4H_{10} concentration qualitatively exhibit a trend similar to that of CH_4 in gas mixtures. At *n*-C_4H_{10} concentrations greater than 40 cm^3(STP)/cm^3, the E_P^C of *n*-C_4H_{10} increases with increasing *n*-C_4H_{10} concentration until it reaches a plateau at approximately -13.9 ± 1.5 kJ/mol. Because *n*-C_4H_{10} permeability coefficients are not affected by the presence of CH_4, the E_P^C values for *n*-C_4H_{10} are the same in both pure and mixed gas cases.

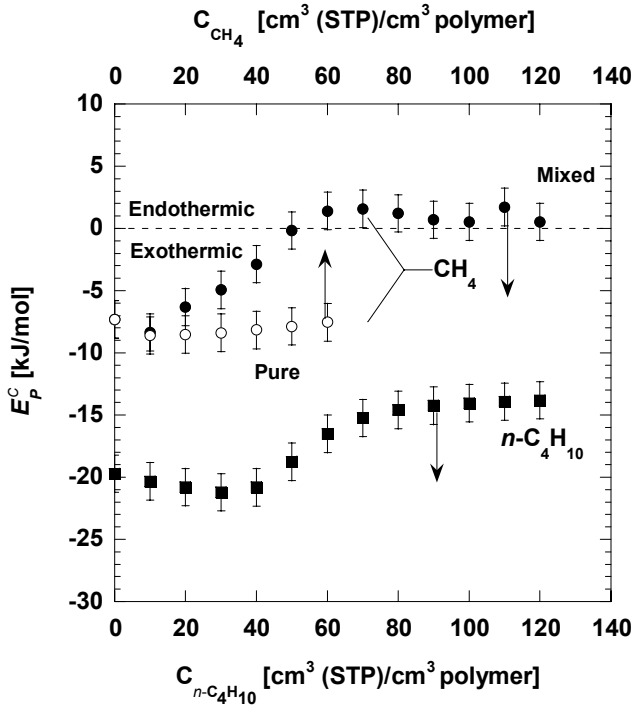

Figure 7.5 Activation energies of permeation of CH_4 and n-C_4H_{10} as a function of penetrant concentration at the upstream face of the film. The n-C_4H_{10} activation energies of permeation are estimated based on mixed gas data, while both pure and mixed gas estimates of the CH_4 activation energies are provided. There is essentially no difference between the pure and mixed gas n-C_4H_{10} permeability data in PTMSP, so the activation energies of permeation for n-C_4H_{10} are the same, within the uncertainty in the measurements, in both pure and mixed gas cases.

7.6 MIXED GAS DIFFUSIVITY

The concentration-averaged CH_4 and n-C_4H_{10} diffusion coefficients in mixtures were estimated using Eq. (7.2) and are presented in Figures 7.6(a) and (b), respectively. The presence of n-C_4H_{10} considerably reduces the CH_4 diffusion coefficient in the polymer even at low levels of n-C_4H_{10} sorption. For example, at 35°C, the CH_4 diffusion coefficient decreases more than 70%, from 7.0×10^{-5} cm^2/s in pure gas at infinite dilution (the point at an n-C_4H_{10} activity of zero in Figure 7.6(a)), to 2.0×10^{-5} cm^2/s when the

upstream n-C_4H_{10} activity is 0.20. In contrast, n-C_4H_{10} diffusion coefficients increase with increasing n-C_4H_{10} activity (*cf.*, Figure 7.6(b)). For n-C_4H_{10}, there is no measurable difference between pure and mixed gas diffusivity values; that is, the effect of CH_4 on n-C_4H_{10} diffusion coefficients is negligible.

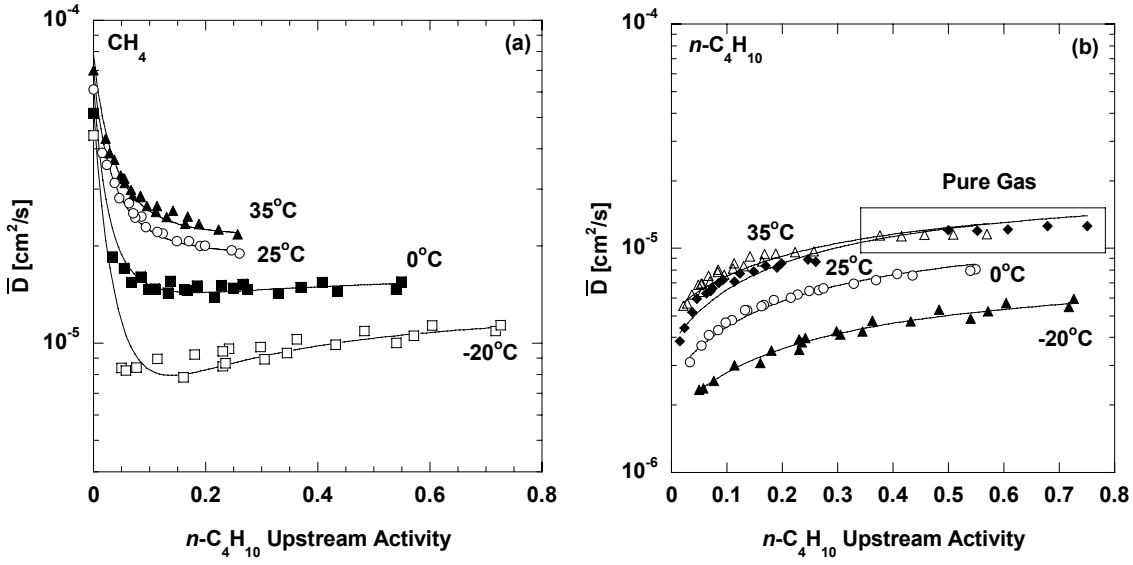

Figure 7.6 The average effective diffusion coefficient of: (a) CH_4 and (b) n-C_4H_{10} as a function of n-C_4H_{10} activity in the feed mixtures. The solid lines in (a) are predictions from Eq. (7.10) using the parameters in Table 7.2. The lines in (b) are predictions from Eq. (7.5) using the parameters in Table 7.1.

The blocking effect, which acts to reduce CH_4 diffusivity due to the presence of n-C_4H_{10}, and the competitive sorption effect, which acts to reduce CH_4 solubility due to the presence of n-C_4H_{10} [10], are both responsible for the mixed gas permeability depression in Figure 7.3(a). Figures 7.7(a)-(d) present the ratio of CH_4 mixed gas permeability, solubility, and diffusivity to those of pure gas at infinite dilution as a function of n-C_4H_{10} activity at 35, 25, 0, and -20°C, respectively. The CH_4 permeability decrease in the mixture is substantial: at -20°C and 0.73 n-C_4H_{10} activity, the mixed gas CH_4 permeability in PTMSP is only 3.3% of the pure gas value. Both solubility and

diffusivity contribute to this reduction, with solubility reduction (*i.e.,* competitive sorption) generally contributing somewhat more to the overall permeability reduction than diffusivity reduction.

The local effective diffusion coefficient, D_A, characterizes the ability of a penetrant to migrate through a polymer at a particular, well-defined penetrant concentration [17]. Pure gas D_A values were calculated from the slope of the sorption isotherm from Chapter 6 and the pressure dependence of permeability using Eq. (5.4). The local effective diffusion coefficients of *n*-C_4H_{10} in *n*-C_4H_{10}/CH_4 mixtures were also calculated using Eq. (5.4) because *n*-C_4H_{10} permeability, diffusivity, and solubility in these mixtures are essentially unaffected by the presence of CH_4. In Eq. (5.4), $dP_A/df_{A,2}$ is estimated from the measured *n*-C_4H_{10} fugacity dependence of *n*-C_4H_{10} mixture permeability in the polymer, and df_A/dC_A is estimated from the pure gas sorption isotherms of *n*-C_4H_{10} in PTMSP presented in the previous chapter.

Figure 7.8(a) presents D_A values for *n*-C_4H_{10} in the mixture as a function of *n*-C_4H_{10} concentration. The *n*-C_4H_{10} diffusion coefficients increase with increasing *n*-C_4H_{10} concentration, similar to the trend presented in Figure 7.6(b). At sufficiently high *n*-C_4H_{10} concentration, the *n*-C_4H_{10} diffusion coefficient reaches a plateau and no longer changes with *n*-C_4H_{10} concentration in the polymer.

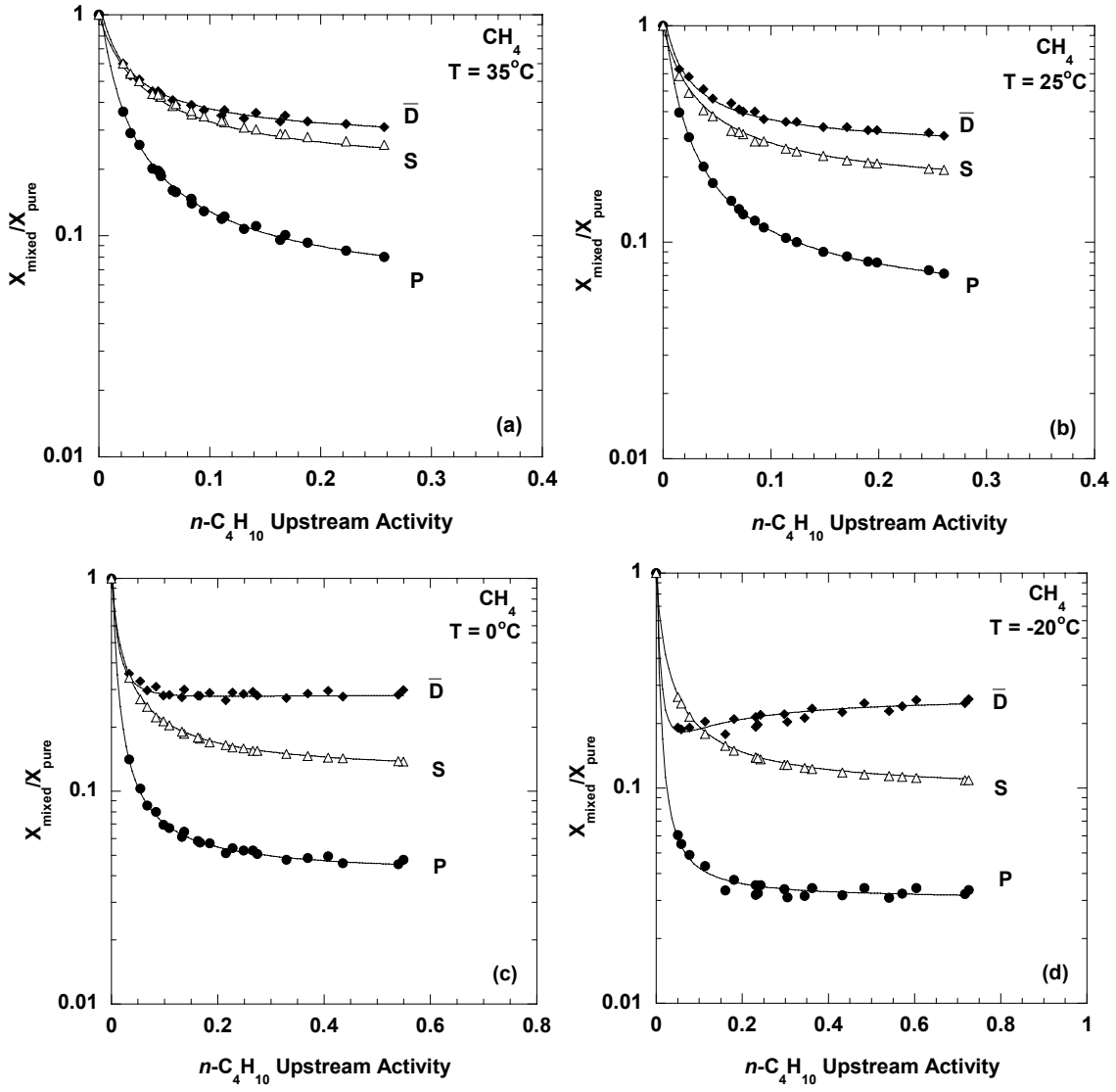

Figure 7.7 The ratio of CH_4 mixed gas permeability (P), solubility (S), and diffusivity ($\bar{D}$) coefficients to those of pure gas at infinite dilution as a function of *n*-C_4H_{10} activity at (a) 35°C, (b) 25°C, (c) 0°C, and (d) -20°C. The total feed pressure was from 1.1 – 14.6 atm. The solid lines are predictions of the dual mode models (*i.e.,* Eqs. (2.17), (7.9), (7.4), (7.10), and (2.18)).

The local effective diffusion coefficients of CH_4 in mixtures (*i.e.,* D_B), which depend on *n*-C_4H_{10} concentration in the polymer, were estimated using Eq. (5.6). A different formula (Eq. (5.6) instead of (5.4)) is used to calculate the local effective diffusion coefficients of CH_4 in mixtures because these values depend sensitively on *n*-C_4H_{10} concentration. Figure 7.8(b) presents the local effective diffusion coefficients of CH_4 in mixtures as a function of *n*-C_4H_{10} concentration at the upstream side of the membrane. There is a minimum in the local CH_4 diffusion coefficient with concentration that was not apparent previously in Figure 7.6(a). For example, at 35°C, the CH_4 local effective diffusion coefficient initially decreases with increasing *n*-C_4H_{10} concentration, from 7.0×10^{-5} cm^2/s in pure gas (infinite dilution) to a minimum value of approximately 1.5×10^{-5} cm^2/s in the presence of 32 cm^3(STP) *n*-C_4H_{10}/cm^3 polymer. At higher *n*-C_4H_{10} concentrations, the CH_4 local diffusion coefficients increase, reaching a value of 2.2×10^{-5} cm^2/s in the presence of 58 cm^3(STP) *n*-C_4H_{10}/cm^3 polymer. This trend can perhaps be rationalized by a competition between two phenomena: (1) blocking of the large, interconnected free volume elements in PTMSP by *n*-C_4H_{10}, which hinders CH_4 transport, and (2) plasticization of the film by *n*-C_4H_{10} sorption, which increases the CH_4 diffusion coefficient. At low *n*-C_4H_{10} concentration, *n*-C_4H_{10} sorption occurs predominantly in the Langmuir regions [10], with little or no plasticization. Thus, the blocking effect is stronger than the plasticization effect at lower *n*-C_4H_{10} concentrations. As a result, CH_4 diffusion coefficients initially decrease with increasing *n*-C_4H_{10} concentration. As *n*-C_4H_{10} concentration increases, the Langmuir region becomes progressively more saturated, resulting in a greater fraction of *n*-C_4H_{10} sorption in the Henry's law region [10], rendering plasticization more important. In addition, the blocking effect should reach a maximum, hypothetically, as the Langmuir region becomes saturated. At higher *n*-C_4H_{10} concentrations, plasticization overcomes the

blocking effect, and, consequently, the CH_4 diffusion coefficient increases with increasing *n*-C_4H_{10} concentration.

Throughout this study, the magnitude of the CH_4 diffusion coefficient *reduction* due to blocking effect is considerably greater than the CH_4 diffusion coefficient *enhancement* due to plasticization effect, as shown in Figure 7.8(b). For example, at 25°C, the blocking effect decreases the CH_4 local effective diffusion coefficient by a factor of five, from 6.1×10^{-5} cm^2/s in pure gas (infinite dilution) to 1.3×10^{-5} cm^2/s in the presence of 39 cm^3(STP) *n*-C_4H_{10}/cm^3 polymer. In contrast, the plasticization effect increases the CH_4 local diffusion coefficient by a factor of only approximately two, from 1.3×10^{-5} to 2.2×10^{-5} cm^2/s, as *n*-C_4H_{10} concentration goes from 39 to 60 cm^3(STP)/cm^3.

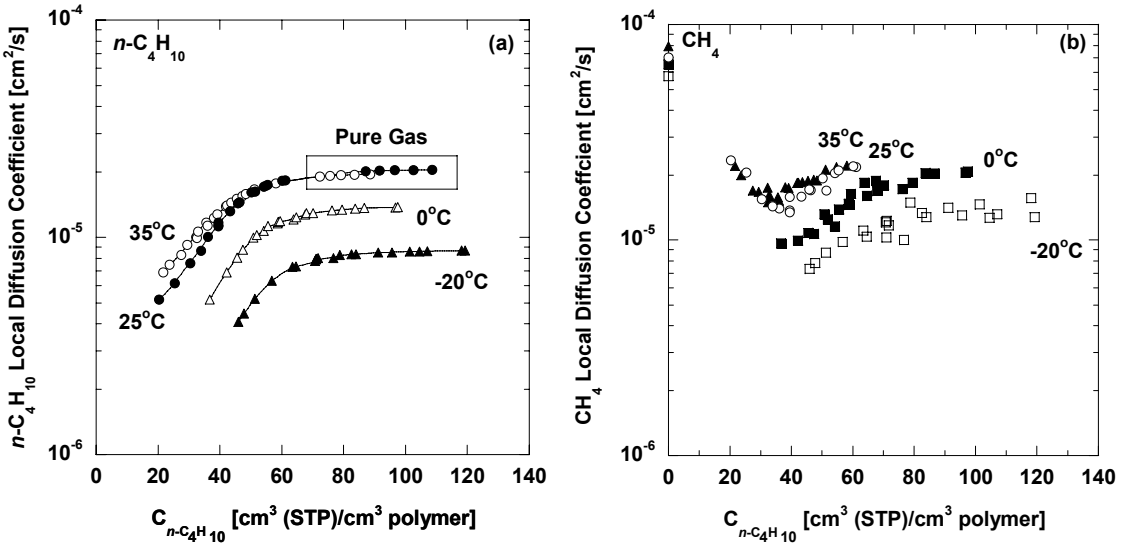

Figure 7.8 Local diffusion coefficients as a function of *n*-C_4H_{10} concentration in the polymer: (a) *n*-C_4H_{10} and (b) CH_4. For comparison, pure gas *n*-C_4H_{10} data (*i.e.,* the data points in the box) are presented along with the mixed gas data. The solid lines in (a) are predictions of the dual mode permeability model (*i.e.,* Eq. (7.6)). The pure gas CH_4 local diffusion coefficients are reported at 4.4 atm upstream pressure.

7.7 EFFECT CONCENTRATION ON ACTIVATION ENERGY OF DIFFUSION

The temperature dependence of gas diffusivity in pure gas and mixtures can be characterized using Eq. (2.11). The activation energy of diffusion, E_D, at a fixed penetrant concentration can be determined as follows [16]:

$$E_D^C = -R\left(\frac{d\ln \bar{D}_A}{d\left(1/T\right)}\right)_C \tag{7.3}$$

where E_D^C is the activation energy of diffusion when the penetrant concentration is C. Figure 7.9 shows that although E_D^C for pure CH_4 is not a strong function of concentration, the E_D^C of CH_4 in gas mixtures depends on *n*-C_4H_{10} concentration, where it exhibits a maximum (12.2 ± 1.5 kJ/mol) at 50 cm^3(STP)/cm^3 *n*-C_4H_{10}. For comparison, the mixed gas E_D^C of CH_4 in PDMS in the presence of 50 cm^3(STP)/cm^3 *n*-C_4H_{10} is 12.1 kJ/mol. The increase in CH_4 E_D^C as *n*-C_4H_{10} concentration increases may be related to the blocking effect by *n*-C_4H_{10} that hinders CH_4 transport through the polymer. As *n*-C_4H_{10} competitively occupies the more facile permeation pathways, methane transport is restricted to routes requiring more energy. As *n*-C_4H_{10} concentration increases, the plasticization effect, which enhances CH_4 transport and reduces E_D^C, begins to dominate. This phenomenon is shown in Figure 7.9, where the E_D^C of CH_4 decreases with increasing *n*-C_4H_{10} concentration at high *n*-C_4H_{10} concentrations. The E_D^C of *n*-C_4H_{10} also shows a concentration dependence similar to that of the E_D^C of CH_4 in mixture. The E_D^C of *n*-C_4H_{10} reaches a maximum value of 15.4 ± 1.5 kJ/mol at a *n*-C_4H_{10} concentration of 50 cm^3(STP)/cm^3. However, the dependence of E_D^C of *n*-C_4H_{10} on *n*-C_4H_{10} concentration is weaker than that of CH_4 in gas mixtures.

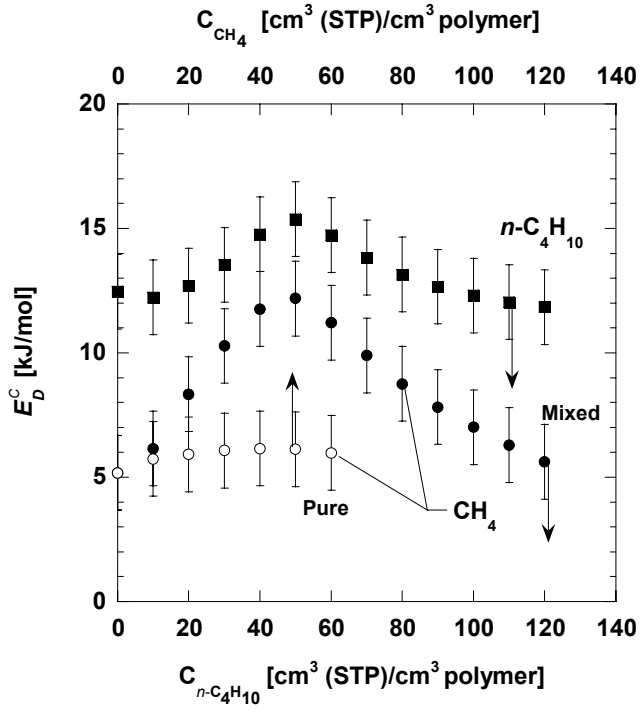

Figure 7.9 Pure and mixed gas activation energy of diffusion for CH_4 and *n*-C_4H_{10} as a function of penetrant concentration in the polymer at the upstream face of the film. The *n*-C_4H_{10} activation energies of diffusion are estimated based on mixed gas data. There is essentially no difference between the pure and mixed gas *n*-C_4H_{10} diffusivity data in PTMSP, so the activation energies of diffusion of *n*-C_4H_{10} are the same, within the uncertainty in the measurements, in both pure and mixed gas cases. The error bars were determined using the propagation of errors method [11].

7.8 DUAL MODE PERMEABILITY MODEL

7.8.1 Pure Gas

The dual mode permeability model (Eq. (2.17)) describes the pure gas permeability data reasonably well. The values of k_D, C_H', and b for CH_4 and *n*-C_4H_{10} in PTMSP have been reported the previous chapter. The best fit $\overline{D}_D$ and $\overline{D}_H$ values for CH_4, determined by plotting experimental pure gas permeability data versus $[(1+bf_2)]^{-1}$, are reported in Table 7.1. The CH_4 pure gas permeability values calculated using Eq. (2.17)

and the parameters in Table 7.1 are represented by solid lines in Figure 7.1(a). The concentration average diffusion coefficient for gas A, $\bar{D}_A$, is given by the dual mode model as follows [12]:

$$\bar{D}_A = \frac{\bar{D}_{D_A} k_{D_A} + \bar{D}_{H_A} \dfrac{C'_{H_A} b_A}{1 + b_A f_{A,2}}}{k_{D_A} + \dfrac{C'_{H_A} b_A}{1 + b_A f_{A,2}}} \tag{7.4}$$

Values of the concentration averaged diffusion coefficient according to Eq. (7.4) for *n*-C_4H_{10} at pure gas conditions are represented by the lines in Figure 7.2(a).

7.8.2 Mixed Gas

The dual mode permeability model can be extended to mixtures, as shown in Eqs. (2.20) and (2.21). In the remainder of this chapter, the subscripts A and B correspond to *n*-C_4H_{10} and CH_4, respectively. This model describes pure and mixed gas *n*-C_4H_{10} permeability data reasonably well. The best fit $\bar{D}_D$ and $\bar{D}_H$ values for *n*-C_4H_{10} were determined by plotting the experimental pure and mixed gas permeability data versus $[(1+b_A f_{A,2}+b_B f_{B,2})]^{-1}$ and are recorded in Table 7.1. Values of *n*-C_4H_{10} pure and mixed gas permeability as calculated by this model using the parameters in Table 7.1 are the solid lines in Figures 7.1(b) and 7.4. The concentration average diffusion coefficient, $\bar{D}_A$, for *n*-C_4H_{10} in pure gas and mixtures is given by the dual mode model as follows [18]:

$$\bar{D}_A = \frac{\bar{D}_{D_A} k_{D_A} + \bar{D}_{H_A} \dfrac{C'_{H_A} b_A}{1 + b_A f_{A,2} + b_B f_{B,2}}}{k_{D_A} + \dfrac{C'_{H_A} b_A}{1 + b_A f_{A,2} + b_B f_{B,2}}} \tag{7.5}$$

where the subscripts A and B correspond to *n*-C_4H_{10} and CH_4, respectively. Calculations according to Eq. (7.5) are represented as solid lines in Figures 7.2(b) and 7.6(b). Table

7.1 shows that $\bar{D}_D$ is greater than $\bar{D}_H$, consistent with previous results for PTMSP and glassy polymers in general [2,12]. The local effective diffusion coefficient, D_A, for *n*-C_4H_{10} can be calculated using the dual mode model as follows [2]:

$$D_A = \frac{\bar{D}_{D_A} k_{D_A} + \bar{D}_{H_A} \dfrac{C'_{H_A} b_A}{\left(1 + b_A f_{A,2} + b_B f_{B,2}\right)^2}}{k_{D_A} + \dfrac{C'_{H_A} b_A}{\left(1 + b_A f_{A,2} + b_B f_{B,2}\right)^2}} \tag{7.6}$$

Despite the reasonable estimates for *n*-C_4H_{10} permeability data, the mixed gas model cannot predict mixed gas CH_4 permeability data using the pure gas $\bar{D}_D$ and $\bar{D}_H$ of CH_4 recorded in Table 7.1. In fact, no single set of dual mode diffusion coefficients could fit simultaneously the pure and mixed CH_4 permeability data. This inability of the mixed gas permeability model to account for the changes in permeability of a light gas in PTMSP has been previously recognized [3]. While the model appropriately accounts for competitive sorption effects in mixtures, it does not consider the blocking effect observed in PTMSP. That is, in the original formulation of the model, the CH_4 dual mode diffusion coefficients are not allowed to depend on the concentration of *n*-C_4H_{10}. To capture this effect, a concentration dependence of $\bar{D}_H$ is introduced in the dual mode mixed gas permeability model using the following empirical relation:

$$\bar{D}_{H_B} = \bar{D}_{Ho_B} \exp\left(-\alpha_H \bar{C}_{H_A}\right) \tag{7.7}$$

where the subscripts A and B correspond to *n*-C_4H_{10} and CH_4, respectively, $\bar{D}_{Ho_B}$ is the CH_4 diffusion coefficient in Langmuir region at infinite dilution, α_H is a parameter that quantifies the blocking effect in the Langmuir region induced by the condensable *n*-C_4H_{10}

molecules, and $\overline{C}_{H_A}$ is the average *n*-C_4H_{10} concentration in the Langmuir region, defined as:

$$\overline{C}_{H_A} = \frac{C'_{H_A} b_A f_{A,2}}{2\left(1 + b_A f_{A,2} + b_B f_{B,2}\right)} \tag{7.8}$$

The blocking effect is a consequence of the high level of *n*-C_4H_{10} sorption in the larger free volume elements in the polymer (*i.e.,* Langmuir region) [4]. As such, the decrease in CH_4 mixed gas diffusion coefficients is only attributed to the *n*-C_4H_{10} concentration in the Langmuir region, as shown in Eq. (7.7).

Substituting Eq. (7.7) into (2.21) yields a modified dual mode mixed gas permeability model for CH_4:

$$P_B = k_{D_B}\overline{D}_{D_B} + \frac{C'_{H_B} b_B \overline{D}_{Ho_B} \exp\left(-\alpha_H \overline{C}_{H_A}\right)}{1 + b_A f_{A,2} + b_B f_{B,2}} \tag{7.9}$$

Eq. (7.9) captures both the competitive sorption effect and the blocking effect in CH_4 mixture permeation in PTMSP and describes the pure and mixed gas CH_4 permeability data reasonably well. The best fit $\overline{D}_D$, $\overline{D}_H$, and α_H of CH_4 based on pure and mixed gas data are recorded in Table 7.2. Permeability coefficients calculated according to Eq. (7.9) using the parameters from Table 7.2 are represented by solid lines in Figure 7.3(a). The $\overline{D}_D$ of CH_4 obtained from Eq. (7.9) (Table 7.2) is an order of magnitude less than that determined from the pure gas measurements (Table 7.1). The α_H values increase with decreasing temperature; the $\overline{D}_D$ and $\overline{D}_H$ values increase as temperature increases. A linear concentration dependence of $\overline{D}_{H_B}$ (*i.e.,* $\overline{D}_{H_B} = \overline{D}_{Ho_B}\left(1 - \alpha_H \overline{C}_{H_A}\right)$) could also describe the permeability data as well, but the best fit parameters determined this way lead to negative $\overline{D}_{H_B}$ values, which are physically unrealistic. Theoretically, one might also consider the plasticization effect of the Henry's law region in Eq. (7.9) by

introducing a concentration dependent $\bar{D}_D$ (*i.e.,* $\bar{D}_{D_B} = \bar{D}_{Do_B} \exp\left(\alpha_D \bar{C}_{D_A}\right)$) [2]. However, when fitting the experimental data to such a model, it is difficult to obtain unique values for α_D, the plasticization parameter, because the plasticization effect is weak relative to the blocking effect. That is, the plasticization effect is not very apparent from Figures 7.3(a) and 7.6(a). The expression for $\bar{D}_B$ according to the modified dual mode permeability model (Eq. (7.9)) is:

$$\bar{D}_B = \frac{\bar{D}_{D_B} k_{D_B} + \bar{D}_{Ho_B} \exp\left(-\alpha_H \bar{C}_{H_A}\right) \dfrac{C'_{H_B} b_B}{1 + b_A f_{A,2} + b_B f_{B,2}}}{k_{D_B} + \dfrac{C'_{H_B} b_B}{1 + b_A f_{A,2} + b_B f_{B,2}}} \tag{7.10}$$

A comparison of calculations according to Eq. (7.10) and experimental data is shown in Figure 7.6(a).

Table 7.2 shows $\bar{D}_H$ values that are greater than $\bar{D}_D$ values. This result is in contrast to the usual trend in glassy polymers, where $\bar{D}_D$ is usually greater than $\bar{D}_H$ [2,12]. The source of the discrepancy is not known at this time. Another unexplained trend found in this study is the similarity between the $\bar{D}_D$ values in PTMSP for CH_4 from the mixture data (Table 7.2) and *n*-C_4H_{10} (Table 7.1), despite the fact that CH_4 is smaller than *n*-C_4H_{10}, so one would anticipate that its diffusion coefficients would be larger. Nevertheless, this model provides a convenient mathematical expression for gas and vapor permeation in PTMSP.

Table 7.2 CH_4 dual mode diffusion coefficient parameters based on Eq. (7.9) using pure and mixed gas data

T (^oC)	$\bar{D}_D$ x 10^6 (cm^2/s)	$\bar{D}_{Ho}$ x 10^6 (cm^2/s)	α_H
-20	12 ± 1	63 ± 7	0.11 ± 0.01
0	15 ± 1	74 ± 8	0.077 ± 0.008
25	16 ± 2	86 ± 6	0.055 ± 0.006
35	18 ± 2	98 ± 7	0.058 ± 0.006

Gas diffusivity is often correlated with the amount of fractional free volume (FFV) in the polymer [19,20]. Gas diffusivity commonly increases as the amount of FFV in the polymer increases [12]. Figure 7.10 presents the CH_4 effective diffusion coefficients in pure gas and mixtures in PTMSP, at various *n*-C_4H_{10} and CH_4 concentrations and temperatures, as a function of inverse local FFV in the polymer/penetrant mixture. The local FFV values were estimated from the experimental sorption and dilation data in PTMSP reported in Chapter 6, using Eq. (5.9). Figure 7.10 shows no distinct trend in diffusion coefficients with FFV in PTMSP. Part of the trend actually shows an increase in CH_4 diffusion coefficients with decreasing FFV. The reasons for this lack of coherence with the free volume model are not immediately known, in part due to a lack of similar literature data (*i.e.,* where FFV in the polymer/penetrant mixture is estimated based on experimental data). In Chapter 5, the effective diffusion coefficients of CH_4 and *n*-C_4H_{10} in PDMS increase as the FFV in the polymer/penetrant mixture increases [16]. Although further study of this phenomenon may result a better understanding of the relationship between gas diffusivity and FFV in the polymer, it appears that FFV is not the only factor contributing to the temperature and concentration dependence of diffusion coefficients in PTMSP.

A key question regarding the permeation properties of PTMSP has been whether the primary mechanism is via preferential sorption and surface diffusion along the walls of interconnected free volume elements (or pores) in this very high free volume polymer. Srinivasan *et al.* and Pinnau and Toy suggested that this was the case [3,4]. Additionally, Singh found rather compelling evidence that PTMSP is, in fact, a "borderline" material between conventional, dense, low free volume polymers and microporous materials such as microporous carbon [21]. Singh's studies compared the gas diffusion coefficients calculated from transient kinetic uptake experiments with those estimated from steady state permeability and sorption measurements, similar to the techniques used in this manuscript. Order of magnitude differences were observed in the diffusion coefficients estimated by these two methods, clearly suggesting that most of the gas transport in PTMSP was through interconnected free volume elements or "pores" inherently present in the material due, presumably, to its intrinsically high free volume and unusual distribution of free volume [22,23]. However, the models and data analysis considered in this study can be applied to both microporous and nonporous materials. Thus, while the data presented in this study do not definitively prove that the dominant mechanism for gas and vapor transport in PTMSP occurs via micropore transport, they are consistent with such an interpretation.

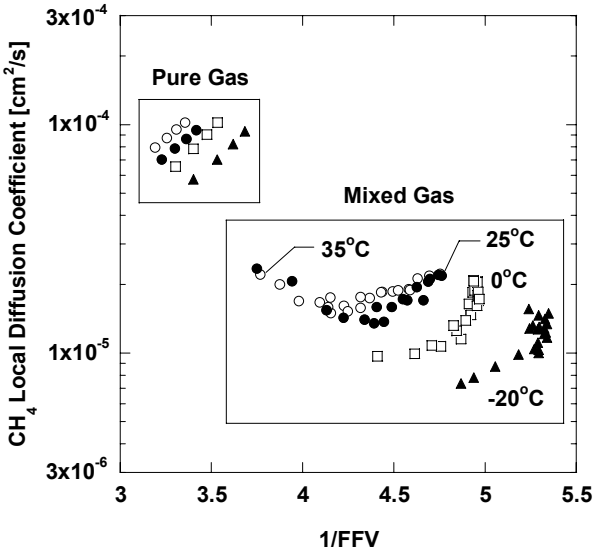

Figure 7.10 Correlation between fractional free volume of the polymer/penetrant mixtures and effective diffusion coefficients of CH_4 in PTMSP at various penetrant concentrations and temperatures. The FFV was estimated based on penetrant concentrations at the upstream face of the film as described in Chapter 5.

7.9 SELECTIVITY

7.9.1 Permeability Selectivity

Figure 7.11(a) presents mixed gas *n*-C_4H_{10}/CH_4 permeability selectivity in PTMSP as a function of *n*-C_4H_{10} upstream activity in the mixtures. At low *n*-C_4H_{10} activity, the permeability selectivity increases with increasing *n*-C_4H_{10} activity. For example, at 25°C, *n*-C_4H_{10}/CH_4 mixed gas permeability selectivity increases two-fold from 25 to 51, as *n*-C_4H_{10} upstream activity increases from 0.02 to 0.11. At higher *n*-C_4H_{10} activity (>0.1), the permeability selectivity apparently reaches a plateau. The permeability selectivity increases with decreasing temperature: *e.g.,* the *n*-C_4H_{10}/CH_4 mixed gas permeability selectivity at 0.22 *n*-C_4H_{10} upstream activity increases from 43 to 197 as temperature decreases from 35 to -20°C. Figure 7.11(b) presents the ratio of the

n-C_4H_{10}/CH_4 mixed gas to pure gas permeability selectivity at various temperatures. Due to CH_4 permeability depression in the mixture, the permeability selectivities determined from the mixture measurements are considerably higher than those estimated from pure gas data. These differences between the pure and mixed gas permeability selectivities are even greater at higher *n*-C_4H_{10} activity and lower temperature. For example, at 0^oC and 0.54 *n*-C_4H_{10} upstream activity, the mixed gas permeability selectivity is approximately 22 times higher than the pure gas selectivity.

7.9.2 Diffusivity Selectivity

Figure 7.12(a) presents *n*-C_4H_{10}/CH_4 mixed gas diffusivity selectivity in PTMSP as a function of *n*-C_4H_{10} upstream activity and temperature. The diffusivity selectivity increases with increasing *n*-C_4H_{10} activity. For example, at 0^oC, the diffusivity selectivity increases from 0.17 to 0.54 as *n*-C_4H_{10} upstream activity increases from 0.03 to 0.54. This trend is observed in part due to the decrease in CH_4 diffusion coefficient when *n*-C_4H_{10} is present in the mixture (*i.e.,* the blocking effect). The *n*-C_4H_{10} diffusion coefficients also increase with increasing *n*-C_4H_{10} upstream activity. Interestingly, this trend is relatively insensitive to temperature. The diffusivity selectivity data at various temperatures, in general, nearly fall on a single master curve. The *n*-C_4H_{10}/CH_4 diffusivity selectivities in PTMSP determined in this study are between 0.15 and 0.54. Figure 7.12(b) presents the ratio of the *n*-C_4H_{10}/CH_4 mixed gas to pure gas diffusivity selectivity at various temperatures. The diffusivity selectivities determined from the mixed gas measurements are higher than those estimated from the pure gas data, due to the blocking effect that considerably reduces CH_4 diffusion coefficient in mixtures. With the exception of the data at -20^oC, the difference between mixed gas and pure gas diffusivity selectivities generally increases with increasing *n*-C_4H_{10} upstream activity. As indicated in Figure 7.6(a), the CH_4 diffusivity at -20^oC increases modestly at *n*-C_4H_{10}

activities greater than approximately 0.05, presumably due to plasticization of the polymer by *n*-C_4H_{10}. This increase in mixed gas CH_4 diffusion coefficients at -20°C causes the decrease in the diffusivity selectivity ratio observed at -20°C in Figure 7.12(b).

7.9.3 Solubility Selectivity

Based on our mixed gas sorption study in PTMSP (Chapter 6), the *n*-C_4H_{10}/CH_4 mixed gas solubility selectivity in PTMSP decreases with increasing *n*-C_4H_{10} activity and temperature, as shown in Figure 7.13(a), because *n*-C_4H_{10} solubility decreases more than CH_4 solubility with increasing *n*-C_4H_{10} activity. For instance, at -20°C, the *n*-C_4H_{10}/CH_4 mixed gas solubility selectivity decreases from 690 to 480 as *n*-C_4H_{10} activity increases from 0.05 to 0.24. At 35°C, the solubility selectivity decreases from 175 to 96 as *n*-C_4H_{10} activity increases from 0.03 to 0.26. As shown in Figure 7.13(b), the solubility selectivities determined from the mixed gas measurements are considerably higher than those estimated from pure gas data, due to the competitive sorption effect, which decreases CH_4 solubility in the mixture [10]. These differences between pure and mixed solubility selectivities are even greater at higher *n*-C_4H_{10} activity and lower temperature.

Table 7.3 compares pure and mixed gas *n*-C_4H_{10}/CH_4 permeability, solubility, and diffusivity selectivities at various temperatures. The permeability selectivities determined from mixed gas measurements are higher than those estimated from pure gas data. The difference is a result of both higher solubility and diffusivity selectivity in mixtures relative to those in pure gas. Table 7.3 presents the ratios of the mixed gas selectivities to those of pure gas. The mixed gas permeability selectivity at 35°C is 6.8 times higher than that estimated from pure gas measurements, and the deviation is greater at lower temperatures: at -20°C, the mixed gas permeability selectivity is 32 times higher than the pure gas values. At this temperature, the solubility and diffusivity selectivities are 8.8 and 4.4 times, respectively, higher than their pure gas values.

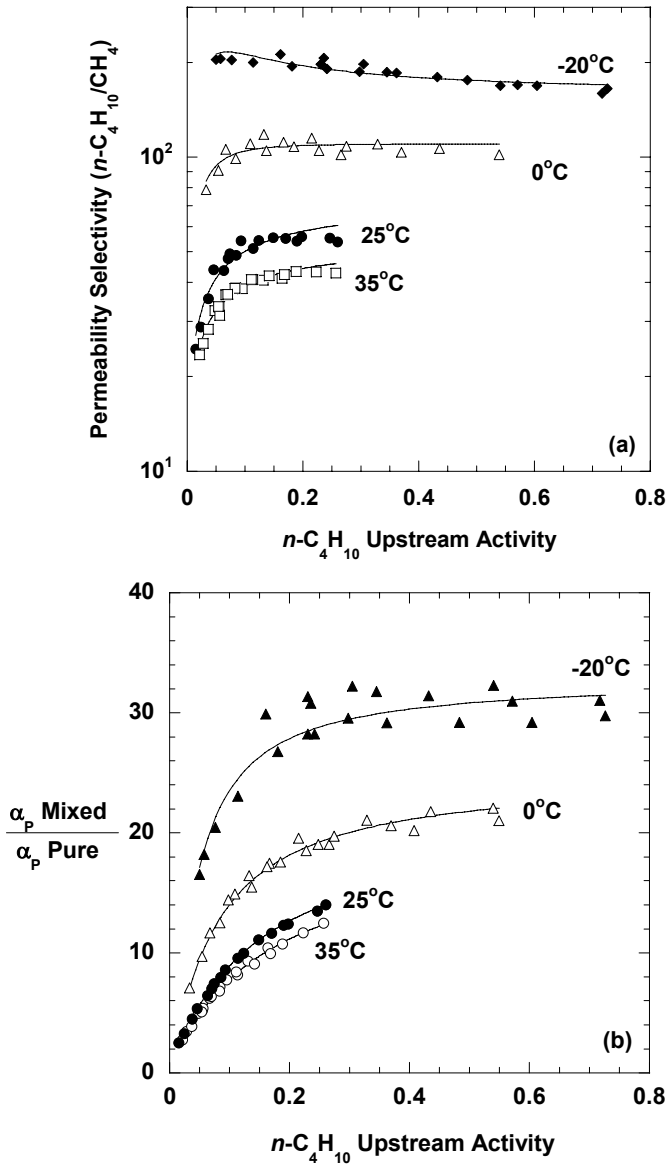

Figure 7.11 (a) Mixed gas n-C_4H_{10}/CH_4 permeability selectivity in PTMSP as a function of n-C_4H_{10} upstream activity. (b) Ratio of n-C_4H_{10}/CH_4 mixed gas to pure gas permeability selectivity in PTMSP. The pure gas permeability selectivity is calculated from n-C_4H_{10} permeability at different n-C_4H_{10} upstream activity values and CH_4 pure gas permeability at infinite dilution. The lines represent predictions of the dual mode mixture permeability model (*i.e.,* Eqs. (2.17) and (7.9)).

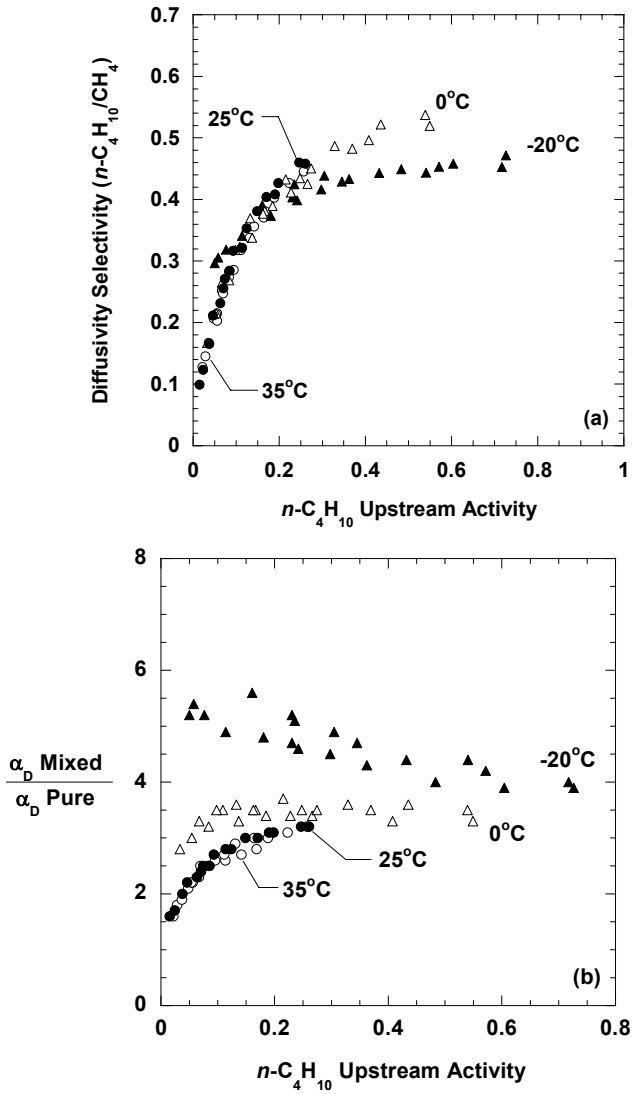

Figure 7.12 (a) Mixed gas n-C_4H_{10}/CH_4 diffusivity selectivity in PTMSP as a function of n-C_4H_{10} upstream activity. (b) Ratio of n-C_4H_{10}/CH_4 mixed gas to pure gas diffusivity selectivity in PTMSP. The pure gas diffusivity selectivity is calculated from n-C_4H_{10} diffusivity values at the indicated n-C_4H_{10} upstream activity values and CH_4 pure gas diffusivity at infinite dilution.

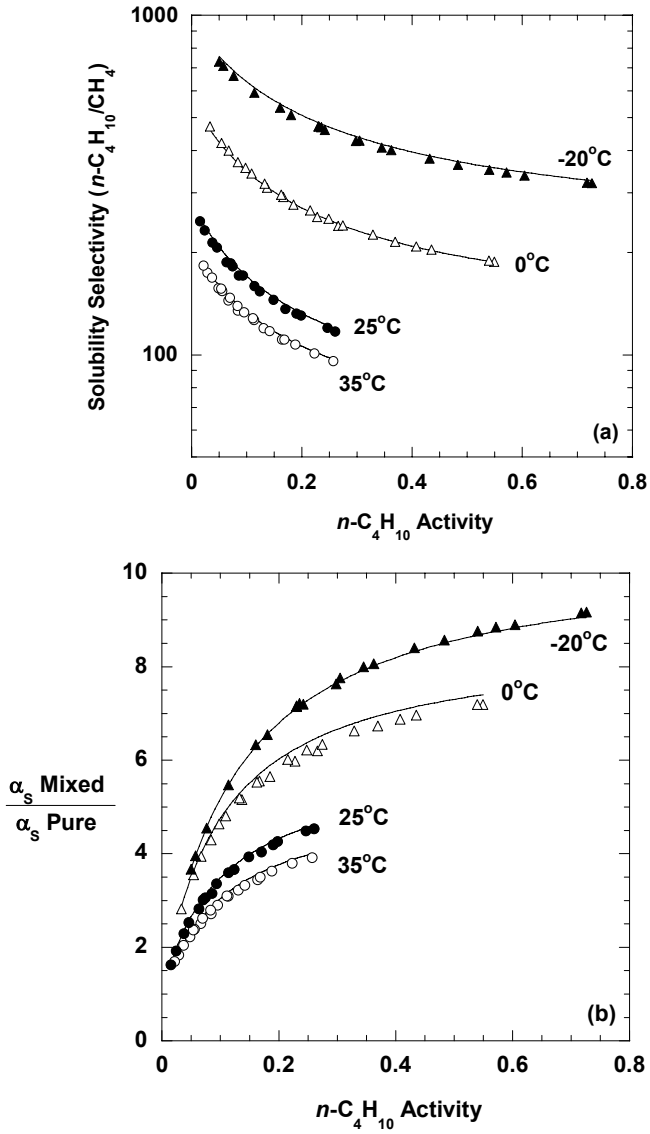

Figure 7.13 (a) Mixed gas n-C_4H_{10}/CH_4 solubility selectivity in PTMSP as a function of n-C_4H_{10} activity in the mixture. (b) Ratio of n-C_4H_{10}/CH_4 mixed gas to pure gas solubility selectivity in PTMSP. The pure gas solubility selectivity is calculated from n-C_4H_{10} pure gas solubility at the indicated n-C_4H_{10} activity values and CH_4 pure gas solubility in the limit of zero CH_4 fugacity. The lines represent predictions of the dual mode sorption model (*i.e.,* Eqs. (2.18) and (2.19)).

Table 7.3 Effect of temperature on pure and mixed gas *n*-C_4H_{10}/CH_4 permeability, solubility, and diffusivity selectivities

T (^oC)	Permeability Selectivity			Solubility Selectivity			Diffusivity Selectivity		
	Mixed[a]	Pure[b]	Mixed/Pure	Mixed[a]	Pure[b]	Mixed/Pure	Mixed[a]	Pure[b]	Mixed/Pure
-20	167 ± 8	5.2 ± 0.3	32 ± 2	351 ± 18	40 ± 2	8.8 ± 0.4	0.48 ± 0.05	0.11 ± 0.01	4.4 ± 0.5
0	109 ± 5	5.7 ± 0.3	19 ± 1	251 ± 13	40 ± 2	6.2 ± 0.3	0.43 ± 0.04	0.13 ± 0.01	3.5 ± 0.4
25	51 ± 3	5.4 ± 0.3	9.5 ± 0.6	159 ± 8	44 ± 2	3.6 ± 0.2	0.32 ± 0.03	0.12 ± 0.01	2.8 ± 0.3
35	38 ± 2	5.6 ± 0.3	6.8 ± 0.4	139 ± 7	50 ± 3	2.8 ± 0.1	0.27 ± 0.03	0.11 ± 0.01	2.5 ± 0.3

[a]Feed composition: 6 mol% *n*-C_4H_{10}; feed pressure: 4.4 atm. The permeate side of the film was swept with helium.

[b]Estimated using *n*-C_4H_{10} mixture properties at the upstream conditions specified above[a] and CH_4 pure gas properties at infinite dilution from Tables 7.1 and 6.2.

7.10 CONCLUSIONS

Although *n*-C_4H_{10} transport properties are essentially unaffected by the presence of CH_4, CH_4 permeability in PTMSP is considerably reduced by the presence of *n*-C_4H_{10}. This depression in CH_4 permeability arises from competitive sorption, which reduces CH_4 solubility in mixtures, and blocking, which reduces CH_4 diffusivity in mixtures. The mixed gas CH_4 permeability data can be predicted using a modified dual mode mixture permeability model. The *n*-C_4H_{10}/CH_4 permeability selectivity increases with increasing *n*-C_4H_{10} upstream activity and decreasing temperature due to the competitive sorption and blocking effects, both of which favor *n*-C_4H_{10} permeation over that of CH_4. The *n*-C_4H_{10}/CH_4 diffusivity selectivity also increases with increasing *n*-C_4H_{10} upstream activity, but it is a weak function of temperature. On the other hand, the *n*-C_4H_{10}/CH_4 solubility selectivity decreases with increasing *n*-C_4H_{10} activity and temperature. The difference between the *n*-C_4H_{10}/CH_4 permeability selectivity in pure gas and mixtures in PTMSP is due to both solubility and diffusivity effects.

7.11 REFERENCES

[1] R. D. Raharjo, H. J. Lee, B. D. Freeman, T. Sakaguchi, and T. Masuda, "Pure gas and vapor permeation properties of poly[1-phenyl-2-[p-(trimethylsilyl)phenyl]acetylene] (PTMSDPA) and its desilylated analog, poly[diphenylacetylene] (PDPA)", Polymer, 46 (2005) 6316-24.

[2] T. C. Merkel, V. Bondar, K. Nagai, and B. D. Freeman, "Sorption and transport of hydrocarbon and perfluorocarbon gases in poly(1-trimethylsilyl-1-propyne)", Journal of Polymer Science: Part B: Polymer Physics, 38 (2000) 273-96.

[3] R. Srinivasan, S. R. Auvil, and P. M. Burban, "Elucidating the mechanism(s) of gas transport in poly[1-(trimethylsilyl)-1-propyne] (PTMSP) membranes", Journal of Membrane Science, 86 (1994) 67-86.

[4] I. Pinnau and L. G. Toy, "Transport of organic vapors through poly(1-trimethylsilyl-1-propyne)", Journal of Membrane Science, 116 (1996) 199-209.

[5] Y. Ichiraku, S. A. Stern, and T. Nakagawa, "An investigation of the high gas permeability of poly(1-trimethylsilyl-1-propyne)", Journal of Membrane Science, 34 (1987) 5-18.

[6] K. Nagai, T. Masuda, T. Nakagawa, B. D. Freeman, and I. Pinnau, "Poly[1-(trimethylsilyl)-1-propyne] and related polymers: synthesis, properties and functions", Progress in Polymer Science, 26 (2001) 721-98.

[7] Y. Hu, M. Shiotsuki, F. Sanda, and T. Masuda, "Synthesis and extremely high gas permeability of polyacetylenes containing polymethylated indan/tetrahydronaphthalene moieties", Chemical Communications, submitted.

[8] S. Matteucci, Y. Yampolskii, B. D. Freeman, and I. Pinnau, "Transport of gases and vapors in glassy and rubbery polymers", in Y. Yampolskii, I. Pinnau and B. D. Freeman (Eds.), Materials Science of Membranes, John Wiley & Sons, Ltd., Chichester, 2006.

[9] W. J. Koros, A. H. Chan, and D. R. Paul, "Sorption and transport of various gases in polycarbonate", Journal of Membrane Science, 2 (1977) 165-90.

[10] R. D. Raharjo, B. D. Freeman, and E. S. Sanders, "Pure and mixed gas CH_4 and *n*-C_4H_{10} sorption and dilation in poly(1-trimethylsilyl-1-propyne)", Polymer, in press.

[11] P. R. Bevington, Data Reduction and Error Analysis for the Physical Sciences, 3rd ed., McGraw-Hill, New York, NY, 2002.

[12] K. Ghosal and B. D. Freeman, "Gas separation using polymer membranes: an overview", Polymers for Advanced Technologies, 5 (1994) 673-97.

[13] T. Masuda, Y. Iguchi, B.-Z. Tang, and T. Higashimura, "Diffusion and solution of gases in substituted polyacetylene membranes", Polymer, 29 (1988) 2041-9.

[14] T. C. Merkel, Z. He, I. Pinnau, B. D. Freeman, P. Meakin, and A. J. Hill, "Effect of nanoparticles on gas sorption and transport in poly(1-trimethylsilyl-1propyne)", Macromolecules, 36 (2003) 6844-55.

[15] S. Pauly, "Permeability and diffusion data", in E. A. Grulke (Ed.), Polymer Handbook, John Wiley & Sons, Ltd., Toronto, 1999.

[16] R. D. Raharjo, B. D. Freeman, D. R. Paul, G. C. Sarti, and E. S. Sanders, "Pure and mixed gas CH_4 and *n*-C_4H_{10} permeability and diffusivity in poly(dimethylsiloxane)", Journal of Membrane Science, in press.

[17] W. J. Koros and M. W. Hellums, "Transport properties", in J. I. Kroschwitz (Ed.), Encyclopedia of Polymer Science and Technology, Wiley, New York, 1990, pp. 724-802.

[18] W. J. Koros, R. T. Chern, V. Stannett, and H. B. Hopfenberg, "A model for permeation of mixed gases and vapors in glassy polymers", Journal of Polymer Science: Part B: Polymer Physics, 19 (1981) 1513-30.

[19] M. H. Cohen and D. Turnbull, "Molecular transport in liquids and glasses", Journal of Chemical Physics, 31 (1952) 1164-9.

[20] W. M. Lee, "Selection of barrier materials from molecular structure", Polymer Engineering and Science, 20 (1980) 65-9.

[21] A. Singh, Gas and vapor sorption and permeation properties of high free volume glassy polymers, Ph.D. Dissertation, North Carolina State University, Raleigh, NC, 1997.

[22] V. P. Shantarovich, I. B. Kevdina, Y. P. Yampolskii, and A. Y. Alentiev, "Positron annihilation lifetime study of high and low free volume glassy polymers: effects of free volume sizes on the permeability and permselectivity", Macromolecules, 33 (2000) 7453-66.

[23] A. J. Hill, B. D. Freeman, M. Jaffe, T. C. Merkel, and I. Pinnau, "Tailoring nanospace", Journal of Molecular Structure, 739 (2005) 173-8.

Chapter 8: Conclusions and Recommendations

8.1 CONCLUSIONS

This dissertation focused on studying the competitive sorption, diffusion, and permeation effects in solubility selective polymers. In this study, *n*-C_4H_{10}/CH_4 mixtures were selected as the model vapor/gas mixture. The polymers of choice were poly(dimethylsiloxane) (PDMS) and poly(1-trimethylsilyl-1-propyne) (PTMSP). Although these two polymers shares similarity as vapor selective materials, the origins of their vapor selectivities are very different. The Si-O linkage in the backbone chain of PDMS has a very high segmental mobility [1]. Due to the very flexible polymer chain, the rubbery PDMS has a weak size sieving ability, and therefore, it is more permeable to larger, more condensable organic vapors than to smaller, less condensable, permanent gas [2]. In contrast, the polymer chain in glassy PTMSP is very rigid due to the C=C linkage in the backbone [3,4]. However, the combination of the rigid polymer chain and the bulky side group hinders chain segmental motion and restrains polymer chains from packing efficiently, creating large and possibly interconnected free volume elements in the polymer matrix [3,4]. This very open structure attenuates the polymer's ability to discriminate between large and small molecules. Therefore, unlike conventional glassy polymers, PTMSP is vapor selective [3]. The difference between the sorption and transport mechanisms in PDMS and those in PTMSP leads to interesting differences in their mixture sorption and transport properties.

8.1.1 Poly(dimethylsiloxane) (PDMS)

In rubbery PDMS, CH_4 permeability, solubility, and diffusion coefficients in the polymer are enhanced by the presence of *n*-C_4H_{10}. Plasticization by *n*-C_4H_{10} increases CH_4 diffusion coefficients in the polymer. The presence of *n*-C_4H_{10} also provides a more favorable environment for CH_4 sorption, which results in an increase in CH_4 solubility. On the other hand, the presence of CH_4 in the mixture does not influence *n*-C_4H_{10} sorption and transport properties, presumably due to the low solubility of methane in the polymer.

The *n*-C_4H_{10}/CH_4 mixture permeability selectivity increases as *n*-C_4H_{10} activity increases and temperature decreases, and it is lower than that estimated from pure gas experiments, especially at high *n*-C_4H_{10} activity and lower temperature. This deviation is a result of both lower solubility and diffusivity selectivities in mixtures relative to those in pure gas. The mixture diffusivity selectivity varies little with *n*-C_4H_{10} activity and temperature. Plasticization in PDMS increases the diffusivity of CH_4 and *n*-C_4H_{10} by a similar amount, so it has little influence on diffusivity selectivity. The mixture solubility selectivity in PDMS increases with increasing *n*-C_4H_{10} activity and decreasing temperature, and changes in solubility selectivity are mainly responsible for the increase in mixture permeability selectivity with increasing *n*-C_4H_{10} activity and decreasing temperature in PDMS.

Several models were used to describe the mixture data. The FFV model fails to collapse all of the mixture diffusivity data into a single master curve. Nevertheless, to a rough approximation, the experimental data obey this model. A modified activated state diffusion model successfully describes the increase in CH_4 permeability and diffusivity in the presence of *n*-C_4H_{10}. The ternary Maxwell-Stefan model predicts the mixture data based on pure gas data and a single adjustable parameter. According to this model, the

convective flow contribution to the overall flux in mixture permeation experiments was small (*i.e.,* < 5% for CH_4 and < 15% for *n*-C_4H_{10}).

8.1.2 Poly(1-trimethylsilyl-1-propyne) (PTMSP)

In contrast to the mixture results in PDMS, in glassy PTMSP, the presence of *n*-C_4H_{10} decreases CH_4 mixture permeability, solubility, and diffusion coefficients in the polymer. The larger, more soluble *n*-C_4H_{10} molecules occupy most of the sorption sites in the Langmuir region, reducing methane mixture solubility considerably. The blocking effect hinders CH_4 transport through the pore-like channels in PTMSP, and therefore, depresses CH_4 mixture diffusion coefficients. Both the competitive sorption effect and the blocking effect are responsible for the depression of CH_4 permeability in mixtures. As in PDMS, the presence of CH_4 does not have measurable influence on *n*-C_4H_{10} sorption and transport properties in PTMSP.

The mixture permeability selectivity increases with increasing *n*-C_4H_{10} activity and decreasing temperature, and it is higher than that estimated from the pure gas measurements. This difference is due to both higher solubility and diffusivity selectivities in mixtures relative to those in pure gas, as discussed in Chapter 7. The mixture solubility selectivity in PTMSP decreases with increasing *n*-C_4H_{10} activity and temperature. The mixture diffusivity selectivity increases with increasing *n*-C_4H_{10} activity.

The dual mode sorption model for mixture successfully captures the competitive sorption effect between CH_4 and *n*-C_4H_{10}, as shown in Chapter 6. However, the dual mode mixture permeability model cannot describe the depression of CH_4 permeability in the presence of *n*-C_4H_{10}. This mixture model appropriately accounts for the competitive sorption effect in mixtures, but it does not consider the blocking effect observed in PTMSP. To capture this effect, the dual mode mixture permeability model was modified by introducing a *n*-C_4H_{10} concentration dependence into the CH_4 diffusion coefficient in

the Langmuir region. This modified model describes the CH_4 mixture permeability data in PTMSP reasonably well.

8.2 RECOMMENDATIONS

8.2.1 Other Gas Mixtures

CO_2/CH_4 mixtures would be an excellent candidate for a future study. CO_2 removal from raw natural gas is required to increase the heating value of natural gas and reduce corrosion during its transport and distribution [5]. Compared to the conventional method (*e.g.,* amine absorption), membrane separation can offer a cheaper, smaller, and less energy consuming alternative separation method [5,6].

Another gas pair of interest is C_3H_6/C_3H_8. Olefin/paraffin separation is very important in the petroleum industry [7]. The conventional technology for this separation is low temperature distillation, which requires an extensive amount of energy [7]. There is considerable interest in alternative separation techniques, such as membrane separation [5].

Apart from their industrial importance, studies of other gas mixtures will provide a better fundamental understanding of penetrant sorption and transport mechanisms that take place in PDMS and PTMSP, in particular. In this present study, only a mixture of non polar gases of widely varying condensability (*i.e., n*-C_4H_{10}/CH_4) was considered. A study of CO_2/CH_4 mixtures would add a polar/non polar gas pair to the mixture database. A study on C_3H_6/C_3H_8 mixtures would add a gas pair of very similar condensability where the mixture solubilities of both components should be influenced by the presence of the other component.

8.2.2 Conventional Glassy Polymers

Although Sanders *et al.* [8] previously studied mixed gas sorption in poly(methyl methacrylate) (PMMA), to the best of our knowledge, a comprehensive set of mixed gas permeability, solubility, and diffusivity data in a conventional glassy polymer has never been reported. It is of interest to compare such data with those in ultra high free-volume PTMSP presented in this study. For example, one could study the mixture behavior of a low free volume, glassy polymer such as polycarbonate. Polycarbonate has been used in a number of gas separation applications [9], and its pure gas sorption and transport properties have been studied thoroughly in the literature [10-12].

In addition, the availability of such data will help understanding the correlation between FFV and diffusion coefficient in glassy polymers. The difficulty in interpreting the correlation between FFV and diffusion coefficient in PTMSP, as shown in Figure 7.10, is partly due to the lack of similar data in the literature. As such, it is difficult to determine whether the trend in Figure 7.10 is exclusive to ultra high-free volume glassy polymer such as PTMSP, or if it is common to glassy polymers in general.

8.2.3 New Model for PTMSP

Although the modified dual mode mixture permeability model developed in this study (Chapter 7) describes the experimental CH_4 mixture permeability data reasonably well, the physical significance of the model parameters are not very clear. In addition, the use of this model to describe the blocking effect exerted by *n*-C_4H_{10} molecules on CH_4 is rather empirical. Development of a new model that has a more sound theoretical basis to capture this effect and has more clear physical significance of its parameters should be beneficial, as it lays a theoretical foundation for the gas and vapor transport mechanism in PTMSP. One could reasonably start by considering existing pore-flow transport models [13]. Since penetrant transport in PTMSP possibly lies in a transition region

between pore-flow and solution-diffusion [14], combination between the solution-diffusion and pore-flow models might be necessary to more completely describe the gas and vapor transport behavior in PTMSP.

8.3 REFERENCES

[1] S. A. Stern, V. M. Shah, and B. J. Hardy, "Structure-permeability relationships in silicone polymers", Journal of Polymer Science: Part B: Polymer Physics, 25 (1987) 1263-98.

[2] T. C. Merkel, V. I. Bondar, K. Nagai, B. D. Freeman, and I. Pinnau, "Gas sorption, diffusion, and permeation in poly(dimethylsiloxane)", Journal of Polymer Science: Part B: Polymer Physics, 38 (2000) 415-34.

[3] T. C. Merkel, V. Bondar, K. Nagai, and B. D. Freeman, "Sorption and transport of hydrocarbon and perfluorocarbon gases in poly(1-trimethylsilyl-1-propyne)", Journal of Polymer Science: Part B: Polymer Physics, 38 (2000) 273-96.

[4] R. Srinivasan, S. R. Auvil, and P. M. Burban, "Elucidating the mechanism(s) of gas transport in poly[1-(trimethylsilyl)-1-propyne] (PTMSP) membranes", Journal of Membrane Science, 86 (1994) 67-86.

[5] R. W. Baker, Membrane Technology and Applications, 2nd ed., John Wiley & Sons, New York, 2004.

[6] H. Lin and B. D. Freeman, "Gas permeation and diffusion in cross-linked poly(ethylene glycol diacrylate)", Macromolecules, 39 (2006) 3568-80.

[7] R. B. Eldridge, "Olefin/paraffin separation technology: a review", Industrial & Engineering Chemistry Research, 32 (1993) 2208-12.

[8] E. S. Sanders, High-pressure sorption of pure and mixed gases in glassy polymers, Ph.D. Dissertation, North Carolina State University, Raleigh, N.C., 1983.

[9] R. W. Baker, "Future directions of membrane gas separation technology", Industrial & Engineering Chemistry Research, 41 (2002) 1393-411.

[10] W. J. Koros, A. H. Chan, and D. R. Paul, "Sorption and transport of various gases in polycarbonate", Journal of Membrane Science, 2 (1977) 165-90.

[11] G. K. Fleming and W. J. Koros, "Dilation of polymers by sorption of carbon dioxide at elevated pressures. 1. Silicone rubber and unconditioned polycarbonate", Macromolecules, 19 (1986) 2285-91.

[12] S. M. Jordan, G. K. Fleming, and W. J. Koros, "Permeability of carbon dioxide at elevated pressures in substituted polycarbonates", Journal of Polymer Science: Part B: Polymer Physics, 28 (1990) 2305-27.

[13] D. D. Do, Adsorption Analysis: Equilibria and Kinetics, Series on Chemical Engineering, Imperial College Press, London, 1998.

[14] I. Pinnau and L. G. Toy, "Transport of organic vapors through poly(1-trimethylsilyl-1-propyne)", Journal of Membrane Science, 116 (1996) 199-209.

Appendix A: Fugacity Calculations

The Soave-Redlich-Kwong (SRK) equation of state is given by: [1,2]

$$p = \frac{RT}{\hat{V} - b} - \frac{a}{\hat{V}\left(\hat{V} + b\right)} \tag{A.1}$$

where p is pressure (atm), R is the gas constant (82.06 atm cm^3/K/mol), T is absolute temperature (K), $\hat{V}$ is the molar volume of the gas (cm^3/mol), and a and b are model parameters. For mixtures, a and b depend on gas composition as shown below:[1]

$$a_m = \sum_i^N \sum_j^N X_i X_j \left(a_i a_j\right)^{1/2} \left(1 - \bar{k}_{ij}\right) \tag{A.2}$$

$$b_m = \sum_i^N X_i b_i \tag{A.3}$$

where X_i is the mol fraction of component i in the mixture, N is the number of components in the mixture, a_i and b_i are the SRK parameters for component i, and $\bar{k}_{ij}$ is the binary interaction coefficient between components i and j. The $\bar{k}_{ij}$ value for CH_4 and n-C_4H_{10} (0.0056) was obtained from Knapp et al. [3]. Poling et al. offer the following rules for calculating pure component SRK parameters:[1]

$$a_i = \frac{0.42747 R^2 T_{c_i}^{\ 2}}{p_{c_i}} \left[1 + m_i \left(1 - T_{r_i}^{\ 1/2}\right)\right]^2 \tag{A.4}$$

$$b_i = \frac{0.08664 R T_{c_i}}{p_{c_i}} \tag{A.5}$$

where T_{c_i} (K) and p_{c_i} (atm) are the critical temperature and pressure of component i, respectively. The term m_i is given by:[1]

$$m_i = 0.48 + 1.574 w_i - 0.176 w_i^2 \tag{A.6}$$

where w_i is the acentric factor of component *i*. Values of p_{c_i}, T_{c_i}, and w_i were obtained from Poling et al. [1].

For a pure gas, fugacity can be related to pressure as follows:[1]

$$\ln\frac{f_i}{p_i} = -\ln\left(\frac{\hat{V}-b_i}{\hat{V}}\right) - \frac{a_i}{b_i RT}\ln\left(\frac{\hat{V}+b_i}{\hat{V}}\right) + Z - 1 - \ln Z \tag{A.7}$$

where f_i is the fugacity of component *i*, and Z is the compressibility factor:

$$Z = \frac{p\hat{V}}{RT} = \frac{\hat{V}}{\hat{V}-b_i} - \frac{a_i}{RT\left(\hat{V}+b_i\right)} \tag{A.8}$$

For a gas mixture, the fugacity of component *i* can be calculated as follows:[4]

$$\ln\frac{f_i}{pX_i} = \frac{b_i}{b_m}\left(Z-1\right) - \ln\left(Z - \frac{pb_m}{RT}\right) - \frac{2\sum_j^N y_j\left(a_i a_j\right)^{1/2}\left(1-\bar{k}_{ij}\right)a_m b_i / b_m}{RTb_m}\ln\left(1+\frac{b_m}{\hat{V}}\right) \tag{A.9}$$

The *n*-C_4H_{10} activity is defined as the ratio of *n*-C_4H_{10} fugacity to the saturation fugacity at a given temperature (f/f_{sat}) [5]. The saturation fugacity is the fugacity at the saturation pressure (p_{sat}), and p_{sat} is estimated using the Wagner equation [1]:

$$\ln p_{sat} = \frac{A(1-T_r) + B(1-T_r)^{1.5} + C(1-T_r)^3 + D(1-T_r)^6}{T_r} \tag{A.10}$$

where T_r is the reduced temperature (T/T_c), T_c is the gas critical temperature, and *A*, *B*, *C*, and *D* are constants from Poling et al. [1]. The saturation fugacity can then be calculated using Eq. (A.7).

REFERENCES

[1] B. E. Poling, J. M. Prausnitz, and J. P. O'Connell, The Properties of Gases and Liquids, 5th ed., McGraw-Hill, New York, NY, 2001.

[2] G. Soave, "20 years of Redlich-Kwong equation of state", Fluid Phase Equilibria, 82 (1993) 345-59.

[3] H. Knapp, R. Doring, L. Oellrich, U. Plocker, and J. M. Prausnitz, Vapor-liquid equilibria for mixtures of low boiling substances, Chemistry Data Series, Vol. 6, DECHEMA, Great Neck, NY, 1989.

[4] E. S. Sanders, High-pressure sorption of pure and mixed gases in glassy polymers, Ph.D. Dissertation, North Carolina State University, Raleigh, 1983.

[5] P. J. Flory, Principles of Polymer Chemistry, Cornell University Press, Ithaca, NY, 1953.

Appendix B: Calculations of Effective Diffusion Coefficients in Mixtures

Fick's law for binary mixture transport through a polymer film can be written as follows: [1]

$$N_A = -D_A \frac{dC_A}{dx} \tag{B.1}$$

$$N_B = -D_B \frac{dC_B}{dx} \tag{B.2}$$

where the subscripts A and B represent n-C_4H_{10} and CH_4, respectively. To transform N_A and N_B to P_A and P_B, Eq. (B.1) and (B.2) are integrated across the membrane thickness. For n-C_4H_{10}, this step is straightforward since there is essentially no change in n-C_4H_{10} sorption and transport properties in the presence of CH_4. On the other hand, it is obvious from Figure 11 that transport of CH_4 across the film depends on n-C_4H_{10} concentration. To introduce that dependence at a fundamental level, the diffusion coefficient of CH_4 must be written as a function of n-C_4H_{10} concentration. Since n-C_4H_{10} concentration changes across the thickness of the film, its impact on CH_4 diffusion coefficient must be properly averaged. In this regard, it is useful to write Eq. (B.2) in an equivalent form that explicitly recognizes the importance of n-C_4H_{10} concentration (*i.e.,* C_A) on the CH_4 diffusion coefficient and flux:

$$N_B = -D_B\left(C_A\right)\frac{dC_B}{dC_A}\frac{dC_A}{dx} \tag{B.3}$$

Dividing Eq. (B.3) by (B.1) and rearranging yields:

$$\frac{N_B}{N_A}\frac{D_A\left(C_A\right)}{D_B\left(C_A\right)} = \frac{dC_B}{dC_A} \tag{B.4}$$

Integrating Eq. (B.4) across the film gives:

$$\frac{N_B}{N_A}\int_{C_{A,1}}^{C_{A,2}} \frac{D_A\left(C_A\right)}{D_B\left(C_A\right)}\,dC_A = \int_{C_{B,1}}^{C_{B,2}} dC_B \tag{B.5}$$

Using the permeability defined in Eq. (2.1) and assuming that $f_{B,1}$, $C_{A,1}$, and $C_{B,1}$ are approximately zero, which is true in this study, the mixed gas permeability of CH_4, P_B, can be written as a function of P_A, $f_{A,2}$, and D_A as follows:

$$P_B = P_A f_{A,2} \frac{S_B}{\int_0^{C_{A,2}} \frac{D_A\left(C_A\right)}{D_B\left(C_A\right)}\,dC_A} \tag{B.6}$$

where S_B is the solubility coefficient of CH_4 at the upstream face of the film (*i.e.,* $S_B = C_{B,2}/f_{B,2}$).

REFERENCE

[1] S. Matsui and D. R. Paul, "A simple model for pervaporative transport of binary mixtures through rubbery polymeric membranes", Journal of Membrane Science, 234 (2004) 25-30.

Appendix C: Maxwell-Stefan Equations

For one-dimensional transport, the Maxwell-Stefan equations for a ternary system are: [1]

$$n_A + \left(\frac{n_A w_B - n_B w_A}{w_m} \right) \varepsilon_A = -\rho D_A \frac{dw_A}{dx} \tag{C.1}$$

$$n_B + \left(\frac{n_B w_A - n_A w_B}{w_m} \right) \varepsilon_B = -\rho D_B \frac{dw_B}{dx} \tag{C.2}$$

where n_A [g/(cm^2 s)]and n_B [g/(cm^2 s)] are the mass fluxes of penetrants A and B; and w_A, w_B, and w_m are the weight fractions of penetrant A, penetrant B, and polymer, respectively, in the system. In this analysis, D_A and D_B are taken to be functions of the total penetrant content in the polymer: [2]

$$D_A = \langle D_A \rangle_o \exp\left(\beta \left(w_A + w_B \right) \right) \tag{C.3}$$

$$D_B = \langle D_B \rangle_o \exp\left(\beta \left(w_A + w_B \right) \right) \tag{C.4}$$

where $\langle D_A \rangle_o$ and $\langle D_B \rangle_o$ are infinite dilution mutual diffusion coefficients, and β is an empirical adjustable parameter. The terms ε_A and ε_B are defined follows: [1]

$$\varepsilon_A = \frac{MW_A}{MW_B} \frac{D_A}{D_{BA}} \tag{C.5}$$

$$\varepsilon_B = \frac{D_B}{D_{BA}} \tag{C.6}$$

where D_{BA} is the coupling diffusion coefficient between penetrant B and A. MW_A and MW_B are the molecular weights of penetrant A and B, respectively. Like D_A and D_B, D_{BA} is assumed to depend on the total penetrant weight fraction in the polymer (*i.e.,* $D_{BA} = \langle D_{BA} \rangle_o \exp\left(\beta \left(w_A + w_B \right) \right)$).

At steady state, when w_m is close to unity, and when w_{Al} and w_{Bl} are zero, which are reasonable approximations in this study, integration of Eqs. (C.1) and (C.2) yields:

$$n_A\int_0^l dx + n_A\varepsilon_A\int_0^l w_B\,dx - n_B\varepsilon_A\int_0^l w_A\,dx = \int_{w_{Al}}^{w_{A0}} \rho\langle D_A\rangle_o \exp\left(\beta\left(w_A + w_B\right)\right)dw_A \tag{C.7}$$

$$n_B\int_0^l dx + n_B\varepsilon_B\int_0^l w_A\,dx - n_A\varepsilon_B\int_0^l w_B\,dx = \int_{w_{Bl}}^{w_{B0}} \rho\langle D_B\rangle_o \exp\left(\beta\left(w_A + w_B\right)\right)dw_B \tag{C.8}$$

The terms $\int_0^l w_A\,dx$ and $\int_0^l w_B\,dx$ can be estimated from the pure gas concentration profile: [3]

$$\int_0^l w_A\,dx = \frac{\exp\left(\beta w_{A0}\right)lw_{A0}}{\exp\left(\beta w_{A0}\right)-1} - \frac{l}{\beta} \equiv \hat{w}_A \tag{C.9}$$

$$\int_0^l w_B\,dx = \frac{\exp\left(\beta w_{B0}\right)lw_{B0}}{\exp\left(\beta w_{B0}\right)-1} - \frac{l}{\beta} \equiv \hat{w}_B \tag{C.10}$$

Substituting Eqs. (C.9) and (C.10) into Eqs. (C.7) and (C.8) and evaluating the integrals yields:

$$n_A l + \left(n_A\hat{w}_B - n_B\hat{w}_A\right)\varepsilon_A = \frac{\rho\langle D_A\rangle_o}{\beta}\left[\exp\left(\beta\left(w_{A0} + \overline{w}_B\right)\right) - \exp\left(\beta\overline{w}_B\right)\right] \tag{C.11}$$

$$n_B l + \left(n_B\hat{w}_A - n_A\hat{w}_B\right)\varepsilon_B = \frac{\rho\langle D_B\rangle_o}{\beta}\left[\exp\left(\beta\left(w_{B0} + \overline{w}_A\right)\right) - \exp\left(\beta\overline{w}_A\right)\right] \tag{C.12}$$

where $\overline{w}_A$ and $\overline{w}_B$ are the average weight fractions of penetrant *A* and *B*, respectively, in the film, which are estimated from the pure gas concentration profile:

$$\overline{w}_A = \frac{\hat{w}_A}{l} \tag{C.13}$$

$$\overline{w}_B = \frac{\hat{w}_B}{l} \tag{C.14}$$

Solving Eqs. (C.11) and (C.12) simultaneously gives:

$$n_A = \frac{\dfrac{\rho\langle D_A\rangle_o}{\beta}\left[\exp\left(\beta\left(w_{A0}+\overline{w}_B\right)\right)-\exp\left(\beta\overline{w}_B\right)\right]\left(l+\varepsilon_B\hat{w}_A\right) + \dfrac{\rho\langle D_B\rangle_o}{\beta}\left[\exp\left(\beta\left(w_{B0}+\overline{w}_A\right)\right)-\exp\left(\beta\overline{w}_A\right)\right]\varepsilon_A\hat{w}_A}{\left(l+\varepsilon_A\hat{w}_B\right)\left(l+\varepsilon_B\hat{w}_A\right)-\varepsilon_B\hat{w}_B\varepsilon_A\hat{w}_A} \tag{C.15}$$

$$n_B = \frac{\dfrac{\rho\langle D_B\rangle_o}{\beta}\left[\exp\left(\beta\left(w_{B0}+\overline{w}_A\right)\right)-\exp\left(\beta\overline{w}_A\right)\right]\left(l+\varepsilon_A\hat{w}_B\right) + \dfrac{\rho\langle D_A\rangle_o}{\beta}\left[\exp\left(\beta\left(w_{A0}+\overline{w}_B\right)\right)-\exp\left(\beta\overline{w}_B\right)\right]\varepsilon_B\hat{w}_B}{\left(l+\varepsilon_B\hat{w}_A\right)\left(l+\varepsilon_A\hat{w}_B\right)-\varepsilon_A\hat{w}_A\varepsilon_B\hat{w}_B} \tag{C.16}$$

Eqs. (C.15) and (C.16) can be expressed in terms of permeability coefficients as follows:

$$P_A = \frac{\dfrac{\rho\langle D_A\rangle_o}{\beta}\left[\exp\left(\beta\left(w_{A0}+\overline{w}_B\right)\right)-\exp\left(\beta\overline{w}_B\right)\right]\left(l+\varepsilon_B\hat{w}_A\right) + \dfrac{\rho\langle D_B\rangle_o}{\beta}\left[\exp\left(\beta\left(w_{B0}+\overline{w}_A\right)\right)-\exp\left(\beta\overline{w}_A\right)\right]\varepsilon_A\hat{w}_A}{\left(l+\varepsilon_A\hat{w}_B\right)\left(l+\varepsilon_B\hat{w}_A\right)-\varepsilon_B\hat{w}_B\varepsilon_A\hat{w}_A} \times \frac{22414}{MW_A}\frac{l}{f_{A,2}} \tag{C.17}$$

$$P_B = \frac{\dfrac{\rho\langle D_B\rangle_o}{\beta}\left[\exp\left(\beta\left(w_{B0}+\overline{w}_A\right)\right)-\exp\left(\beta\overline{w}_A\right)\right]\left(l+\varepsilon_A\hat{w}_B\right) + \dfrac{\rho\langle D_A\rangle_o}{\beta}\left[\exp\left(\beta\left(w_{A0}+\overline{w}_B\right)\right)-\exp\left(\beta\overline{w}_B\right)\right]\varepsilon_B\hat{w}_B}{\left(l+\varepsilon_B\hat{w}_A\right)\left(l+\varepsilon_A\hat{w}_B\right)-\varepsilon_A\hat{w}_A\varepsilon_B\hat{w}_B} \times \frac{22414}{MW_B}\frac{l}{f_{B,2}} \tag{C.18}$$

The importance of frictional coupling effects in mixture permeation can be quantified by taking the ratio of the second term on the left hand side of Eqs. (C.11) and (C.12) to the total left hand side of Eqs. (C.11) and (C.12) as follows:

$$\varphi_A = \frac{\left(n_A \hat{w}_B - n_B \hat{w}_A\right)\varepsilon_A}{n_A l + \left(n_A \hat{w}_B - n_B \hat{w}_A\right)\varepsilon_A} \tag{C.19}$$

$$\varphi_B = \frac{\left(n_B \hat{w}_A - n_A \hat{w}_B\right)\varepsilon_B}{n_B l + \left(n_B \hat{w}_A - n_A \hat{w}_B\right)\varepsilon_B} \tag{C.20}$$

where φ_A and φ_B are coupling factors. In the absence of frictional coupling (*i.e.,* ε_A=ε_B=0 or φ_A=φ_B=0), the Maxwell-Stefan equations reduce to Fick's Law for transport of each component independently through the polymer:

$$n_A = -\rho D_A \frac{dw_A}{dx} \tag{C.21}$$

$$n_B = -\rho D_B \frac{dw_B}{dx} \tag{C.22}$$

REFERENCES

[1] D. R. Paul, "Reformulation of the solution-diffusion theory of reverse osmosis", Journal of Membrane Science, 241 (2004) 371-86.

[2] R. M. Barrer, J. A. Barrie, and J. Slater, "Sorption and diffusion in ethyl cellulose. Part III. Comparison between ethyl cellulose and rubber", Journal of Polymer Science, 27 (1958) 177-97.

[3] S. Matsui and D. R. Paul, "A simple model for pervaporative transport of binary mixtures through rubbery polymeric membranes", Journal of Membrane Science, 234 (2004) 25-30.

Appendix D: Supplementary Figures

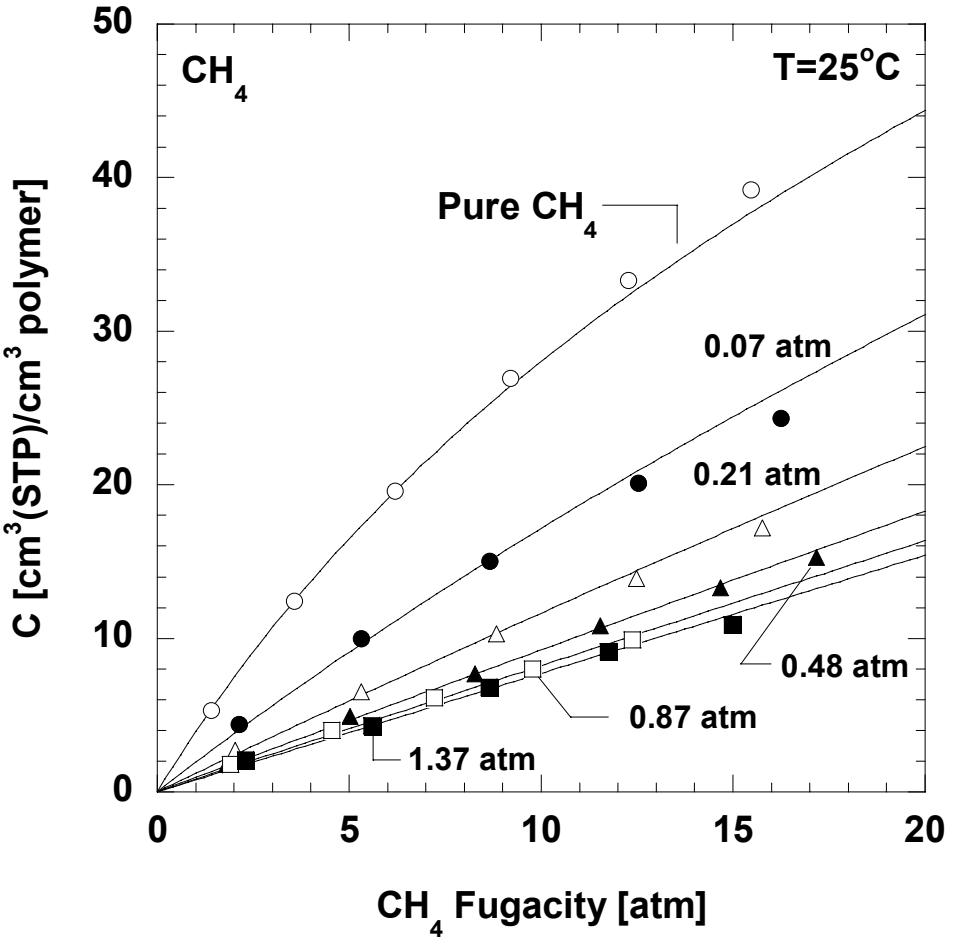

Figure D.1 Pure and mixed gas sorption isotherms of (a) CH_4 and (b) n-C_4H_{10} as a function of CH_4 fugacity in the mixture at 25°C. Each isotherm is determined at a nominally fixed n-C_4H_{10} fugacity, whose value (in atm) is given by the numbers in the figures. These n-C_4H_{10} fugacities are averages over the course of each sorption isotherm. The average n-C_4H_{10} activities (f/f_{sat}) in these isotherms are: (○) 0 (*i.e.,* pure CH_4), (●) 0.029 ± 0.006, (△) 0.10 ± 0.01, (▲) 0.21 ± 0.01, (□) 0.38 ± 0.01, and (■) 0.61 ± 0.01. The f_{sat} of n-C_4H_{10} at 25°C is 2.26 atm. The uncertainties represent the standard deviation of the average values. The lines represent the dual mode sorption model fits using the parameters in Table 6.2.

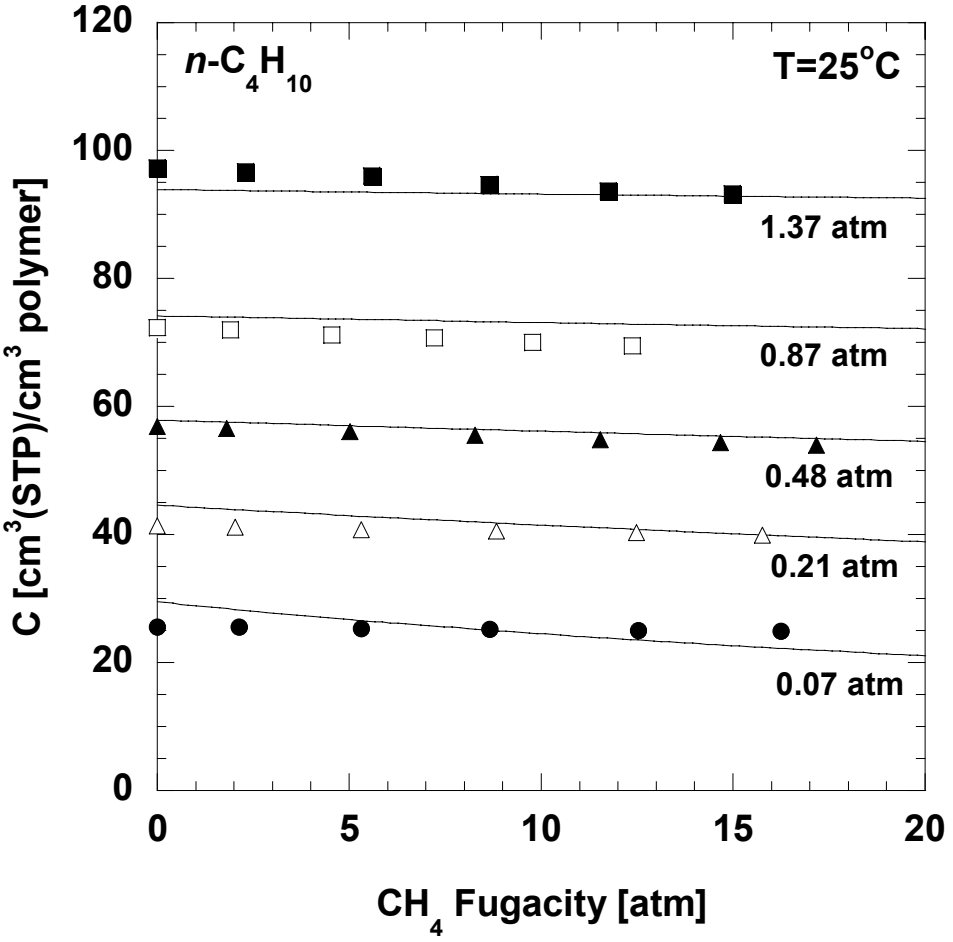

Figure D.1 Pure and mixed gas sorption isotherms of (a) CH_4 and (b) n-C_4H_{10} as a function of CH_4 fugacity in the mixture at 25°C. Each isotherm is determined at a nominally fixed n-C_4H_{10} fugacity, whose value (in atm) is given by the numbers in the figures. These n-C_4H_{10} fugacities are averages over the course of each sorption isotherm. The average n-C_4H_{10} activities (f/f_{sat}) in these isotherms are: (○) 0 (*i.e.,* pure CH_4), (●) 0.029 ± 0.006, (△) 0.10 ± 0.01, (▲) 0.21 ± 0.01, (□) 0.38 ± 0.01, and (■) 0.61 ± 0.01. The f_{sat} of n-C_4H_{10} at 25°C is 2.26 atm. The uncertainties represent the standard deviation of the average values. The lines represent the dual mode sorption model fits using the parameters in Table 6.2.

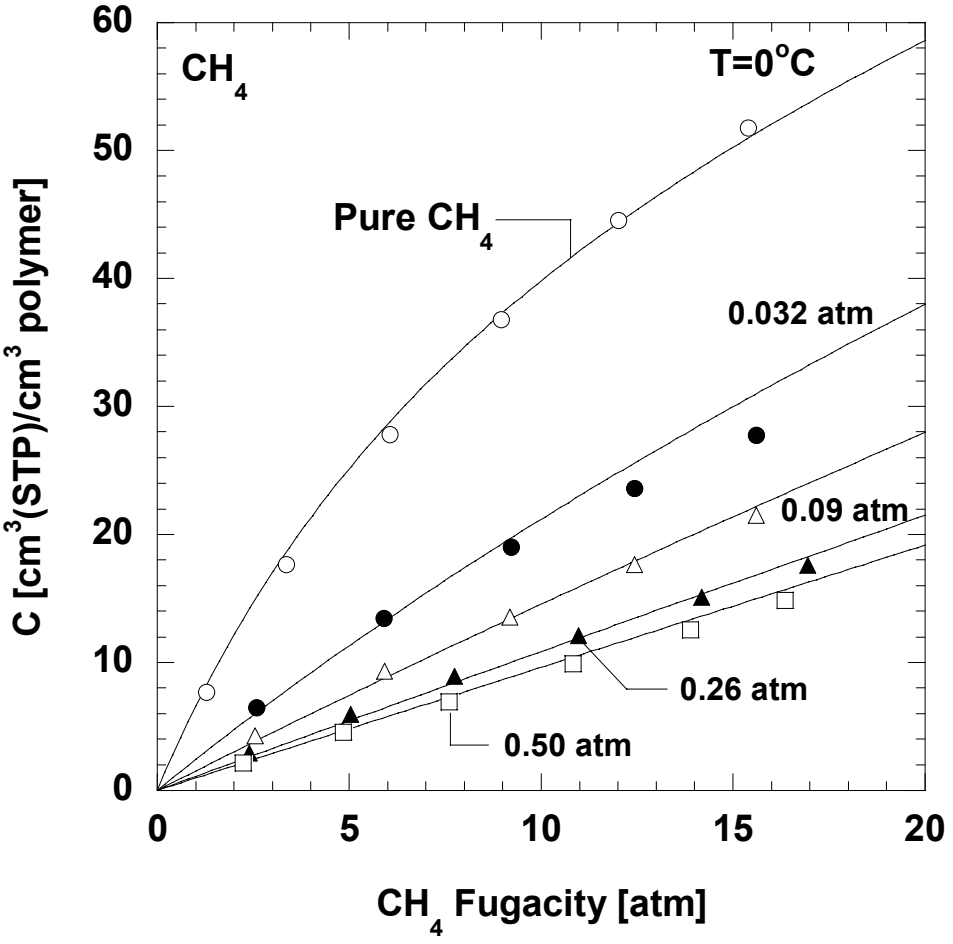

Figure D.2 Pure and mixed gas sorption isotherms of (a) CH_4 and (b) n-C_4H_{10} as a function of CH_4 fugacity in the mixture at 0°C. Each isotherm is determined at a nominally fixed n-C_4H_{10} fugacity, whose value (in atm) is given by the numbers in the figures. These n-C_4H_{10} fugacities are averages over the course of each sorption isotherm. The average n-C_4H_{10} activities (f/f_{sat}) in these isotherms are: (○) 0 (*i.e.,* pure CH_4), (●) 0.033 ± 0.006, (△) 0.09 ± 0.01, (▲) 0.26 ± 0.01, and (□) 0.51 ± 0.01. The f_{sat} of n-C_4H_{10} at 0°C is 0.99 atm. The uncertainties represent the standard deviation of the average values. The lines represent the dual mode sorption model fits using the parameters in Table 6.2.

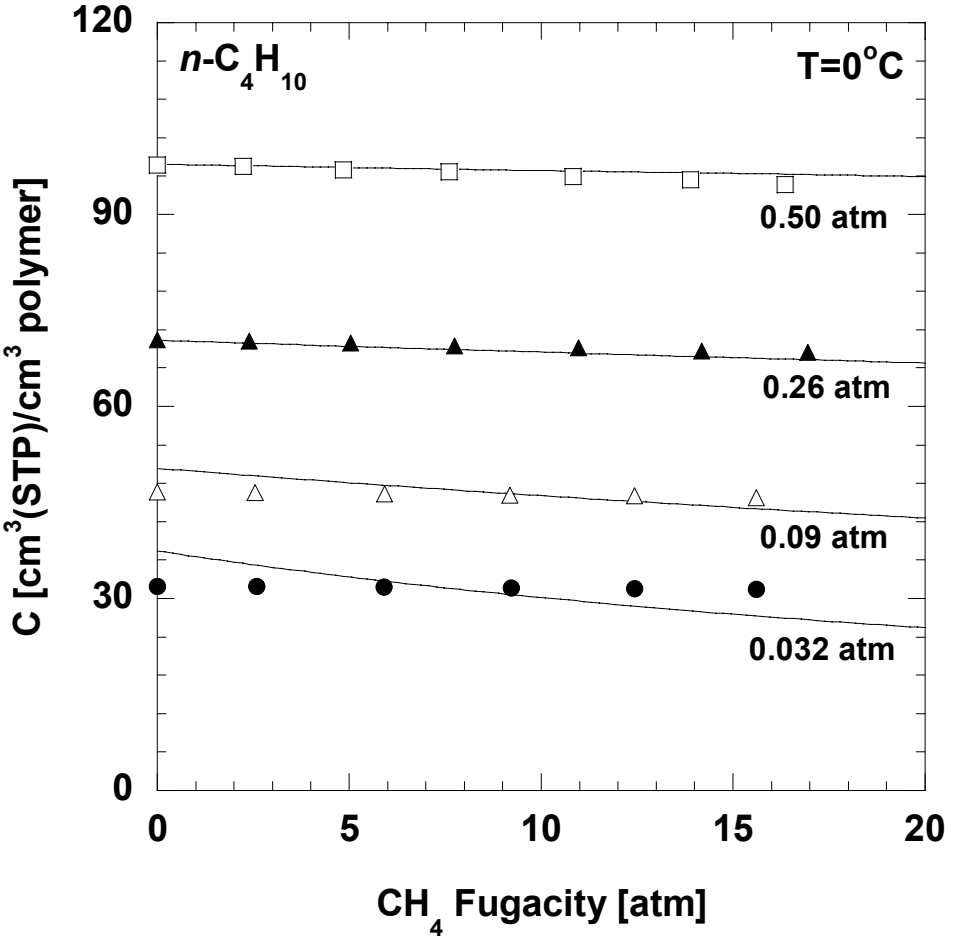

Figure D.2 Pure and mixed gas sorption isotherms of (a) CH_4 and (b) n-C_4H_{10} as a function of CH_4 fugacity in the mixture at 0°C. Each isotherm is determined at a nominally fixed n-C_4H_{10} fugacity, whose value (in atm) is given by the numbers in the figures. These n-C_4H_{10} fugacities are averages over the course of each sorption isotherm. The average n-C_4H_{10} activities (f/f_{sat}) in these isotherms are: (○) 0 (*i.e.,* pure CH_4), (●) 0.033 ± 0.006, (△) 0.09 ± 0.01, (▲) 0.26 ± 0.01, and (□) 0.51 ± 0.01. The f_{sat} of n-C_4H_{10} at 0°C is 0.99 atm. The uncertainties represent the standard deviation of the average values. The lines represent the dual mode sorption model fits using the parameters in Table 6.2.

Bibliography

DIPPR Physical and Thermodynamic Properties, http://dippr.byu.edu/public/chemsearch.asp,

N. A. Al-Baghli and K. F. Loughlin, "Adsorption of methane, ethane, and ethylene on titanosilicate ETS-10 zeolite", Journal of Chemincal Engineering Data, 50 (2005) 843-8.

R. W. Baker, "Future directions of membrane gas separation technology", Industrial & Engineering Chemistry Research, 41 (2002) 1393-411.

R. W. Baker, Membrane Technology and Applications, 2nd ed., John Wiley & Sons, New York, 2004.

R. M. Barrer, J. A. Barrie, and J. Slater, "Sorption and diffusion in ethyl cellulose. Part III. Comparison between ethyl cellulose and rubber", Journal of Polymer Science, 27 (1958) 177-97.

R. M. Barrer, J. A. Barrie, and N. K. Raman, "Solution and diffusion in silicone rubber I - A comparison with natural rubber", Polymer, 3 (1962) 595-603.

J. A. Barrie, K. Munday, and M. Williams, "Sorption and diffusion of hydrocarbon vapors in glassy polymers", Organic Coatings and Plastics Chemistry, 39 (1978) 187-91.

P. R. Bevington, Data reduction and error analysis for the physical sciences, 2nd ed., McGraw-Hill, New York, NY, 1992.

A. Bondi, Physical Properties of Molecular Crystals, Liquids, and Glasses, John Wiley and Sons, New York, 1968, pp. 25-97.

E. S. Burnett, "Compressibility determinations without volume measurements", Journal of Applied Mechanics, 3 (1936) 136-40.

E. Buss, "Gravimetric measurement of binary gas adsorption equilibria of methane-carbon dioxide mixtures on activated carbon", Gas Separation and Purification, 9 (1995) 189-97.

M. Catte, C. Achard, C.-G. Dussap, and J.-B. Gros, "Prediction of gas solubilities in pure and mixed solvents using a group contribution method", Ind. Eng. Chem. Res., 32 (1993) 2193-8.

M. H. Cohen and D. Turnbull, "Molecular transport in liquids and glasses", Journal of Chemical Physics, 31 (1952) 1164-9.

M. G. De Angelis, T. C. Merkel, V. I. Bondar, B. D. Freeman, F. Doghieri, and G. C. Sarti, "Hydrocarbon and fluorocarbon solubility and dilation in poly(dimethylsiloxane): comparison of experimental data with predictions of the Sanchez-Lacombe equation of state", Journal of Polymer Science: Part B: Polymer Physics, 37 (1999) 3011-26.

S. S. Dhingra and E. Marand, "Mixed gas transport study through polymeric membranes", Journal of Membrane Science, 141 (1998) 45-63.

S. V. Dixon-Garrett, K. Nagai, and B. D. Freeman, "Ethylbenzene solubility, diffusivity, and permeability in poly(dimethylsiloxane)", Journal of Polymer Science: Part B: Polymer Physics, 38 (2000) 1461-73.

D. D. Do, Adsorption Analysis: Equilibria and Kinetics, Series on Chemical Engineering, Imperial College Press, London, 1998.

J. H. Dymond, K. N. Marsh, R. C. Wilhoit, and K. C. Wong, The Virial Coefficients of Pure Gases and Mixtures, Vol. 21, Springer, Darmstadt, Germany, 2002.

R. B. Eldridge, "Olefin/paraffin separation technology: a review", Industrial & Engineering Chemistry Research, 32 (1993) 2208-12.

D. G. Elliot, R. J. J. Chen, P. S. Chappelear, and R. Kobayashi, "Vapor-liquid equilibrium of methane-*n*-butane system at low temperatures and high pressures", Journal of Chemical and Engineering Data, 19 (1974) 71-7.

G. K. Fleming and W. J. Koros, "Dilation of polymers by sorption of carbon dioxide at elevated pressures. 1. Silicone rubber and unconditioned polycarbonate", Macromolecules, 19 (1986) 2285-91.

G. K. Fleming, Dilation of silicone rubber and glassy polycarbonates due to high pressure gas sorption, Ph.D Dissertation, University of Texas at Austin, Austin, TX, 1988.

P. J. Flory, Principles of Polymer Chemistry, Cornell University Press, Ithaca, NY, 1953.

M. Ghisellini, M. Quinzi, M. Giacinti Baschetti, F. Doghieri, G. Costa, and G. C. Sarti, "Sorption and diffusion of vapors in PTMSP and PTMSP/PTMSE copolymers", Desalination, 149 (2002) 441-5.

K. Ghosal and B. D. Freeman, "Gas separation using polymer membranes: an overview", Polymers for Advanced Technologies, 5 (1994) 673-97.

A. J. Hill, B. D. Freeman, M. Jaffe, T. C. Merkel, and I. Pinnau, "Tailoring nanospace", Journal of Molecular Structure, 739 (2005) 173-8.

J. Horiuti, "The solubility of gas and coefficient of dilatation by absorption", Scientific Papers of the Institute of Physical and Chemical Research, 17 (1931) 125-256.

Y. Hu, M. Shiotsuki, F. Sanda, and T. Masuda, "Synthesis and extremely high gas permeability of polyacetylenes containing polymethylated indan/tetrahydronaphthalene moieties", Chemical Communications, submitted.

Y. Ichiraku, S. A. Stern, and T. Nakagawa, "An investigation of the high gas permeability of poly(1-trimethylsilyl-1-propyne)", Journal of Membrane Science, 34 (1987) 5-18.

F. P. Incropera and D. P. DeWitt, Fundamentals of Heat and Mass Transfer, John Wiley & Sons, New York, NY, 1996.

S. M. Jordan and W. J. Koros, "Permeability of pure and mixed gases in silicone rubber at elevated pressures", Journal of Polymer Science: Part B: Polymer Physics, 28 (1990) 795-809.

S. M. Jordan, G. K. Fleming, and W. J. Koros, "Permeability of carbon dioxide at elevated pressures in substituted polycarbonates", Journal of Polymer Science: Part B: Polymer Physics, 28 (1990) 2305-27.

Y. Kamiya, Y. Naito, T. Hirose, and K. Mizoguchi, "Sorption and partial molar volume of gases in poly(dimethylsiloxane)", Journal of Polymer Science: Part B: Polymer Physics, 28 (1990) 1297-308.

Y. Kamiya, Y. Naito, K. Terada, K. Mizoguchi, and A. Tsuboi, "Volumetric properties and interaction parameters of dissolved gases in poly(dimethylsiloxane) and polyethylene", Macromolecules, 33 (2000) 3111-9.

H. Knapp, R. Doring, L. Oellrich, U. Plocker, and J. M. Prausnitz, Vapor-liquid equilibria for mixtures of low boiling substances, Chemistry Data Series, Vol. 6, DECHEMA, Great Neck, NY, 1989.

W. J. Koros, A. H. Chan, and D. R. Paul, "Sorption and transport of various gases in polycarbonate", Journal of Membrane Science, 2 (1977) 165-90.

W. J. Koros and D. R. Paul, "Transient and steady-state permeation in poly(ethylene terephthalate) above and below the glass transition", Journal of Polymer Science, Polymer Physics Edition, 16 (1978) 2171-87.

W. J. Koros, D. R. Paul, and G. S. Huvard, "Energetics of gas sorption in glassy polymers", Polymer, 20 (1979) 956-60.

W. J. Koros, R. T. Chern, V. Stannett, and H. B. Hopfenberg, "A model for permeation of mixed gases and vapors in glassy polymers", Journal of Polymer Science: Part B: Polymer Physics, 19 (1981) 1513-30.

W. J. Koros and M. W. Hellums, "Transport properties", in J. I. Kroschwitz (Ed.), Encyclopedia of Polymer Science and Technology, Wiley, New York, 1990, pp. 724-802.

I. R. Krichevsky, "Thermodynamics of an infinitely dilute solution in mixed solvents. I. The Henry's coefficient in a mixed solvent behaving as an ideal solvent", Zhournal Fizicheskoi Khimii, 9 (1937) 41-7.

S. Y. Lee and B. S. Minhas, "Effect of gas composition and pressure on permeation through cellulose acetate membrane", AICHE Symposium Series, 84 (1970) 93-101.

W. M. Lee, "Selection of barrier materials from molecular structure", Polymer Engineering and Science, 20 (1980) 65-9.

P. Li and H. Tezel, "Adsorption separation of N_2, O_2, CO_2, and CH_4 gases by β-zeolite", Microporous and Mesoporous Materials, 98 (2007) 94-101.

H. Lin and B. D. Freeman, "Gas solubility, diffusivity and permeability in poly(ethylene oxide)", Journal of Membrane Science, 239 (2004) 105-17.

H. Lin and B. D. Freeman, "Gas permeation and diffusion in cross-linked poly(ethylene glycol diacrylate)", Macromolecules, 39 (2006) 3568-80.

T. Masuda, Y. Iguchi, B.-Z. Tang, and T. Higashimura, "Diffusion and solution of gases in substituted polyacetylene membranes", Polymer, 29 (1988) 2041-9.

S. Matsui and D. R. Paul, "A simple model for pervaporative transport of binary mixtures through rubbery polymeric membranes", Journal of Membrane Science, 234 (2004) 25-30.

S. Matteucci, Y. Yampolskii, B. D. Freeman, and I. Pinnau, "Transport of gases and vapors in glassy and rubbery polymers", in Y. Yampolskii, I. Pinnau and B. D. Freeman (Eds.), Materials Science of Membranes, John Wiley & Sons, Ltd., Chichester, 2006.

C. C. McDowell, B. D. Freeman, and G. W. McNeely, "Acetone sorption and uptake kinetic in poly(ethylene terephtalate)", Polymer, 40 (1999) 3487-99.

T. C. Merkel, V. Bondar, K. Nagai, B. D. Freeman, and Y. Yampolskii, "Gas sorption, diffusion, and permeation in poly(2,2-bis(trifluoromethyl)-4,5-difluoro-1,3-dioxole-*co*-tetrafluoroethylene)", Macromolecules, 32 (1999) 8427-40.

T. C. Merkel, V. I. Bondar, K. Nagai, B. D. Freeman, and I. Pinnau, "Gas sorption, diffusion, and permeation in poly(dimethylsiloxane)", Journal of Polymer Science: Part B: Polymer Physics, 38 (2000) 415-34.

T. C. Merkel, V. Bondar, K. Nagai, and B. D. Freeman, "Sorption and transport of hydrocarbon and perfluorocarbon gases in poly(1-trimethylsilyl-1-propyne)", Journal of Polymer Science: Part B: Polymer Physics, 38 (2000) 273-96.

T. C. Merkel, Z. He, I. Pinnau, B. D. Freeman, P. Meakin, and A. J. Hill, "Effect of nanoparticles on gas sorption and transport in poly(1-trimethylsilyl-1propyne)", Macromolecules, 36 (2003) 6844-55.

A. S. Michaels, W. R. Vieth, and J. A. Barrie, "Diffusion of gases in poly(ethylene terephthalate)", Journal of Applied Physics, 34 (1963) 13-20.

A. Morisato, B. D. Freeman, I. Pinnau, and C. G. Casillas, "Pure hydrocarbon sorption properties of poly(1-trimethylsilyl-1-propyne) (PTMSP), poly(1-phenyl-1-propyne) (PPP), and PTMSP/PPP blends", Journal of Polymer Science: Part B: Polymer Physics, 34 (1996) 1925-34.

M. H. V. Mulder, T. Franken, and C. A. Smolders, "Preferential sorption versus preferential permeability in pervaporation", Journal of Membrane Science, 22 (1985) 155-73.

K. Nagai and T. Nakagawa, "Effects of aging on the gas permeability and solubility in poly(1-trimethylsilyl-1-propyne) membranes synthesized with various catalysts", Journal of Membrane Science, 105 (1995) 261-72.

K. Nagai, T. Masuda, T. Nakagawa, B. D. Freeman, and I. Pinnau, "Poly[1-(trimethylsilyl)-1-propyne] and related polymers: synthesis, properties and functions", Progress in Polymer Science, 26 (2001) 721-98.

V. Nitsche, K. Ohlrogge, and K. Sturken, "Separation of organic vapors by means of membranes", Chemical Engineering Technology, 21 (1998) 925-35.

K. C. O'Brien, W. J. Koros, and T. A. Barbari, "A new technique for the measurement of multicomponent gas transport through polymeric films", Journal of Membrane Science, 29 (1986) 229-38.

J. P. O'Connell and J. M. Prausnitz, "Thermodynamics of gas solubility in mixed solvents", AIChE Journal, 3 (1964) 347-51.

H. Okuno, T. Nishida, and T. Uragami, "Preferential sorption and permeation of binary liquid mixtures in poly(vinyl chloride) membrane by pervaporation", Journal of Polymer Science: Part B: Polymer Physics, 33 (1995) 299-307.

D. R. Paul, "Reformulation of the solution-diffusion theory of reverse osmosis", Journal of Membrane Science, 241 (2004) 371-86.

S. Pauly, "Permeability and diffusion data", in J. Brandrup, E. H. Immergut and E. A. Grulke (Eds.), Polymer Handbook, John Wiley & Sons, Ltd., Toronto, 1999.

I. Pinnau, C. G. Casillas, A. Morisato, and B. D. Freeman, "Hydrocarbon/hydrogen mixed gas permeation in poly(1-trimethylsilyl-1-propyne) (PTMSP), poly(1-phenyl-1-propyne) (PPP), and PTMSP/PPP blends", Journal of Polymer Science: Part B: Polymer Physics, 34 (1996) 2613-21.

I. Pinnau and L. G. Toy, "Transport of organic vapors through poly(1-trimethylsilyl-1-propyne)", Journal of Membrane Science, 116 (1996) 199-209.

I. Pinnau and Z. He, "Pure- and mixed-gas permeation properties of polydimethylsiloxane for hydrocarbon/methane and hydrocarbon/hydrogen separation", Journal of Membrane Science, 244 (2004) 227-33.

B. E. Poling, J. M. Prausnitz, and J. P. O'Connell, The Properties of Gases and Liquids, 5th ed., McGraw-Hill, New York, NY, 2001.

D. S. Pope, W. J. Koros, and G. K. Fleming, "Measurement of thickness dilation in polymer films", Journal of Polymer Science: Part B: Polymer Physics, 27 (1989) 1173-7.

D. S. Pope, W. J. Koros, and H. B. Hopfenberg, "Sorption and dilation of poly(1-(trimethylsilyl)-1-propyne) by carbon dioxide and methane", Macromolecules, 27 (1994) 5839-44.

R. S. Prabhakar, T. C. Merkel, B. D. Freeman, T. Imizu, and A. Higuchi, "Sorption and transport properties of propane and perfluoropropane in poly(dimethylsiloxane) and poly(1-trimethylsilyl-1-propyne)", Macromolecules, 38 (2005) 1899-910.

R. S. Prabhakar, R. Raharjo, L. G. Toy, H. Lin, and B. D. Freeman, "Self-consistent model of concentration and temperature dependence of permeability in rubbery polymers", Industrial & Engineering Chemistry Research, 44 (2005) 1547-56.

J. M. Prausnitz, R. N. Lichtenthaler, and E. G. de Azevedo, Molecular Thermodynamics of Fluid-Phase Equilibria, 3rd ed., Prentice-Hall, Inc., Upper Saddle River, NJ, 1999.

R. D. Raharjo, B. D. Freeman, and E. S. Sanders, "Pure and mixed gas CH_4 and *n*-C_4H_{10} sorption and dilation in poly(1-trimethylsilyl-1-propyne)", Polymer, in press.

R. D. Raharjo, B. D. Freeman, D. R. Paul, G. C. Sarti, and E. S. Sanders, "Pure and mixed gas CH_4 and *n*-C_4H_{10} permeability and diffusivity in poly(dimethylsiloxane)", Journal of Membrane Science, in press.

R. D. Raharjo, H. J. Lee, B. D. Freeman, T. Sakaguchi, and T. Masuda, "Pure gas and vapor permeation properties of poly[1-phenyl-2-[p-(trimethylsilyl)phenyl]acetylene] (PTMSDPA) and its desilylated analog, poly[diphenylacetylene] (PDPA)", Polymer, 46 (2005) 6316-24.

R. D. Raharjo, B. D. Freeman, and E. S. Sanders, "Pure and mixed gas CH_4 and *n*-C_4H_{10} sorption and dilation in poly(dimethylsiloxane)", Journal of Membrane Science, 292 (2007) 45-61.

A. Rojey, C. Jaffret, S. Cornot-Gandolphe, B. Durand, S. Jullian, and M. Valais, Natural Gas Production Processing Transport, Editions Technip, Paris, 1997.

B. H. Sage, B. L. Hicks, and W. N. Lacey, "Phase equilibria in hydrocarbon systems. The methane-butane system in two-phase region", Journal of Industrial and Engineering Chemistry, 32 (1940) 1085-92.

E. S. Sanders, High-pressure sorption of pure and mixed gases in glassy polymers, Ph.D. Dissertation, North Carolina State University, Raleigh, N.C., 1983.

E. S. Sanders, W. J. Koros, H. B. Hopfenberg, and V. Stannett, "Mixed gas sorption in glassy polymers: equipment design considerations and preliminary results", Journal of Membrane Science, 13 (1983) 161-74.

E. S. Sanders, W. J. Koros, H. B. Hopfenberg, and V. Stannett, "Pure and mixed gas sorption of carbon dioxide and ethylene in poly(methyl methacrylate)", Journal of Membrane Science, 18 (1984) 53-74.

J. Schultz and K.-V. Peinemann, "Membranes for separation of higher hydrocarbons from methane", Journal of Membrane Science, 110 (1996) 37-45.

V. M. Shah, B. J. Hardy, and S. A. Stern, "Solubility of carbon dioxide, methane, and propane in silicone polymers: effect of polymer side chains", Journal of Polymer Science: Part B: Polymer Physics, 24 (1986) 2033-47.

V. P. Shantarovich, I. B. Kevdina, Y. P. Yampolskii, and A. Y. Alentiev, "Positron annihilation lifetime study of high and low free volume glassy polymers: effects of free volume sizes on the permeability and permselectivity", Macromolecules, 33 (2000) 7453-66.

I. Shulgin and E. Ruckenstein, "Prediction of gas solubility in binary polymer + solvent mixtures", Polymer, 44 (2003) 901-7.

A. Singh, Gas and vapor sorption and permeation properties of high free volume glassy polymers, Ph.D. Dissertation, North Carolina State University, Raleigh, NC, 1997.

A. Singh, B. D. Freeman, and I. Pinnau, "Pure and mixed gas acetone/nitrogen permeation properties of polydimethylsiloxane [PDMS]", Journal of Polymer Science: Part B: Polymer Physics, 36 (1998) 289-301.

J. M. Smith, H. C. V. Ness, and M. M. Abbott, Introduction to Chemical Engineering Thermodynamics, McGraw-Hill, New York, NY, 2001.

G. Soave, "20 years of Redlich-Kwong equation of state", Fluid Phase Equilibria, 82 (1993) 345-59.

R. Srinivasan, S. R. Auvil, and P. M. Burban, "Elucidating the mechanism(s) of gas transport in poly[1-(trimethylsilyl)-1-propyne] (PTMSP) membranes", Journal of Membrane Science, 86 (1994) 67-86.

S. A. Stern, P. J. Gareis, T. F. Sinclair, and P. H. Mohr, "Performance of a versatile variable-volume permeability cell. Comparison of gas permeabiltiy measurements by the variable-volume and variable-pressure methods", Journal of Applied Polymer Science, 7 (1963) 2035-51.

S. A. Stern, V. M. Shah, and B. J. Hardy, "Structure-permeability relationships in silicone polymers", Journal of Polymer Science: Part B: Polymer Physics, 25 (1987) 1263-98.

K. Toi, G. Morel, and D. R. Paul, "Gas sorption and transport in poly(phenylene oxide) and comparisons with other glassy polymers", Journal of Applied Polymer Science, 27 (1982) 2997-3005.

G. J. van Amerongen, "The permeability of different rubber to gases and its relation to diffusivity and solubility", Journal of Applied Physics, 17 (1946) 972-85.

D. W. van Krevelen, Properties of Polymers: Their Correlation with Chemical Structures; Their Numerical Estimation and Prediction from Additive Group Contribution, 3rd ed., Elsevier Science, Amsterdam, 1990, pp. 71-107.

F. Vigne-Maeder and A. Auroux, "Potential maps of methane, water, and methanol in silicalite", Journal of Physical Chemistry, 94 (1990) 316-22.

J.-S. Wang and Y. Kamiya, "Concurrent measurements of sorption and dilation isotherms and diffusivity for polysulfone membrane/carbon dioxide system", Journal of Membrane Science, 98 (1995) 69-76.

H. C. Wiese, J. Jacobs, and B. H. Sage, "Phase equilibria in the hydrocarbon systems. Phase behavior in the methane-propane-*n*-butane system", Journal of Chemical and Engineering Data, 15 (1970) 82-91.

L. C. Witchey-Lakshmanan, H. B. Hopfenberg, and R. T. Chern, "Sorption and transport of organic vapors in poly(1-trimethylsilyl-1-propyne)", Journal of Membrane Science, 48 (1990) 321-31.

L. C. Witchey-Lakshmanan, H. B. Hopfenberg, and R. T. Chern, "Dilation of poly[1-(trimethylsilyl)-1-propyne] during sorption of *n*-nonane", Journal of Polymer Science: Part B: Polymer Physics, 31 (1993) 1545-53.

P. Zoller and D. Walsh, Standard Pressure-Volume-Temperature Data for Polymers, Technomic, Lancaster, PA, 1995.

Vita

Roy Damar Raharjo was born on June 13th, 1981 to Djastra Hernadi and Elly Susanti in Semarang, Indonesia. After graduating from Loyola High School, Semarang in 1999, he attended Purdue University in West Lafayette, Indiana. He finished his undergraduate study in 3 years and received a Bachelor of Science degree in Chemical Engineering from Purdue University in Spring 2002. He enrolled in the University of Texas at Austin the following fall to pursue a doctoral degree in Chemical Engineering under the guidance of Professor Benny D. Freeman.

Permanent address: Graha Candi Golf A1 no. 3
Semarang, 50274
INDONESIA

This dissertation was typed by Roy Damar Raharjo.